UNIVERSITÀ DEGLI STUDI DI PADOVA

FACOLTÀ DI INGEGNERIA

DIPARTIMENTO DI INGEGNERIA MECCANICA, SETTORE MATERIALI

Corso di Laurea Magistrale in Ingegneria dei Materiali

Eu^{3+} ion as a luminescent structural probe for studying the biomineralization processes in sol-gel derived bioactive glasses: a preliminary study.

Relatore interno: prof. Alessandro Martucci

Tutor esterno: prof. Jean-Marie Nedelec

Laureando: Simone Tiozzo

Matricola: 603130-IR

Anno accademico 2010-2011

A tutti coloro che
hanno creduto in me...

To all the people who
have believed in me...

Foreword

The following work constitutes the conclusion of a nine months research activity, mainly carried out abroad in the Erasmus LLP Placement framework within the *Laboratoire des Materiaux Inorganiques* (LMI) of the Blaise Pascal University (Clermont 2) and the *École Nationale Supérieure de Chimie de Clermont-Ferrand* (ENSCCF), and concluded in the *Dipartimento di Ingegneria Meccanica - Settore Materiali* of the University of Padua.

The choice of performing almost the whole experimental part of my Master Degree thesis in a foreign university, in France, was not a simple one to undertake, since it involved the need of living far from home and from the people I love for six months, with all the practical and emotional difficulties of the case; moreover, it meant also leaving the comfort and security of a well known university department, wherein I spent five great years during my studies, for an unknown laboratory, with the consequent need of dealing with further problems like integration with other students and researchers, earning from scratch the trust of teachers and technicians, being continuously considered as a "foreign body", a freelancer, by all the institutions, etc.

Nevertheless, in Clermont-Ferrand I had the opportunity of working on the subject that interests me the most, that is the study of biomaterials from the biological and physico-chemical point of view, while improving my knowledge of French and testing myself, both from the academic and human point of view, against a series of tasks that never would I have faced staying in Padua; those opportunities of personal and intellectual growth, in the end, are the reasons why I chose the path that has led me to this point, to writing exactly these words on this page.

Coming to the subject of this thesis, in the following sections we will trace back the first steps that I helped to make in the pursue of an ambitious challenge: the development of a "novel" characterization technique, meant to shed some new light on the mechanisms that control the reactivity of a biomaterial when it is implanted in a living tissue. In detail, the issue I dealt with (with the help of the French research team) was the need of a new method to detect and accurately quantify the crystallization of the nano-scale layer of hydroxyl-

carbonate-apatite (HCA) that grows on the surfaces of bioactive glasses when they are put in contact with biological media.

The possible solution we have devised for this tricky problematic is based on the doping of bioactive glasses with low amounts of Eu^{3+} ions: in fact, those cations are luminescence emitting centers with high sensitivity to the degree of symmetry of the site they occupy, so they can work as a structural probe, that is they can tell us if they are in a glassy or crystalline environment through some characteristic spectral features. This way, since, as we will demonstrate, Eu is capable of entering inside the HCA lattice, it is possible to detect apatite crystallization on bioactive glasses via recognition of said features, which, specifically, are very narrow emission peaks located at well defined wavelengths and with peculiar intensity ratios.

What I actually did to help in the development of this technique was a preliminary study, i.e. I carried out a series of tests meant to verify if the solution we suggest is really effective: I tried to understand how Eu^{3+} ions behave when the glass is immersed in biological simulated fluids; if they are actually capable of entering the HCA nanocrystals precipitating on the glass surfaces; if they modify the dissolution and crystallization behavior of the base glass; if they significantly alter the glass network; if they lower the bioactivity of the material, and to what extent; etc. Summarizing, I tried to explore the scientific feasibility of this "novel" characterization technique, leaving economic (e.g. is this technique cost-effective?) and operative (e.g. how can we quantify HCA crystallization from spectroscopic data?) considerations to further studies on the subject.

Before starting our journey through the five chapters of this thesis, I would like to point out the reason why I insist in writing "novel" between brackets: what I did was, in the end, none other thing than a site selective luminescence spectroscopy study on the samples resulting from *in vitro* bioactivity tests; though to the extent of our knowledge this was never attempted before in the case of bioactive glasses, so that it can be actually regarded as a new approach, site selective spectroscopy analyses are widespread all over the literature, and have been carried out for decades on all sorts of materials; looking at my research activity from this latter perspective, nothing radically new has been done, and I can poetically consider myself just as a "tiny dwarf, sitting on top of a giant's shoulders".

In the first part of this work we will provide the reader the necessary introductive information to allow him to understand the experimental observations and deductions we will develop in the second part; in particular:

- In Chapter 1 we will report a general introduction on biomaterials, and especially on bioglasses and on the way they can be synthesized;
- In Chapter 2 we will describe the peculiar reactions, going by the name of biomineralization processes, that take place when a bioactive glass is immersed in natural or simulated body fluids;
- In Chapter 3 we will deal with the various characterization techniques we exploited during our researches, and we will provide a simple introduction to the luminescent features of Eu^{3+} ions;
- In Chapter 4 we will first present a theoretical overview on our research strategy, then we will deal with our doped bioactive glasses, describing their sol-gel synthesis protocol and showing the results provided by the various techniques we exploited to characterize them from the structural and textural point of view;
- Finally, in Chapter 5 we will focus on the study of the biomineralization processes taking place upon immersion of our samples in simulated biological fluids; in particular, first we will present the results obtained via our newly developed luminescence method, based on site selective Eu^{3+} ions spectroscopy, and then we will exhibit all the complementary evidences that can validate said results.

Last but not least, I want to point out that this Master Degree thesis is edited in English in order to be easily understood by both parts interested in this research activity, the Italian University of Padua and the French LMI/ENSCCF; I apologize since now for all the errors I have surely committed in writing it.

Simone Tiozzo

Table of contents

Part One: Introductory information

Part Two: Experimental data

Part One:

Introductory information

Chapter one: Introduction to bioactive glasses

Thanks to the great discoveries of the last century in the fields of medicine, surgery and pharmacology, life expectancy in the developed countries is making giant steps towards medium lifespans surpassing 80 years, and people over sixty years old already represent more than 20% of the total population in the European continent (Eurostat 2008); if we look to Fig. 1.1, we can clearly understand what great improvements have been made in 100 years:

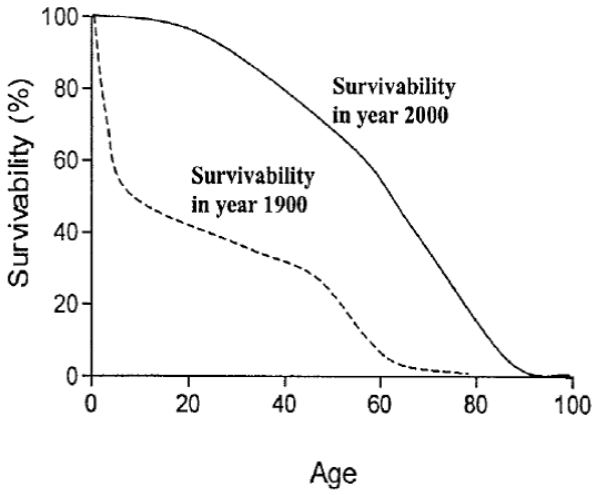

Fig. 1.1: Comparison between survivability trends in 1900 and 2000 (from ref. [63])

Facing the ageing of the population is a challenging task, since the human body naturally and unavoidably (at least for now) undergoes a functional degradation with time, and so it is becoming more and more difficult to ensure, together with survivability, also a satisfactory quality of life all along a person's lifespan. In achieving this latter purpose a great asset is represented by the so called spare part surgery, a branch of surgery dealing with the substitution of damaged tissues and organs with functional ones, that is dealing with grafts.

Since auto-grafts (the donor being the same person as the receiver) are not always possible, and allo-grafts (the donor being another human being) have stringent compatibility constraints due to the high risk of rejection, the development and improvement of artificial prostheses has become an extremely active field of research for biomedical engineering.

In the last decades enormous progresses have been made both in the case of functional (heart valves, hemodialysis filters, artificial blood vessels, artificial skin etc) and structural

prostheses (Charnley total hip joint replacement, inter-vertebral spacers, knee prostheses, etc), thanks to the joint efforts of surgeons, biologists and engineers; but to achieve further improvements in implant performances, it is surely necessary to continue the development of the *biomaterials*, that is of those materials specifically designed to intimately interact with the human body.

1.1: Classification of biomaterials

Defining what exactly a *biomaterial* is is not a simple issue; in 1986 the Consensus Conference of the European Society for Biomaterials proposed the following definition:

"A biomaterial is a non-viable material used in a medical device intended to interact with biological systems".

However, over the years this definition is starting to be less and less fitting to the reality of biomaterials research, since the "non-viable" connotation excludes completely the whole tissue engineering field, which is demonstrating increasingly promising for various applications such as fully organic artificial heart valves, bio-engineered skin, scaffolds for in vitro tissue regeneration, etc.

Nevertheless, the reported definition points out the most important feature biomaterials must possess to be considered as such: since they must interact in some way with biological tissues, they must not harm these latter, nor they must interfere with their normal functionality. This requirement can be translated into the most peculiar property of biomaterials, i.e. their so called *biocompatibility*:

"Biocompatibility is the capability of a material not to induce negative effects in the biological environment it is implanted into"

The various metallic, ceramic, polymeric or composite biomaterials can be classified in some different ways, depending on the peculiar feature kept into account:

From the point of view of the <u>effects</u> of the interaction <u>on the biomaterial</u>, we distinguish:

- <u>Biostable</u> materials: their structure and texture remains unaltered even after long term interaction with biological tissues; some examples are Al_2O_3, Au, TiO_2, UHMWPE (Ultra High Molecular Weight Poly-Ethylene).

- Biodegradable materials: after interaction with biological environment their structure or texture results modified to some extent; e.g. bioglasses, PGA, PLA, calcium phosphates.

Considering the effects of the implant on the body:

- Bioinert materials: they simply do not interact with the surrounding tissues, therefore they neither harm nor induce a positive response in the body; this category is extensively overlapped to that of biostable materials.
- Bioactive materials: after implantation they undergo some specific alterations to their structure and texture that promote a strong and direct bond with the host tissues; a few examples are bioglasses, HA, A/W glass-ceramic, Cerabone, Ceravital, etc. Most of these materials are bioceramics specifically designed to act like bone substitutes, or, in any case, to develop an intimate bond with osseous tissue.
- Bioresorbable materials: the action of biological fluids or of cells on these materials induces their partial or complete degradation into a series of chemical species that can be readily assimilated by the body, without any hazard; e.g. PGA, PLA, porous HA, β−TCP.

As the title of this thesis clearly suggests, in this work we will deal with some glasses whose peculiar composition and textural features are such that they can be classified among the so called bioactive materials; moreover, being glasses for biomedical applications, they can also be referred to as "bioglasses", though with some abuse of language.

1.2: Bioglasses

With the name "bioglass" it is common use to denote every type of glass specifically designed to be implanted inside the human body; as stated above, this is a tolerated abuse of nomenclature, since only certain biocompatible glasses belonging to the SiO_2−Na_2O−CaO−P_2O_5 system can be rigorously named Bioglass®.

The most interesting feature of the amorphous materials belonging to this group of bioceramics is that they exhibit marked bioactivity behavior: this means that, as we will discuss in detail in Chapter 2 (and experimentally demonstrate in Chapter 5 in the case of our doped glasses), after implantation they are capable of developing on their surfaces a layer of hydroxyl-carbonate-apatite practically identical to the mineral part of natural bone, and therefore they can be readily colonized by osteoblasts, which results in fast and intimate osteo-integration without foreign body reaction. Moreover, the degradation byproducts of this

interaction (mainly silicate ions released because of the hydrolytic action of biological fluids on the amorphous network) play an active role in stimulating bone regeneration, thus enhancing the speed and effectiveness of the integration process.

The invention of the first bioglass dates back to 1969, when Larry Hench prepared his first sample of what was to become the worldwide renowned Bioglass® 45S5; this material had the composition reported in Table 1.1, and from *in vivo* tests it proved to be the first glass ever to be capable of establishing a strong bond with osseous tissue. This outstanding achievement was connected to the peculiar reactions taking place at the interface implant / bone, that will be described in detail in Chapter 2.

Oxide	Weight %	Molar %
SiO_2	45	46.1
Na_2O	24.5	24.4
CaO	24.5	26.9
P_2O_5	6	2.6

Tab. 1.1: Chemical composition of LL Hench's original Bioglass® 45S5

This material derived from the hypothesis that a glass very rich in CaO and P_2O_5 could be able to develop a calcium phosphate layer on its surfaces when left in contact with biological tissues; the idea indeed proved to be correct, and after more than forty years, BG 45S5 is still commercialized and actively studied.

On the wake of the success of this bioceramic, the biocompatibility and bioactivity properties of other glasses in the quaternary system SiO_2−Na_2O−CaO−P_2O_5 as well as in other oxides systems was investigated. The results of these studies allowed to deepen the knowledge on the role of the various oxides, to understand the limit compositions that had not to be trespassed to preserve bioactivity, to discover which oxides enhanced what aspect of the reactivity of the glass, etc. Giving a detailed description of the progresses made in over of forty years of research in the field is not possible in these few lines, so we invite the reader to refer to reviews on the subject such as ref. [3], [42], [59] or [60], or to textbooks like ref. [67].

A minor, non representative sample of the many compositions proposed and studied over time just by LL. Hench's research team is reported in Tab. 1.2:

Designation	SiO_2	Na_2O	CaO	CaF_2	P_2O_5	B_2O_3	Al_2O_3
45S5.4F	46.1	24.4	16.2	10.8	2.6	0	0
45S5	46.1	24.4	26.9	0	2.6	0	0
#1(S63.5P6)	65.7	15.0	15.5	0	2.6	0.4	0.6
#9(S53P4)	53.9	22.6	21.8	0	1.7	0	0
#10(S45P7)	46.6	24.1	24.4	0	3.0	1.8	0
52S4.6	52.1	21.5	23.8	0	2.6	-	-
55S4.3	55.1	20.1	22.2	0	2.6	-	-
60S3.8	60.1	17.7	19.6	0	2.6	-	-
42SF	42.1	26.3	17.4	11.60	2.6	-	-
46SF	46.1	24.4	16.14	10.76	2.6	-	-
49SF	49.1	23.0	15.18	10.12	2.6	-	-
52SF	52.1	21.5	14.28	9.52	2.6	-	-
55SF	55.1	20.1	13.32	8.88	2.6	-	-
60SF	60.1	17.7	11.76	7.84	2.6	-	-
49S(gg)	50.	0	46.	0	4.	-	-
54S(gg)	55.	0	41.	0	4.	-	-
58S(gg)	60.	0	36.	0	4.	-	-
63S(gg)	65.	0	31.	0	4.	-	-
68S(gg)	70.	0	26.	0	4.	-	-
72S(gg)	75.	0	21.	0	4.	-	-
77S(gg)	80.	0	16.	0	4.	-	-
86S(gg)	90.	0	6.	0	4.	-	-

Tab. 1.2: Chemical compositions (expressed in molar percentages) of a few of the various bioactive glasses studied by L.L. Hench & coworkers

In the beginning all the bioglasses were prepared by the traditional, millennial fusion method; obviously, this required very high temperatures (up to over 1450°C) and the use of platinum crucibles (common refractory crucibles would intolerably contaminate the material); it involved the need of large amounts of alkaline modifier oxides to lower the melting point of the batch, and caused problems in the case of volatile oxides; it precluded to achieve compositions exhibiting liquid / liquid immiscibility (e.g. very high SiO_2 contents), etc. Moreover, the obtainable shapes for the implants were highly restricted by the very few forming technologies exploitable (mainly pouring the melt into moulds of proper design).

Therefore, bioglasses made a great leap onwards when they started to be synthesized using the sol-gel method (in Tab. 1.2 sol-gel derived sampes are marked (gg): gel glasses).

1.3: The sol-gel synthesis route

The sol-gel route is a synthesis method based on reactions of inorganic polymerization taking place in solution (aqueous or organic); the precursors can be generally of two types: alcoxydes, that is chemical species having formula $M(-O-R)_n$, where M is a metallic or metalloid atom (normally referred to as the "metallic center" of the molecule), and R are organic moieties such as methyl-, ethyl-, isopropyl-, etc; or metallic salts, such as nitrates, chlorides, etc, sometimes in hydrated form.

When these precursors are put in contact with water and proper catalysts (in the simplest cases acidic or basic catalysis is sufficient), they give rise to hydrolysis and inorganic poly-condensation reactions, that lead to the following results:

- In the beginning, tiny oligomeric clusters of sub-colloidal size (1 ÷ 10 nm) are formed, so what before was a solution of reactants becomes a dispersion going by the name of **sol**;
- Then, over time, these nano-clusters continue growing, and start binding to each other, eventually forming an interconnected continuous skeleton, inside whose (interconnected) porosity a liquid phase constituted by molecules of solvent and of not yet reacted precursors is contained; the system in these conditions is called **gel**.

After the gel is formed, it normally undergoes a solvent evaporation process (drying step), carried out in different ways depending on the purposes, and then, finally, it is calcined / annealed at higher temperature to yield a densified solid material. Since throughout the whole synthesis process the environment conditions are mild, that is no high pressures or high temperatures are exploited (in most cases T < 800°C), the sol-gel route is ascribable to the category of *Soft Chemistry* methods.

Depending on the peculiar operations carried out on the sol or on the gel, different final solid products can be obtained, such as: nanoparticules, e.g. SiO_2 NP synthesized following the Stöber method; thin films, when the sol is deposited on the substrate (e.g. via dip-coating, spin-coating, etc) and becomes a gel in situ; powders, obtained by quickly drying of the gel and successive grinding; monoliths, via drying and calcination steps carried out in controlled environment and at very low speed; aerogels, by performing the drying step in super-critic conditions; fibers, if the fiber is pulled from the sol; etc (see Fig. 1.2 for some examples of the many possible products obtainable exploiting the sol-gel route)

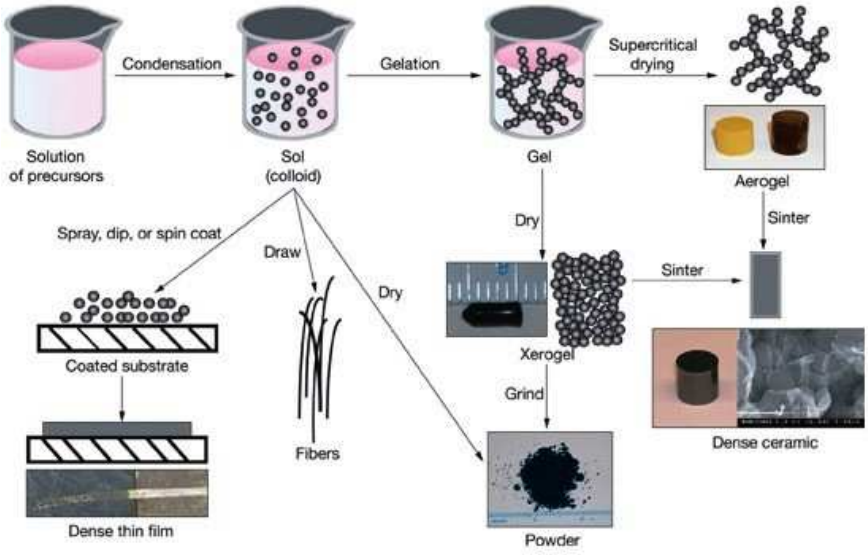

Fig. 1.2: The sol-gel method and some of its potentialities (from www.llnl.gov/str/May05/Satcher.html)

Even though being modified and doped in various different ways, still bioglasses are essentially silica based amorphous materials, therefore they can be synthesized following a sol-gel route just like many other glasses.

The first researchers to explore this path were R. Lin, A.E. Clark and L.L. Hench, that in 1991 published the article *An investigation of bioactive glass powders by sol-gel processing* (ref. [71]), in which they demonstrated not only that a series of Na_2O-free[1] bioglasses in the system SiO_2−CaO−P_2O_5 could be successfully synthesized exploiting the sol-gel method, but also that these materials exhibited better bioactive properties with respect to melt-derived glasses having equivalent compositions.

Since then, a lot of progresses have been made, for example it was possible to demonstrate that the presence of P_2O_5, though significantly promoting biomineralization processes (as we will see in Par. 4.2.1, it facilitates the nucleation of HCA crystals), is not necessary for bioactivity, since binary SiO_2−CaO glasses are bioactive as well (see ref. [12], [40] and [41]).

The synthesis of bioactive glasses is generally carried out using a mix of alcoxides (precursors for Si and P) and metal salts (reactants for modifying cations such as Ca, Mg, Zn, etc) in alcoholic solution (generally the parent alcohol of the Si precursor), and involves the hydrolysis and condensation reactions schematized below:

[1] Since exploiting the sol-gel route there is no need of lowering the melting point of the batch, Na_2O was not necessary in the composition anymore.

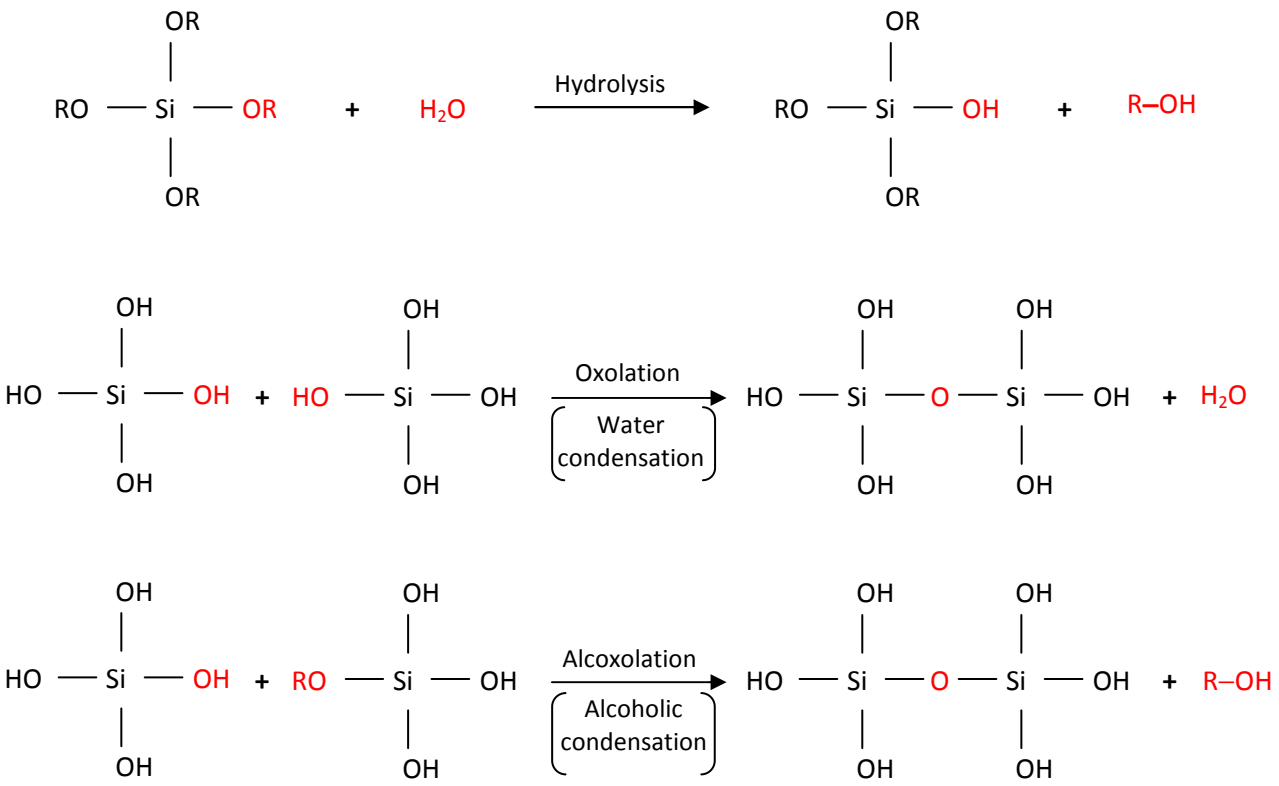

More explanations on the protocol of synthesis actually exploited in the case of our Eu doped bioactive glasses, along with detailed information on the behavior of Ca and Eu precursors throughout the whole process will be reported in Par. 4.2.3.

By properly tailoring the synthesis and thermal treatment (drying and annealing) conditions, it is possible to control to a very fine extent the properties of the final product, both from a structural and textural point of view; to achieve this result, it is possible to act on a broad series of experimental parameters, amongst which we can cite:

- Alcoxides / water ratio: it influences the average degree of hydrolysis (that is the mean number of −OR moieties hydrolyzed) of precursors attained prior to condensation;
- Nature and concentration of the catalyst: acidic catalysis induces the formation of linear polymeric chains with fewer ramifications (optimal for films, powders and monoliths), while basic catalysis promotes ramification and thus yields globular structures similar to pearl necklaces (optimal for NP);
- Type of moieties attached to the metal center: it has consequences on the degree of connectivity of the amorphous silicate network, on the reactivity of the precursors, on the interactions with the solvent, on the type of surface the final material will exhibit to the environment, etc.

- Nature of the solvent: it influences the kinetics of hydrolysis and condensation reactions;
- Temperature and duration of heat treatments: they have a strong impact on the degree of densification of the final product, therefore they deeply influence all the textural properties of the material (higher temperature and longer annealing generally causing a decrease in specific surface area, total pore volume, pore size, degree of porosity, etc).

In the production of bioactive glasses the sol-gel route has a long series of advantages over the traditional melting of powders method; among them:

- **Homogeneity**: hydrolysis and condensation reactions occur in solution, that is in liquid phase, therefore the mixing of precursors takes place up to a molecular scale; in melt derived glasses, on the contrary, the high viscosity of the batch prevents such intimate homogenization (high temperature refining of the batch is thus needed);
- **Purity**: with respect to melting, the sol-gel method eliminates the risk of contaminations deriving from crucibles, refractory lining of the furnace, impurities in the raw materials (flint sand, carbonates, etc);
- **Low temperatures**: an homogeneous and qualitatively excellent sol-gel derived bioglass can be obtained at temperatures as low as 600°C, while exploiting the traditional method the batch must be heated up at least at 1450°C;
- **Extreme compositions**: the phase diagram SiO_2−CaO (reported in Fig. 1.3) presents a liquid / liquid immiscibility region at higher SiO_2 concentrations, therefore at high silica content the traditional route does not yield an homogeneous glass, but a biphasic material (since already in the beginning the melt was phase separated), with one Ca-rich and one Si-rich phase. The sol-gel method, on the contrary, can easily yield glasses with compositions like 75% SiO_2 − 25% CaO, as demonstrated in ref. [49] (where such composition is called B75).
- **Simplicity**: sol-gel syntheses are normally extremely simple (see Par. 4.2.3 for an example of protocol) to carry out, so they can be easily transferred to an industrial scale; moreover, this method is especially suitable for the realization of coatings.
- **Tailored porosity**: through an accurate design of synthesis parameters it is possible to tailor the textural properties of the final material to one's needs; moreover, exploiting a series of advanced templating methods (inverse opal, replica, addition of surfactants), it is also possible to structure the porosity, obtaining ordered or even hierarchically organized pores (see for example the meso- and macro-structured bioactive glasses of ref. [23]);

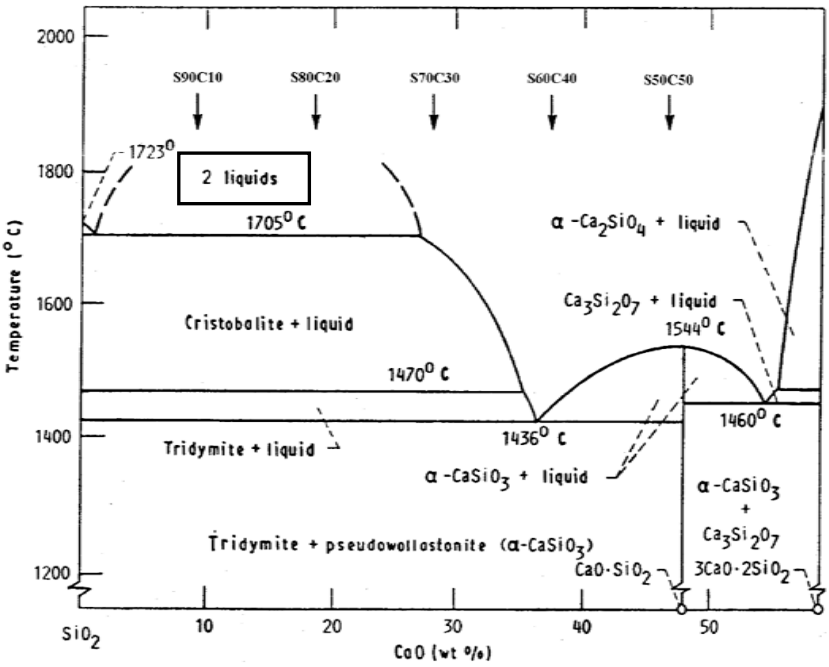

Fig. 1.3: SiO_2 – CaO phase diagram (from ref. [12])

- **Increased bioactivity**: thanks to the positive interplay between high specific surface area, pore volume and pore size (in the meso-porosity range, see Chapter 3), it has been demonstrated by various researchers[2] and for various materials that sol-gel derived glasses are more bioactive than melt derived ones having identical composition.

All the above mentioned features cooperate in making the sol-gel route the best available way to synthesize bioactive glasses, and are exactly the reasons that led us to the choice of the exploited synthesis protocol; for more information, we invite the reader to refer to Par. 4.2.3.

1.4: Osseous tissue

As we have already said, bioglasses are meant to be implanted in the human body and are especially designed to form an intimate strong bond to osseous tissues; some of them, belonging to the category of Class A bioactive materials (see Chapter 2), are even capable of bonding to soft tissues such as cartilages or tendons.

Before continuing on with the description of bioactivity processes, it is therefore better to present a brief overview on the most important features of bone tissue.

[2] Just to make a few examples, we can cite: T. Kokubo et al, *J. Am. Ceram. Soc.* 75 (1992) 2094; A.E. Clark, L.L. Hench, *J. Biomed. Mater. Res.* 28 (1994) 693; P. Sepulveda, L.L. Hench, *J. Biomed. Mater. Res.* 61 (2002) 301; D.L. Wheeler et al, *J. Orthop. Res.* 18 (2000) 140; M. Hamadouche et al, *J. Biomed. Mater. Res.* 54 (2001) 560.

Osseous tissue is hierarchically organized, and its global structure can be decomposed into a series of levels belonging to different dimensional scales: (A) macrostructure, (B) microstructure, (C) sub-microstructure and (D) nanostructure (see. Fig. 1.4).

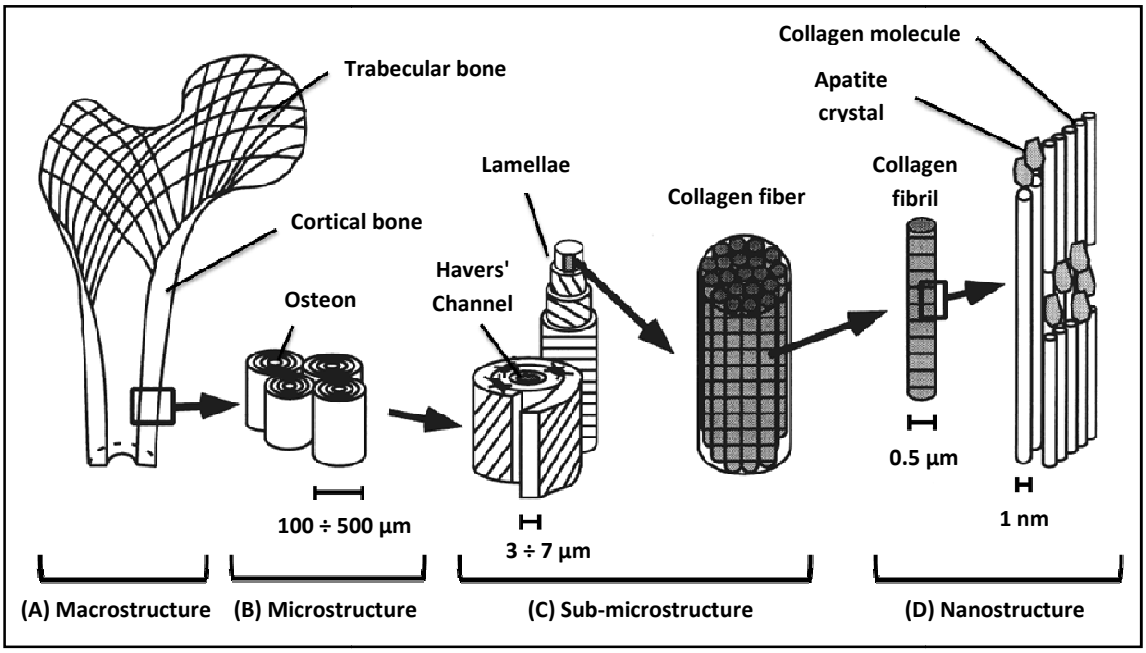

Fig. 1.4: Bone hierarchical structural organization

(A) At a macroscopic level, it is possible to distinguish between two types of bone tissue: trabecular bone (also called spongy bone), which is mainly located in the inner part of bones, especially at the extremities of long ones (tibia, femur, etc), is extremely porous (porosity > 70%) and contains bone marrow; and cortical bone, more compact than the first (porosity < 20%), located in the external, cortical part of bones and having structural, load bearing function.

(B) From the microstructural point of view, trabecular bone is made up of *trabeculae*, thin struts (made of collagen fibers and apatite crystals) forming an interconnected highly porous network; compact bone, on the contrary, is made up of osteons (or Haversian Systems), which are cylindrical structures exhibiting a further level of organizartion.

(C) Passing to the sub-microscopic scale, osteons are constituted by a certain number of lamellae, concentrically wound around the axial Havers' Channel; these lamellae are made of collagen fibers, organized in a cholesteric liquid crystal phase.

(D) At a nano-scale, each of these fibers can be divided into a series of fibrils, which in turn are made up of collagen molecules and inorganic nanocrystals (having their c axis aligned to that of the fibrils), tightly bound together.

These latter crystals are disk or globular shaped and of nanometric size (20 ÷ 30 nm), and are made of hydroxyl-carbonate-apatite (HCA), a calcium phosphate of formula:

$$\mathbf{Ca_{10-x}(PO_4)_{6-x}(CO_3\ ;\ HPO_4^{3-})_x(OH)_{2-x}}$$

In particular, HCA is a non stoichiometric hydroxyl-apatite ($Ca_{10}(PO_4)_6(OH)_2$) in which a part of the phosphate ions are substituted by carbonate (CO_3^{2-}, whose mean weight percentage oscillates between 3.2 and 5.8%$_{wt}$) and hydrogenophosphate (HPO_4^{2-}) ions. More detailed information on its crystallographic structure, on its unit cell, and on the point group symmetry of its lattice sites will be provided in Par. 4.1.2.

HCA constitutes more or less the 50% of human bone weight, and represents the mineral part of osseous tissues extra-cellular matrix (ECM), responsible for the hardness and compressive strength of bones; on the other hand, collagen molecules constitute the organic part of ECM, and give to the bone its toughness and flexural strength; the rest of the osseous tissue is made up of different types of cells, amongst which the most important (and specific to this type of tissue) are:

- **Osteoclasts**: they are gigantic poly-nucleated cells (deriving from the fusion of pre-osteoclasts) responsible for the physiological resorption of the bone ECM; in particular, they are capable of degrading collagen molecules via some specific enzymes, while they can dissolve HCA by lowering the local pH (HA is unstable at pH < 4.5).
- **Osteoblasts**: they exert an action exactly opposite to that of osteoclasts, since they are responsible for the production of new ECM, that is for the synthesis of collagen molecules and for the direction of biomineralization (precipitation of new HCA crystals).
- **Osteocytes**: they are basically inactive osteoblasts trapped inside the ECM they themselves synthesized; their function is fundamental since, being connected with each other by a network of *canaliculi*, they allow the circulation of nutrients, minerals and other molecules throughout the whole bone thickness, thus ensuring viability to the tissue.

Our skeleton is always in a dynamic equilibrium between osteoclast resorption and osteoblast regeneration of osseous tissue, and these processes are accurately regulated by various molecular signals, in turn stimulating or inhibiting one or the other depending on the needs: e.g. in presence of a fracture, osseous regeneration is stimulated, while when there is a metabolic Ca^{2+} deficiency in the body, bone resorption is accelerated.

Chapter Two: Bioactive glasses and their bio-mineralization processes

In this chapter we will describe the various processes that take place on the surfaces of bioactive glasses when they are put in contact with natural or simulated biological fluids. In particular, we will first point out the capital importance of type A bioactivity in ensuring a rapid and successful osteo-integration of the implant, thus leading to long term stability of this latter and to fast health recovery of the patient; then we will outline the various steps the biomineralization process is usually divided into, giving for each a detailed explanation; then we will focus on the peculiar features that render bioactive glasses capable of stimulating bone regeneration; finally, we will present the ways bioactive efficiency is usually assessed.

2.1: Bioactivity properties of bioglasses

As we have previously said, a lot of silicate based amorphous materials for biomedical applications are commonly referred to as bioglasses; this name stays mainly for the fact that they are all biocompatible, thus suitable for intimate and long term contact with biological tissues, and does not necessarily claim some form of connection with L.L. Hench's original Bioglass® composition.

In addition to biocompatibility, most of these glasses exhibit also bioactive behavior, that is they are capable of establishing a strong, direct, quick and intimate bond with the host osseous tissue they are implanted into, without any formation whatsoever of fibrotic capsule, i.e. without causing any foreign body reaction. This effect is due to two main reasons: first, when they are in contact with biological fluids, bioglasses are capable of developing on their surfaces an Hydroxyl-carbonate-apatite layer, which is recognized by the body as *self* and thus is readily populated by osteoblasts; second, their peculiar ionic release stimulates osseous regeneration in a series of ways that leads to fast growth of bone on the glasses.

Moreover, the vast majority of bioglasses belongs to the "Type A (or Class A) bioactive materials" class, that is they exhibit the following four characteristic features:

1. The material is capable of bonding both to bone and soft connective tissues (tendons, cartilages, ligaments, etc.)
2. The material is *osteo-conductive*, that is growth of new bone tissue (mineralized extra-cellular matrix vascularized and populated by cells) is possible on its surfaces;
3. The material is *osteo-inductive* (also osteo-*productive*), i.e. actively promotes the growth of osseous tissue in the region of the implant by stimulation of differentiation and proliferation of osteoblasts;
4. The material is progressively resorbed (not necessarily to a complete extent) as the new biological tissue is formed;

On the contrary, Class B bioactive materials (various calcium phosphates, porous hydroxyl-apatites, many biocompatible glass ceramics, etc) are not capable of bonding to soft tissues, are not or only marginally resorbable, and are **not** osteo-inductive.

The above mentioned features make bioglasses more efficient than Class B bioactive materials for applications in the biomedical field, like filling and reparation of osseous defects, or coating for shafts of implanted prostheses; in particular, it has clinically been demonstrated that bioglasses bond to the bone they are implanted into in a faster and stronger way, as shown in Fig. 2.1, where a comparison between the temporal evolutions of the amounts of newly formed osseous tissue in the perimplantar region is reported for three types of materials (data expressed in percentages normalized with respect to a sample of healthy bone).

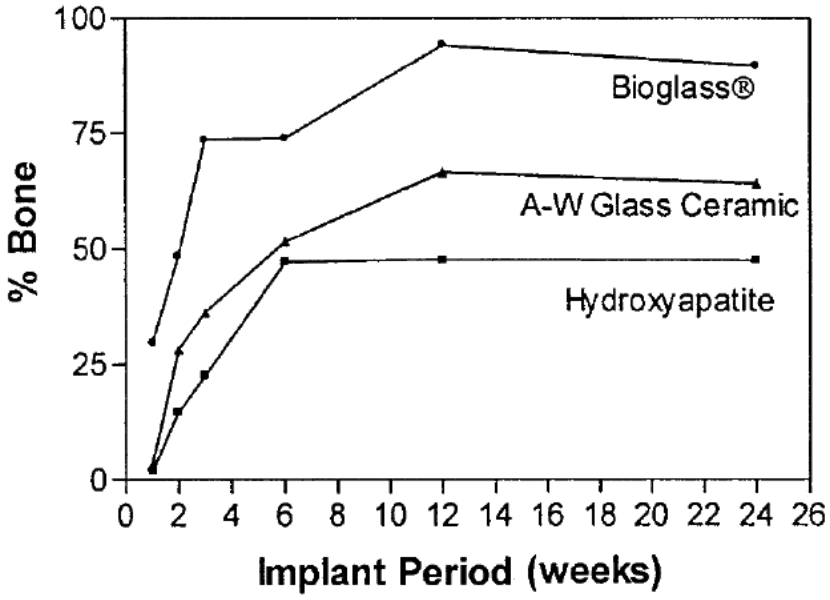

Fig. 2.1: Evolution of the amount of newly formed bone in the perimplantar region (from [57])

The better performances of bioactive glasses are not limited to bone regeneration rate alone, but extend to many other parameters involved in the health recovery of the patient (see Fig. 2.2), and this leads for example to an increased percentage of success of prosthetic implants coated with bioglass with respect to uncoated ones, or to an extremely low number of patients needing revision surgery both in the short and long term.

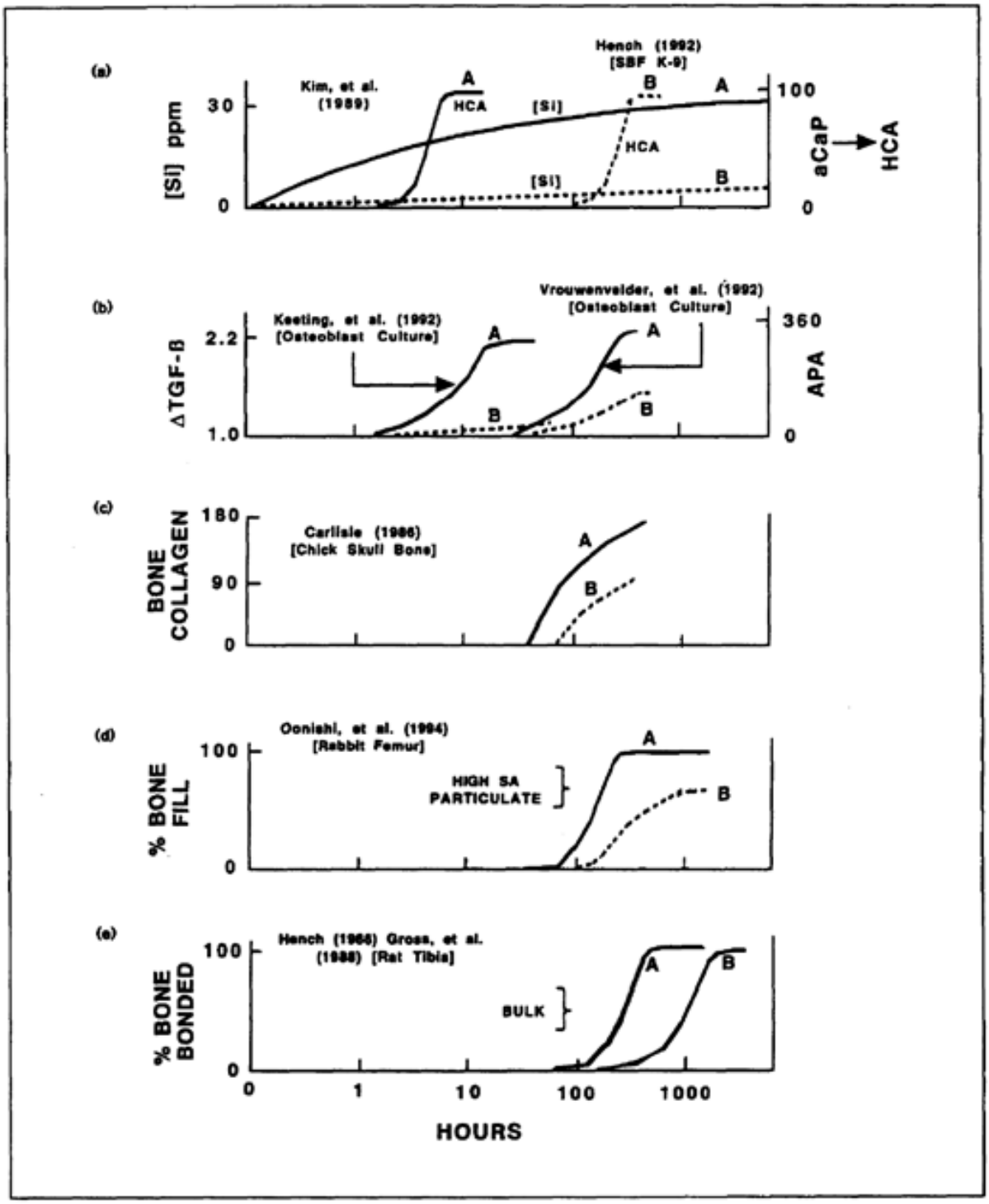

Fig. 2.2: Comparison between Class A and Class B bioactive materials' performances

It results clearly evident from Fig. 2.2 that the kinetics of the interactions with host tissues are way faster in the case of bioactive glasses (A curves): the formation of HCA crystallites inside the amorphous calcium phosphates layer takes place well before (a), and the release of silicate ions in the perimplantar region (a) stimulates the local production of TGF-β (b), a powerful molecular signal that in turn induces the differentiation of osteo-progenitor stem cells into osteoblasts and the proliferation of these latter; since these cells are responsible for the synthesis of bone extra-cellular matrix (mainly collagen fibers, c) and for its mineralization with HCA crystals, their increased activity in turn causes a faster tissue regeneration (d, e), and therefore a faster recovery of the patient's damaged functionality.

All these positive qualities of bioactive glasses translate themselves into an increased rate of success in clinical applications: for example, one of the first fields Bioglass® 45S5 (the "father" of all bioglasses, being the first one invented) implants were applied to was the substitution of the three ossicles (malleus, incus and stapes) of middle ear; after more than twenty years of extremely satisfactory results, and many hundreds of patients successfully healed, statistical data demonstrate that short term rejection of bioglass implants is an extremely rare eventuality, and even in the long period the cases of extrusion or displacement of the synthetic ossicles are limited to an extremely low percentage of patients (see Fig. 2.3).

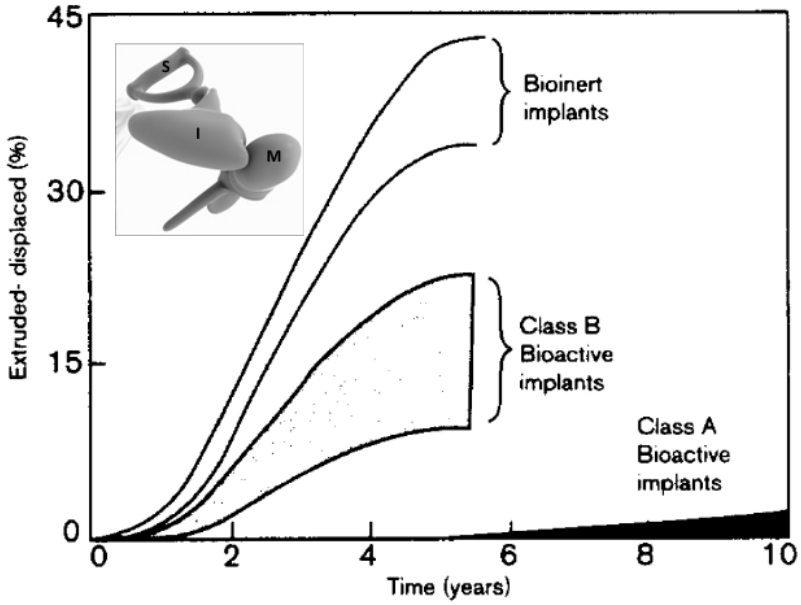

Fig. 2.3: Comparison between short and long term rejection incidences for prosthetic ossicles of the middle ear made of different biomaterials

2.2: Biomineralization processes in bioactive glasses

The strong bioactivity properties exhibited by most of the biomaterials commonly (and improperly) classified under the name of bioglasses are tightly connected to the peculiar interaction dynamics these amorphous materials are capable of establishing when they are put in contact with living tissues. In particular, it's exactly the series of reactions taking place on the surface of bioactive glasses when immersed in biological fluids (i.e. mainly blood) that explains their capability of bonding directly to the bones. In turn, said dynamics find their origin in both structural and textural features of the glasses, that is in composition, degree of network modification, specific surface area, total pore volume, pore size and shape, etc.

Though having considerably different chemical compositions, all the existing bioglasses share certainly one feature: they are all *hydrolytically unstable*, i.e. once immersed in natural or simulated biological fluids (that obviously are aqueous solutions), their amorphous network undergoes a gradual degradation, accurately designed to generate a beneficial reaction in the osseous tissue.

In particular, this structural and compositional development leads to the formation of an interfacial layer enriched in calcium and phosphate ions, both drawn from the liquid phase and deriving from glass leaching and dissolution processes; this layer is substantially made up of amorphous calcium phosphates doped in Si (due to the presence of the residual silicate network), and over time progressively evolves first incorporating OH^- and CO_3^{2-} ions issuing from the biological environment, and, later, crystallizing in the form of hydroxyl-carbonate-apatite, a phase practically coincident with the mineral / inorganic component of human bones.

This layer of HCA results bio-mimetic, and plays a fundamental role in the bioactivity behavior, since it constitutes the main cause of the osteo-conductivity properties of the material: in fact, being, as stated above, extremely similar to the osseous mineral ECM, the HCA layer is recognized as *self* by the body, and thus it does not lead to chronic inflammatory response or to foreign body reaction (attack of leukocytes and of the immune system, culminating with the isolation of the implant inside a capsule of fibrotic tissue), but, on the contrary, it is readily populated by osteoblasts.

These latter cells then start proliferating and synthesizing collagen fibers (whose function is to bind together the precipitated apatite crystals), meanwhile also releasing molecular signals and growth factors that stimulate the neo-vascularization of the perimplantar region; all this

eventually leads to the growth of a layer of new, living and functional osseous tissue, acting as a natural, strong bridge between original bone and artificial implant.

This way the fixation of the prosthesis to the host tissues is not merely mechanical, that is due to the surface roughness of the material, or just biological, i.e. due to the growth of new tissue inside the surface porosity (interpenetration), but is ascribable to a more strong, intimate connection, since the bone bonds directly to the surface layer of the bioactive glass, or better, it actually grows from there.

The physico-chemical processes leading to biomineralization (i.e. formation of the HCA layer) in bioglasses have been intensely studied by many researchers in the past decades, and the knowledge on this subject has been developed up to an almost complete extent, at least from the qualitative point of view; L.L. Hench, inventor of Bioglass®, and his coworkers have divided the reactions taking place at the interface between bioactive glass and biological medium into a series of steps, schematically represented in Fig. 2.4 (see ref. [61], but almost all Hench's articles report this very same scheme in the introductory part):

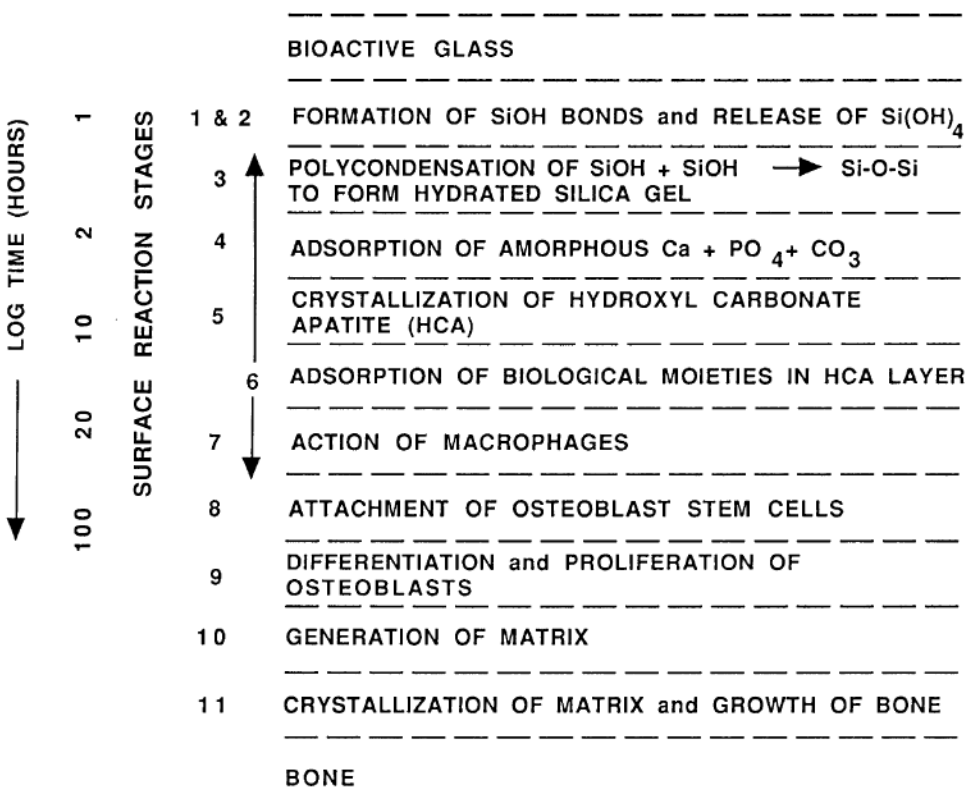

Fig. 2.4: Scheme by L.L. Hench, representing the various steps biomineralization processes on bioglasses can be divided into

1) Fast ionic exchange: since bioactive glasses are normally heavily modified (in order to be hydrolytically unstable), they are rich of alkaline and alkaline earth ions, and therefore they are very prone to leaching when immersed in biological fluids; in particular, Na^+, K^+, Ca^{2+} and Mg^{2+} ions are quickly released by the amorphous network, while H^+ (H_3O^+) ions enter the glass, leading to an intense depletion in modifiers of the surface layer and to the formation of silanol (Si−OH) groups:

$$\equiv Si - O - Na \; + \; H^+ \longrightarrow \equiv Si - OH \; + \; Na^+$$

$$\equiv Si - O - Ca^+ \; + \; H^+ \longrightarrow \equiv Si - OH \; + \; Ca^{2+}$$

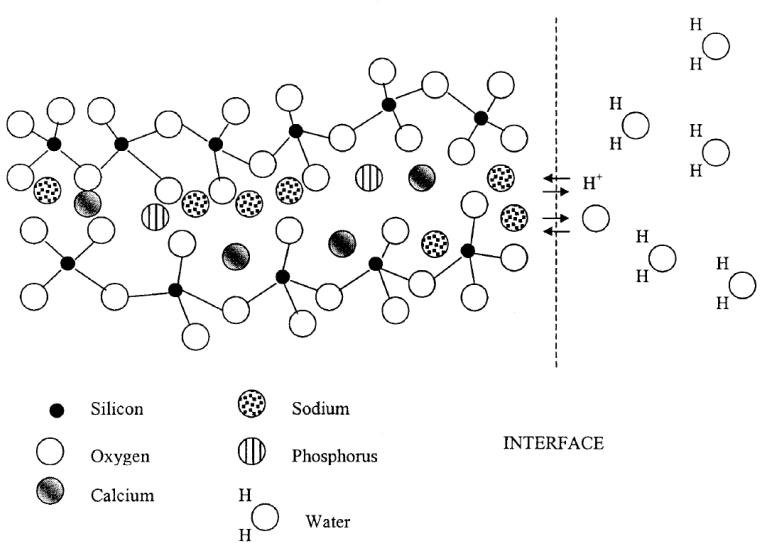

2) Depolymerization of the network: due to its specifically designed high content in modifier oxides, the network of bioactive glasses has very low hydrolytic resistance, and therefore the water molecules contained in blood plasma can easily induce the breaking (via hydrolysis reaction) of Si−O−Si bonds, with formation of surface silanols and release of $Si(OH)_4$ groups inside the liquid:

$$\equiv Si - O - Si \equiv \; + \; H_2O \longrightarrow \equiv Si - OH \; + \; HO - Si \equiv$$

3) Formation of a surface silica-hydrogel layer: the presence of high concentrations of Si−OH groups on the surfaces induces the formation by polycondensation reactions of an hydrated layer (approximately 100 µm thick) rich in silica and extremely porous, thus especially prone to the absorption of biological fluids (containing water, ions, but also proteins, growth factors, etc).

4) Formation of an amorphous calcium phosphates (Ca-P) layer: Ca^{2+}, Mg^{2+}, PO_4^{3-} and other ions, both issuing from the biological fluids or deriving from the glass leaching and dissolution processes, migrate by diffusion towards this silica gel layer; as a consequence, a new layer (around 50 µm thick) rich in Ca and P is formed on the surfaces of the bioglasses. Due to its composition, this latter is commonly referred to as "amorphous calcium phosphates (Ca-P) layer", and its existence can be easily deduced by the concentration profiles of Fig. 2.5, acquired with an electron microprobe on a 45S5 Bioglass® implant integrated inside a rat bone (from ref. [59]). The identification of the Ca-P layer is even more straightforward if we look to Fig. 2.6, where we reported the 2D chemical cartographies acquired via PIXE-RBS microprobe analyses on an *in vitro* bioactivity tested sample of B67,5[1] bioactive glass grains (from ref. [49]).

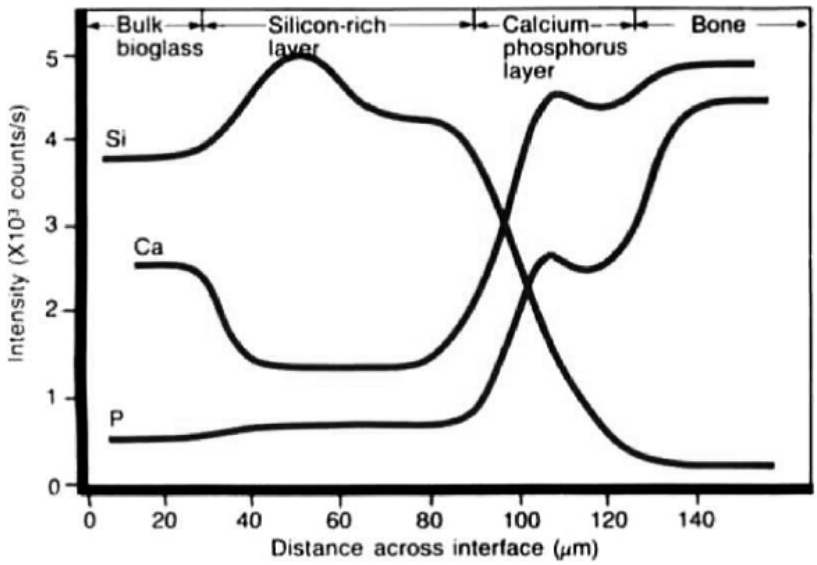

Fig. 2.5: Concentration profiles determined by electron microprobe analyses on a Bioglass® 45S5 implant integrated in rat bone

5) Hydroxyl-carbonate-apatite crystallization: the just described Ca-P layer is gradually enriched also in OH^- and CO_3^{2-} ions, drawn from the biological medium, so at a certain point crystallization of Hydroxyl-carbonate-apatite, $Ca_{10-x}(PO_4)_{6-x}(CO_3,HPO_4)_x(OH)_{2-x}$ (with $0<x<2$) takes place, starting from preferential nucleation sites provided by the underlying porous silica gel layer or by calcium phosphate nano-clusters present in the original glassy matrix (see Par. 4.2.1). The crystals are initially of nanometric size, but in a few days they grow up to a dimension of around one hundred of nm (see Par. 4.1.1).

[1] Moreover, this latter material is exactly the bioactive glass we studied in the present work, that is the base glass we started from to conduct our study on the effects and potentialities of Eu doping.

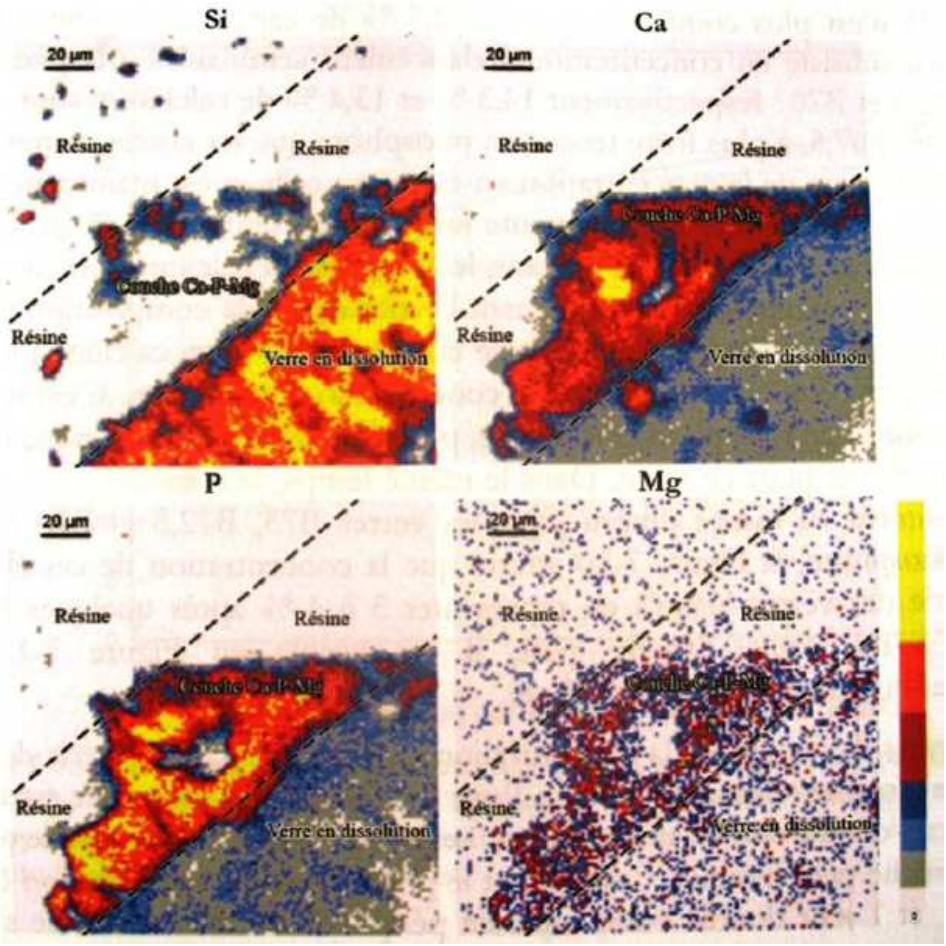

Fig. 2.6: Two-dimensional PIXE-RBS chemical cartographies of the cross section of a B67,5 bioactive glass granule after 7 days of in vitro bioactivity testing

The layer of HCA thus formed exhibits a high degree of bio-mimesis with the osseous matrix, both from a structural (composition, crystallinity, degree of substitution CO_3^{2-} VS HPO_4^{2-}) and textural (specific surface area, pore size) point of view, therefore not only macrophages and neutrophils (step 7 of Pic. 2.4) adhere to the surface of biomineralized glass grains, but also osteoblasts and osteo-progenitor stem cells are able to do so (step 8). Once adhesion and morphological spreading of osteoblasts has taken place, these latter start to proliferate (step 9) and to synthesize collagen fibers (step 10), which bind the HCA nanocrystals together, toughening the layer.

All these processes, together with the vascularization of the resulting perimplantar neo-formed ECM, lead to the formation of new living osseous tissue, practically indistinguishable from natural cortical bone.

2.3: Osteo-inductivity properties of bioactive glasses

The biologically induced formation of an HCA layer on the surfaces of the material when put in contact with natural or simulated body fluids ("biomineralization") can be regarded as the most distinctive feature of bioactive glasses, and is responsible for their osteo-conductivity; moreover, the study of biomineralization processes is exactly the aim of the present work, therefore in the following chapters we will almost exclusively focus on the precipitation of apatitic crystals during *in vitro* bioactivity tests, and on their detection via a series of different characterization techniques.

Nevertheless, what really makes bioactive glasses so successful for biomedical applications is not their osteo-conductivity alone, otherwise synthetic HA implants would exhibit more or less the same performances: when we switch to *in vivo* conditions, in fact, the real crucial feature of bioglasses, rendering them Class A bioactive, is their osteo-inductivity, i.e. their capability to actively stimulate bone regeneration. This trait will not be covered in great detail in this thesis, except for probe validation purposes in Chapter 5, since Eu^{3+} ions are of no use in studying the processes underlying osteo-inductivity; therefore, for completeness' sake, and to render more clear the observations that will be made in Par. 5.3.4, in this section we will present a brief panoramic on this subject.

Many studies have been published about the effects of the ionic products released by bioactive glasses during interaction with body fluids (see for example ref. [57], [62], [63] and [65]), and most of them agree in individuating in Si ions deriving from hydrolytic dissolution of the amorphous network the principal factor stimulating bone regeneration. In particular, it has been demonstrated that the presence of proper concentrations of silicate (and, to a minor extent, also calcium) ions in the perimplantar area are capable of:

- stimulating the differentiation of osteo-progenitor stem cells located in the surrounding tissues into osteoblasts;
- stimulating the mitotic proliferation of mature osteoblasts;
- potentiating the production of tropo-collagen, the protein collagen fibers are made up of;
- potentiating the expression of specific membrane receptors and of molecular signals involved in bone growth and reparation.

Consequently, it's the bioglass itself that, without further need of functionalization with

growth factors (such as, for example, BMPs, i.e. bone morphogenetic proteins[2]), actively and directly stimulates the osseous tissue to grow on its surfaces and to repair the existing damage (which is artificially induced in the case of the implantation of a coated prosthesis, or already present in the case of porous bioactive granules for bone defects filling).

Proof of the preceding statements can be found in various published articles, where many parameters and aspects connected to bone regeneration are monitored by establishing a comparison between bioglass samples and bioinert control references; as a non exhaustive collection of evidences, we hereby report the following data:

- Number of osteoblasts: after only four days of interaction between 45S5 Bioglass® granules and biological fluids, the number of mature and active osteoblasts present in the perimplantar region reaches the 155% (± 6.5%) of the value registered for a bioinert reference (see ref. [62]).
- IGF II, Insulin-like Growth Factor II: IGF II is a powerful molecular signal that promotes osteoblast mitosis, and therefore stimulates the proliferation of osseous cells, and, indirectly, the synthesis of extra cellular matrix; normally it can be found (in inactive form) attached to a protein named IGFBP-3, and to be cleaved from it, thus passing to an activated form, it needs the joint action of two enzymes: Metalloproteinase-2 (MMP2) and Cathepsin-D. By monitoring the concentration of the four mentioned biomolecules one can discover that in the case of a bioactive glass left in contact with biological fluids for four days, significantly higher values can be detected with respect to an inert material:

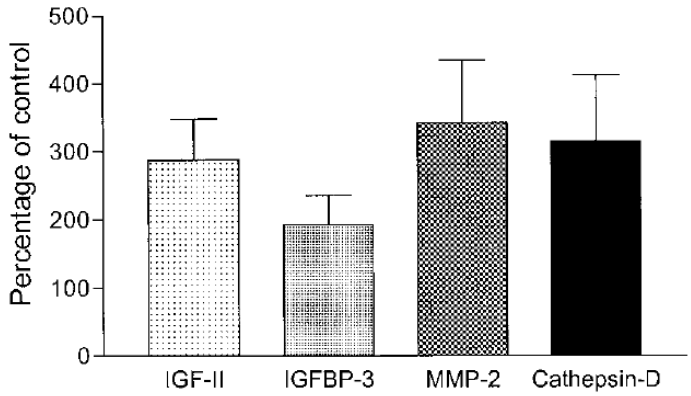

Fig. 2.7: Concentrations of four proteins involved in bone regeneration processes in the case of the perimplantar region of a Bioglass® 45S5 sample after 4 days of interaction (see ref. [65]).

[2] Coating the implants with bioresorbable polymer gels containing BMPs to ensure a slow but constant release (deriving from gel degradation) of molecular signals stimulating bone regeneration is a research strategy that has been explored in recent years to enhance the bonding performances of orthopedic prostheses; even though effective, this solution has as serious drawback the enormous expensiveness of BMPs (≈ 1200$/mg).

- Alkaline-Phophatase: it is an enzyme synthesized exclusively by mature osteoblasts, so it can be exploited as a marker to quantify the degree of cellular differentiation; in particular, after six days of interaction with Bioglass® 45S5 granules, the specific activity of alkaline-phosphatase in the perimplantar area can be found to be slightly increased if compared to the case of an inert reference (see Pic. 2.8, from [63]).

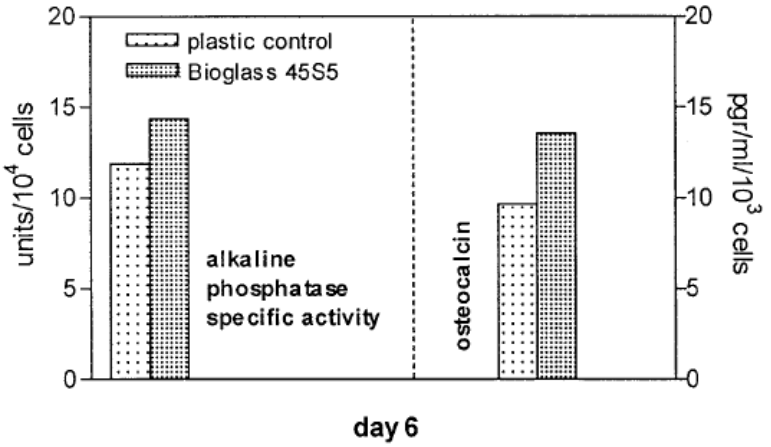

Fig. 2.8: Concentrations of proteins characteristic of osteo-genesis processes detected in the case of a six days old cell culture on a Bioglass® 45S5 sample.

- Osteocalcin: osteocalcin is a non collagenous protein characteristic of the bone ECM, whose synthesis by osteoblasts is tightly connected to the mineralization and reconstruction phase of osseous tissue; the concentration shown in Pic. 2.8 for the Bioglass® 45S5 sample appears evidently higher than the one registered for the control, testifying a superior osteo-genetic activity on the surface of the bioactive implant.

Once the beneficial effects of bioactive glasses on bone growth have been ascertained, to identify what are the actual causes of these improved performances it is necessary to analyze which alterations are brought about in the perimplantar region by the presence of a bioglass sample; moreover, it can be extremely interesting to investigate if for osteo-inductivity effects to take place, the physical presence of a bioglass implant is necessary, or if, on the contrary, it is sufficient that just the products of its hydrolytic dissolution are put in contact with living tissues (or cell cultures).

From this latter point of view, in reference [65] Xynos, Hench *et al.* demonstrated that simply exposing an healthy osseous tissue sample to a simulated biological solution

(specifically, DMEM, i.e. Dulbecco's Modified Eagle Medium, a cell culture medium whose features will be treated in some detail in Par. 5.1.1) previously left in contact for six days with some Bioglass® 45S5 granules (which were then removed from the liquid prior to the tissue assay) induced the stimulation of osteoblast proliferation and activity.

This evidence indisputably proves that osteo-inductivity is not directly connected to some structural or textural property of bioglasses, but is due to the ionic species released by them when they are subjected to leaching and hydrolytic attacks by biological fluids. In particular, analyzing the results of ICP-AES measurements on post-interaction DMEM reported in Table 2.1 (from ref. [65] by Xynos), one can easily notice that the only relevant ionic concentration change involves silicate ions, whose content after six days of bioglass granules immersion passes from 0.2 to 16.6 ppm.

Inductively Coupled Plasma Analysis of Control DMEM and Bioglass 45S5-Conditioned DMEM Containing the Ionic Products of Bioactive Glass Dissolution

	Si	Ca	P	Na
Control DMEM	0.19 ± 0.01	76.33 ± 0.96	33.48 ± 0.41	2885 ± 42.72
Bioglass 45S5-conditioned DMEM	16.58 ± 1.78	88.35 ± 2.32	30.45 ± 0.64	2938 ± 24.62

Note. The concentration of Si in the bioactive glass conditioned DMEM solution was 8800% of control ($P < 0.005$), Ca concentration was 110% ($P < 0.05$), and P concentration was 90% of control ($P < 0.001$). No significant differences in Na content were observed. Units are expressed in parts per million.

Table 2.1

Therefore it results reasonably demonstrated that Si ions mediate the activation of a series of biological / cellular mechanisms having as final consequence the stimulation of growth and regeneration of osseous tissue; to prove this in a rigorous, non-phenomenological way, it would be necessary to delve into molecular biology studies on the influence of Si on the expression of certain families of genes (for example those codifying for IGF II, Cathepsin-D, etc), but this thesis is not the appropriate place for such speculations.

As further empirical proof of the fundamental importance of Si on osteo-inductivity properties we can report the fact that porous synthetic biphasic calcium phosphate (BCP, a mixture of HA and β−TCP), though surely being biomimetic, osteo-conductive, bioactive and bioresorbable by the action of osteoclasts, is not osteo-inductive, due to the lack of silicon in its composition, and thus is a Class B bioactive material; on the contrary, Si doped BCP exhibits Class A bioactivity properties (see ref. [66]).

Even though we have stated that osteo-inductivity is not directly related to structural and textural properties of bioactive glasses, obviously these latter features play a fundamental role in determining the kinetics of Si ionic release, and thus an accurate control on them is absolutely crucial to the obtainment of satisfactory osseous regeneration performances: in fact, if silicate ions are released too slowly from the amorphous network, they might not reach the critical concentration necessary for the activation of the above mentioned cellular mechanisms, while, on the other hand, a too fast or too intense Si release might have negative or even cytotoxic effects on osteoblasts. Therefore, in order to maximize the osteo-inductivity of a bioglass, it is necessary to optimize its hydrolytic strength, specific surface area and porosity, so that to achieve the best interplay, leading to an appropriate ionic release rate.

Last but not least, it is important to point out that all the things we have said so far in this section are valid if and only if the bioactive material is put in contact with living osteoblast cells; if on the contrary the glass just interacts with acellular simulated biological fluids (like SBF or DMEM), as in the case of our research activity (see Chapter 5), osteo-inductive features can play no role whatsoever in the biomineralization processes, since no bone cells to be stimulated are present.

2.4: *In vitro* bioactivity tests

From a pure scientific point of view, in order to assess the bioactive efficiency of a bioglass, carrying out *in vivo* clinic implantation trials on human beings would be the best choice, since the gathered data would be directly and thus perfectly representative of the real performances of the material in its final application. Doing so indiscriminately is evidently not even imaginable, neither resorting to extensive *in vivo* testing on laboratory animals is a viable alternative, since it is ethically very questionable, and extremely costly as well.

Therefore, with the aim of minimizing the use of *in vivo* tests, some *in vitro* assay protocols to estimate with which efficiency a bioactive glass would be capable of bonding to bone tissue have been elaborated over time.

To date, the most important and widespread testing method is the one proposed in 1991 by T. Kokubo et al in the article *Solutions able to reproduce in vivo surface-structure changes in bioactive glass-ceramic A-W*, published in the *Journal of Biomedical Materials Research* (24) (see ref. [19]); therein, the authors made the hypothesis that the interactions with real biological tissues could be successfully simulated by immersing the bioactive samples in an

aqueous solution mimicking the ionic composition of human plasma. In that article such artificial solution was named Simulated Body Fluid (SBF), and a recipe for its preparation starting from a series of salts dissolved in deionized water was proposed; the final composition is reported in Tab. 2.2:

	Na^+	K^+	Mg^{2+}	Ca^{2+}	Cl^-	HCO_3^-	HPO_4^{2-}	SO_4^{2-}
Human Plasma	142,0	5,0	1,5	2,5	103,0	27,0	1,0	0,5
Kokubo's SBF	142,0	5,0	1,5	2,5	148,0	4,2	1,0	0,0

Tab 2.2: Comparison between ionic concentrations in human plasma and Kokubo's SBF (data reported in terms of mmol/L)

In particular, Kokubo's testing protocol consists of immersing appropriate amounts of bioactive samples in appropriate volumes of SBF for the desired periods of time at constant body temperature (36.5 ÷ 37°C); after the assay, the post-interaction material is characterized using a series of techniques (see Par. 4.1.1 for more information on this subject), in order to determine the changes induced in its structure and texture by the immersion in SBF.

If it is possible to detect the formation of HCA crystals on the surface of tested samples, then it is reasonable to assume that the same biomineralization processes would take place even in *in vivo* conditions, so that the material would be at least osteo-conductive, and therefore Class B bioactive. Moreover, analyzing the composition of SBF after the assay, it is also possible to determine if the samples release toxic species, and, by estimating the release of silicate ions, if they might be osteo-inductive and thus Class A bioactive.

Twenty years of positive results and hundreds of publications have demonstrated the validity and reliability of this *in vitro* test, that has the advantage of being more simple, quick, cheap and bio-ethical to carry out than every *in vivo* test; obviously, before a bioactive material is actually exploited for the construction of biomedical implants, it must undergo also *in vivo* assays (for more information on the series of tests that must be passed before clinic trials are authorized, see ref. [67] and [73]), but immersion in SBF is extremely helpful for the early stages of development, for example when a lot of compositions need to be tested in order to discover which one is the most suitable for the desired application. Some criticisms, however, might be formulated against Kokubo's method:

- First of all, it is a static method, i.e. the samples stay immersed in SBF inside sealed bottles, while in *in vivo* conditions a dynamic evolution of the system is possible, with released ionic products being withdrawn from the interaction area also by various mechanisms not directly related to biomineralization (fluid flow, metabolic depletion of ions, etc), and with continuous renewal of biological fluids. To overcome this limitation, some dynamic *in vitro* bioactivity testing protocols have been proposed (see for example ref. [2] and [7]), but their execution is more complicated, so they have encountered limited success.
- Second, in the case of bioactive powders, since biomineralization processes are surface driven, the final results are intrinsically connected to the specific surface area of the material, therefore utmost care must be paid in the interpretation and comparison of data arising from different samples. This issue will be discussed in more detail in Par. 5.1.3.
- Third, SBF is merely an ionic solution, while true biological fluids also contain a lot of different biomolecules (proteins, molecular signals, vitamins, glucids, amino acids, etc.), that might potentially alter the kinetics of biomineralization processes to some extent; in order to give more importance to this aspect, and thus to more representatively simulate biological interactions, instead of SBF, Clupper et al (see ref. [72]) proposed to exploit Dulbecco's Modified Eagle Medium (DMEM), a cell culture fluid having ionic concentrations similar to Kokubo's SBF, but containing also a series of biomolecules (see Tab. 5.1 and 5.2 for more information on DMEM composition). This very same approach was adopted also in this work, and a detailed description of our interaction protocol is reported in Paragraph 5.1.2.

Once a biomaterial has proven to be Class B bioactive by developing an HCA layer during *in vitro* testing with Kokubo's method, it is suitable to pass to more advanced *in vitro* tests, like cell adhesion and cell culture assays, citotoxicity tests, ELISA tests, etc. All these latter methods are closer than immersion in SBF to the true conditions the biomaterial would experience when implanted inside living tissues, but involve also much higher costs, the need of expensive biological laboratory equipment, and a superior level of operative complexity.

Nevertheless, they can provide more in depth information on the true behavior of the samples when left in contact with living osseous tissues, and thus they can be exploited, for example, to rigorously verify if a material, besides being osteo-conductive, is also osteo-inductive, that is if it exhibits Class A bioactivity features.

Chapter Three: Characterization techniques

In this chapter we will report some basic information on the characterization techniques we used during our research activity on Eu doped bioactive glasses; we will try to be as clear and introductive as possible, providing the essential explanations necessary to comprehend the observations and deductions we made in our experimental path; but for a deeper understanding of the underlying physical principles (often belonging to quantum mechanics), or for a complete panoramic on the advanced applications and potentialities of the described methods, we invite since now the reader to refer to more specialized literature on the subject.

3.1: ICP-AES, Inductively Coupled Plasma Atomic Emission Spectroscopy

ICP-AES is a very sensitive characterization technique commonly exploited to carry out chemical analyses on liquids, that is to determine the actual concentrations of the various elements present in solution; as the name itself suggests, it is a spectroscopy based technique, that relies on the precise quantification of the photon flux emitted at well defined wavelengths for the assessment of the chemical composition of the samples.

Being an emission method, it requires some source of excitation, which is provided by an inductively coupled plasma, i.e. by a plasma whose energy is supplied via Joule effect by electric currents produced through electromagnetic induction; in brief, the plasma torch works in this way: a flux of Argon gas is channeled tangentially through a quartz tube surrounded by copper induction coils connected to a 30MHz radiofrequency generator; a Tesla coil creates a high voltage, high frequency spark within the gas, providing the necessary ignition to the ionization process; then the alternate currents running inside the external coil create intense azimuthal induced currents (the ionized gas has high electric conductivity) inside this embryonic plasma, thus further ionizing the gas and heating it up to extremely high temperatures (6000 ÷ 10000 K).

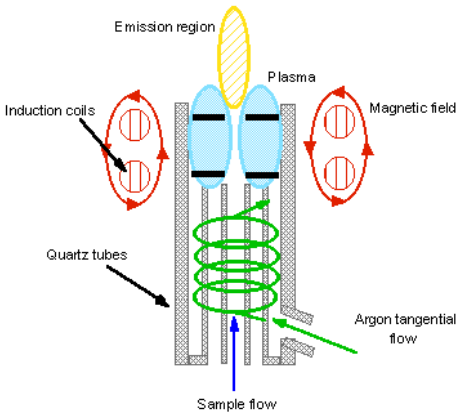

Fig. 3.1: Simplified scheme of an inductively coupled plasma torch

The analysis, in turn, is carried out like this: the liquid sample is nebulized inside the plasma torch, that first completely dissociates to the atomic state the chemical species present in solution, and then causes even the partial ionization of said elements; due to the high energies involved in the process, the peripheral (valence) electrons of these atoms are promoted to excited electronic levels, and when desexcitation takes place, UV-Visible photons are emitted.

Since the quanta of energy emitted in these transitions are characteristic of each element, performing a spectroscopic analysis on the light emitted by the *plume* (i.e. the ionized nebulized sample) allows the identification of the elements present in the initial solution. Moreover, quantitatively comparing the photon flux detected from our samples and from reference solutions of known certified concentrations allows the exact quantification of the chemical composition of the analyzed liquid.

ICP-AES has a series of advantages over other chemical analysis techniques (like, for example, X-ray fluorescence): since the instrument works in a high linearity domain, the construction of reference curves does not need the acquisition of many data, to an extent that even only one point could be enough to build a calibration line (the other point being the zero); the detection sensitivity for certain elements can be pushed up to the impressive limit of a few ppb, and ppm accuracy is granted for almost all the analyzable elements; it is possible to characterize also chemical species having high resistance to thermal decomposition; very small amounts of sample are needed (normally a few mL, depending on the experimental settings). However, there exist also some drawbacks: it is a very expensive technique, both for the initial instrument's price and for the operative costs (Ar is a costly inert gas); in some cases it is neither easy nor cheap to get a reference solution for dosing the desired elements (as happened to us for Europium, see Par. 4.3.1); and, above all, the samples must necessarily be in the liquid form, so that if we want to analyze a solid (like our glass powders), we need first to dissolve it in some way.

During our research activity we exploited ICP-AES measurements for two main purposes: to check that the actual composition of our doped glass powders was really the same as the nominal one (see Par. 4.3.1); and to follow the evolution of the concentrations of Ca, P, Si and Eu ions inside DMEM during *in vitro* bioactivity tests on our doped glasses (see Par. 5.3.4). For this second type of analyses the samples were already in the liquid form, as they were small aliquots of biological simulated fluids collected from the interaction vessels after testing,

so no further sample preparation was needed prior to the characterization; in the first case, on the contrary, we had solid materials, therefore a dissolution process was needed.

In particular, we exploited the *Alkaline fusion* (or Alkaline pearl) method: 100 mg of sample were mixed with 300 mg of lithium methaborate ($LiBO_2$) and put inside a graphite crucible, which was then heated up to 1100°C inside an induction oven for ten minutes; after this step, a viscous "pearl" of amorphous homogeneous material was obtained, and was quickly dropped inside 200 mL of 1M HNO_3 aqueous solution, wherein complete solubilization of the now fritted solid took place; the solution obtained in this way was eventually fed to the plasma torch for chemical analysis.

The analyses were materially carried out in the *Laboratoire Magma et Volcans* of the Blaise Pascal university of Clermont-Ferrand, with a Jobin Yvon ULTIMA-C instrument.

3.2: X ray diffraction measurements

X ray diffraction is one of the most widespread characterization techniques ever invented, and can be applied to the analysis of crystalline as well as mixed amorphous / crystalline compounds in a really enormous number of ways and methods, that can provide a wide range of different information on the samples, going from the identification of phases to the evaluation of residual tensile stresses, from the determination of unit cell parameters and site occupancy factors to quantitative crystal composition analyses, etc.

Since this technique is worldwide renowned, and at least one powder diffractometer is surely available in every research laboratory working on ceramic materials, we will not waste any time in explaining the theoretical principles underlying X ray diffraction measurements, because these concepts are surely well known to the reader. Moreover, we exploited this technique at its most basic level, that is for qualitative identification of the crystalline phases present in our powdered samples, so even the interpretation of the data we acquired does not really need further explanations, since we just performed a comparison between our plots and JCPDS / ICDD database files.

XRD analyses were employed for a series of purposes:

1. To evaluate the influence of Eu_2O_3 content on the devitrification processes that take place upon calcination at 700°C in our doped and undoped sol-gel derived bioactive glasses (see Par. 4.3.4);

2. To evaluate the influence of Eu_2O_3 concentration on the nature and amount of crystalline phases formed within the amorphous matrix of our samples during high temperature heat treatment (800, 900, 1100°C);
3. To demonstrate the actual precipitation of HCA on the surfaces of our doped and undoped bioactive powders after immersion in DMEM, that is after *in vitro* bioactivity tests (see Par. 5.3.1).

The measurements were carried out in the *Dipartimento di Ingegneria Meccanica - Settore Materiali* of the University of Padua, but different experimental parameters, instruments and methods were exploited in the three cases:

1. Our as-synthesized sol-gel derived bioactive glasses calcined at 700°C were characterized using a Bruker AXS D8 Advance powder X-ray diffractometer, exploiting a Bragg-Brentano "$\theta - 2\theta$" set-up; the generator was set at 40kV and 40mA, the analysis range went from 10° to 60°, with a 0.05° step and a sampling interval of 4 seconds.
2. The glasses treated at higher temperature were analyzed using the same instrument and settings, but this time the sampling interval was increased to 10 seconds.
3. On the contrary, the biomineralized powders have been analyzed with a Philips PW1710 diffractometer, using a "glancing angle" set-up, usually employed for the characterization of thin films; the generator was set to 30kV and 40mA, the analysis range spaced from 10° to 60°, with a 0.05° step and sampling interval of 10 seconds, and the selected glancing angle was $\theta_{glancing} = 3°$.

In particular, to perform this latter type of analyses we had to exploit a home-made trick to support our powders: a double sided tape was stuck to a soda lime glass slide, and was homogeneously covered with the samples, thus roughly simulating a film; this way, even with a tiny amount of material (a few tens of milligrams) it was possible to obtain a very good diffraction signal, comparable with the one detected from powder diffraction analyses, which however normally require way bigger amounts of sample (around 500 mg).

All the acquired diffractograms bearing distinct crystalline features, that is those deriving from point 2 and point 3 measurements, were analyzed with the help of the software *Xpowder 2004 Pro*, to identify which JCPDS files matched best the detected Bragg peaks.

3.3: Nitrogen adsorption measurements

The sol-gel protocol we exploited to synthesize our Eu doped bioactive glasses (see Par. 4.2.1) was expressly tailored to yield powders having a non negligible degree of porosity, since this latter plays a fundamental role in the reactions that take place on our samples when they are immersed in biological simulated fluids; therefore, characterizing our glasses from the textural point of view turned out to be a matter of utmost importance to understand their behavior during in vitro bioactivity tests and to study the effects of the dopant Eu ions on biomineralization processes.

In the following paragraphs we will describe the methods we employed to carry out such characterizations, assuming that the reader is already familiar with the concepts of open porosity, pore volume, specific surface area, adsorption of gases, etc. If this was not the case, we invite him to refer to introductory textbooks on the subject, or to specialized but yet comprehensible books like: S. Lowell et al, *Characterization of porous solids and powders: surface area, pore size and density*, Kluwer Academic Publishers, 2004 (ref. [53]).

3.3.1: Adsorption isotherms and their classification

When dealing with porous samples, a wide range of textural characterization techniques are available, each one being better suited for the analysis of a certain class of materials, depending on the peculiar size (micro-, meso- or macro-pores[1]), shape (cylindrical, ink-bottle, funnel, slit-shaped, etc) and type of the pores (open interconnected, or closed): in particular, among the most widespread we can cite gas sorption methods, mercury intrusion methods, and thermo-porosimetry methods.

Since our samples were synthesized following a protocol just slightly different from the well established one exploited by other members of the research team, we expected our Eu doped glasses to bear the same type of pores as in ref. [23] and [49], that is to contain a network of interconnected, more or less cylindrical-shaped mesopores. Therefore we decided to characterize their textural properties by performing on them nitrogen adsorption measurements with a Quantachrome Autosorb AS1 instrument.

[1] Micro-pores = pores having diameter < 2nm;

Meso-pores = pores having diameter between 2 and 50 nm;

Macro-pores = pores whose diameter is > 50nm.

This kind of analyses relies on the determination of the so called *adsorption isotherms*: these curves, as the name itself suggests, are built at constant temperature (in particular at the boiling point of liquid nitrogen, i.e. T = 77.35 K = −195.8°C) gathering point-by-point information on adsorption equilibrium states; in fact, when a certain gas (called *adsorptive*) is put in contact with a porous sample (called *adsorbent*), the system reaches a dynamic equilibrium state in which part of the gas molecules stay in the gaseous state, and part is physisorbed[2] onto the surface of the solid (becoming thus *adsorbate* molecules).

The actual amount of adsorbed molecules depends on a series of factors: first and obvious, on the amount of sample, therefore it is necessary to work with specific quantities (referred to a gram or kilogram of material); on the couple adsorbent/adsorptive, since the interaction between them can be more or less weak; on the selected temperature, higher T involving lower adsorbed amounts, due to the more intense thermal vibrations; on the relative pressure P/P_0 of the adsorptive gas (where P_0 is the vapor saturation pressure of N_2 at the given T), since higher pressures mean higher amounts of gas molecules available for adsorption; and, last but not least, on the specific surface area and degree of porosity of the adsorbent, since for example a wider surface (for the same amount of sample) coupled with a lot of interconnected pores can host a bigger number of molecules.

Therefore, measuring for each relative pressure value the exact amount of gas physisorbed on the surfaces of the sample (manometric or gravimetric methods can be exploited for this purpose) allows the construction of the isotherm curve (specific amount adsorbed vs P/P_0) and, thence, the deduction of useful information on the specific surface area, porous volume, average pore size, etc of the analyzed material. In particular, it is common practice to acquire both adsorption and desorption data, that is to cover a range of relative pressures going from 0.05 to around 1 (adsorption branch), and then returning back to 0.05 (desorption branch).

Even without the need of further data treatment, the isotherm's shape itself carries qualitative information on the type of pores present in the sample: the IUPAC classified (see ref. [51], [52] and [53]) six prototypes of nitrogen adsorption isotherms, with four kinds of hysteresis loops, reported respectively in Fig. 3.2 and 3.3; however, in real samples various combinations of said types can be encountered very often.

[2] *Physisorption* is a (normally) fully reversible adsorption process based on weak van der Waals interactions between adsorbent and adsorbate; on the contrary, *chemisorption* is an irreversible adsorption process based on strong chemical bonds, i.e. involving the formation of covalent or ionic bonds between gas molecules and the surface of the adsorbent.

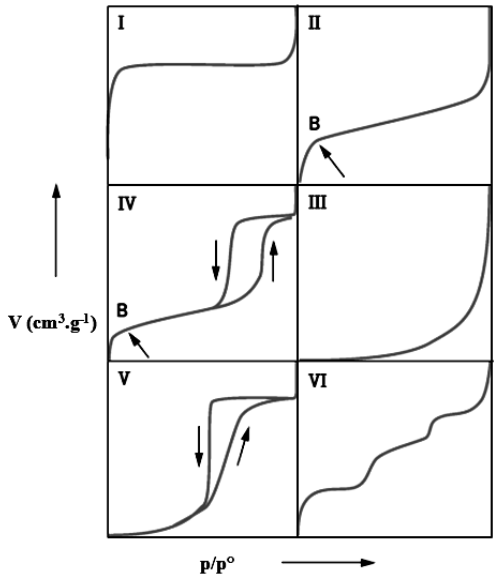

Fig. 3.2: IUPAC classification of nitrogen adsorption isotherms (from [52])

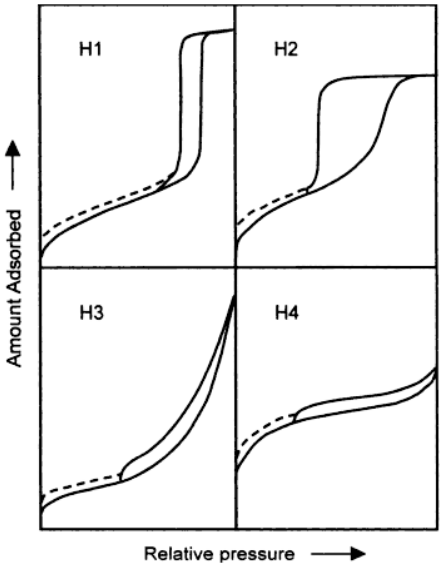

Fig. 3.3: IUPAC classification of hysteresis loops in N_2 adsorption isotherms (see [53])

For what concerns the isotherm's shape:

- **Type I** isotherms exhibit a saturation trend, and are typical of exclusively microporous samples, where the pores are filled at very low relative pressures (way < 0.05);
- **Type II** isotherms exhibit a continuous increase in the amount adsorbed with P/P_0, and are characteristic of non-porous or macro-porous samples, where multi-molecular adsorption takes place (i.e. the adsorbate layer thickens in a very gradual way);
- **Type IV** isotherms show two distinctive features: a saturation plateau at higher relative pressures and, above all, a characteristic hysteresis loop starting from P/P_0 values around 0.42, connected to nitrogen capillary condensation inside the mesopores of the samples;
- **Type III and V** isotherms are encountered only rarely, and are the variants of type II and IV curves in the case of very weak adsorbent/adsorbate interactions.
- **Type VI** isotherms have been observed only recently, and exhibit a typical stepwise growth; they are characteristic of samples with highly homogeneous surfaces, on which adsorption takes place monolayer by monolayer.

On the other hand, as regards the hysteresis loops:

- **H1 loops** are typical of mesoporous samples having a very narrow pore size distribution;
- **H2 loops** are characteristic of samples bearing highly interconnected mesopores;

- **H3 loops** are observed when the capillary condensation takes place in materials having a compliant structure;
- **H4 loops** are typical of microporous samples with slit shaped pores.

Therefore, just by carefully observing the acquired isotherms one can gain some considerable knowledge on the analyzed materials; however, to derive from the plots some quantitative information such as specific surface area (SSA), total specific open pore volume, mean pore size, etc, it is necessary to treat the acquired data exploiting some physico-mathematic models, like the BET (Brunauer−Emmett−Teller) theory for the calculation of SSA values or the BJH (Barrett−Joyner−Halenda) method for the determination of pore size distributions.

3.3.2: Specific surface area calculations

Knowing with precision the specific surface area of our samples is very important, since, as we will see in Chapter 5, those data are needed to calculate the exact amount of powder to be put inside the interaction vessel for bioactivity testing purposes; moreover, estimating the textural alterations brought about by the doping process is very interesting, since it allows us to understand to which extent Eu^{3+} ions modify the glasses they are meant to study. To calculate the SSA values of our powders from the acquired isotherms we exploited the most renowned and commonly used method existing, that is Brunauer Emmett and Teller's one, generally referred to as "BET theory".

This method, dating back to 1938, adapts the mono-layer chemisorption model designed by Langmuir to the case of multi-molecular physisorption; in particular, the fundamental hypotheses here are: 1) adsorptive molecules can physisorb on the adsorbent's surface forming infinite (stacked) layers; 2) contiguous adsorption layers do not interact with each other; 3) adsorption phenomena can be described by the Langmuir theory, both in the case the molecules bond directly to the solid and in the case they bond to a previously adsorbed layer (obviously, in the two situations the values of adsorption enthalpy are different).

Starting from these three postulates, after a series of deductions (not reported here; if the reader is interested in the rigorous demonstration of the method, he is invited to refer to [52] and [53]) the three researchers derived the following formula, valid for a range of relative

pressures going approximately from 0.05 to 0.35, and known today as *BET transformed equation*:

$$\frac{1}{V_{ads} \cdot \left(\frac{P_0}{P} - 1\right)} = \frac{C - 1}{C \cdot V_{mono}} \left(\frac{P}{P_0}\right) + \frac{1}{C \cdot V_{mono}} .$$

Here V_{mono} is the volume of nitrogen (per gram of powder) necessary to form a complete and compact monolayer of adsorbed molecules on the surfaces of the sample, and C is a parameter connected to the intensity of the interactions adsorbate/adsorbent, calculated as $C = exp\left(\frac{E_{m/s} - E_{m/m}}{RT}\right)$, where $E_{m/s}$ = adsorption enthalpy of the first layer of molecules and $E_{m/m}$ = adsorption enthalpy of the following layers (assumed equal to the heat of liquefaction, since in this case the interaction is between molecules of adsorbate).

As it is straightforward to notice, by plotting $\frac{1}{V_{ads} \cdot \left(\frac{P_0}{P} - 1\right)}$ VS $\left(\frac{P}{P_0}\right)$, which is extremely easy since V_{ads} and P/P_0 data can be extracted from the adsorption isotherm, one should obtain a straight line having slope equal to $\frac{C - 1}{C \cdot V_{mono}}$ and intercept equal to $\frac{1}{C \cdot V_{mono}}$; therefore, starting from experimental adsorption data, it is possible to calculate by linear best fit the value of V_{mono} and C, and once the value of V_{mono} and the average area occupied by a nitrogen molecule (σ_{N_2} = 0.162 · 10^{-18} m^2) are known, the specific surface area of the sample can be determined as $SSA_{BET} = \frac{V_{mono} \cdot N_A \cdot \sigma_{N_2}}{V_{N_2}}$ (where N_A is the number of Avogadro and V_{N_2} is the molar volume of nitrogen).

The SSA values obtained exploiting this simple method, however, can be considered rigorously valid only if the isotherm is of type II or IV (with capillary condensation beginning beyond P/P_0 = 0.35), while their reliability becomes a bit lower when the sample contains also micropores (isotherms of partial type I character, and/or hysteresis loops of H4 kind).

To characterize our samples from the textural point of view we carried out nitrogen adsorption measurements acquiring 20 points for the adsorption branch and 20 points for the desorption branch of the isotherm, i.e. P/P_0 values went from 0.05 to 1 and back again through steps of 0.05; in particular, to assess the SSA value we applied the BET method to the first seven experimental points of the adsorption branch, that is for P/P_0 values of: 0.05, 0.10, 0.15, 0.20, 0.25, 0.30 and 0.35; on the other hand, to calculate the total pore volume we exploited the V_{ads} value acquired at $P/P_0 \approx 1$, when total pore filling with condensed N_2 takes place.

On the data of the desorption branch we applied also the BJH method for the determination of meso-pore size distribution and average pore size, but our samples were not rigorously suitable for that elaboration: in fact, they contain a non negligible amount of micropores, as we will see in Chapter 4, so the BJH method (extremely sensitive to micropores) didn't provide sufficiently reliable data.

3.4: Raman spectroscopy

Raman spectroscopy is a highly versatile characterization technique suitable for studying not only amorphous and crystalline materials, but also substances in the liquid and gaseous states, and the information it provides can give us an insight into the vibrational properties of the analyzed samples. Since similar (but not identical, see section 3.5) information can be acquired through conventional or Fourier-Transformed infrared spectroscopy, it's common use to say that Raman and IR spectroscopies are complementary characterization techniques.

The physical principle underlying Raman spectroscopy is the inelastic scattering of light by a medium, and was first discovered in the case of liquids by Chandrasekhara Venkata Raman (1888-1970, Nobel prize for Physics in 1930) in 1928. In the following pages we'll try to provide an introductory explanation of the physical basis and of the main features of this technique; for a more complete and deeper understanding the reader should refer to specialized literature on the subject.

3.4.1: The inelastic scattering of light

Let's consider a substance made up of molecules, like something in the liquid or gaseous state[3]; when it is irradiated by a beam of monochromatic light of frequency v_0, its molecules can absorb the electromagnetic wave through various mechanisms, depending on the amount of energy hv_0 transported by the quantum of radiation. If the incident light is in the visible range, the absorption of the photons can result in the promotion of an electron of the molecule to a higher energy state, referred to as a *virtual energy level*[4].

Since this excited state is unstable, the molecule then quickly returns to a less energetic state

[3] If we switch to solids (both crystals and glasses), the phenomenon becomes a bit more complicated, since the structural units in this case are no more independent from each other, but the underlying physical principle stays exactly the same.

[4] It's important to point out that, in contrast with what happens in the case of fluorescence phenomena, this virtual energy level doesn't need to coincide with a discrete (i.e. permitted) energy state of the molecule (see scheme in the next page).

through different other mechanisms, some of which are of non-radiative nature, and some of which on the contrary involve the reemission of the absorbed energy under the original form of electromagnetic wave; these latter give rise to what we call the scattering of light.

This reemission, however, can be of elastic or inelastic nature:

- Elastic or Rayleigh diffusion: the emitted wave has the same frequency v_0 of the incident one, thus it has also the same energy;
- Inelastic or Raman diffusion: the emitted wave's frequency v is different from the incident one v_0; in particular:
  - if $v < v_0$, the diffused beam is less energetic than the incident one, and thus the molecule has absorbed part of the radiative energy to attain a final excited state, whose distance from the ground state is equal to $h(v_0 - v)$; this goes by the name of Raman Stokes diffusion, and the difference between the wavenumbers $\left(\text{being } \bar{\nu} = {}^{1}/_{\lambda}\right)$ of the two waves, $\bar{\nu}_0 - \bar{\nu}$, is called *Raman shift*.
  - if $v > v_0$, the molecule was already in an excited state of energy $E = E_{ground\ state} + h(v - v_0)$ when it absorbed the light, and by relaxing radiatively to the ground state it has given its "excess" energy $h(v - v_0)$ to the diffused wave, which this way results more energetic than the incident one; this is called Raman anti-Stokes scattering.

The following scheme intuitively shows the differences between the aforementioned scattering effects, and also a comparison with two other important radiative absorption and desexcitation phenomena: IR absorption and fluorescence.

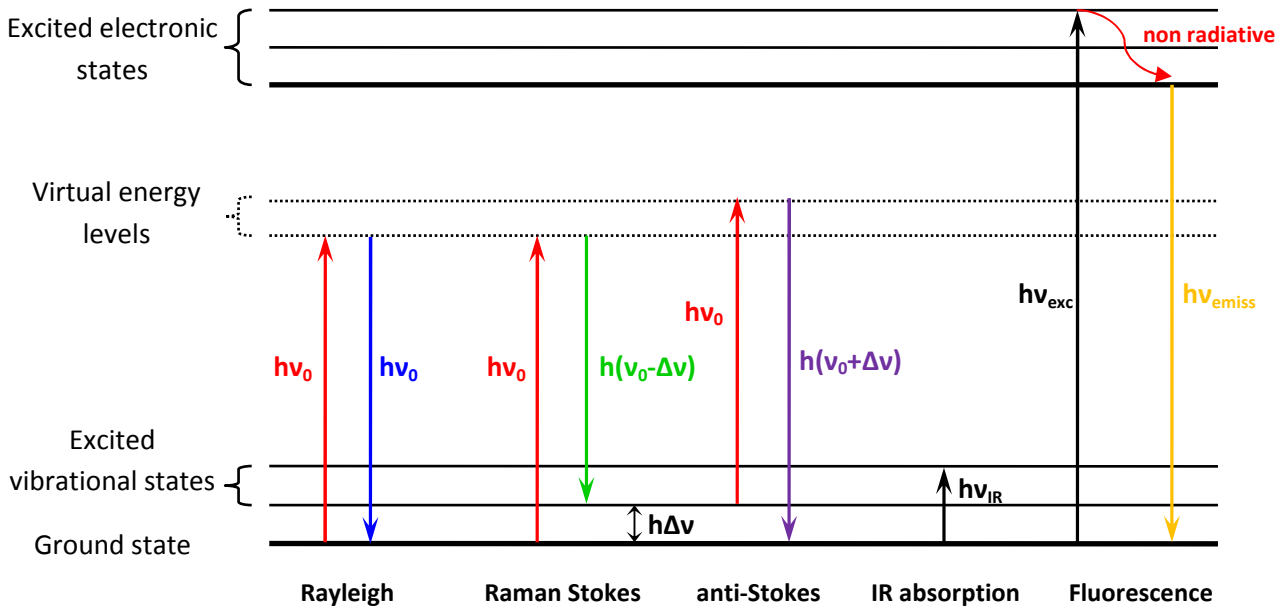

Since the energy difference between Raman diffused and incident waves is equivalent to the energy gap between an excited vibrational state and the ground state, studying inelastically diffused light allows us to gather information on the various modes of vibration of the scattering molecule, and thus on which chemical bonds are present inside of it.

Experimentally it's possible to find that the anti-Stokes diffused component is less intense than the Stokes component; this happens because for a molecule being already in an excited state is far less probable than attaining it after excitation and radiative desexcitation. More precisely, it is reasonable to assume that the scattering intensity from a certain virtual level is proportional to the population of that level, which in turn is obviously proportional to the population of the starting level, i.e. the one occupied before the absorption of the radiative quantum $h\nu_0$.

Now, according to Boltzmann's statistic, the population of a level is proportional to the term $exp\left(-\frac{E_{state}}{K_B T}\right)$, so the higher an energy level, the less it's populated; this way, it's straightforward to understand how the anti-Stokes component can be even 1000 times (since the relationship is exponential) less intense than the Stokes component. In turn, Raman Stokes scattering too is several orders of magnitude less intense than Rayleigh scattering (approximately only the 0.0001% of scattered photons are inelastically diffused), since a transition from an excited (virtual) level to a less energetic, but still excited, state is less probable then the transition to the ground state.

Boltzmann's statistic explains also the fact that Raman spectroscopy normally provides information only on the lowest vibrational levels of the emitter: the Raman Stokes diffusion requires that the final state attained by the molecule is an excited one, so only the less energetic among the excited states, i.e. the first rotational or vibrational excited states of the electronic ground state, are suitable to return enough signal to be detected. For this reason, Raman spectroscopy is sometimes referred to as an infrared technique, but this is scientifically inappropriate: the provided information is on vibrational levels, whose transitions between each other would involve energies in the IR range, but the technique normally exploits visible light.

Basically, to acquire the Raman signal it is necessary to focalize the detection on the "right" or on the "left" side of the Rayleigh scattering peak (i.e. around $\nu_{incident}$): at lower energies it is possible to find Raman Stokes scattering peaks, while at higher energies, but in exactly

symmetric positions (since the vibrational levels involved in the inelastic diffusion remain the same) we can find the Raman anti-Stokes emission.

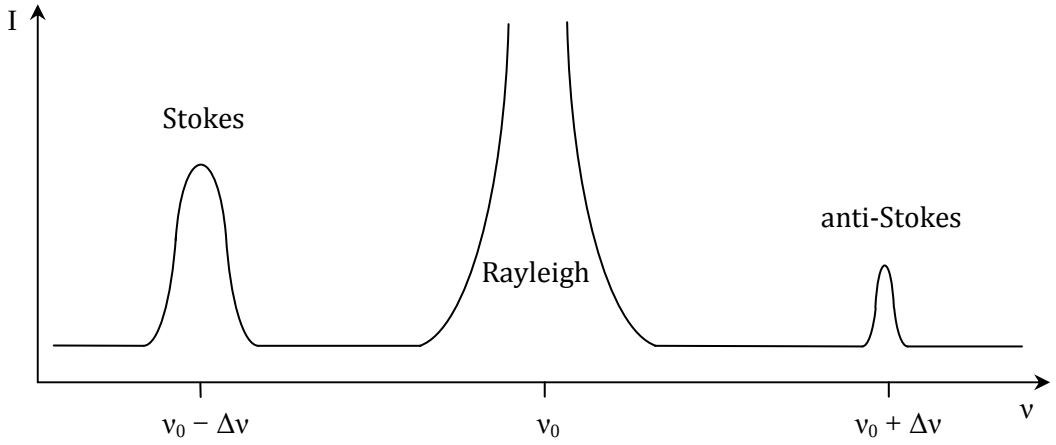

Unfortunately, things are way more complex than what the preceding few lines let us believe, since the formal description of transitions between energy states and of interactions between molecules and electromagnetic waves require quantum mechanics and group theory considerations, and thus various selection rules apply; this thesis is not an appropriate place for such complicated speculations, so here we will just say that in order to be permitted, and thus to return a detectable signal, the transition from a virtual level to an excited vibrational state (Raman stokes emission) or *vice versa* (absorption prior to anti-Stokes diffusion) must involve a change in the polarizability of the scattering molecule; when this happens, the vibrational mode connected to said excited energy level is referred to as a "Raman active" mode, and the higher the difference in polarizability between states, the stronger the intensity of the Raman emission arising from that level.

This means that, depending on the peculiar symmetry of the analyzed molecule, some vibrational modes may be IR active (involving a variation in the electric dipole moment of the molecule) but not Raman active, or *vice versa*, while some others may be both Raman and IR active (or inactive); that's the reason why Raman and IR spectroscopies, though being both used to study the vibrational "fingerprints" of molecules, yield slightly different data, and thus should not be considered competitive, but, on the contrary, complementary techniques.

What we have just said is rigorously valid only for liquids and gases; if the scattering medium is in the solid state, either amorphous or, even worse, crystalline, the interactions between different vibrating structural units, the degree of periodicity of the lattice, etc create new constraints on the vibrational modes, so the aforementioned selection rules change

significantly, while some other new interesting features make their appearance: e.g. boson peaks at low Raman shifts in glassy materials, providing information on the degree of mid-range order of the network, or again, spectral fingerprints of acoustic and optical phonons propagating through the crystalline lattice.

For more detailed considerations on the huge amount of information one can infer from Raman spectra of solids, as well as for a complete overview on the various advanced characterization techniques based on the Raman effect (such as Surface Enhanced Raman Spectroscopy, Coherent anti-Stokes Raman Spectroscopy, Hyper Raman, etc), once again we invite the reader to refer to specialized handbooks and textbooks on the subject.

3.4.2: Raman spectrophotometers

Trying to keep the explanation as simple as possible, a Raman spectrophotometer is basically made up of:

- a source of monochromatic light, which nowadays is a laser in the visible (Ar^+ laser) or in the NIR (Nd:YAG) range. It provides the scattering molecule/crystal the necessary energy for the promotion of its electrons to the virtual energy level. The use of a NIR source allows for the reduction of background fluorescence, which sometimes can mask the Raman peaks; however, since the intensity of Raman scattered light is proportional to $(\nu_{incident})^4$, lowering too much the frequency of the incident light can be detrimental to obtaining a good signal to noise ratio.
- a first series of collimation and monochromator optics (built-in in the laser cavity), to select only one wavelength of the laser beam (Ar^+ lasers, for example, emit with different intensities at various λ such as 351.1 nm, , 454.6 nm, 496.5 nm, 514.5 nm, 1092.3 nm, etc.) and direct it on the sample, which is kept in position by a sample holder; generally the beam impinges normally on the sample.
- a second group of collection optics, generally positioned at 90° with respect to the incident beam, in order to avoid the detection of transmitted light; these optics must collect the scattered radiation, filter off the Rayleigh peak and disperse the various components of the inelastically diffused light, in order to permit the spectral decomposition[5].

[5] Alternatively, a Michelson's interferometer coupled with Fourier-Transformed treatment of the acquired data might also be used to carry out the spectroscopic analysis.

- a detector, whose function is converting the photon flux in an electric signal suitable for digital processing; in the past photomultiplier tubes were the best choice for this purpose, but nowadays they're progressively being replaced by CCD cameras.

3.4.3: Raman micro-spectroscopy measurements

Since the Raman effect involves just the scattering of light, its promising application to microscopic analyses was explored early on (the first commercial instrument dates back to 1973); coupling a Raman spectrophotometer with an optical confocal microscope permits, in fact, to focalize the incident beam and the collection of diffused light on extremely small volumes of sample (up to an order of magnitude of 1 μm^3), and thus to determine their local chemical nature (i.e. which bonds are vibrating in that exact spot where the analysis was focalized thanks to the microscope), or to draw some interesting chemical cartographies.

The really high spatial resolution of this analytical technique, its complete non-destructivity, the tiny amounts of sample required to detect a good quality signal and the absolute lack of sample preparation (one just needs to put some grains of powder on a glass microscope slide) led us to choose this characterization tool for probing HCA crystallization on the post-interaction doped and non-doped bioactive glasses:

- spatial resolution: being able to localize the analysis on such small volumes allows us to study the vibrational behavior only of the interfacial interaction layer, by focalizing the laser beam exactly on the surface of the glass grains (or just a bit over it). This way, the intensity of the light inelastically scattered from the amorphous calcium phosphates and from HCA crystals is maxed out, while minimizing the signal coming from the underlying silica-based glass. The result is a spectrum with very high phosphate peaks and mid-to-low silica peaks (see Par. 5.3.3).
- non destructivity: working with highly expensive Eu doped materials implies synthesizing really small amounts of bioactive glasses (less than 2g for each batch), and since even the *in vitro* bioactivity tests are costly, destructive testing on post-interaction powders is out of discussion. Being completely non destructive and requiring just a spatula tip of material to provide satisfactory results, Raman micro-spectroscopy is an excellent choice for the characterization of the vibrational structure of our samples; in comparison, it's way better than FT-IR transmission spectroscopy, since it does not require the use of special home-made and potentially sample contaminating solutions (see the paragraph on FTIR) to avoid the loss of the analyzed powders.

However, this technique has also some unavoidable drawbacks:

- low speed: compared to FTIR, its direct competitor, the available micro-Raman spectrophotometer required much longer acquisition times to yield good results: approximately 10 minutes for an acceptable spectrum with Raman shifts ranging from 200 to 1560 cm^{-1}, against less than 4 minutes for an FTIR transmission spectrum in the whole mid-infrared range, from 400 to 4000 cm^{-1}.
- absence of tabular data: IR absorption peaks tables are widespread all over the literature, and extensive transmission FTIR characterizations have been carried out on bioactive glasses of compositions really close to mine, so attributing one vibrational mode to a detected IR peak is almost straightforward; on the contrary, Raman tables practically don't exist, and finding some bibliographic reference aiding in the identification of Stokes scattering peaks turned out to be quite difficult.

The spectrophotometer used during the research activity was a Jobin Yvon T64000, coupled with a confocal microscope (using the 50x optics); the monochromatic light beam was provided by the 514.5nm line of an Ar^{+} laser (1.5 W of power at the exit of the generator, corresponding to approximately 41mW on the sample); the collection optics was constituted by a Notch filter (to chop the Rayleigh scattering) coupled with a monochromator (1800 lines/mm); the detection was carried out by a nitrogen-cooled multichannel CCD camera, over a range of Raman shifts going from 200 to 1560 cm^{-1}; in particular, the global spectrum was divided into three parts, separately acquired and then merged together, each of which was collected twice for averaging purposes, with 100 sec accumulation time (for a total analysis time of 600 sec, i.e. 10 minutes). At least three spectra were acquired for each analyzed sample, focusing the beam on different spots; if the acquired data showed reasonable agreement, than one of the plots was saved, while in case of consistent differences, other spots were probed until an "average" recurring pattern was found.

3.5: Infrared spectroscopy

Infrared spectroscopy is by far the most widespread characterization technique employed in the study of the structural / vibrational features of both amorphous and crystalline samples, as well as of gases and liquids; for this reason, we will not spend a lot of words (as we've just done for micro-Raman) in the description of its physical basis, or on its pro's and con's, for we assume that the reader is already well familiar with all this.

To provide just a brief panoramic, when a beam of infrared light impinges on a sample, the incident photons can be absorbed by the material's structural units if their frequency matches the characteristic ν of a vibrational mode of said unit, i.e. if a resonance effect takes place; from a quanto-mechanic point of view, this corresponds to the fact that the energy carried by the incident photon coincides with the energy gap between the ground state of the molecule/unit and one of its excited vibrational levels; therefore, when the photon is absorbed, a transition between the mentioned levels takes place.

Since the distance between said energy states (and therefore the wavenumber of the absorbed IR light quantum) is characteristic both of the vibrating structural unit and of the peculiar vibrational mode involved in the transition, by carrying out a spectroscopic study on the absorption of the incident IR wave one can derive a lot of useful information on which units are present in the sample and how they vibrate. This kind of analyses can thus allow the recognition of the vibrational fingerprint of the structural units constituting the analyzed material, that is, in a nutshell, can provide information on which bonds resonate inside the sample, and with what intensity.

However, infrared absorption is intrinsically a quanto-mechanic phenomenon, therefore not all the possible transitions between vibrational states are permitted, but some selection rules apply: in particular, in order for a certain vibrational mode to be IR-active, i.e. to be able to yield a transition upon direct absorption of an IR photon, it must involve a change in the net electric dipole momentum of the structural unit. For example, let us consider a CO_2 molecule:

- The symmetric stretching of the C=O bonds, ν_{sym}(C=O), does not induce a change in the net dipole moment, because this latter, due to the linear geometry of the molecule, remains constantly equal to zero; this vibrational mode is therefore IR-inactive.
- On the contrary, the antisymmetric stretching is IR-active, since it causes an "unbalance" in the moments of the two C=O bonds, that results in a change in the net dipole moment of the whole molecule.

Depending on the number N of atoms it is made up of and on its linear or non-linear geometry, a molecule can have either 3N−5 (linear) or 3N−6 possible vibrational modes; these latter can be classified in various families, amongst which we can cite for example the symmetric and asymmetric stretching, involving the change in the relative distances of atoms without alterations in the bond angle; or the scissoring, involving the exactly opposite effect; etc (refer to specialized textbooks for more detailed information on this subject).

IR absorption spectroscopic analyses can be performed detecting either the fraction of light transmitted by the sample or the reflected one (this latter case will be discussed no further in this work); to practically carry out infrared spectroscopy transmission measurements one can exploit mainly two experimental approaches to irradiate the sample:

- Using a continuous excitation source (an IR lamp) and selecting step by step the wavelength to be directed onto the sample through a monochromator, like normally happens in UV − visible spectroscopy;
- Or coupling the IR source with a Michelson's interferometer and with Fourier transformed treatment of the recorded data; this is what goes by the name of Fourier Transformed IR spectroscopy.

This latter solution is definitely the fastest, since it allows the acquisition of an absorption spectrum over the complete Mid-infrared range (4000 ÷ 400 cm^{-1}) in just a few seconds; and the detected signal is way stronger, since it's the whole source's intensity (modulated in wavelength by the interferometer) that impinges at any time on the sample; so it is not surprising that the overwhelming majority of modern research instruments for IR analyses is made up of FTIR spectrophotometers.

Infrared absorption data can be recorded across the spectrum in terms of transmittance percentage ($T_{\%}$) or in terms of absorbance (Abs), where:

$$T_{\%} = \frac{I_{transmitted}}{I_{incident}} \cdot 100 \qquad \text{and} \qquad Abs = \log_{10}\left(\frac{I_{incident}}{I_{transmitted}}\right) ;$$

depending on the peculiar field of research, the two ways are exploited almost equivalently: for example, in the study of biomineralized bioactive glasses (i.e. in our case) the majority of literature data is published in terms of transmittance, so with our analyses we decided to follow in this path, but there is no scientific reason to choose one method over the other.

During our research activity we performed FTIR spectroscopy measurements on Eu doped bioactive glasses prior and after in vitro bioactivity testing, with the purpose of demonstrating the actual formation of HCA crystals on the surface of our powders during immersion in simulated biological fluids. In Chapter 4 and 5 we will present the specific features we exploited to recognize the characteristic vibrational fingerprint of HCA; for now we will just describe the peculiar method we exploited in order not to lose the analyzed material.

As we have already said in Par. 3.4.3, due to the very small amounts of material subjected to bioactivity tests, losing the analyzed powders would have led us to a premature complete depletion of our samples, with consequent impossibility of carrying out further characterizations; therefore, the idea of sacrificing a few milligrams of biomineralized glass to create (together with KBr powder, transparent to IR light) a compress for each analysis was not extremely tempting.

Nevertheless, we needed to support our samples in some way to place them into the sample-holder, so we came out with a home-made solution: we put our powders in between two slabs of KBr normally used to build a containment cell for FTIR analyses on liquids. In particular, for each analysis a spatula tip of sample was first put in the center of one of the slabs, then spread onto it as much as possible (in order to be sure not to completely extinguish the incident beam), then finally blocked in position by superimposition of the second slab; the sandwich slab/powder/slab was eventually mounted inside the sample holder, paying utmost care not to move it too roughly (or else grains of powder could have spilt out).

The analyses covered the whole Mid-infrared range, from 4000 to 400 cm^{-1}, with a resolution of 2 cm^{-1} and 128 accumulations (to yield the best quality results we could attain), and were carried out on a Perkin-Elmer 2000 FTIR spectrophotometer. Due to the peculiar home-made trick we exploited for sample-supporting, slightly different amounts of powder were characterized each time, so the acquired spectra never resulted rigorously quantitatively comparable between each other. Nevertheless, their qualitative features (such as relative intensities of the various peaks, for example) provided us a lot of useful information on our doped bioactive glasses, allowing us to demonstrate the actual formation of HCA crystals upon interaction with DMEM for all our bioactivity tested compositions (though with considerable differences in the precipitation extent).

3.6: Eu^{3+} ions and their luminescence features

Europium is a rare earth element belonging to the family of the lanthanides; it was discovered in 1896 by the French chemist Eugène-Anatole Demarçay, and is the most reactive among the lanthanides: it oxidizes very quickly to Eu_2O_3 in air, even spontaneously igniting at temperatures above 150°C; it has two stable oxidation numbers, +2 and +3, the latter one being the most stable in air atmosphere, and can form many compounds with halogens and chalcogens, as well as being capable of forming nitrates (hydrated or not).

In its metallic state it has no practical application whatsoever, while on the contrary many compounds containing Eu(II) or Eu(III) find scientific as well as technological applications for their luminescence (fluorescence in most cases) properties: for example Eu^{3+} ions are used as dopant in amorphous hosts for the construction of lasers for optoelectronics; $(Y,Eu)_2O_3$ is employed as red phosphor in CRT-TV sets and fluorescent lamps, while Eu doped yttrium ortho-vanadate was the red phosphor that in the 1960s revolutionized the CRT industry, allowing the construction of monitors of much increased brightness than before.

Eu in its elemental state has electronic configuration:	[Xe] $4f^7$ $6s^2$
While Eu^{2+} ions have ground electronic configuration:	[Xe] $4f^7$
And Eu^{3+} has ground electronic configuration:	[Xe] $4f^6$

3.6.1: Eu^{3+} ions' energy levels

As reported above, the fact that Eu^{3+} ions have an external $4f^6$ electronic configuration is their most important trait, and is responsible for most of their fluorescence features. First of all, it is important to point out that the 4f orbitals exhibit an interesting behavior going by the name of "*lanthanides contraction*": the 4f wavefunctions tend to progressively contract when the number of $4f^n$ electrons increases from n = 0 (La) to n = 14 (Lu), so that in the case of Eu the maximum 4f density of probability is already located closer to the nucleus than in the case of 5s and 5p orbitals. With a certain abuse of language, we could say that 4f orbitals are located below the 5s and 5p outer shells, and that these two latter have a sheltering effect on 4f electrons, which therefore show only low sensitivity to external electric fields (just like the other inner shells).

To be more precise, we should say that, due to the lanthanides contraction effect, the 4f electrons' wavefunctions exhibit only weak interactions with the wavefunctions of the electrons of any adjacent ions; therefore, Eu^{3+} immersed in any crystal field (i.e. surrounded by any disposition, ordered or disordered, of any type of ions) behaves more or less in the same way from the photoluminescence point of view, that is its energy level scheme remains more or less unchanged, just as if it were always in "free ion" (i.e. in void) conditions.

The underlined "more or less", however, is of capital importance, since slight variations in the energetic whereabouts of the various levels occur when the sites occupied by Eu ions have different point group symmetry, or the intensity of the crystal field (CF) is dissimilar due to the presence of different surrounding ions; and it is exactly this series of slight but yet

relevant (and detectable) differences that, together with other features we will point out in the following pages, makes Eu^{3+} ions perfectly suited to be used as a luminescent structural probe.

The peculiar energy scheme deriving from the $4f^6$ electronic configuration is what renders Eu ions capable of giving rise to fluorescence phenomena; however, in order to understand how electrons can occupy the different levels, a lot of complex quanto-mechanic considerations need to be made.

First of all, Eu^{3+} is far from being an hydrogenoid ion, that is an ion with one single electron, since it has 60 of them; fortunately, the first 54 e^- belonging to complete inner shells and to the 5s and 5p complete orbitals give no contribution to the levels involved in luminescence transitions, therefore only the 6 4f electrons must be kept into account. Nevertheless, 6 electrons can be accommodated into 7 4f orbitals in a huge number of different configurations (3003, to be exact), called electronic *micro-states*, and depending on the peculiar combination of quantum numbers of the 6 electrons, these micro-states will have different energies (i.e. it's the way all the six electrons occupy the 4f orbitals that determines the energy state of the ion).

However, many microstates, even if configurationally different, are equivalent from an energetic point of view (this effect is called degeneration), and can be grouped inside what we call *spectroscopic terms of Russel-Saunders*, whose denomination depends on the total angular momentum of the micro-state. To compute the energy of a certain electronic configuration / spectroscopic term we must resort to quantum physics and perturbation theory, that is we must use a series of Hamiltonian operators.

In particular, for rare earth ions like Eu^{3+} it is possible to demonstrate that the global Hamiltonian can be decomposed in the following way:

$$H = H_{config.} + H_{interel.} + H_{spin/orbit} + H_{CF}$$

and that in the above reported formula, the order of magnitude of the various Hamiltonians is such that each of them can be considered practically independent from the ones on its right, and to be a higher order perturbation of the ones on its left: for example, H_{config} is almost completely independent from $H_{interel}$, while H_{CF} is just a minor perturbation of $H_{spin/orbit}$.

- **H_{config}** keeps into account the electrostatic Coulombian interactions between the various electrons and the positively charged nucleus; by far it is the most important contribution, leading to the distribution of the electrons in the various orbitals of the atom/ion. With a

certain degree of approximation it can be calculated as the sum of the mono-electronic contributions of each e^-.

- $\mathbf{H_{interel}}$ accounts for the inter-electronic repulsions, and its effects can be translated into the spectroscopic terms of Russel-Saunders; in particular, the orbital momentums $\vec{l}$ of the 6 4f electrons sum vectorially up to yield a global orbital angular momentum $\vec{L}$, while the spin momentums $\vec{s}$ sum vectorially up to give the global spin momentum $\vec{S}$; cross interactions between spin and orbital momentums are considered negligible.

  Each micro-state has its own set of 6 $\vec{l}$ and $\vec{s}$ vectors, and through a complex and long method (for more information refer to specialized literature, or to [56]) in dependence of these latter it is possible to group the various states into a series of spectroscopic terms denoted $\mathbf{^{2S+1}\Gamma}$, where 2S+1 represents the total spin multiplicity of the term (S being the scalar projection of the maximum $\vec{S}$ attained by the various states belonging to the term) and Γ is a letter connected to the maximum L of the state (L being the scalar projection of the maximum $\vec{L}$ of the term; Γ = S, P, D, F, G, H, I, … for L = 0, 1, 2, 3, 4, 5, 6, …).

  If we did not consider any further perturbations, the spectroscopic terms would identify the different energy levels of the ion; following Hund's rules, the fundamental term between them could be identified as the one having the highest spin multiplicity and, in case of two or more terms having the same 2S+1 value, as the one having also the maximum orbital degeneration (i.e. the one containing more micro-states).

- $\mathbf{H_{spin/orbit}}$ keeps into account the interactions between spin and orbital momentums neglected at the previous point; in particular, the Russel-Saunders coupling model theorizes that these interactions induce the appearance of a total angular momentum J = L + S, and this causes the splitting of each term into (2S+1) levels if S<L, or (2L+1) levels if L<S; these latter are denoted $\mathbf{^{2S+1}\Gamma_j}$, where j assumes values between |L-S| and |L+S|. Moreover, each of these levels is 2J+1 times degenerated, and the fundamental level can be identified as the one belonging to the fundamental spectroscopic term and having: the lowest J value if the 4f orbitals are less than half filled ($La^{3+} \rightarrow Eu^{3+}$); J = S! if they are exactly half filled (Gd^{3+}); the highest J value if the orbitals are more than half filled ($Tb^{3+} \rightarrow Lu^{3+}$).

- $\mathbf{H_{CF}}$ accounts for the interactions between electrons of the REE ion and the external electric field generated by surrounding charges, i.e. what we call the electric crystalline field. Thanks to the lanthanides contraction effect, however, the 4f electrons are well sheltered from the CF, so this interaction causes further splitting of each level into sub-

levels having only slightly different energy values (internal Stark effect)[6]. Nevertheless, these little but detectable splittings depend on the point group symmetry and on the intensity of the crystal field, so a spectroscopic study on the luminescence features of Eu ions hosted in a material can yield structural information on the sites the emitting centers occupy in the host lattice.

Giving a more detailed or rigorous description of the quanto-mechanic basis of luminescence phenomena, on the Stark effect or on the way the energies of the different levels are calculated is way beyond the purposes of this work, so we will spend no more words on this subject, inviting the reader to refer to specialized textbooks if he seeks such information.

We conclude this paragraph showing on the right the energy level scheme calculated by Ofelt[7] for Eu^{3+} ions hosted inside LaF_3 (the picture shows only the part interested in luminescence phenomena); evidently, due to the differences in host lattices and in constituting chemical species, the Eu^{3+} ions used to dope our bioactive glasses will experience a different CF, and therefore will have a slightly dissimilar energy scheme. Nevertheless, as already stated, thanks to the lanthanides contraction effect the differences are only of minor entity, and therefore what is shown in Fig. 3.4 remains approximately valid (except for exact energy values).

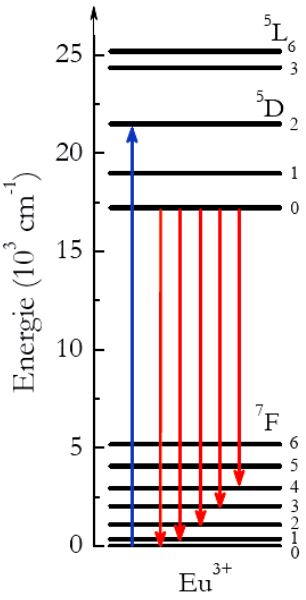

Fig. 3.4: Energy level scheme

The fundamental manifold is made up of 7 ^7F_J energy levels (J going from 0 to 6), with the ground state being the $^7F_0$, while the first available excited levels commonly interested by luminescence phenomena are the $^5D_0$, $^5D_1$, $^5D_2$, $^5D_3$ and $^5L_6$.

3.6.2: Luminescence phenomena in Eu^{3+} ions

Luminescence (also called fluorescence) phenomena in the case of Eu^{3+} ions are tightly connected to transitions between the few energy levels we've just cited; as we have shown in the scheme at Par. 3.4.1, prior to the emission of luminescence photons, the active center (i.e.

[6] For transition metals' ions, on the contrary, since the valence electrons are not sheltered from the action of the CF, the Hamiltonian H_{CF} is of capital importance, and has almost the same order of magnitude as $H_{interel}$; this renders their energy scheme extremely sensitive to the environment.

[7] G.S. Ofelt, *Structure of the f^6 configuration with application to Rare-Earth ions*, The Journal of Chemical Physics, 1963, 38(9): p. 2171-2180

the Eu^{3+} ion) must be brought into an excited state. This effect can be triggered in many ways, ranging from direct excitation of the center itself by absorption of a photon of proper wavelength, to energy transfer from other sensitizer complexes, to high energy excitation of the host lattice (as in the case of scintillation). If we keep as simple as possible, taking into account only the first excitation mechanism, then in order to be able to detect a luminescence signal we have first to excite our material by directing against it a beam of light having suitable energy.

In fact, in this case, differently from the Raman effect, excitation must involve a transition to some permitted energy level, therefore we can detect luminescence emission only if we excite in a correct way the target, i.e. by tuning the source to a wavelength corresponding to a transition from the ground state to one of the above mentioned excited states ($^5D_0$, $^5D_1$, etc).

When this result is achieved, two different pathways may be followed by the Eu^{3+} excited ion, depending on the peculiar level it was "promoted" into:

- If this latter coincides with the $^5D_0$, after a characteristic delay, called luminescence decay lifetime, the emitting center effectuates a transition towards the ground manifold, normally attaining a ^7F_J level with $J \leq 6$; this transition is associated with the emission of a luminescence photon having energy exactly equal to the gap between the two levels involved in the radiative transition.
- If on the contrary the excited state has higher energy, then usually non radiative relaxation towards the $^5D_0$ takes place, followed by radiative desexcitation into the ^7F_J manifold (as described above). However, it is also possible that desexcitation with emission of fluorescence photons takes directly place from the $^5D_1$ or $^5D_2$ levels, but this event is much less probable, therefore the emission intensities detected for $^5D_1 \rightarrow {}^7F_J$ or $^5D_2 \rightarrow {}^7F_J$ transitions are far lower than the ones arising from $^5D_0 \rightarrow {}^7F_J$.

A typical emission spectrum of Eu^{3+} ions hosted in an amorphous environment upon excitation in the $^5D_2$ level is reported in Fig. 3.5; we have labeled the various transitions according to what is reported in literature on the subject.

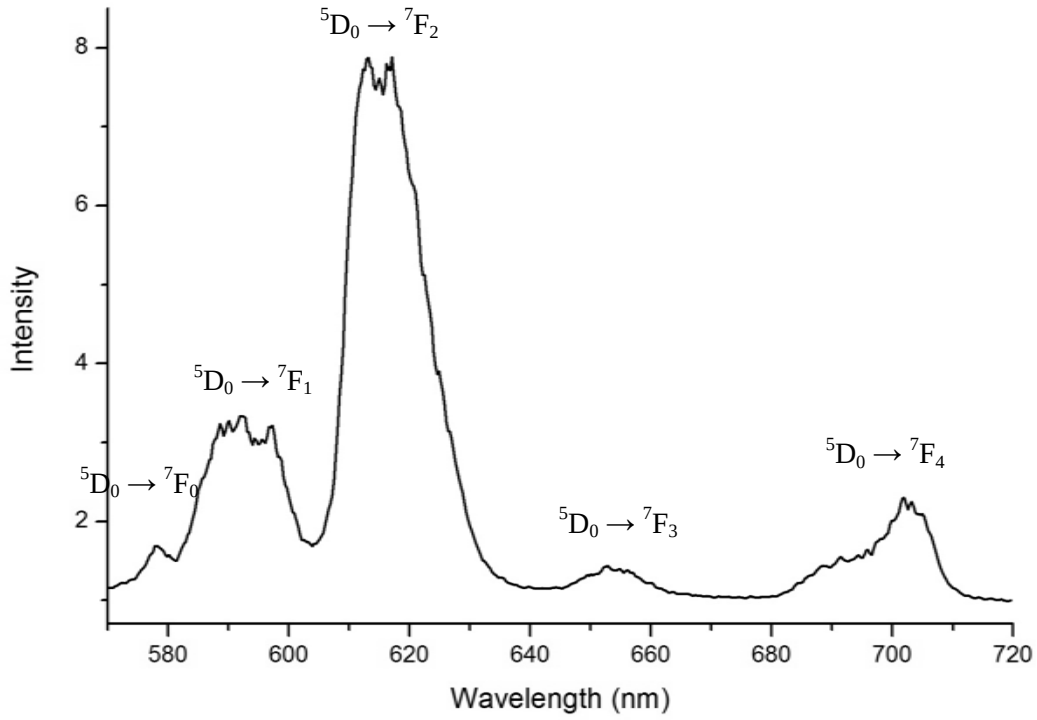

Fig. 3.5: Typical emission spectrum of Eu^{3+} ions in glassy environment (excitation in the $^5D_2$)

Not everything is as straightforward as it may seem, however, since the physical principle underlying these processes belongs to quantum mechanics; therefore, some complex selection rules exist, and not all the transitions between energy levels are permitted.

In particular, two types of transitions exist, depending on the peculiar quantum operator involved, and each one has its own set of rules:

- Dipolar electric (DE) transitions: of electric nature are the $^5D_0 \rightarrow {}^7F_0$, $^5D_0 \rightarrow {}^7F_2$ and $^5D_0 \rightarrow {}^7F_3$ transitions; here the rules are: $|\Delta J| \leq 6$ (and if at least one of the two levels has J = 0, then $|\Delta J|$ = 2 to 6); $\Delta S = 0$ and $\Delta L = \pm 1$. This latter rule goes by the name of Laporte's rule, and basically states that dipolar electric transitions can take place only between levels having different parity states (i.e. different kinds of symmetry in their orbitals' wavefunctions). Now, in the case of Eu^{3+} ions the transitions involve levels all deriving from 4f orbitals, so they would be parity forbidden; moreover, the excited levels have a total spin multiplicity of 5, while the ground manifold has 2S+1 = 7, therefore the transitions would be also spin forbidden. However, when Eu ions are contained in a crystalline host, the odd CF terms mix the 4f (odd parity) and 5d (even parity) wavefunctions (acquisition by 4f of partial 5d character), rendering these rules less strict, and the transitions become possible. On the other hand, when the site occupied by Eu has

no inversion center, the possibility of vibronic coupling (association of dipolar electric transitions with lattice vibrational modes breaking the symmetry/parity of one of the two states), leads to the observation of vibronic transitions.

- Dipolar magnetic (DM) transitions: $^5D_0 \rightarrow {}^7F_1$ and $^5D_0 \rightarrow {}^7F_4$ transitions are of magnetic nature, and therefore exhibit lower intensity and lower sensitivity to the CF; this time Laporte's rule states that the parity must not change in the transition, i.e. $\Delta L = 0$ (so Eu's 4f → 4f transitions are permitted); moreover, $\Delta S = 0$ and $\Delta J = 0,\pm1$ (but $0 \rightarrow 0$ forbidden).

For a more complete and in depth description of dipolar transitions, of selection rules and of their exceptions we invite the reader to refer to specialized textbooks like ref. [54].

3.6.3: Eu^{3+} ions as a luminescent structural probe

A lot of features contribute in making Eu^{3+} ions very suitable for the application as a luminescent structural probe; among them, we can cite:

- Distance between excited and ground states: the wide energy gap between the lowest excited state ($^5D_0$) and the highest level of the fundamental manifold ($^7F_6$) makes non radiative relaxation across the whole energy gap extremely unlikely to happen; therefore, the yield of radiative desexcitation is quite high.
- Recognizable spectra: since the lanthanides contraction effect shelters Eu 4f electrons from the external CF, different CFs (both in site symmetry and intensity) don't revolution too much the spectral emission features, so a typical emission fingerprint is always easily recognizable.
- Low but detectable CF sensitivity: even if what said above is true, nevertheless the crystalline field produces detectable effects on the spectra, so by enumerating the number of emission lines and evaluating their lambda shifts one can infer a lot of useful information on the point group symmetry of the site or sites occupied by Eu ions inside the host lattice. Moreover, it is straightforward to distinguish luminescent centers accommodated in amorphous networks from centers inside crystalline lattices, since in the former case emission spectra exhibit broad bands due to inhomogeneous broadening[8], while in the latter sharp peaks are to be expected.

[8] In an amorphous host there is no long range order, so Eu ions end up occupying a great variety of sites, with small but appreciable differences between each other (that's the reason behind the adjective "inhomogeneous"); this leads to minor differences in the emission features of each center, that convoluted one over the other, lead to the detection of broad bands instead of narrow well resolved peaks.

However, the main reason that explains the great success of Eu^{3+} as a structural probe, employed in a really wide range of research fields, lies in the fact that both its ground state, $^7F_0$, and its lowest emitting (that is excited) state, $^5D_0$, have total angular moment j = 0. This makes these two levels mono-degenerated (i.e. their total degeneracy (2J+1) is 1), and therefore the radiative transition between them has as detectable consequence the appearance of one single peak in the high energy part of the emission spectrum, at around 575 ÷ 580 nm.

Obviously, what we have just said is true if and only if there exists only one kind of site occupied by Eu ions; if on the contrary the host lattice has for example two different sites that accommodate our REE, in the two cases the CF experienced by the emitting centers would be a bit different, and therefore some differences in the Stark splittings of the various levels would arise; consequently, the $^5D_0 \rightarrow {}^7F_0$ (and *vice versa*) transitions for the two sites would take place with the emission (or absorption) of photons having slightly different lambdas, and therefore in the spectra we would detect two $0 \rightarrow 0$ peaks instead of one.

In practice, from a very simplified point of view we might say that the number of emission peaks we can detect in the $^5D_0 \rightarrow {}^7F_0$ region of the spectrum coincides with the number of inequivalent sites occupied by Eu^{3+} ions in the sample's lattice. However, this is practically true only when the excitation is unselective (for example when we excite in the UV range), that is when all the Eu ions, unregarding of the type of site occupied, are actually excited, and can thus emit at their characteristic wavelengths.

On the contrary, when we tune our light source to selectively excite Eu ions occupying just one of the sites, that is when the incident photons have energy exactly equal to the gap between ground and emitting states of one of the two "types" of Eu, then we are able to detect only the fluorescence signal arising from centers accommodated in said sites (and thus, among the other consequences, only one $0 \rightarrow 0$ peak can be observed).

This, in a nutshell, is the basic principle of site selective luminescence spectroscopy: selectively exciting just one set of centers to detect its specific emission spectral signature, or, alternatively, selectively observing one characteristic emission peak to acquire the specific excitation spectrum[9] of the site responsible for said emission.

[9] An *emission* spectrum is acquired by fixing the excitation wavelength and progressively scanning the detected lambda over the desired range of wavelengths (for the emission from the $^5D_0$ level the most commonly studied range is $570 \rightarrow 720$ nm); an *excitation* spectrum, on the contrary, is acquired by fixing the detection wavelength and varying the lambda of the incident exciting beam over the range $250 \rightarrow 550$ nm.

Once identified the luminescence features of the different sites, peak enumeration, peak integration and energetic calculations can yield a lot of interesting data on the crystal (or amorphous) structure of the analyzed material, like identification of the point group symmetry of the site occupied by REE ions, estimation of the degree of preferential site occupancy, etc.

3.6.4: Luminescence spectroscopy measurements

Luminescence measurements constitute the heart and soul of this thesis, since the innovative method we strived to develop for the detection of biologically induced precipitation of HCA crystals on bioactive glasses is based on site selective spectroscopy studies.

As we will describe in better detail in Chapter 4, we made the hypothesis that by doping with Eu^{3+} ions the starting bioactive glasses we could induce the precipitation of Eu doped HCA crystals; therefore, assuming that the sites occupied by the emitting centers in the two phases (amorphous glass and crystalline HCA) were considerably different in both site symmetry and CF intensity, we tried first to discover the correct wavelengths to be exploited to selectively excite one or the other, and then proceeded to the identification of the characteristic spectral signatures of Eu ions in glass and in HCA.

To do so, we carried out a series of luminescence measurements, acquiring a lot of emission and localized excitation spectra ($^7F_0 \rightarrow {}^5D_0$ transition range), as well as some global (300 → 550 nm) excitation spectra; some luminescence decay measurements were performed too.

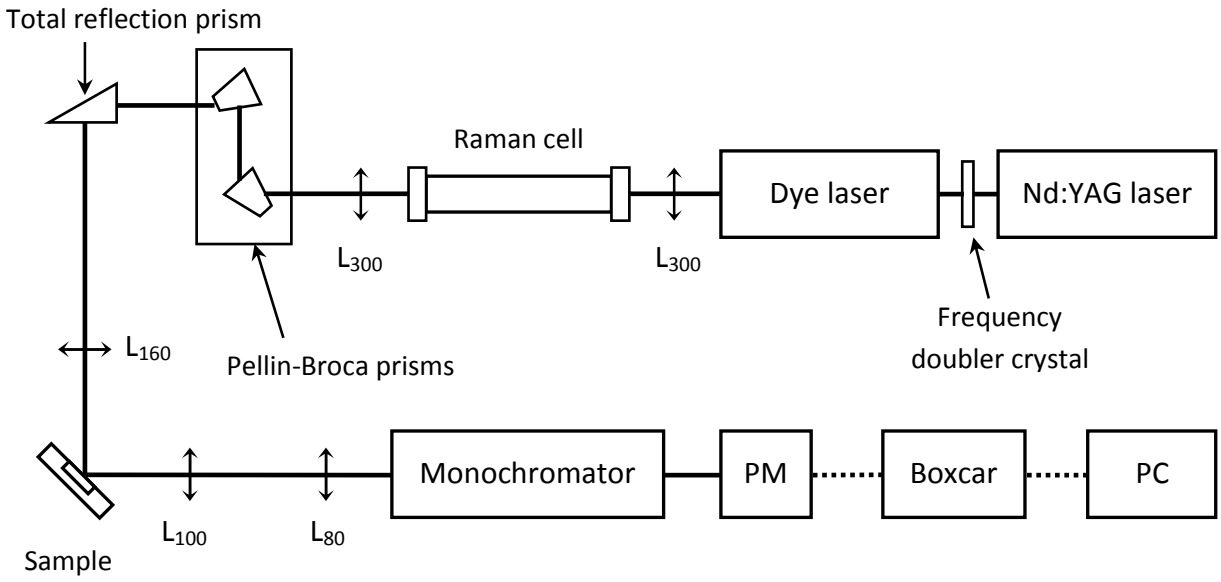

Fig. 3.6: Scheme of the optical set-up exploited for emission measurements

To acquire our emission spectra as well as our localized excitation spectra we used the optical set-up schematically reported in Fig. 3.6; the experimental parameters exploited for each measurement will be described in detail in Chapter 5, when we will expose the path we followed to develop our fluorescence based new characterization method for the study of biomineralization processes.

Some luminescence decay measurements were performed exploiting the same optical set-up of Fig. 3.6, but connecting a digital oscilloscope to the photomultiplier (PM) instead of a boxcar; the aim of these analyses was mainly to determine the characteristic decay lifetimes of Eu ions hosted in the different identified sites.

The few complete excitation spectra we were able to collect were acquired using a Xenon lamp as excitation source, coupled with a Jobin-Yvon Triax 550 and a Jobin-Yvon Triax 180 monochromators for the selection of the incident and detected wavelengths (2mm aperture size for both); the detection was assured by a CCD camera.

In all the luminescence measurements I was guided and taught by prof. Rachid Mahiou, director of the *Laboratoire des Materiaux Inorganiques* of the Blaise Pascal University of Clermont-Ferrand, to whom I address my most sincere and grateful thanks for all the help he gave me in learning from scratch what fluorescence is and how a site selective spectroscopy analysis is meant to be performed.

Part Two:

Experimental data

Chapter Four: Eu^{3+} doped bioactive glasses

In this chapter we will first present the reasons that have led us to the choice of undertaking this research activity, and all the literature data that gave us hints on how we could reach the desired results; then we will describe the experimental and logic path we have followed to pursue our aims; finally, we will provide information on the synthesized bioactive glasses: textural properties, structural characterizations, crystallization behaviors, etc.

4.1: An overview of the research

4.1.1: The issue: how to detect HCA crystallization on bioactive glasses

As already mentioned in the preceding chapters, one of the most important features of bioactive glasses is that, when they are left in contact with true or simulated biological fluids, they are capable of forming an interfacial layer of amorphous calcium phosphates (Ca-P), which crystallizes over time as hydroxyl-carbonate-apatite (HCA), a phase extremely similar to the mineral part of natural human bone; this leads to the recognition of the biomaterial as *self* by the organism, and thus to the avoidance of any *foreign body reaction* (chronic inflammation, immune defense system response, formation of a thick fibrotic capsule, etc).

Thanks to the formation of the HCA layer and to the controlled release of ionic species (like Si^{4+} solvated ions) stimulating bone regeneration, a bioactive implant is readily populated by osteoblasts and osteo-progenitor stem cells, and a very good and intimate degree of osteo-integration is attained in much less time than in the case of bioinert materials.

While the qualitative behavior of bioactive glasses has been extensively studied since the 70's, so that now our knowledge reaches a quite complete extent, much less has been written from the quantitative point of view on the dynamics and kinetics of the physico-chemical processes involved in the interaction with biological media.

This might partly be due to the lack of a really efficient characterization technique, capable of detecting and rigorously quantifying the precipitation of the apatite layer, especially at low interaction delays, when the absolute amount of HCA is negligible with respect to the total mass of the sample and the crystals are still of nanometric size, and not well crystallized.

To study the biomineralization processes, in the last decades many characterization techniques have been used, with different degrees of success and precision; in the following lines the principal methods and their features will be exposed:

- X-ray Diffraction (XRD): from a theoretical point of view, this should be the best technique to detect and quantify the exact composition of a crystalline sample. Comparing the acquired diffraction data with the JCPDS/ICDD reference database should permit a precise identification of the phases, while Rietveld refinement on the detected patterns should provide extremely accurate and complete quantitative information.
  From the practical point of view, however, in the case of bioactive glasses the low amount of formed crystalline phase with respect to the amorphous base glass and Ca-P layer, the tiny dimension of the crystallites and the high degree of defectivity of their lattices are all detrimental to obtaining good quality diffraction patterns; the data a conventional powder XRD analysis can acquire from post-interaction samples are often not much better than what is shown in Fig. 4.1 and 4.2:

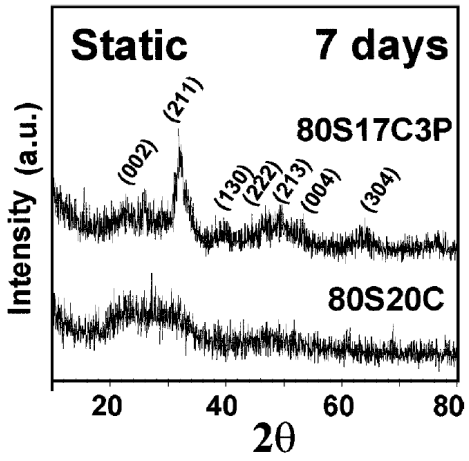

Fig. 4.1: Powder XRD patterns of two bioactive sol-gel derived glasses after 7 days of static immersion in SBF (from [2])

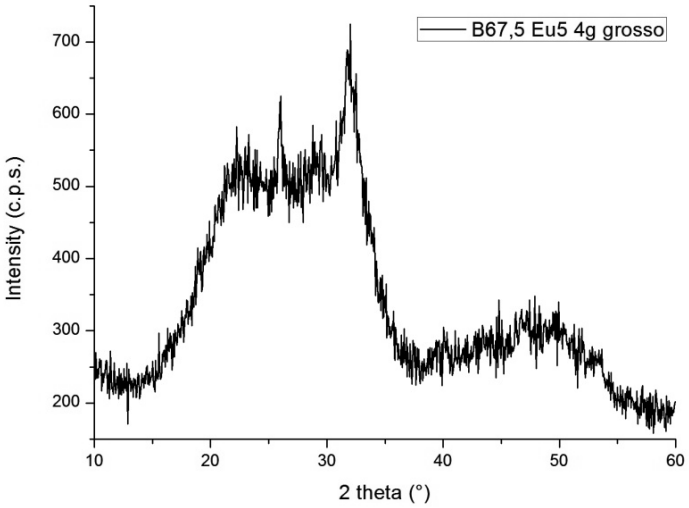

Fig. 4.2: Powder XRD pattern of one of our doped bioactive glasses after 4 days of immersion in DMEM (see Chap. 5)

Evidently, for such plots the application of Rietveld refinement is downright impossible, and even the identification of the crystalline phases is somewhat uncertain: if we didn't have complementary information from other characterization techniques, or we didn't exactly know what to expect, recognizing those broad, feeble and noisy peaks as HCA would be quite challenging.

Slightly better results can be obtained passing from a Bragg-Brentano (also known as "θ - 2θ") to a thin-films glancing angle XRD set up; this is the only sensible way to characterize glass monoliths after *in vitro* bioactivity testing (since the HCA layer is formed on the sole surface), but can yield interesting signal improvements also in the case of powdered samples, which, however, must be mounted on the sample holder exploiting some easy home-made tricks, such as covering with powder a double-sided tape stuck to a soda-lime glass slide or to a Si wafer piece. The typical diffraction patterns acquirable via thin films XRD in the case of post-interaction bioactive glasses are reported in Fig. 4.3 (monolith) and 4.4 (powders).

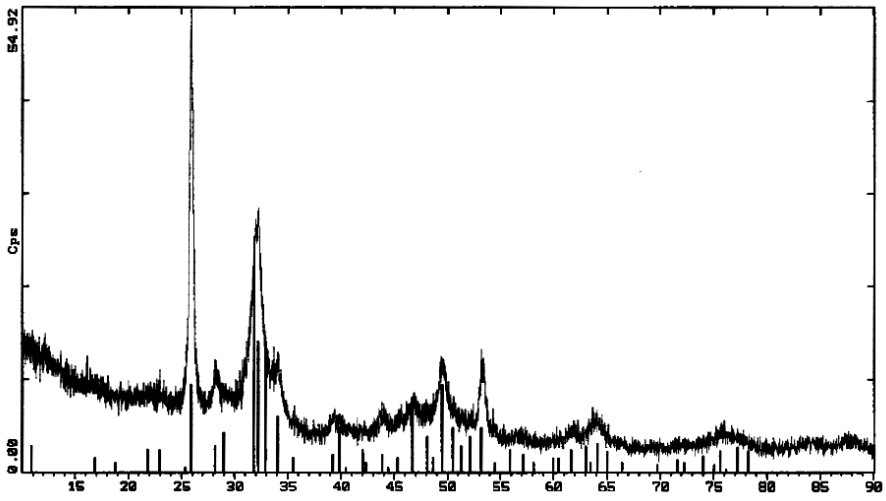

Fig. 4.3: TF-XRD pattern of the surface of a Bioglass® 45S5 monolith after 7 days in SBF (from [32])

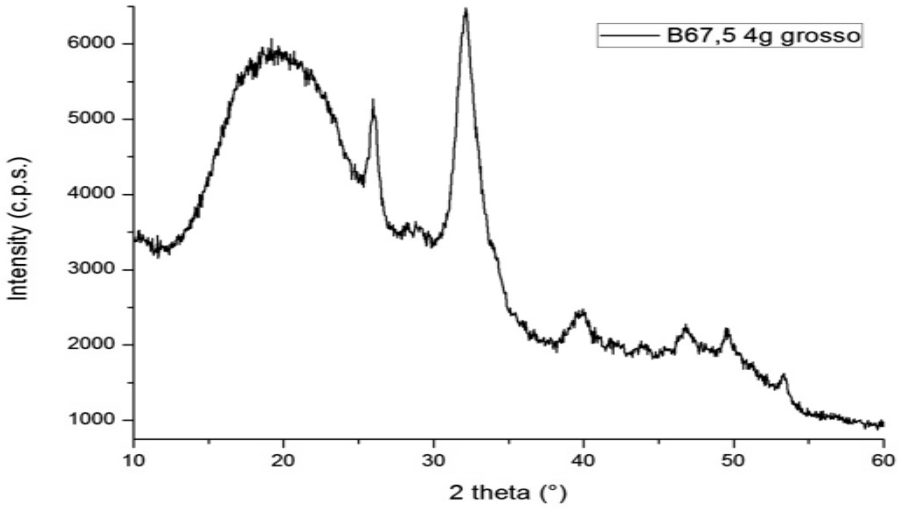

Fig. 4.4: TF-XRD pattern of our non-doped bioactive glass powder after 4 days in DMEM (see Chap. 5)

The absence of diffraction peaks, however, is not a sufficient condition to infer that no biomineralization has taken place: for example, in the case of M. Vallet-Regi's 80S20C

glass, FTIR spectra, SEM + EDX and TEM + electron diffraction all confirm (see ref. [2]) that tiny HCA crystals actually precipitated on the surface of the samples, even though the XRD data show a perfectly amorphous pattern (see Fig. 4.1).

In fact, according to LeGeros et al[1], apatite crystals must consist of more than 20 unit cells in order to return a detectable XRD signal, and must be much bigger if we desire a good quality diffractogram, with thin and well resolved peaks; taking into account the HA lattice parameters (a = 0.94 nm; c = 0.69 nm) and symmetry (hexagonal, $P6_3/m$), and observing that, at least in the beginning, it shows preferred growth along the c axis, giving rise to abnormally high (002) reflections at 26° (see ref. [2], [32], [37], [45]), a minimum detectable size for the nanocrystallites of HCA can be estimated around 15 nm.

- Fourier-Transformed InfraRed spectroscopy (FTIR): this is by far the most used technique for the characterization of pre- and post-interaction samples (see ref. [1], [2], [7], [9], [13], [22], etc), and both transmission and reflection (ATR) analyses are reported in literature. This method has the advantage of being very simple, fast and inexpensive and of requiring little to none sample preparation (in most cases, just compressing the powdered sample along with KBr in the shape of a disc). Unfortunately, it has a non-negligible drawback: while it is easy to make comparisons between groups of acquired spectra, extracting quantitative information from them is quite problematic, and the attainable accuracy is not satisfactory.

  The typical IR signature of a bioactive glass with an apatitic layer on its surface can be found on top (7 days) of Fig. 4.5, where the evolution of IR spectra with in vitro bioactivity testing time is depicted in the case of a binary ($80\%_{mol}$ SiO_2 ÷ $20\%_{mol}$ CaO) sol-gel derived glass (from ref. [2]).

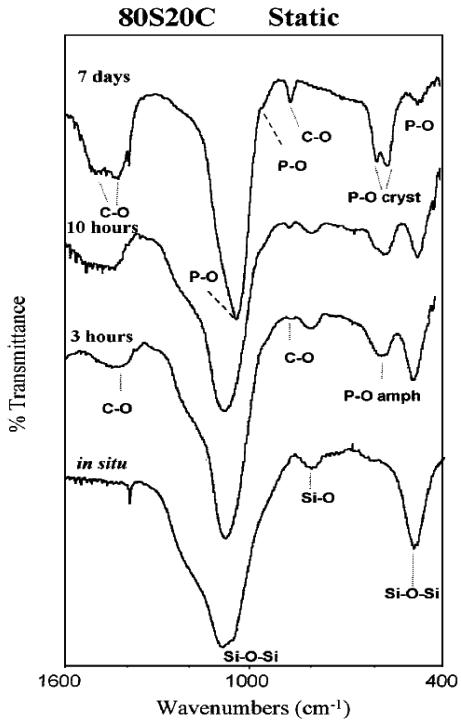

Fig. 4.5: Evolution of IR spectra of a bioactive glass during in vitro bioactivity testing, from [2]

The spectral feature used to identify HCA crystallization is principally the couple of peaks located at around 560 and 600 cm^{-1}, labeled "P-O cryst." in the picture. As we will see in the next chapter, those easily recognizable peaks, corresponding to P-O bonds resonating

[1] J.P. LeGeros, O.R. Trautz, and R.Z. LeGeros, in *Transations of the American Crystal. Association* (1965), p. 40

in an apatitic environment[2], become more and more intense with biological interaction time. Of great interest are also the C-O peaks, while the OH bands (not represented in Fig. 4.5, since they occur at higher wavenumbers) are less reliable.

- Raman and micro-Raman spectroscopy: complementary but, in practice, often competitive with FTIR, Raman effect exploiting spectroscopic techniques offer some interesting advantages over conventional IR structural/vibrational analyses: first of all, Raman active modes are different from IR active modes, and in this case P-O (in particular the symmetric vibration peak at 960 cm^{-1} of Raman shift) and C-O vibrations are highly enhanced over Si-O-Si bands; secondly, water molecules are almost completely incapable of giving inelastic diffusion, so *in situ* "real time" measurements are possible (see ref. [36]), that is bioglass samples can be directly analyzed while still immersed and interacting in biological simulated fluids.

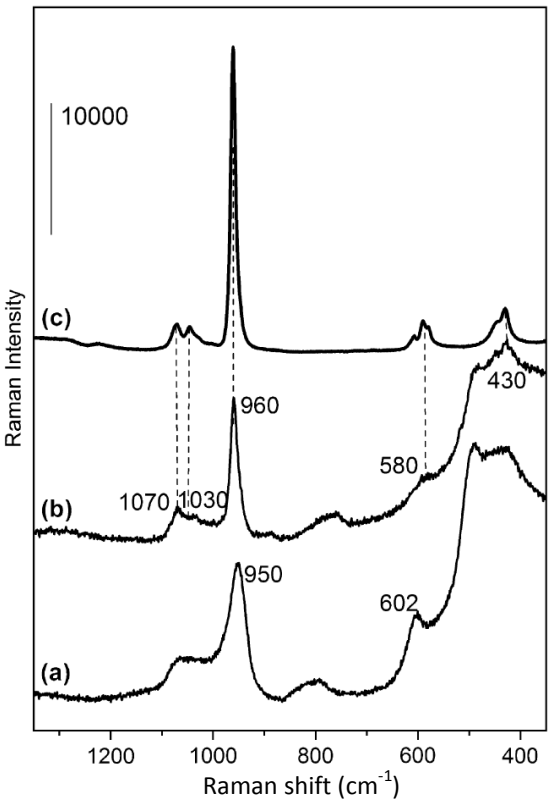

Fig. 4.6: Raman spectra of HA (c) and bioactive glass samples before (a), and after 7 days of interaction (b)

Moreover, if a Raman micro-spectrophotometer is used, it is possible to focalize the beam on the Ca-P surface layer, therefore further maximizing the phosphate signal over the silicate one. However, since literature data on the application of Raman spectroscopy to bioactive glasses is far less widespread than for FTIR analyses, the exact and definitive attribution of inelastic scattering peaks can sometimes be more difficult, e.g. for glasses quite different from those of published articles.

The typical spectral signature of a bioactive glass that has developed an HCA layer on its surface after interaction with a biological medium is reported in Fig. 4.6 (for a glass of nominal composition 77%$_{wt}$ SiO_2, 14%$_{wt}$ CaO and 9%$_{wt}$ P_2O_5; from ref. [36]); the most important, intense and recognizable features are the peaks at 960, 1070 and 1080 cm^{-1} of Raman shift, which are respectively

[2] Elliot J.C., *Structure and chemistry of the apatites and other calcium orthophosphates,* Vol. 18, Studies in inorganic chemistry, Amsterdam Elsevier 1994, p. 59.

associated to the symmetric apatitic P-O vibration, asymmetric apatitic P-O stretching, and carbonate C-O vibration.

As for FTIR spectroscopy, the principal drawback of this characterization technique is that quantitative reliable analyses are quite difficult to carry out.

- Scanning Electron Microscopy (SEM): this microscopy technique is extremely helpful in observing the morphology of the Ca-P amorphous or crystalline layer developed on the surface of bioactive glasses after exposure to biological fluids; basically, it allows us to directly "see" the HCA crystals growing on the samples (Fig. 4.7). However, at low interaction times, when HCA is still in the form of tiny nanocrystallites, the resolution of the most common instruments is not high enough to yield satisfactory results.

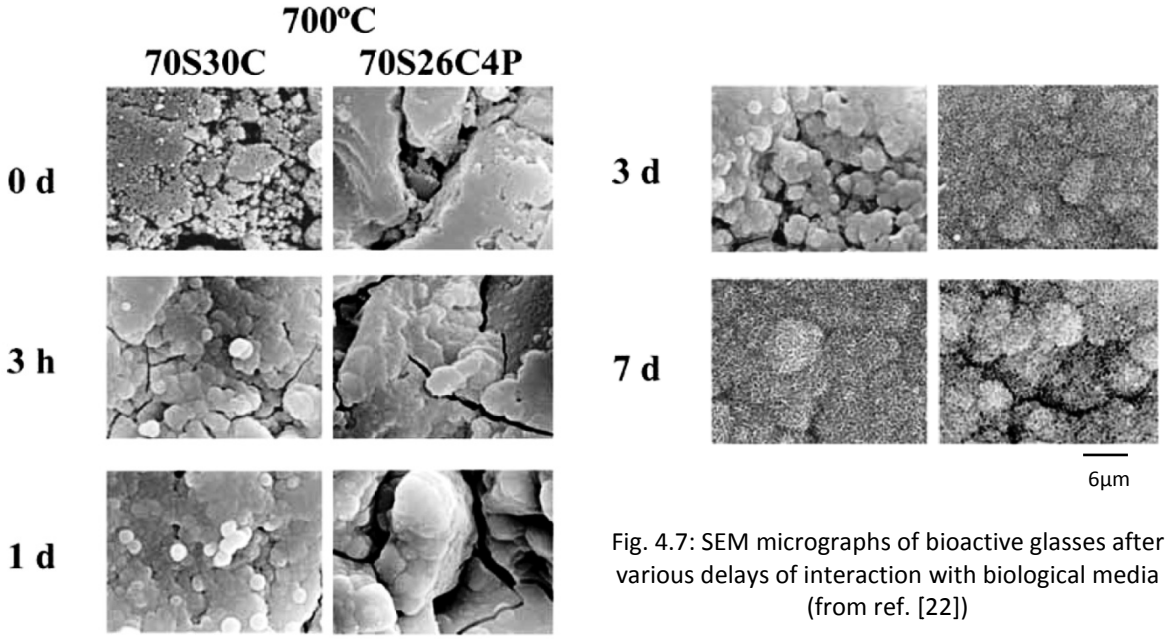

Fig. 4.7: SEM micrographs of bioactive glasses after various delays of interaction with biological media (from ref. [22])

Moreover, the Energy Dispersive X-ray probes (EDX), commonly coupled to SEM's for conducting chemical characterizations, provide insufficiently reliable compositional data, and, above all, cannot confirm if what appears on the screen is actually in a crystalline or amorphous form. This way, the recognition of HCA solely relies on the calculation of the Ca/P ratio of the analyzed spot, but since the determination of Ca and P content is not so accurate, deviations from the theoretical value of 1.667 are to be expected, even for reference or synthetic HA crystals.

Therefore, this method of characterization, though intuitive and simple (sample preparation is not so complicated or time consuming, especially if ESEM's are used),

cannot be considered the best choice for detecting and, especially, for quantifying the biomineralization of bioactive glasses.

- Transmission Electron Microscopy (TEM): with this technique the maximum attainable resolution is far better than with SEM, and direct observation of HCA nanocrystals as little as a few tens of nanometers is possible (see Fig. 4.8). Moreover, the possibility of carrying out electron diffraction (ED) analyses allows for the actual recognition of the crystalline structure of the sample, so it is really possible to determine if the observed crystal is HCA, or not.

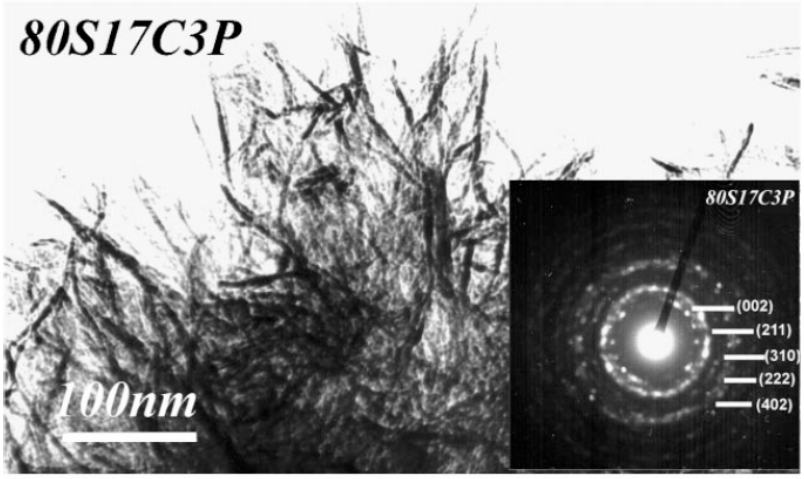

Fig. 4.8: TEM micrograph showing a particle scraped from a bioactive glass surface after 7 days of bioactive testing, made up of clustered needle-like HCA crystals of approximately 150nm length. Inset: ED pattern of the same particle (from ref. [2]).

Though extremely powerful, the couple TEM+ED is affected by some severe drawbacks: first of all, the complex and time-consuming procedures necessary to prepare the ultra-thin sections needed for the analysis, and the great expensiveness of the instrument.

Most of the discoveries made in the bioactive materials field have exploited these characterization techniques, and much has been said and written on the subject in fifty years; however, in order to push further and deeper our knowledge on biomineralization processes, a new tool, capable of providing quantitative as well as qualitative information, even at low interaction times (the first dozens of hours), might be extremely useful. And who knows what new technological improvements shedding some new light on these phenomena could bring?

4.1.2: The clues suggesting a possible new solution

As already said in the previous chapter, thanks to their easily recognizable spectral signatures and to their high sensitivity to the symmetry and intensity of the crystalline field acting on the site they occupy, Europium trivalent ions have been extensively used as a luminescent structural probe to study a great variety of crystalline and amorphous materials, belonging to the most disparate research fields: bioresorbable materials for drug delivery such as mesostructured HA (ref. [24]), fluorescent dyes for cell staining like doped TCP nanocrystals (ref. [5]), phosphors as $LuPO_4$ and YPO_4 (ref. [46]), scintillating crystals like Lu_2SiO_5 (ref. [47]), etc.

The information obtained through site selective spectroscopy luminescence analyses on those samples has allowed, for example, to deepen the knowledge on the existence of different lattice sites occupied by ions, to deduct their point group symmetry and to estimate their degree of preferential occupancy.

Moreover, doping amorphous materials with little amounts of Eu^{3+} can allow for the discovery of nanometric size crystals developed inside the glassy matrix upon heat treatment, undetectable by X-ray diffraction because of their tiny dimensions (see ref. [20]). This is made possible since rare earth ions in crystalline environments give rise to characteristic emission spectra with narrow, well resolved peaks, while when hosted inside amorphous, highly disordered networks, they produce emission spectra with broad, sometimes overlapping bands (see Par. 4.3.7).

In particular, selective excitation of Eu^{3+} ions in the two different kind of environments is possible since therein the luminescent centers experience different crystalline fields (both in intensity and symmetry), and thus their emitting level energy scheme results quite different; therefore, site selective emission spectra yield radically different information, not only from the point of view of shape and position (λ) of peaks, but also from the point of view of luminescence decay lifetimes (see ref. [4]).

Only a few articles (ref. [4] and [20]) on the successful doping with Eu^{3+} ions of bioactive glasses (belonging to the ternary system $SiO_2{-}CaO{-}P_2O_5$) are reported in literature; for the synthesis, an alcoholic solution sol-gel route has been exploited[3]: Silicon and Phosphorus

[3] However, this path is no more than a slight modification of Saravanapavan and Hench's sol-gel protocol for the synthesis of binary $SiO_2{-}CaO$ bioactive glasses; see ref. [12], [40] and [41], and Par. 4.2.1.

precursors are in the form of alcoxides, respectively TEOS (Tetra-Ethyl-Ortho-Silicate, $Si-(O-C_2H_5)_4$), and TEP (Tri-Ethyl-Phosphate, $O=P-(O-C_2H_5)_3$), while Calcium and Europium precursors are hydrated nitrates, $Ca(NO_3)_2 \cdot 4H_2O$ and $Eu(NO_3)_3 \cdot 6H_2O$. After proper synthesis, gelation and heat treatment procedures, the resulting glasses are generally homogeneous and transparent, and their emission spectra upon excitation at 394nm (in the ^5L_j manifold, which relaxes non radiatively to the ^5D_j levels) bear the typical signature of Eu^{3+} ions occupying amorphous sites, i.e. high inhomogeneous broadening of the peaks, with strong overlapping of the various components of each transition (see Fig. 4.9).

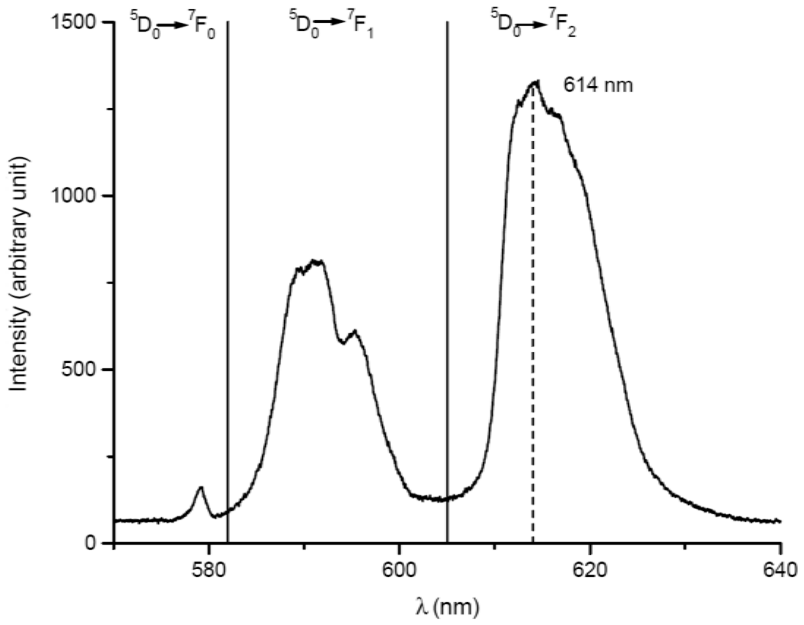

Fig. 4.9: Emission spectrum (λ_{exc} = 394nm) of a 75%$_{mol}$ SiO_2 – 19% CaO – 6% P_2O_5 bioactive glass doped with Eu in such a way that the ratio Eu/Ca+Eu = 0.5% (from ref. [20])

Eu^{3+} ions have also been diffusedly used to study the structure of Hydroxylapatite crystals through site selective luminescence spectroscopy: Eu doped HA have been synthesized both at high (950°C in the case of ref. [11], 650°C for ref. [30]) and low (37 to 100°C in ref. [28]) temperatures exploiting sol-gel techniques, and both the "pure" coprecipitation and the "mixed" alcoxides-nitrates routes have been successfully explored.

Inside the crystalline lattice the rare earth cations place themselves in sites normally occupied by Ca^{2+} ions (see ref. [11], [24], [25], [28], [30]); this substitution is possible and relatively favored[4] since the two ionic radii are not much dissimilar, approximately 1 Å for

[4] Drouet, Rey *et a*l in ref. [28] report that the Eu/(Ca+Eu) ratios experimentally determined for their synthesized crystals are very close to the theoretic values, meaning that almost all the Eu ions present in their precursor solutions have been preferentially incorporated over Ca in the HA lattice.

Ca^{2+} and 0,95 Å for Eu^{3+} (both in the same conditions of coordination; see ref. [28] and [55]), but obviously requires some form of compensation for the difference in net electric charges.

Various charge compensation mechanisms have been proposed for both natural and synthetic HA; adopting the same symbolic notation of [28] (where a square represents an ionic vacancy, and M_{Ca}^{+} stays for a monovalent cation occupying a Ca site), they are:

$$(1) \quad Ca^{2+} + HPO_4^{2-} \longrightarrow Eu^{3+} + PO_4^{3-}$$

$$(2) \quad Ca^{2+} + \boxdot_{OH} \longrightarrow Eu^{3+} + OH^{-}$$

$$(3) \quad 2Ca^{2+} \longrightarrow Eu^{3+} + M_{Ca}^{+}$$

$$(4) \quad Ca^{2+} + OH^{-} \longrightarrow Eu^{3+} + O^{2-}$$

$$(5) \quad 3Ca^{2+} \longrightarrow 2Eu^{3+} + \boxdot_{Ca}$$

While mechanism (3) needs the presence of monovalent cations such as alkali metals ions or NH_4^{+} groups, and therefore it is possible only for natural apatites and for certain synthesis protocols, the others are all theoretically plausible; however, experimental evidences tend to validate mechanisms (4) and (5) above the others.

In particular, equation (5) states that increasing dopant concentrations lead to an increase in the defectivity of the lattice, and this is confirmed both by XRD analyses, since higher Eu% gives rise to less resolved diffraction peaks[5], and by chemical titrations, since the (Ca+Eu)/P ratio decreases slightly with Eu concentration (see ref. [28]).

On the other hand, equation (4) is consistent with the high substitution yield of Eu over Ca (see note 4), which might be due to the higher stability of the $Eu^{3+}-O^{2-}$ bond with respect to the $Ca^{2+}-OH^{-}$ bond, ascribable to its higher degree of covalence. Moreover, this mechanism is also consistent with the site selective luminescence spectroscopy studies reported by Ternane (ref. [11]) and Long (ref. [30]).

In particular, non-selective excitation (λ_{exc}= 254nm at 20K) of Ternane's Eu doped HA crystals, synthesized at high temperature (950°C), yields the following spectrum (Fig. 4.10):

[5] However, the inferior degree of crystallization detected in the case of highly doped HA may also be due to an hindering or inhibiting effect of Eu^{3+} ions, which are more likely to stabilize the non-yet-apatitic surface layer of the growing crystals over their well-apatitic core (see ref. [28]).

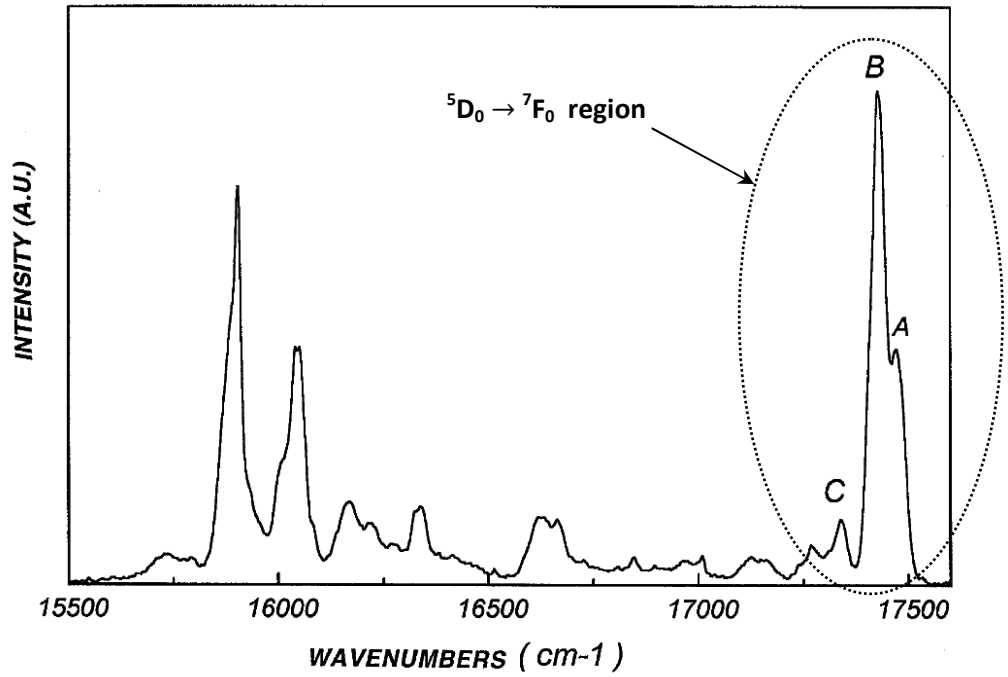

Fig. 4.10: Emission spectrum of Ternane's Eu doped HA upon excitation at 254nm (from ref. [11])

The most evident spectral feature is the presence of three quite well resolved peaks in the $^5D_0 \rightarrow {}^7F_0$ region (see ellipse above); since, as previously said in Chap. 3, this dipolar electric transition takes place between non degenerated energy states, detecting three emission peaks at three different wavenumbers implies that three inequivalent emitting sites exist in the lattice. In HA, however, Eu substitutes for Ca, and only two different Ca sites are present (see ref. [11], [26], [30]), so it is sensible to state that A and B peaks, which are only slightly shifted from each other, are connected to the same site, but with different "neighbors" in the second coordination shell (see ref. [11]).

The two Ca sites in HA are usually labeled Ca(I) and Ca(II), and can be described as follows:

- **Ca(I)**: occupies the 4(f) position on the ternary axes, is coordinated by 9 oxygen atoms and has a C_3 point group symmetry;
- **Ca(II)**: occupies the 6(h) position, is coordinated by 6 oxygen atoms and by 1 hydroxyl (sevenfold total coordination) and has a C_s symmetry (even lower than C_3); moreover, 6 Ca(II) ions describe a six-pointed star shape on a plane perpendicular to the 6_3 screw axis, in the center of which lies an OH^- group (or the other ions substituting for it, like Cl^- for chloroapatites and F^- for fluoroapatites).

A scheme representing the projection on the base plane (001) of the HA unit cell is reported in Fig. 4.11; inside the broken line circle we highlighted the star-shaped "channel" of Ca(II) ions encircling the OH group.

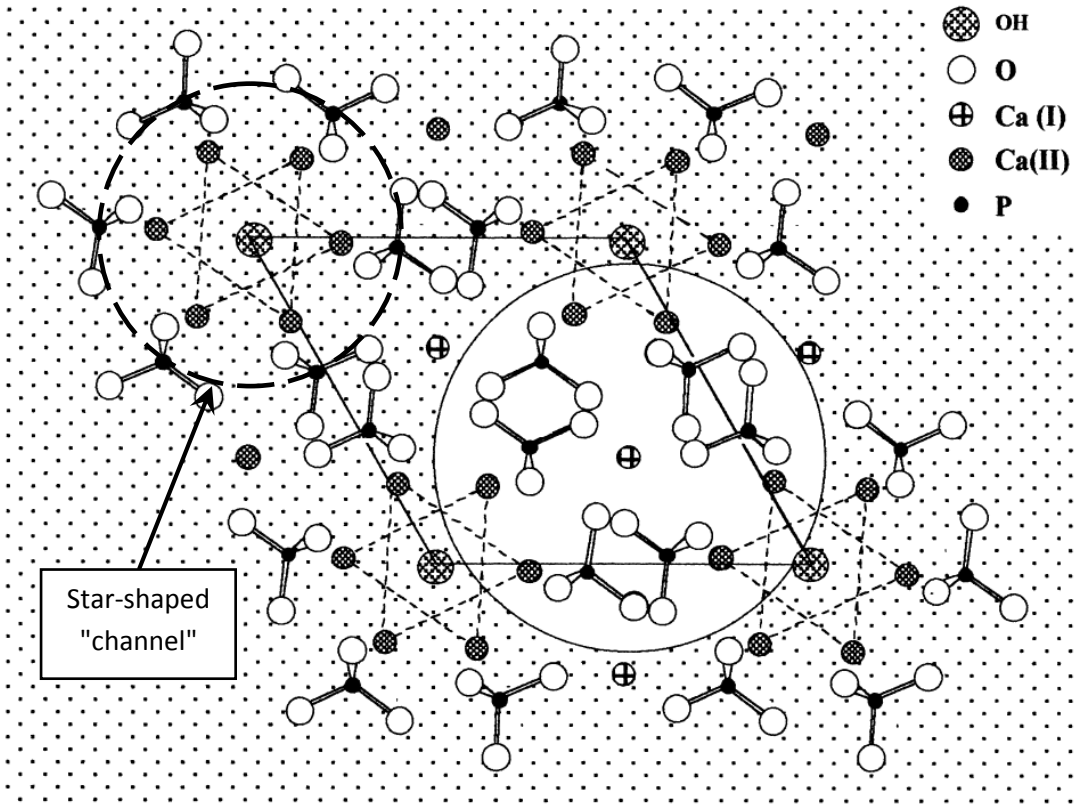

Fig. 4.11: Schematic projection of the HA unit cell on the base plane (from ref. [26])

When Eu occupies a Ca(II) site, the most plausible charge compensation mechanism is $Ca^{2+} + OH^{-} \longrightarrow Eu^{3+} + O^{2-}$, due to the high proximity with the OH^{-}; but the chemical bond between Eu^{3+} and O^{2-} is so much more covalent and strong than the one between Ca^{2+} and OH^{-}, that the site symmetry changes from C_s to a pseudo $C_{\infty v}$ (see ref. [30]). Since for this latter symmetry the $^5D_0 \rightarrow {}^7F_0$ transition is permitted by the selection rules, the resulting emission intensity is very big, so it is possible to ascribe the A and B abnormally high peaks to Eu^{3+} ions occupying Ca(II) sites (see ref. [11]).

On the contrary, when Eu occupies the Ca(I) site, the charge compensation mechanism number (4) becomes no longer possible, due to the increased distance from the OH^{-}, and thus no covalent Eu−O bond is formed; therefore, no deformation of the site symmetry takes place, and so the related emission intensity stays as low as usual for a prohibited $^5D_0 \rightarrow {}^7F_0$

transition. All of this said, it's only logical to ascribe the C emission peak of Fig. 4.10 to Eu ions occupying Ca(I) sites (see ref. [11]).

Since the aforementioned Eu−O pseudo-covalent bond is very stable, preferential occupancy of Ca(II) sites over Ca(I) sites is reported (ref. [11]), but much can change with synthesis protocol, firing temperature, crystallite size, etc. (see ref. [28] and [30]); moreover, the stability of that bond makes the A and B emission decay lifetimes much shorter than C's: respectively 436 and 438 µs against 848 µs (see Fig. 4.12 and ref. [11]).

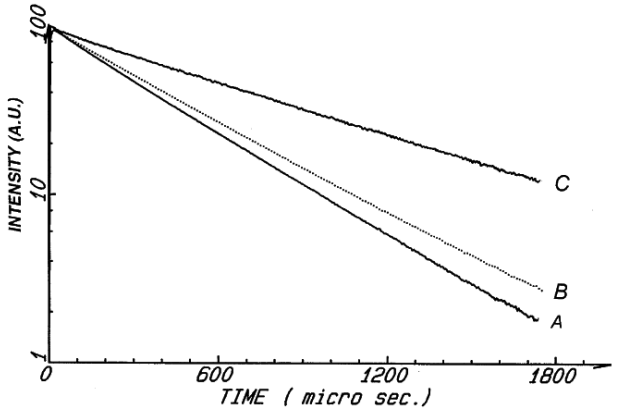

Fig. 4.12: Luminescence decay plots of Eu:HA; excitation and detection are both site selective (see ref. [11])

Last but not least, there is published evidence (see ref. [29]) that free Eu^{3+} ions in aqueous solution are not only readily and preferentially adsorbed on the surface of apatitic crystals, but can also penetrate to some depth inside the crystal lattice, obviously substituting for Ca^{2+} ions.

4.1.3: The research strategy

Gathering together all the information reported in the preceding paragraphs, a possible solution to the problem of detecting and (maybe) quantifying the biomineralization of bioactive glasses comes forth: doping the glasses with Eu^{3+} ions in order to carry out site selective luminescence spectroscopy analyses on the post-interaction samples.

In fact, we have seen that Eu doped glasses show a typical amorphous broad band emission, while Eu doped Hydroxylapatite bears an highly distinctive spectral signature, with sharp peaks and uncommonly intense $^5D_0 \rightarrow {}^7F_0$ transitions; we've also learned that doped HA can be synthesized at temperatures as low as 37°C, and we know that when bioactive glasses are immersed in biological simulated fluids at 37°C, an HCA layer precipitates on their surfaces.

Therefore it is plausible that Eu doped bioactive glasses develop a layer of Eu doped HCA on their surfaces upon immersion in biological media, thus allowing the detection of the biomimetic crystals *via* site selective spectroscopy measurements.

If that is true, by carrying out opportune luminescence analyses on bioactivity tested samples it should be possible to either excite Eu ions in the glass phase and/or Eu ions in the

crystallized layer, and thus to detect their two different spectral signatures, that is broad emission bands and/or thin peaks, maybe overlapped, most probably with different luminescence decay lifetimes. Moreover, since we have seen that Eu ions are extremely sensitive to their surrounding crystalline environment, the doped HCA luminescent "fingerprint" should be detectable even at low interaction time, when the precipitating crystals are still of nanometric size (see ref. [20]) and therefore invisible to most of the other characterization techniques.

The path we chose to verify if the underscored hypothesis was correct, and thus to determine whether the use of Eu^{3+} ions as a luminescent structural probe is an effective asset in detecting bioactive glasses' biomineralization or not, was, in a nutshell, the following:

1) Individuate a "base" glass of well documented bioactivity;
2) Dope it with various amounts of Eu following a synthesis protocol of documented effectiveness, granting a good degree of homogeneity to the final materials;
3) Thoroughly characterize the structural, textural and luminescence properties of the thus obtained products, in order to better understand the effects of the dopant on the glass network and on his hydrolytic and crystallization behavior;
4) Carry out *in vitro* bioactivity tests on the synthesized glass powders following a standardized procedure, possibly reported in literature;
5) Analyze the post-interaction samples from the structural and spectroscopic points of view, searching for evidences of HCA crystallization through "traditional" (i.e. FTIR, micro-Raman, XRD and SEM+EDX; plus ICP-AES on post-interaction fluids) as well as "unconventional" (i.e. site selective spectroscopy) techniques;
6) Compare the obtained results to determine whether the information provided by our "new" technique is consistent with other "classic" experimental and theoretical data.

Of course, even if the luminescent probe proved itself an effective characterization tool for studying biomineralization processes, that is if it was capable of detecting HCA crystallization better than the other present analytic techniques, it would need nevertheless to be carefully validated; in fact, it is absolutely necessary to verify that the doping process does not significantly alter the base glass behavior, at least for what concerns the aspects involved in bioactivity dynamics and kinetics, since a probe altering its target's properties is completely unreliable and therefore useless.

From this latter point of view, we must take into account many aspects, most of which are related to the obvious differences existing between Ca and Eu ions, and design appropriate ways to discover if those differences yield invalidating effects:

- The net charge of Eu is 3+, while the charge of Ca is 2+, but their ionic radii are quite similar[6], therefore the electric field surrounding Eu^{3+} ions is slightly more intense than the one existing around Ca^{2+} ions. This might potentially alter the bioactive behavior of the glasses in a few ways:
  - Eu might be more difficult to leach from the network than Ca during the initial ionic exchange step (see. Chap. 1), leading to possible delays in the attainment of the supersaturation critical level for the precipitation of doped HCA;
  - due to its higher field strength, Eu might be less effective in modifying the glass network, thus increasing the hydrolytic resistance and plausibly reducing or slowing down the release of soluble Si^{4+} ions (which is crucial because they stimulate bone regeneration, see Chap. 1);

  Moreover, again due to its relatively high field strength, Eu might behave like Al^{3+} [7], i.e. it might act as a network modifier at low concentrations and as a network former at high concentrations.

  To verify whether these modifications took place or not, and if Eu behavior was "linear" or "aluminium-like", we synthesized and tested various bioactive glasses with different dopant concentrations, so that from ICP-AES analyses on interaction fluids it has been possible to notice if some trend in leachability and ionic release actually existed.

- As it's reported for one particular synthesis protocol (ref. [28]), even in our experimental conditions Eu might slightly hinder or even inhibit (at high percentages) the formation of HCA crystals, both upon heating and during in vitro testing. If this effect was never negligible, not even at the lowest degree of doping, it would be extremely detrimental to the purpose of this research, since this would mean that our luminescent probe alters significantly the very same biomineralization processes it was designed to study, and thus is completely useless.

[6] Respectively 0.95 and 1 Å according to [30]; 1.09 and 1.14 Å according to www.chemicool.com.

[7] Al, however, has approximately half the ionic radius of Eu: $r_{Al^{3+}} \approx 0.54\,\AA$, so its Field Strength $\propto {}^{Z}/_{{r_{ion}}^{2}}$ is way higher than Eu's.

To discover if that's the case, both the as synthesized glasses and the post-interaction samples have been thoroughly characterized not only through site selective luminescence spectroscopy, but also with more "conventional" techniques, in order to confirm the actual precipitation of HCA crystals and determine their quantitative variations.

- The almost physiologic conditions of *in vitro* bioactivity tests are slightly different from those reported in literature for the syntheses of Eu doped HA: for sure we are very far from the 650°C of Long (ref. [30]) or the 950°C of Ternane (ref. [11]), but even if compared with the 37 ÷ 100°C of Drouet and Rey (ref. [28]), the chemical species in solution are very different (see Chap. 5), and even some organic components like vitamins and amino acids are present.

  This way, even if it did not inhibit or alter the biomineralization processes, Eu might still not be able to enter our HCA lattice[8], thus remaining in the amorphous calcium phosphates (Ca-P) layer, within the glass network or in solution.

  To understand where Eu actually went during bioactivity testing, the information provided from luminescence, FTIR, micro-Raman, XRD and ICP-AES analyses has been cross-referenced; we can tell since now that the appearance of narrow peaks in the right positions of the emission spectra, the confirmation of HCA precipitation by FTIR, Raman and XRD data, and the absence of Eu^{3+} ions from interaction media testified by ICP-AES, altogether confirm the actual formation of Eu doped HCA on the surface of our samples[9].

Last but not least, before continuing on to the detailed description of the experimental part of the research activity, some words need to be spent on our rare earth element itself.

Surely Eu is not a natural component of the human body, and, though being referred to as only lightly toxic in many articles (see ref. [28] and [5]), with a LD50 PO[10] of 5000 mg/kg for rats in the case of $Eu(NO_3)$, nevertheless at high concentrations it might have cytotoxic or metabolic alteration effects on cells. This, however, is not a "real" problem from our point of view, since our doped glasses are not meant to be implanted in human patients, but are just a research tool to shed some new light on the interaction behavior of bioactive materials in

[8] However, the high substitution yield of Eu over Ca (see ref. [28]), due to the great stability of Eu-O bonds, should grant the feasibility of the Eu doped HCA precipitation even in our case.

[9] Obviously, a considerable amount of Eu remains also inside the glassy core of the grains of bioactive powder, especially in the biggest ones.

[10] LD50 PO means "lethal dose 50 per oral route", and it's the orally absorbed amount of substance needed to cause the death of the 50% of an animal testing population.

contact with biological fluids. The only actual drawback of cytotoxicity would be the impossibility to exploit the luminescent structural probe also in the second step of *in vitro* testing protocol (interaction with simulated body fluids being the first one), i.e. for cellular adhesion essays and cell culture tests on samples.

Concluding, Eu is unfortunately a highly expensive material: 10g of quality europium nitrate, $Eu(NO_3)_3 \cdot 6H_2O$ at 99.99%[11] purity, may cost even more than 600 €, and in order to have enough material to carry out the necessary analyses, 500mg of it are averagely needed for each synthesis. Even with proper research funding, the use of such a costly material can be questionable, and, in order to be justified, it requires the obtainable results to be of great quality and innovation; as we will show in the following chapters, at the moment such results have not yet been reached, but the technique is very promising.

4.2: The synthesized bioactive glasses

4.2.1: The bioactive base glass: B67,5

In order to follow in the path laid by other researchers of the team, as starting bioactive material we chose a sol-gel derived ternary glass belonging to the SiO_2-CaO-P_2O_5 system named **B67,5** (where B stays for bioactive and 67,5 is the weight % of SiO_2), whose composition is reported in Tab. 4.1; the data are shown as percentages of oxides, in agreement with the glassmaking tradition:

Role	Oxide	Weight %	Molar %
Network former	SiO_2	67,5	69,3
Network modifier	CaO	25,0	27,4
Network former	P_2O_5	7,5	3,3

Tab. 4.1: Nominal composition of the B67,5 base glass

Though our choice was forced by the will of preserving the expertise, knowledge and experimental data gathered through years of work on bioactive glasses by the LMI research team, the decision was not merely arbitrary: the B67,5 not only has proven to be bioactive in

[11] The high purity is very important, since rare earth elements are quite difficult to separate from each other, and any RE contamination might lead to undesired spectral features and luminescence artifacts.

earlier studies of the group[12], but is also practically identical to Maria Vallet-Regi's 70S26C4P and 68S glasses, whose pronounced bioactivity properties are reported in several published articles (see for example ref. [22] and [9]), and is very close too to almost every sol-gel derived glass studied by her team (see ref. [1], [2], [7], [37]).

Moreover, many published evidences sum up to indicate our B67,5 as an excellent choice of bioactive glass to start from:

- Being synthesized via the sol-gel method, it's far more bioactive than a melt derived glass of the same composition, because it has a way higher specific surface area and an optimal interplay between pore size and pore volume, which result in a great boost in biomineralization kinetics[13];
- The presence of 7,5%$_{wt}$ P_2O_5 in the composition, though slowing down the initial release of Ca ions and the growth of the amorphous Ca-P interfacial layer, improves the precipitation rate of HCA, whose crystallites grow faster and bigger than in P_2O_5 free glasses (see ref. [7], [22], [37], [49]).

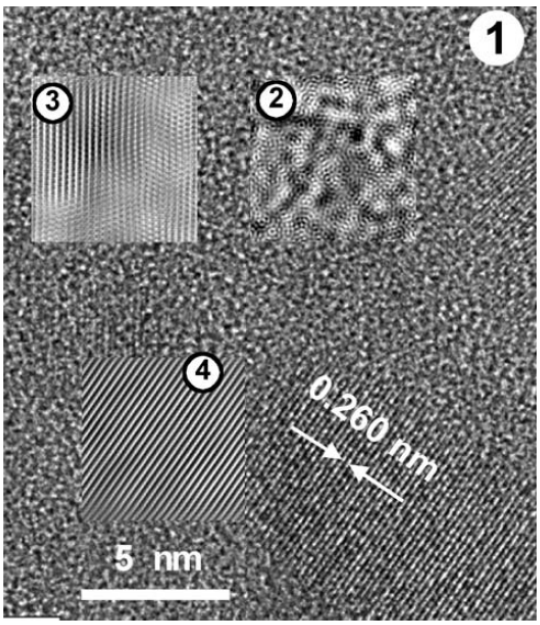

Fig. 4.13: 1) Raw and 2) filtered HR-TEM images of a bioactive glass sample close to our composition; 3) and 4) are filtered details of Ca and P-rich nanometric size crystalline domains inside the amorphous matrix

[12] In particular, Jonathan Lao in his PhD thesis has demonstrated through PIXE-RBS microprobe analyses that after less than 4 days of interaction with biological fluids B67,5 is capable to grow on its surfaces a layer of calcium phosphates whose Ca/P ratio is equal to 1.71, very close to the HA stoichiometric value of 1.67.

[13] For more information on this topic, see:

Li R, Clark AE, Hench LL, *An investigation of bioactive glass powders by sol-gel processing*, J Appl Biomater, 1991;

Vallet-Regi M, Ragel CV, Salinas AJ, *Glasses with medical applications*, Eur J Inorg Chem 2003.

This effect is highly positive for the biomineralization processes, and is due to the fact that upon calcination of the glass, nanometric size crystalline clusters of silicon-doped calcium phosphates precipitate within the glassy matrix, as visible in the HR-TEM image reported in the previous page (Fig. 4.13, from ref. [7]). Depending on the composition and on the calcination temperature, those ordered domains can attain different sizes, and eventually evolve into XRD detectable apatitic crystals if the calcination T is sufficiently high (see ref. [22], lower part of Fig. 4.14 and Par. 4.2.3).

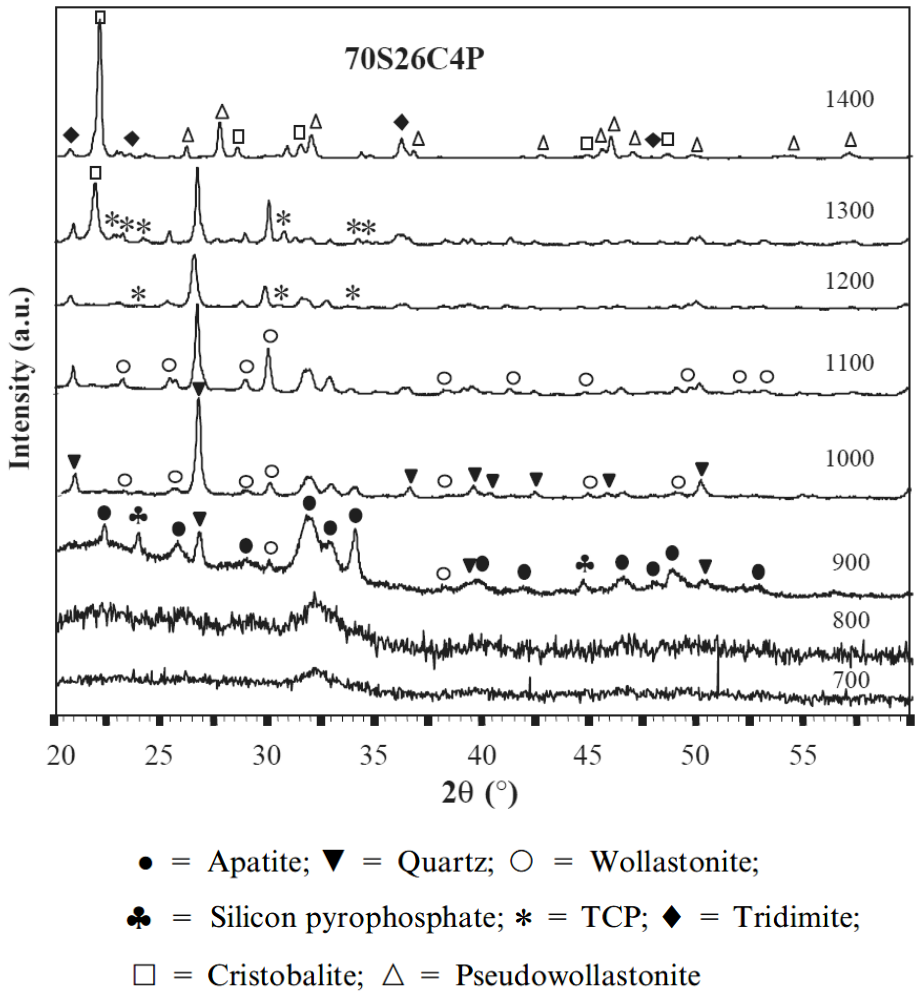

Fig. 4.14: XRD patterns of the aforementioned 70S26C4P bioactive glass, practically identical to our B67,5, calcined at different temperatures (from [22]).

When the bioactive glass is immersed in biological fluids, these nano-clusters provide preferential nucleation sites for HCA precipitation, or better, they are themselves nuclei ready for crystal growth, and thus facilitate and enhance the biomineralization processes.

- Moreover, the presence of P inside the glass network is very helpful for the synthesis of Eu doped glasses, because it aids in preventing RE clusterization (see ref. [21]), and thus

in avoiding problems like concentration self quenching of luminescence (see also Par. 4.3.7); in this, its effect is equivalent to the one of Al^{3+} (see ref. [4]), but while Al is highly detrimental to bioactivity properties (concentrations as low as $3\%_{mol}$ can inhibit the formation of the HCA layer; see ref. [2]), P has an exactly opposite, beneficial effect.

The only relative drawback of this glass is that, containing P_2O_5, the onset of the formation of the Ca-P amorphous layer cannot be easily detected via FTIR or Raman spectroscopy, since it might be masked by the presence of P-O bonds in the glass network.

4.2.2: The series of Eu^{3+} doped bioactive glasses

In order to understand the textural and structural effects brought about by Eu doping, we synthesized various bioactive glasses with different Eu contents; this result was achieved following the research team's usual doping *modus operandi* (see ref. [23] and [49]): starting from the B67,5's "original" composition, we substituted increasing weight percentages ($\%_{wt}$) of CaO with analogous $\%_{wt}$ of Eu_2O_3, leaving unchanged the $\%_{wt}$ of SiO_2 and P_2O_5.

Since their silica content is always equal to $67,5\%_{wt}$, all the synthesized glasses (except for one case, which will be discussed in detail at the end of this paragraph) can be correctly referred to as "doped B67,5 glasses"; in particular, in the following pages we will name them **B67,5 EuX**, where X is the $\%_{wt}$ of CaO that has been substituted by Eu_2O_3. Their nominal compositions, both in $\%_{wt}$ and $\%_{mol}$, are reported in Tab. 4.2:

Name	Weight percentage ($\%_{wt}$) of oxide				Molar percentage ($\%_{mol}$) of oxide			
	SiO_2	P_2O_5	CaO	Eu_2O_3	SiO_2	P_2O_5	CaO	Eu_2O_3
B67,5 Eu1	67,5	7,5	24,0	1,0	69,90	3,29	26,63	0,18
B67,5 Eu2	67,5	7,5	23,0	2,0	70,56	3,32	25,76	0,36
B67,5 Eu3	67,5	7,5	22,0	3,0	71,23	3,35	24,88	0,54
B67,5 Eu4	67,5	7,5	21,0	4,0	71,92	3,38	23,97	0,73
B67,5 Eu5	67,5	7,5	20,0	5,0	72,61	3,42	23,05	0,92
B67,5 Eu10	67,5	7,5	15,0	10,0	76,31	3,59	18,17	1,93

Tab. 4.2: Nominal composition of the synthesized Eu doped bioactive glasses

The choice of introducing in the composition increasing amounts of Eu_2O_3 at the expense of CaO, and not of SiO_2 or P_2O_5, was motivated by two main reasons:

- Eu substitutes for Ca inside the HCA lattice, so carrying out the same substitution even in the base glass was an idea that intuitively sprung into our mind;
- Even bearing a 3+ net charge, having almost the same ionic radius of Ca^{2+} makes Eu's and Ca's electric field strengths (FS) not much different; if we estimate the FS being proportional to $Z/r_{ion}{}^2$, we can calculate[14]:

$$FS_{Eu^{3+}} = A \cdot 3.32\ \text{Å}^{-2}$$

$$FS_{Ca^{2+}} = B \cdot 2.00\ \text{Å}^{-2}$$

  Since these values are sufficiently close, we can make the hypothesis that Ca and Eu both behave as modifiers, and thus both tend to break the continuity of the silicate network, creating non bridging oxygen; obviously, having a stronger FS, Eu should be a less effective modifier than Ca, and thus the substitution we operated might slightly strengthen the glass, making it more difficult to leach and dissolve (as already said in the previous paragraph).
  Moreover, in our opinion Eu electric field intensity is not sufficiently high to allow its classification among the so called "Intermediate Oxides" like Al^{3+}; in fact, if we estimate this latter ion's FS value, we obtain $FS_{Al^{3+}} = C \cdot 10.28\ \text{Å}^{-2}$, which is way higher than Eu's 3.32 Å^{-2}.
  Therefore, even if Eu might not behave exactly in the same way as Ca, nevertheless the differences between them should not be too strong, so the substitution of CaO with Eu_2O_3 in our glasses should be a correct idea.

On the other hand, though motivated by the will of following the research team's *modus operandi*, we must acknowledge that the choice of operating said substitution in terms of weight percentages of oxides might be questionable.

In fact, being Eu_2O_3 a much heavier chemical species than CaO (their respective molar masses are $M_{Eu_2O_3} = 351{,}9$ g/mol VS $M_{CaO} = 56{,}1$ g/mol), the molar amount of Eu_2O_3 needed to attain a given weight percentage is definitely lower than in the case of CaO; this way, the total amount of molecules of modifier oxides (CaO + Eu_2O_3) within the composition decreases with increasing Eu $\%_{wt}$, thus making the heavily doped glasses' networks strong. In particular, if for each bioactive glass we calculate the molar ratio of network modifier oxides

[14] Using the ionic radii of 0.95 Å for Eu^{3+} and 1.00 Å for Ca^{2+} reported in R. D. Shannon, *Acta Cryst.* 1976, A32

($CaO + Eu_2O_3$) / network former oxides ($SiO_2 + P_2O_5$), and use it as a simple tool to estimate the resistance to leaching and hydrolytic dissolution processes, we can find the following values:

Glass	Mod/For ratio
B67,5	0,38
B67,5 Eu1	0,37
B67,5 Eu2	0,35
B67,5 Eu3	0,34
B67,5 Eu4	0,33
B67,5 Eu5	0,32
B67,5 Eu10	0,25

Even if we might assume that the differences of behavior between glasses from B67,5 up to B67,5 Eu5 are only slight and thus reasonably negligible, surely we cannot do so for B67,5 Eu10, whose ratio ≈ 0,25 is too far from B67,5's value of 0,38.

Consequently, in this latter glass two effects might overlap in strengthening the network: the lower modifier / former oxides molar ratio and the lower modifying efficiency of Eu ions VS Ca ions.

In order to separate these two contributions and to understand to what extent the sole Eu doping alters the bioactive behavior of B67,5 Eu10, we synthesized a last glass, named **Molari**, keeping the same molar percentage of Eu_2O_3 as in B67,5 Eu10, and the same modifier / former oxides molar ratio as in B67,5: this way, if Eu^{3+} and Ca^{2+} had the same modifying efficiency, B67,5 and Molari would have exactly the same hydrolytic and leachability resistance, and thus if on the contrary we detected some differences in their two real behaviors, they would exclusively be ascribable to alterations induced by the dopant.

Molari's composition in terms of molar and weight percentages of oxides is the following:

Molari bioactive glass		
Oxide	**Weight %**	**Molar %**
SiO_2	61,59	69,26
CaO	21,15	25,48
P_2O_5	6,84	3,26
Eu_2O_3	10,42	2,00

Tab. 4.3: Composition of Molari bioactive glass

Obviously, having a $\%_{wt}$ of SiO_2 different from 67,5, Molari glass is not a B67,5-type glass.

4.2.3: The protocol of synthesis

All the aforementioned glasses have been synthesized via an alcoholic solution alcoxide hydrolysis/condensation based sol-gel method (see Chap. 2 for introductive information); in particular, since the sample holder of the available optical set-up for luminescence spectroscopic analyses was fit only for powdered samples, we synthesized our glasses under the form of powders. This has rendered all the practical operations very easy and relatively fast, because not working with sol-gel monoliths allowed us to carry out the drying and calcination/stabilization steps without any special constraint on speed or environment[15].

The protocol of synthesis we used for our Eu doped sol-gel glasses is a minor modification of the research team's usual protocol (see ref. [23] and [49]) for obtaining bioactive glass samples, which in turn is none other than a slight modification of a method introduced by P. Saravanapavan and L.L. Hench for binary SiO_2-CaO glasses (see ref. [12], [40] and [41]). In the end, this protocol turns out to be practically identical to the one exploited by M. Vallet Regi's team (see ref. [2], [7], [9], etc.), and to the one exploited for the only literature reported synthesis of Eu doped ternary SiO_2-CaO-P_2O_5 bioactive glasses (see ref. [4] and [20]).

The precursors for the glass network formers, SiO_2 and P_2O_5, are two alcoxides, respectively TEOS and TEP, while the precursors for network modifiers are two nitrates, $Ca(NO_3)_2 \cdot 4H_2O$ and $Eu(NO_3)_3 \cdot 6H_2O$; since TEOS is not miscible with H_2O, the reaction was carried out using ethanol (TEOS's parent alcohol) as solvent of both reactants, and was catalyzed using 2M HCl (acidic catalysis; this is one slight difference from Saravanapavan, who in [12] uses HNO_3 instead of HCl). To ensure the complete hydrolysis of alcoxides before condensation, and thus to obtain a well interconnected three-dimensional network, a large excess of water was used; in particular, the molar ratio H_2O / (TEOS+TEP) was set at 12:1. The volumic ratios H_2O / HCl and H_2O / Et-OH were set respectively at 6:1 and 1:1 (all the ratios are the same as in [12]). The reaction is entirely carried out at room temperature.

All the above reported information is summarized in Tab. 4.4. The protocol of synthesis consists of eight steps, which will be described in detail in the next lines and schematically represented in Fig. 4.15:

[15] For example, drying (i.e. evaporation of both solvent and water from the gel interconnected pores) of sol-gel derived bioactive glass monoliths is often carried out under high humidity conditions (see ref. [9]), for long times and with multiple-step heating programs (see ref. [12]).

Role	Chemical Species	Purity
SiO_2 precursor	TEOS	99,999%
P_2O_5 precursor	TEP	99,8%
CaO precursor	$Ca(NO_3)_2 \cdot 4H_2O$	99,999%
Eu_2O_3 precursor	$Eu(NO_3)_3 \cdot 6H_2O$	99,99%
Solvent	Et-OH	98%
Hydrolyzing agent	H_2O	De-ionized
Catalyst	HCl	2M aqueous solution
H_2O / (TEOS + TEP) molar ratio		12 : 1
H_2O / Et-OH volumic ratio		1 : 1
H_2O / HCl volumic ratio		6 : 1

Tab. 4.4: Reactants summary

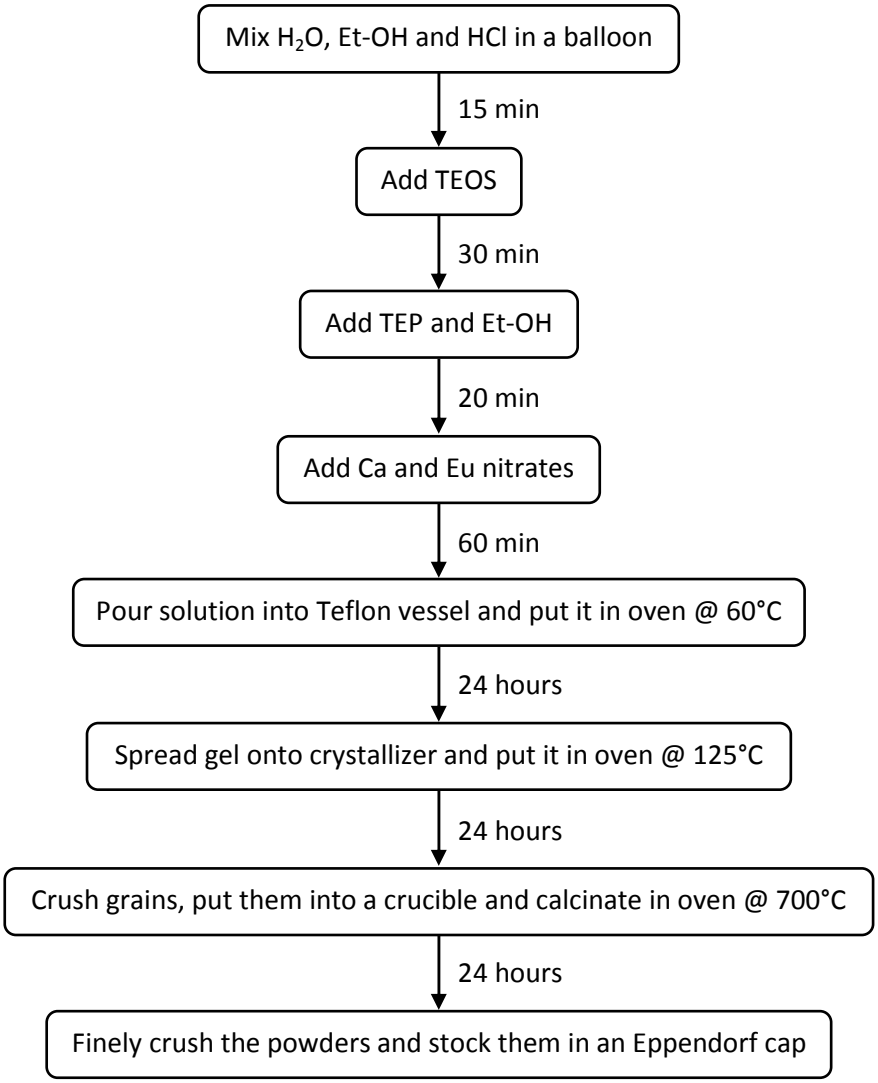

Fig. 4.15: Flow-chart diagram of the synthesis protocol

1) **Mixing of precursors**: in the beginning, the required amounts of H_2O, Et-OH and HCl are mixed together with the help of a magnetic stirrer (kept turned on for the whole reaction time) inside a glass flask of adequate capacity[16]; this latter is sealed with a silicone rubber cap to keep the system as closed as possible, thus preventing for example evaporation of ethanol or absorption of atmospheric moisture by the solution.
2) After 15 minutes of reasonably vigorous[17] stirring, TEOS is added inside the flask;
3) After other 30 minutes, equivalent volumes of TEP and Et-OH are added to the solution;
4) After 20 minutes, Ca and Eu nitrate powders are added to the reaction medium;
5) After another hour of mixing, the resulting *sol* is poured inside some 10mL PTFE (Teflon®) sealed vessels (there's need of approximately one for each gram of final desired product); at this point of the synthesis, inside the liquid phase it is possible to find primary particles of nanometric size (approx. 5 nm; see Lin. et al, ref. [50]);
6) **Gelation and gel-ageing treatment**: the Teflon vessels are put inside an oven at 60°C for 24 hours. During this time, first the primary particles coalesce, forming secondary particles of around 10 ÷ 30 nm of diameter. Then they aggregate, forming a continuous interconnected skeleton (gelation point) that thereafter continues to thicken (ageing). At the end of the 24 hours of treatment, the *gel* has a gelatinous consistency (a bit more solid than a crème-caramel) and must be "fragmented" with a spatula in order to be extracted from the vessel. In particular, the *gel* pieces are spread onto a crystallizer (a glass cylinder with large base and low walls) and divided to a fine extent, in order to maximize their surface for the further treatments.
7) **Drying step**: the crystallizer is put inside an oven at 125°C for 24 hours. During this time ethanol and water both progressively evaporate from the interconnected pores of the gel, leading to gel shrinkage, pore collapse, secondary particle aggregation, etc. At the end of this step, the material is made up of yellowish-white coarse grains, that are then crushed in an agate mortar to yield a finer yellowish powder.
8) **Calcination step**: said powder is placed inside alumina boat-shaped crucibles and put in an oven, where it's heated at a rate of 10°C/min up to the desired calcination temperature, that almost always is 700°C, and then it's kept at this T for 24 hours, after which the oven is let spontaneously cool down to room temperature. During this step of the synthesis the densification of the collapsed gel network takes place: particles start to coalesce through

[16] Since we synthesized maximum 1 or 2g of material for each batch, 25 and 50mL balloons were used.

[17] As an operational habit meant to enhance reproducibility, we tuned the rotation speed so that the vortex-shaped meniscus of the solution remained always approximately a millimeter above the magnetic stirrer.

various mechanisms, and ultimately form a continuous three-dimensional bulky structure, which may or may not retain part of the original interconnected porosity in dependence of the calcination temperature. The calcined product is a white glass powder, that is further finely crushed in an agate mortar and then finally stocked in plastic Eppendorf® caps.

The evolution of the synthesized material throughout the various steps of the protocol is schematically summarized in Fig. 4.16.

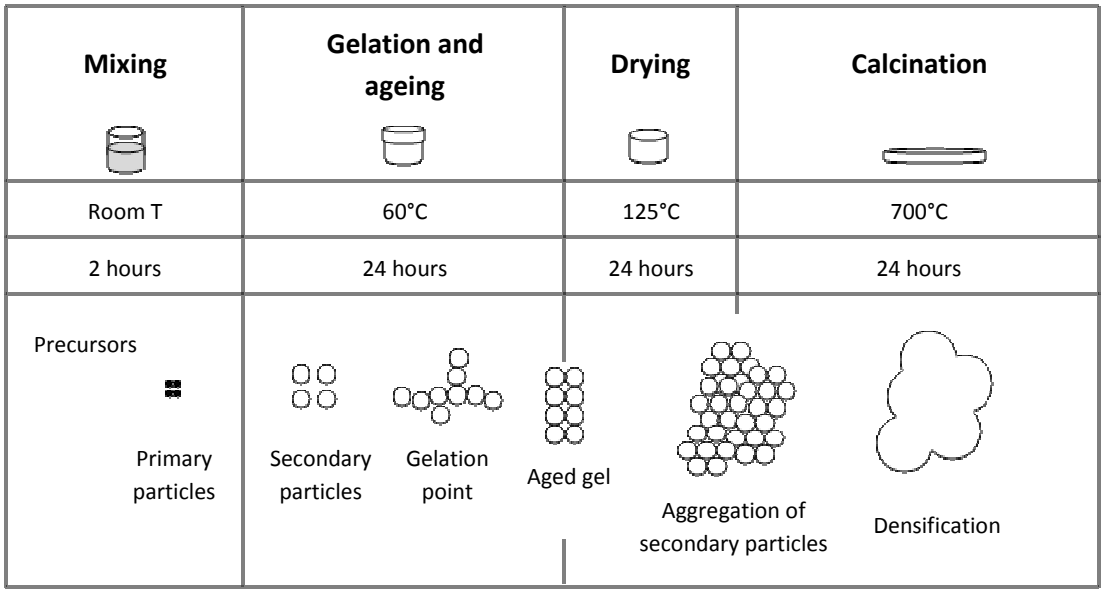

Fig. 4.16: Evolution of the sol-gel glasses throughout the synthesis procedure (from [23])

The choice to exploit a calcination temperature of 700°C was made taking into account many experimental evidences, both newly acquired and derived by previous works of the team (ref. [23] and [49]), as well as various bibliographic references:

- First of all, from TGA (Thermo-Gravimetric-Analysis) plots (see. Par. 4.3.2) it is possible to notice that the complete elimination of nitrates, introduced in the composition by the precursors of Ca and Eu, is possible only at temperatures above 550 ÷ 580°C.
- XRD analyses show that glasses calcined at 700°C are still almost completely amorphous, while those fired at 800, 900 and 1100°C show increasing degrees of crystallinity (see Par. 4.3.4);
- Nitrogen adsorption isotherms show that calcination at 900°C results in complete densification of the glass, as testified by the drastic drop in specific surface area and pore volume with respect to the mean values of glasses calcined at 700°C (see Par. 4.3.3);

- In literature the vast majority of bioactive sol-gel derived glasses in the ternary system SiO_2−CaO−P_2O_5 as well as in the binary system SiO_2−CaO is calcined at 700°C (see Saravanapavan's, Vallet-Regi's, Kreb's, Greenspan's various articles on the subject);
- In previous research works by members of the team (see ref. [23] and [49]) the chosen calcination temperature was always 700°C.

Since we needed to compare our results with the data gathered by other researchers of the team; since we wanted to exploit also some literature information such as FT-IR, Raman and luminescence spectra; since we wanted to keep a certain degree of meso-porosity and an adequately high specific surface area value, owing to their utmost importance in bioactivity processes; since we wanted to avoid having thorough devitrification in our glasses because it could spoil bioactivity as well as complicate the interpretation of results[18]; and since we needed to completely eliminate nitrates from our samples, due to their detrimental effect on bioactivity; then we chose 700°C as systematic calcination temperature.

However, in order to study the effect of Eu doping on the devitrification behavior of our bioactive glasses as well as on their textural and structural properties, we also carried out some calcinations at 800, 900 and 1100°C (see Par. 4.3.4 and 4.3.7).

Before passing to the characterization of the samples resulting from the above described procedure, it is very important to spend some words on the behavior of Ca and Eu precursors during the various steps of the synthesis. In particular, being under the form of nitrates, during the mixing step they are dissolved inside the solution, and thus at the beginning of the gelation treatment free Ca^{2+}, Eu^{3+} and NO_3^- ions are present in the liquid phase along with primary particles deriving from alcoxides (both TEOS and TEP) condensation.

When the material passes beyond the gelation point, it has been demonstrated by Lin et al. (ref. [50]) that those ions are still located in the liquid phase dwelling inside the gelatinous skeleton's interconnected porosity (see Fig. 4.17, which depicts the evolution of Ca^{2+} ions; Eu^{3+} ions, however, behave exactly the same way); this renders the use of vessels in Teflon of primary importance, since the high hydrophobicity of this material should prevent the accumulation of ionic species on the container's walls (see ref. [23]).

[18] For example, having a considerable amount of crystallized HA since the beginning (because of extensive devitrification during calcination) would render the identification of the onset of HCA biologically-induced precipitation extremely difficult.

At the end of the drying step, when no more liquid phase is present, Ca and Eu ions can be found adsorbed on the surfaces of the aggregated SiO_2 secondary particles, that is on the surface of the interconnected collapsed porosity of the dried gel. This means that the actual incorporation of Ca and Eu ions in the SiO_2−P_2O_5 amorphous network takes place only upon heating (starting from 400°C; see ref. [50]) during the calcination step, when silica particles coalesce and diffusion becomes possible; therefore, a correct choice of calcination T and duration is crucial to ensure a good degree of homogeneity to the synthesized glasses.

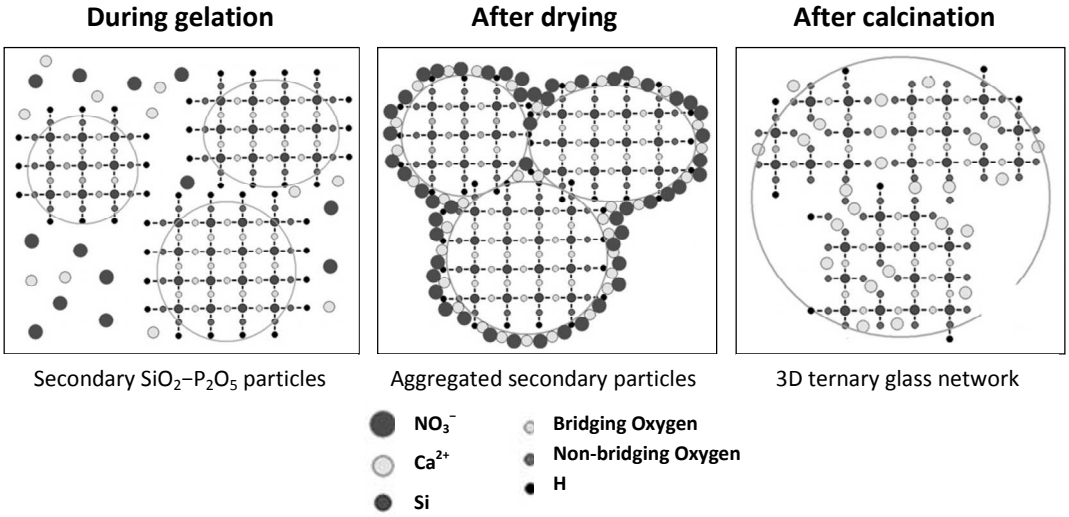

Fig. 4.17: Evolution of Ca^{2+} ions throughout the synthesis steps (from ref. [23] and [50])

From this latter point of view, our choice of calcinating at 700°C for 24 hours seems quite sensible, because, even if the nitrates can be completely eliminated also at 600°C, surely the degree of final homogeneity attainable at 700°C is far superior; maybe heating at 800°C might yield even better results, but the considerable devitrification that takes place at that temperature is unacceptable, so 700°C represents the best compromise between homogeneity and prevention of thorough crystallization.

All the aforementioned issues with nitrates and "free" ions could be avoided if we used alcoxide precursors also for Ca and Eu, as once attempted by Ràmila and Balas (see ref. [1]): this way, in fact, the hydrolysis and condensation reactions would directly yield primary and secondary particles containing all the four Si, P, Ca and Eu. However, depending on the chosen −O−R moieties (2-methoxyethyl in ref. [1]) bound to the metal center, said alcoxides are often either too much (see ref. [1]) or not enough reactive (see ref. [49]), they require specific attention to catalysts, they must be freshly synthesized right before the reaction, this latter needs to be carried out under controlled inert atmosphere (dry Ar or dry N_2), etc.

On the other hand, the homogeneity degree attainable following an "all-alcoxides" synthesis route is not exceptionally higher than the one achievable through a more conventional "alcoxide formers-nitrate modifiers" method, and, above all, the final impact on bioactivity properties is practically negligible (see ref. [1]). Therefore, since the increased operational complexity is not rewarded with significantly better results, we decided to follow the "traditional" alcoxides-nitrates synthesis path.

Moreover, the homogeneity degree of our bioactive glasses is very good, as intuitively shown by the following chemical cartographies (Fig. 4.18), acquired via PIXE-RBS microprobe analysis[19] on a B67,5 Eu5 glass powder compact. As it is easily noticeable, no segregation, clusterization or zoning of ions is detected, at least as far as the resolution of the instrument (0,5 to 5 µm, depending on the settings) allows us to see[20].

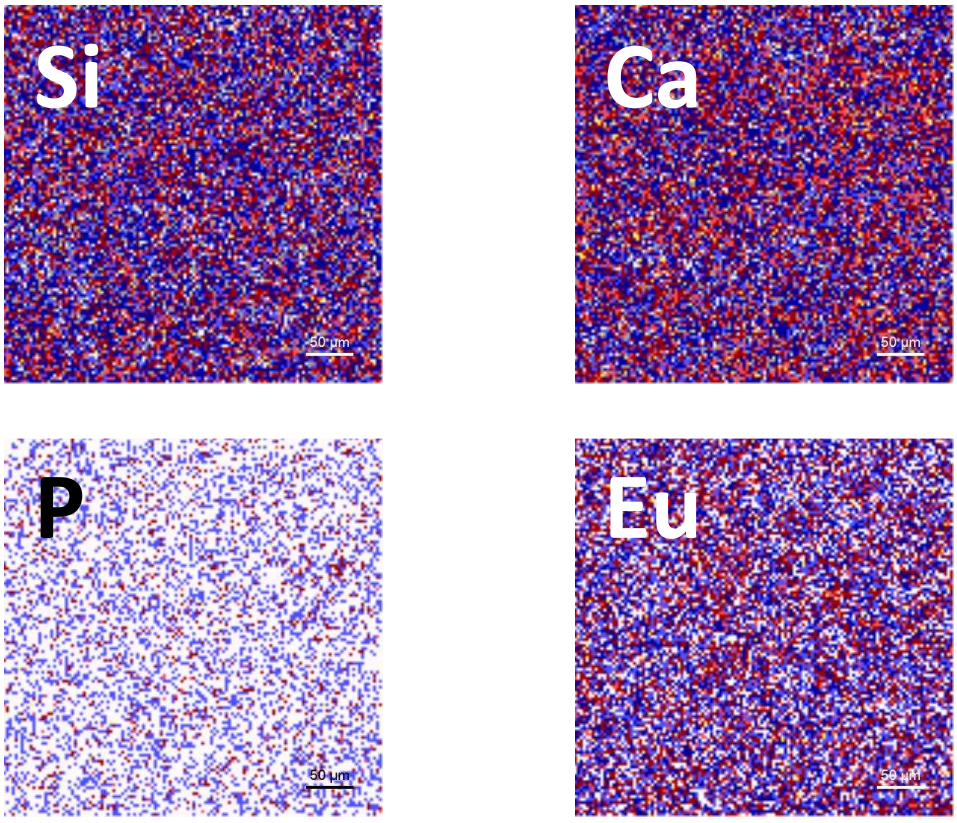

Fig. 4.18: PIXE-RBS chemical cartographies of a B67,5 Eu5 glass compact

[19] Since this characterization technique will never be used again in this work, we won't spend any more words to describe its features, neither will we explain the experimental procedure followed to prepare and analyze the samples. For more information on this subject, please refer to [23] and [49].

[20] The reported cartographies show large scale homogeneity; linear atomic concentration profiles in several directions have also been acquired on a more local scale (measure spots of 1 μm^2), and the results (not shown) demonstrate again a very good degree of homogeneity, with less than 4,8% point-to-point maximum deviations from the average value.

4.3: Characterization of the as synthesized bioactive glasses

4.3.1: Compositional analysis via ICP-AES

First of all, the actual composition of our doped bioactive glasses has been checked through ICP-AES analyses, in order to verify that the exploited protocol of synthesis yielded the desired results; since in order to be fed to the plasma torch the samples must be in the liquid form, the glass powders were dissolved using the alkaline fusion method (for more information on this method and on the characterization technique itself, refer to Chap. 3). The analyses were carried out by Dr. Mhammed Benbakkar at the *Laboratoire Magma et Volcans* of the Blaise Pascal University (Clermont-Ferrand II), and the results are the following:

	Weight percentages ($\%_{wt}$)						
Oxide	B67,5	B67,5 Eu1	B67,5 Eu2	B67,5 Eu3	B67,5 Eu4	B67,5 Eu5	B67,5 Eu10
SiO_2	65.00	64.32	65.14	64.96	64.58	65.09	64.48
CaO	23.69	22.41	22.33	20.92	19.84	20.13	14.58
P_2O_5	6.79	6.87	7.08	6.76	7.12	6.99	7.0
Eu_2O_3	n.a.	n.a.	n.a.	n.a.	n.a.	n.a.	n.a.

Tab. 4.5: Experimental composition of the synthesized bioactive glasses

As it is clearly evident from a comparison of Tab. 4.5 and 4.2, there's a good match between nominal and real values for SiO_2, CaO and P_2O_5 (as already found by other researchers of the team; see ref. [23] and [49]) but Eu_2O_3 data are lacking; this was unfortunately due to the unavailability in the lab of a reference standard (and of a quality certification standard too) with such high Eu $\%_{wt}$ as our samples: none of the rocks stored in the whole geology department contained significant amounts of Eu, so it was impossible for us to create a reference solution by dissolving a mineral with known Eu content via alkaline fusion, and therefore it was impossible to calibrate the instrument for the detection of Eu ions.

The impossibility of knowing the true amount of Eu_2O_3 incorporated in the glass network during the synthesis is a severe drawback, since it forces us to arbitrarily assume as actual percentage of Eu its nominal value, even if we do not have proof of this equivalence; the assumption, however is nevertheless reasonable, since literature data published by Krebs and

Brownstein (ref. [4] and [20]), who exploited a protocol of synthesis practically identical to ours to synthesize almost equivalent glasses, show a very good agreement between nominal and experimentally determined compositions.

4.3.2: Thermal analysis, DTA and TGA plots

Due to technical problems with the available instrumentation, thermal analyses could not be carried out right after the drying step of the syntheses; consequently, small amounts of dried "yellowish" powder (see point 7 of Par. 4.2.3) were stored in closed plastic Eppendorf® caps, and eventually underwent TGA+DTA (Thermo-Gravimetric Analysis + Differential Thermal Analysis) characterization only a few months later. This way, DTA data cannot be strictly considered as representative of the processes that took place upon calcination of the original powders, but still can provide us some useful information.

Regarding said non representativeness, in particular we noticed that effectuating the calcination step a few months after drying resulted in bioactive glass powders with higher specific surface area (SSA) values and with extensive devitrification: B67,5 Eu1 powder calcined right after drying has a mean SSA of 66 m^2/g (see Par. 4.3.3) and underwent only slight devitrification; on the contrary, B67,5 Eu1 powder calcined approximately three months after drying has a SSA value of 184 m^2/g and from site selective spectroscopy analyses (see. Par 4.3.7) shows a very high degree of Hydroxylapatite devitrification (for the identification of the crystalline phase with HA, see Par. 4.3.4, 4.3.7 and Chap. 5).

Coming to the useful information, we can reasonably state that, even if delayed calcination yields significant differences in textural properties and in crystallization behavior, it should nevertheless leave the TGA plots unchanged. The thermal analyses have been carried out starting from room temperature up to 1200°C, with a heating rate of 10°C/min (the same used during real calcination steps) in simple air atmosphere.

The total percentage weight loss varies only slightly with composition, and has a mean value of about 40%, which is consistent with the operative calcination losses (around 42% average) registered during the syntheses. These latter are evaluated by simply weighing the powders before and after calcination, and thus keep into account not only the elimination of volatile species, but also the loss of powder due to convective currents inside the oven, the small loss of material due to attachment of powders to the mortar, etc.

The weight loss always takes place between 90°C (onset of the elimination of humidity reabsorbed after drying) and 550 ÷ 600°C (total elimination of nitrates, associated with a strong endothermic peak; see ref. [12]), while beyond this latter T the variations in sample's weight become negligible. The most substantial weight loss (25 ÷ 30%), however, takes place between 125°C (maximum temperature attained during evaporation treatment) and 250°C, and corresponds to the complete elimination of solvent and water molecules from the interconnected porosity. At higher T, up to 400°C, Saravanapavan and Hench in [12] suggest that evaporation of organic molecules like alcoxy groups might also take place.

Other important, but maybe less reliable (due to the said detected changes in devitrification behavior) feature of the DTA plots is the exothermic peak associated with no weight loss at 850 ÷ 900°C, which can be attributed to crystallization of apatitic crystals; this identification is in good agreement with literature data (see ref. [9]), but there is experimental evidence of slight HA crystallization even at 700°C (see 4.3.4, 4.3.6 and 4.3.7) due to the long duration of the thermal treatment.

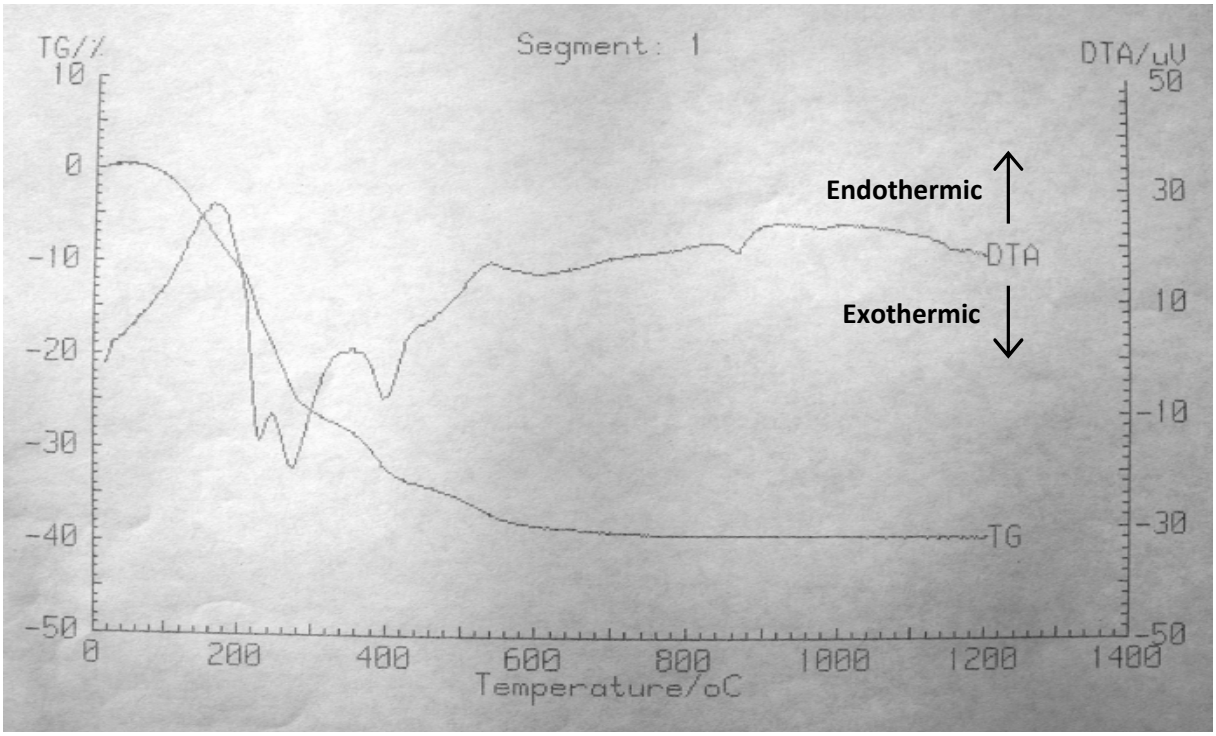

Fig. 4.19: DTA and TGA plots of a B67,5 Eu3 sample

The reported plots are referred to a sample of B67,5 Eu3 glass, but the curves acquired from other powders exhibit more or less the same trends, with just slight differences in the heights of the DTA peaks at 400°C and 550 ÷ 600°C.

4.3.3: Textural effects of Eu doping, Nitrogen adsorption analyses

Almost all the synthesized glasses have been thoroughly characterized through nitrogen adsorption measurements, in order to understand which textural modifications were brought about by the increasing content of Eu^{3+} ions introduced in the composition of our samples.

The various isotherms acquired for powders calcined at 700°C are all very similar, so one for each composition will be reported, in order to make the assignment of their main features as direct and straightforward as possible (too crowded graphics are often difficult to interpret).

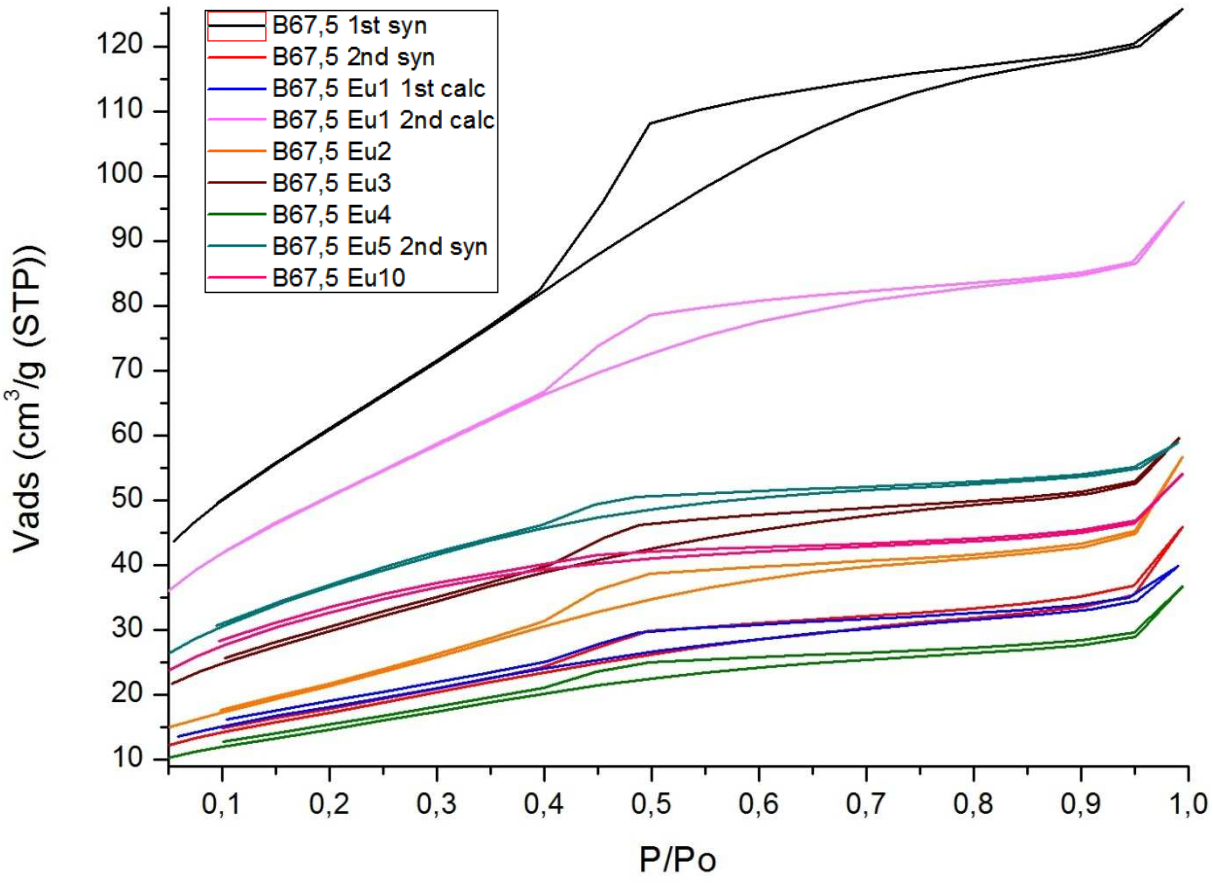

Fig. 4.20: N_2 adsorption isotherms acquired for our doped bioactive glasses (T_{calc} = 700°C)

If we compare the shape of the above reported plots to the IUPAC classification standards (see Fig. 4.21), in our opinion we can recognize hybrid Type I + Type IV isotherms; in particular, since Type I isotherms are usually associated with microporous substrates and Type IV ones are typical of samples with mesopores wherein capillary condensation of the adsorbate can take place (see ref. [51] and [52]), from the isotherms' shapes we can reasonably induce that our samples contain both micro- and mesopores.

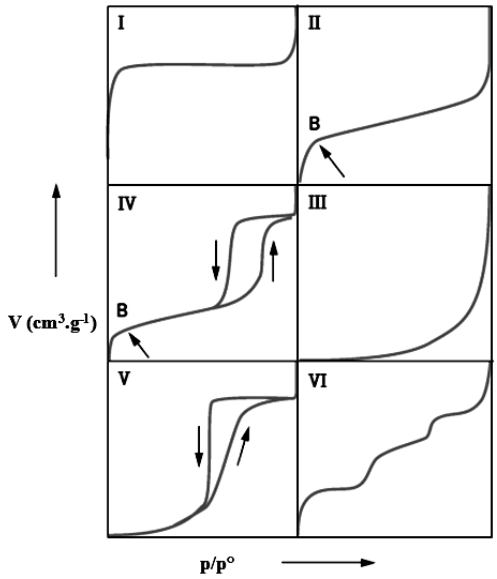

Fig. 4.21: IUPAC classification of nitrogen adsorption isotherms (from [52])

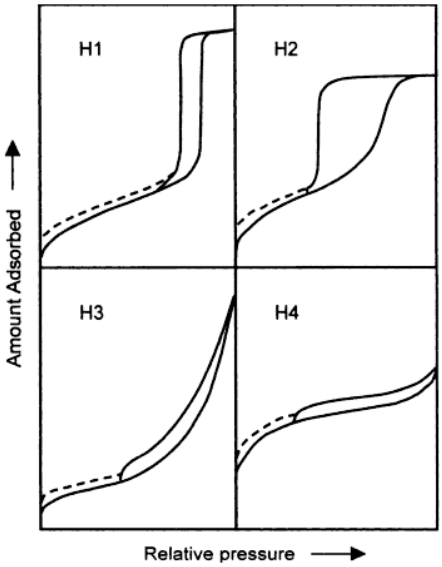

Fig. 4.22: IUPAC classification of hysteresis loops in N_2 adsorption isotherms (see [53])

Switching to hysteresis recognition, our adsorption and desorption branches have more horizontal than vertical nature (H4 feature), but tend to "meet" before reaching the highest relative pressures (H1 feature), so our loops can be classified as IUPAC hybrid H1+ H4 hysteresis (see Fig. 4.22); therefore we can infer that our samples should reasonably contain both mesopores (H1) and narrow (even in the micro- domain) slit shaped pores (H4).

Moreover, many of our experimental curves show low pressure hysteresis, highlighted with dashed lines in Fig. 4.22, meaning that a small part of the adsorbate cannot be desorbed from the sample's surfaces by lowering relative pressure alone; this might be due to the presence of micropores in our bioactive glass powders (see ref. [53], page 44), and is consistent with the partial Type I character of most isotherms and with their H4 loops.

Well different from the above reported isotherms is the plot obtained from the analysis of a B67,5 Eu5 sample calcined at 900°C (on the right): the low pressure hysteresis has disappeared, and the main loop has become practically negligible; moreover, the total pore volume is very low (0,0115cm^3/g), and even the specific surface

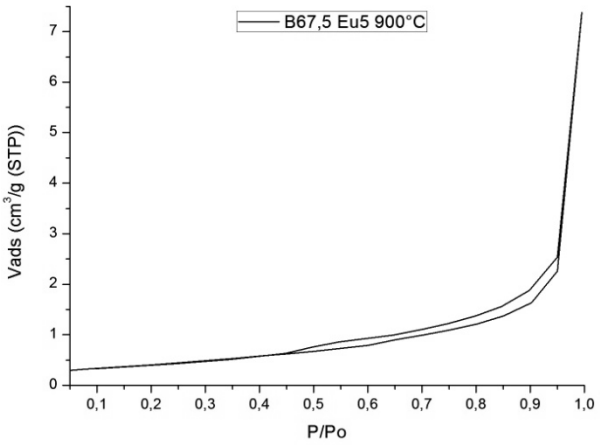

area calculated through the BET method, equal to 1,5 m^2/g, is far lower than the average value for bioactive glasses calcined at 700°C, quantifiable in around 70 ÷ 100 m^2/g.

All these evidences lead us to the conclusion that calcination at $T \geq 900°C$ yields fully densified powders, i.e. it completely eliminates porosity from the samples; therefore, since a high surface area and a high degree of porosity are of utmost importance for a successful bioactive behavior of the glass, 900°C is not a suitable temperature for calcination.

Returning to the isotherms of samples treated at 700°C, we can notice that most of them bear the same features and are located on the lower side of the graph, while two curves slightly different from the others stand out on the top (in pink and black in Fig. 4.20); these latter isotherms are connected with two samples whose synthesis path has been different from the normal protocol:

- **B67,5 1st syn** (black): this glass has undergone gelation treatment inside a disposable plastic polyethylene (Nalgene®) bottle and not in a Teflon vessel. From Fig. 4.20 we can notice that it has the widest hysteresis loop, and from BET and BJH methods applied to the isotherm data we can determine the following values: specific surface area SA = 225 m^2/g; total pore volume V_{pores} = 0.195 cm^3/g; average pore size r_{pores} = 3.5 nm. This means that it is far more porous than the others (see also Tab. 4.6);
- **B67,5 Eu1 2nd calc** (pink): this glass has been calcined only a few months after the drying treatment; it has SA = 184 m^2/g, V_{pores} = 0.149 cm^3/g and r_{pores} = 3.2 nm. Evidently, since the heating program was the same as for the other glasses, some structural rearrangements must have taken place during the stocking period, and after calcination those changes must have yielded a more porous (and more crystallized, as we will see in Par. 4.3.7) glass.

If we now exclude said two anomalous curves, the differences between isotherms noticeable in Fig. 4.20 are principally[21] ascribable to the doping with Eu, be it an effect due to the different behavior of the precursor or a direct effect of the ion itself. In particular, the most straightforward trends we can spot when the Eu content increases are a progressive narrowing of the main hysteresis loop and the appearance (and widening) of low pressure hysteresis.

[21] Obviously, small differences in the operational steps of the syntheses (such as different rotation speeds of stirrers, small delays in the schedule, different room temperatures, etc.) cannot be avoided.

This latter effect suggests that doping our silica based sol-gel glasses with Eu increases the amount of microporosity inside the samples, which is consistent with what found by Ferrari *et al* and what reported in ref. [21] for Eu doped silica xerogels and glasses. On the other hand, since the hysteresis loop is connected to capillary condensation in roughly cylindrical interconnected mesopores (see ref. [52]), its narrowing means that said type of mesopores tends to disappear at high Eu content, either due to a global reduction in mesoporous volume or due to a change in pore shape and organization.

The data provided by the isotherms has been analyzed via application of BET method on the first seven adsorption points and of BJH method on the desorption branch (see Chap. 3), in order to calculate the specific surface area, total pore volume and mean pore size of the samples; the obtained results are reported in Tab. 4.6. It is however necessary to bear in mind that BET and especially BJH methods are designed for mesoporous materials, and thus yield rigorously correct and reliable results only for that type of samples; since a non-negligible part of the porosity of our glasses lies in the micropores domain, as testified by the shape of the adsorption hysteresis, the values reported below must be considered only as semi-quantitative.

Sample	SA (m^2/g)	V_{pores} (cm^3/g)	r_{pores} (nm)
B67,5 2nd syn	64	0.0712	4.4
B67,5 Eu1 1st calc	66	0.0618	3.7
B67,5 Eu2	82	0.0880	4.3
B67,5 Eu3	109	0.0925	3.4
B67,5 Eu4	55	0.0569	4.1
B67,5 Eu5 2nd syn	131	0.0914	2.8
B67,5 Eu10	115	0.0838	2.9
B67,5 1st syn	225	0.195	3.5
B67,5 Eu1 2nd calc	184	0.149	3.2

Tab. 4.6: Textural data from BET and BJH methods (in grey, the two anomolies)

As we can see from the first column of the table, the specific surface area of the samples seems to increase with increasing weight percentages of Eu (except for the B67,5 Eu4 data); a slight increase seems to affect also the total specific pore volume, accounting for both micro- and mesopores; on the contrary, the average pore size seems to become narrower with Eu

content (but in this case the trend is less regular), which is consistent with an increase in microporosity at the expense of mesoporosity, and with the detected narrowing of main condensation hysteresis loops.

Since a complete textural characterization and explanation is not the purpose of this work[22], and since due to microporosity the BJH data aren't even completely reliable, we won't report the BJH pore size distributions of our samples, nor will we spend more words on the textural properties of our Eu doped bioactive glasses.

4.3.4: Influence of Eu^{3+} ions on the devitrification behavior, XRD analyses

With the aim of studying the effects of Eu ions on the devitrification behavior of our materials, we analyzed some of our samples with a conventional X-Ray diffraction powder instrument, exploiting a Bragg Brentano "θ - 2θ" set-up. In particular, we characterized a few "normal" (that is calcined at 700°C) glasses, as well as some other samples purposely calcined at higher temperatures (800, 900, 1100°C).

Below we show the comparison between patterns detected for samples calcined at 700°C:

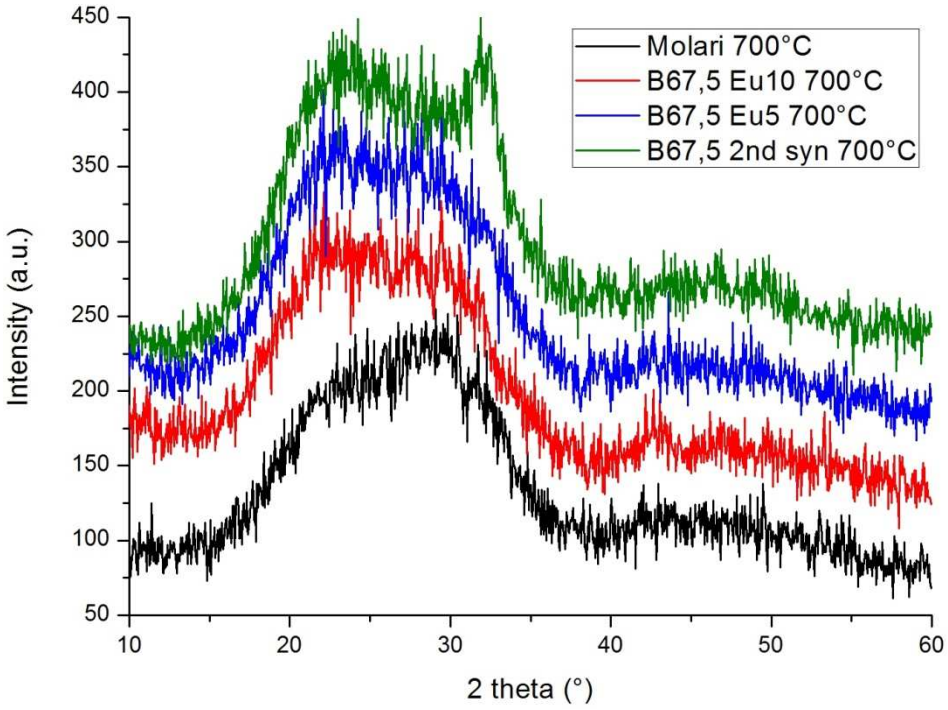

Fig. 4.23: Comparison between diffraction patterns of glasses calcined at 700°C

[22] The textural data are principally needed in order to carry out the in vitro bioactivity tests in the best possible way, that is trying to keep them as reproducible as possible (see Chap. 5).

As it is clearly evidenced, the materials treated at 700°C are almost completely amorphous, even though a minor devitrified phase can be detected in the non doped **B67,5 2nd syn** case; a rigorous identification of this crystalline phase is not possible, since we have only one broad peak at 32°, but comparing Fig. 4.23 with Fig. 4.1 and Fig. 4.2, we can reasonably state that it should be some form of poorly crystallized or nanometric size apatite. At high doping degree, XRD patterns cannot detect devitrification, but this does not mean that devitrification actually does not occur: in fact, it is highly probable that some apatitic crystals are formed upon calcination even in the case of B67,5 Eu5, but they are too tiny to yield significant diffraction effects.

This hypothesis, as well as the identification with some form of apatite, is confirmed by FTIR measurements, that for B67,5, B67,5 Eu1[23] and B67,5 Eu5, but not for B67,5 Eu10 or Molari, show slight apatitic phosphate peaks at 560 ÷ 600 cm^{-1} (see Par. 4.1.1 and Par. 4.3.6). Even the luminescence spectra acquired via site selective excitation (see Par. 4.3.7 and Chap. 5) confirm the presence of Eu doped apatitic crystals in B67,5 Eu1 and B67,5 Eu5, and show that the degree of crystallization decreases with Eu content, up to almost no devitrification at all in B67,5 Eu10 and Molari.

Therefore, considering all the available experimental data, we can state with a reasonable degree of confidence that Eu^{3+} ions have a slight kinetic hindering effect on the crystallization of apatitic crystals upon low temperature heat treatment.

B67,5 and B67,5Eu5 glasses have been calcined also at a higher temperature, in particular at 900°C, to induce a more intense devitrification, and thus to allow a more rigorous identification of the formed crystalline phases. If we compare the two resulting diffraction patterns (Fig. 4.24), acquired with the same instrument and the same experimental settings, we can notice that they are practically identical, both in position and

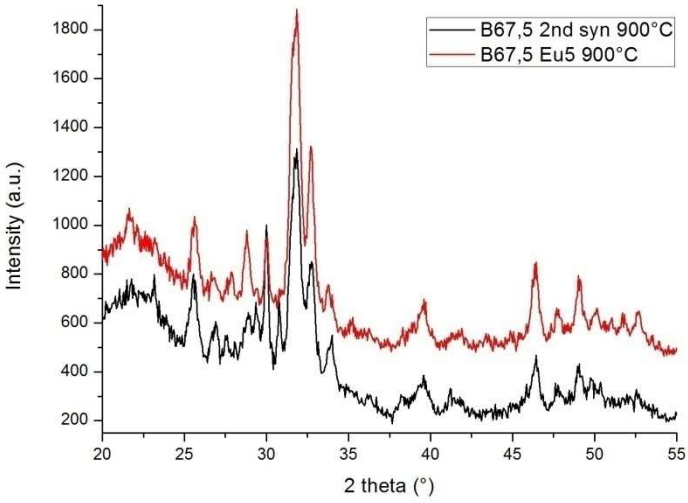

Fig. 4.24: Comparison between XRD patterns of glasses calcined at 900°C

[23] Unfortunately, for this glass there was not enough powder left to carry out powder-XRD analyses.

intensity of the peaks (maybe B67,5 yields a slightly better resolved pattern). However this does not surprise us very much, since within a 24 hours-long high temperature heat treatment, the kinetic hindering effect of Eu^{3+} should be reasonably negligible.

The evolution of devitrifying phases has been followed in B67,5 Eu5 bioactive glass by calcination of powders at 800, 900 and 1100°C; the results are shown in Fig. 4.25:

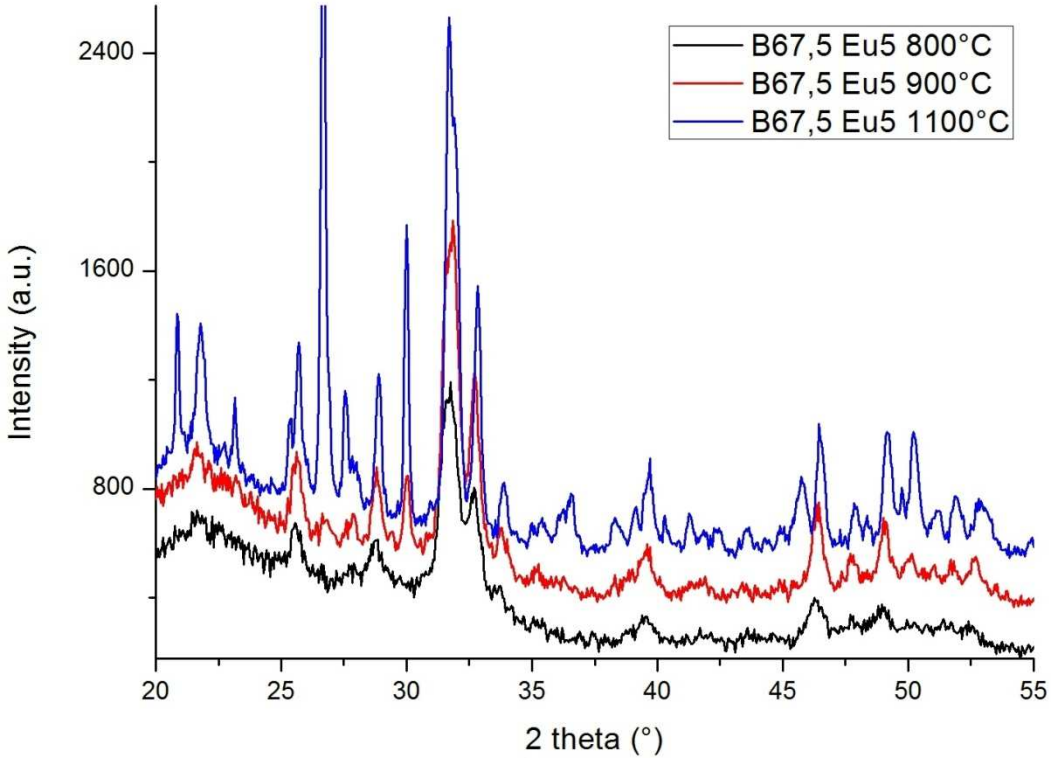

Fig. 4.25: Comparison between B67,5 Eu5 samples calcined at different T_{calc}

As it can be easily noticed, the patterns from the powders treated at 800 and 900°C are very similar (the only relevant differences are at 23.15° and 30°), and exhibit a very good match with an hydroxyl-apatite phase (see below); since the red pattern has more intense and well resolved peaks than the black one, the apatitic phase grows in size and crystallinity with calcination temperature[24], as one would normally expect. On the other hand, increasing the annealing temperature up to 1100°C not only yields better apatite crystals, but also causes the formation of other crystalline phases, as testified by the appearance of new peaks at 20.85°, 25.65°, 27.60°, 36.65° and 45.75°.

As for the identification of the phases, in B67,5 Eu5 calcined at 900°C we can recognize:

[24] This is confirmed also by luminescence spectroscopy analyses, which show that HA characteristic emission peaks grow in intensity passing from a calcination temperature of 800°C to 900°C (see Par. 4.3.7).

- An apatitic phase: good match with Hydroxylapatite, $Ca_{10}(PO_4)_3OH_2$, JCPDS file 9-432;
- Calcium Pyrophosphate: $Ca_2P_2O_7$, JCPDS file 23-871;
- Wollastonite: a calcium silicate, $CaSiO_3$, JCPDS file 42-550;
- β-TCP: $Ca_3(PO_4)_2$, that is the crystal into which HA tends to spontaneously evolve when heated above 900°C, JCPDS file 9-169;

In Fig. 4.26 we report the diffraction pattern of a B67,5 Eu5 sample calcined at 900°C, with superimposed the JCPDS file of HA:

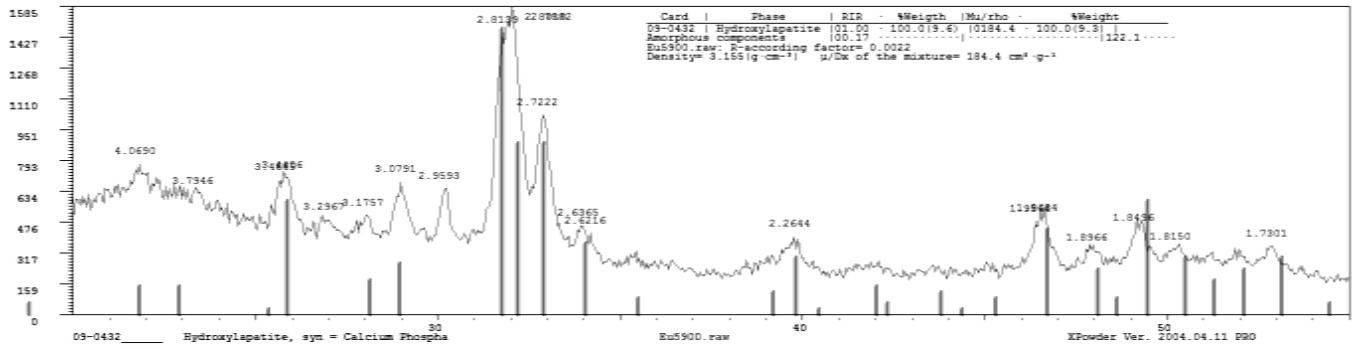

Fig. 4.26: Identification of the apatitic phase in the XRD pattern of B67,5 Eu5 900°C

A very good match can be found also with a Calcium Europium Oxide Silicate, $Ca_2Eu_8(SiO_4)_6O_2$, JCPDS file 29-320, an oxyapatite with the same type of hexagonal unit cell and the same $P6_3/m$ point group of HA, but with slightly different *a* and *c* cell parameters; this is due to the fact that the Bragg peaks of the two said crystals are practically in the same positions (just a few cents of degree shifted from each other).

However, in literature (see ref. [17]) we found out that, in order to synthesize the oxyapatite, a heat treatment at 1400°C for 4 days is necessary, so we can reasonably state that $Ca_2Eu_8(SiO_4)_6O_2$ cannot crystallize under our synthesis conditions; moreover, many other experimental evidences confirm the presence of Eu doped HA in our samples: for example, the luminescent fingerprint of Calcium Europium Oxide Silicate (ref. [17]) is very different from the one detected for our samples, which in turn is identical to the Eu doped HA's one.

Switching to the diffraction pattern registered for B67,5 Eu5 calcined at 1100°C, together with the cited phases (but this time Wollastonite is much more present) we can identify also:

- Quartz: SiO_2, responsible for the huge out-of-scale peak at 26.65°, JCPDS file 33-1161;
- Ca_2SiO_4, another calcium silicate, JCPDS file 23-1042;

4.3.5: Structural characterization by micro-Raman spectroscopy

The synthesized series of Eu doped bioactive glasses has undergone micro-Raman spectroscopy measurements in order to gain some knowledge on the structural units of the amorphous network; as previously said (see Chap 3), this technique allows the identification of the chemical bonds present in our samples from the characteristic energy of their various vibrational modes, provided that the vibration itself causes a net change in the polarizability of the structural unit. Said energy is calculated from the detected Raman shift, which is the difference between the wavenumber of the instrument's incident beam and the wavenumber of the light inelastically scattered by the sample, and thus is related to the characteristic energy difference between the vibrational excited state responsible for the detected Raman scattering and the ground state of the structural unit.

The Raman spectra acquired for our glasses are reported in Fig. 4.27; for our experimental parameters, see Chapter 3.

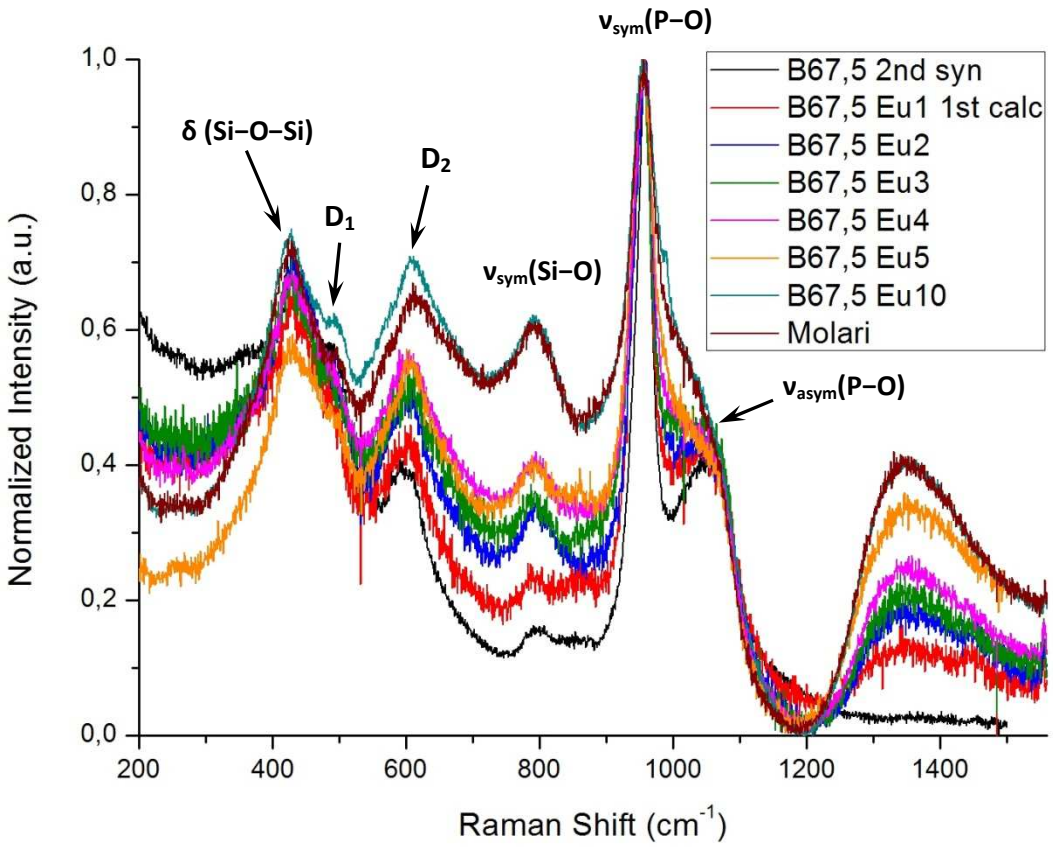

Fig. 4.27: Normalized Raman Stokes spectra of our doped bioactive glasses

Since it was impossible to always employ the same focalization, or to always analyze the same micro-volume of material, the absolute spectra cannot be quantitatively compared to

each other; a qualitative comparison between the height of the peaks, however, is possible if we consider the normalized spectra. In particular, without bibliographic information on which of the peaks could remain reasonably unchanged in our spectra (if any of the like exists), we saw no better solution than normalizing to the intensity of the maximum peak (960 cm^{-1}). This way we obtained almost comparable plots, but we lost the possibility of intuitively evaluate the changes in height of the "reference" peak: in fact, differences in the intensity at 960cm^{-1} manifest themselves in a global lowering or increase in the height of all the other peaks.

This approach might be considered questionable, since for example in the case of a contemporaneous variation in the intensity of many peaks, reference one included, it would be challenging to identify the actual modifications from a normalized spectra; however, it's also true that the compositional and thus structural changes in our series of bioactive glasses are very gradual[25] (we alter 1%$_{wt}$ each time), so the trends should be easily noticeable.

The principal features of our spectra are summarized in Tab. 4.7 (data gathered from ref. [21], [33] and [36]):

Raman Shift (cm^{-1})	Vibrational mode	Description
430	δ(Si–O–Si)	Si–O–Si in-plane bending and out-of-plane rocking
490	D_1	Symmetric breathing of 4 members siloxane rings
603	D_2	Symmetric breathing of 3 members siloxane rings
800	δ_{sym}(Si–O)	Symmetric deformation of the network involving the Si and O atoms
960	ν_{sym}(P–O)	Symmetric vibration of P–O bonds in PO_4^{3-} groups
1060	TO ν_{asym}(Si–O–Si)	Transverse optic antisymmetric stretching of Si–O–Si bonds
1070	ν_{asym}(P–O)	Antisymmetric stretching of P–O bonds in PO_4^{3-} groups
1080	ν(C–O)	Vibration of C–O bonds inside carbonate groups
1250 ÷ 1450	???	Unidentified broadband connected to Eu content

Tab. 4.7: Summary of the most relevant features detectable in our glasses' spectra

What we notice the most in the reported plots is that increasing Eu content causes a progressive increase in the intensity of all peaks, at the expense of the reference 960 cm^{-1} one, ν_{sym}(P–O), which means that this latter becomes less intense; moreover, even the peak at

[25] B67,5 cannot be that different from B67,5 Eu1, and this latter is very similar to B67,5 Eu2, and so on;

around 1070 cm^{-1}, ν_{asym}(P−O), becomes shorter and less resolved from the 960 cm^{-1} one at high doping degree.

Since those two peaks are associated with P−O bonds, and since phosphate groups in a crystalline environment are much more Raman active than in amorphous networks (see ref. [33]), all this might mean that the amount of nanocrystals of HA formed upon calcination decreases with Eu content, which is consistent with what emerges from both XRD (Par. 4.3.4) and FTIR (Par. 4.3.6) analyses.

Another interesting feature is the broad band located at 1250 ÷ 1450 cm^{-1}, that is evidently absent in the base B67,5 glass, and becomes more and more intense with increasing dopant concentration: its height seems to be influenced by Eu $\%_{mol}$ alone, and not by the rest of the glass composition, since B67,5 Eu10 and Molari glasses, having the same Eu_2O_3 $\%_{mol}$ but different molar amounts of other oxides, exhibit bands of the same intensity. No specific information about it has been found in literature, but we can reasonably state that it is due to a luminescence feature of Eu^{3+} ions and not to Raman effect.

In particular, being redshifted of 1250 ÷ 1450 cm^{-1} from the incident laser beam at 514.5 nm, this band is located between 550 and 556 nm, and thus might be connected to the direct radiative desexcitation from the $^5D_1$ level[26] towards the $^7F_1$ level (see Fig. 4.28; the reported data are derived from the experimental spectra we will show in Par. 4.3.7). The very faint (comparable with Raman Stokes signal) detected intensity is consistent with this hypothesis, because the probability of radiative transitions originating from levels different from the $^5D_0$ is very low for Eu^{3+} ions: in fact, the overwhelming majority of the electrons promoted to the $^5D_1$ level normally non radiatively relax to the $^5D_0$ level prior to emitting luminescence photons in the transition to the ground state.

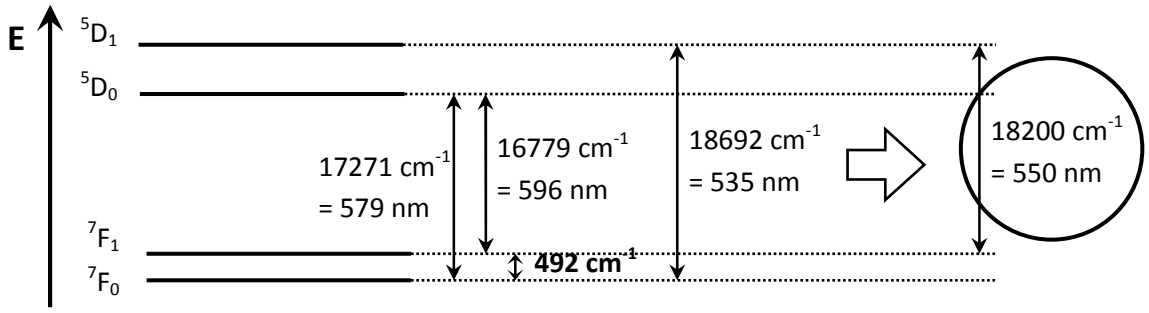

Fig. 4.28: Simplified energy level scheme of Eu^{3+} ions hosted inside the glass network

[26] The transition $^7F_0 \rightarrow {}^5D_1$ takes place upon absorption of photons having λ ≈ 535 nm (see ref. [20]), so the Ar laser, having λ = 514.5 nm, is sufficiently energetic to yield excitation of Eu ions in the $^5D_1$ level.

4.3.6: Structural characterization by FTIR spectroscopy

To complete the structural/vibrational characterization of our as-synthesized bioactive glasses, together with micro-Raman we also carried out some transmission FTIR spectroscopic analyses; as explained in Chapter 3, this technique allows direct promotion of the structural units to excited vibrational states through absorption of IR photons, provided that the resulting transition occurs with a change in the net electric dipole moment of the unit. Since each vibrational mode of a solid has a characteristic energy gap with respect to the ground state, by measuring the transmittance[27] of the sample as a function of the incident beam wavenumber (and thus, energy) we can understand which bonds are present and IR-active in our samples.

For more information on the technique and on the experimental set-up we used for our analyses, we invite the reader to refer to Chapter 3; here we will only recollect that in order to avoid losing the powders we characterized, we didn't exploit the KBr compress method, but, on the contrary, to support our samples inside the instrument we put our powders between two KBr windows normally used to carry out analyses on liquids.

This, though allowing us to be completely non destructive (maybe just a bit sample-polluting), rendered the analyses extremely sensitive to the amount of powder placed between the slabs of KBr, and to its degree of dispersion; therefore, extracting quantitative information from absolute spectra is out of discussion, and only qualitative comparisons between normalized curves will be made.

The normalized spectra acquired for some of our doped bioactive glasses, those that also underwent *in vitro* bioactivity testing, are reported in Fig. 4.29:

[27] Defined as the ratio between transmitted and incident light intensities: $T_{\%} = {I_{transm}}/{I_{incid}} * 100$; this way, the absorption of the beam at a certain wavenumber, corresponding to the presence of a certain bond, is detected as a drop in $T_{\%}$, so transmittance IR peaks are visualized, in practice, as "transmittance wells".

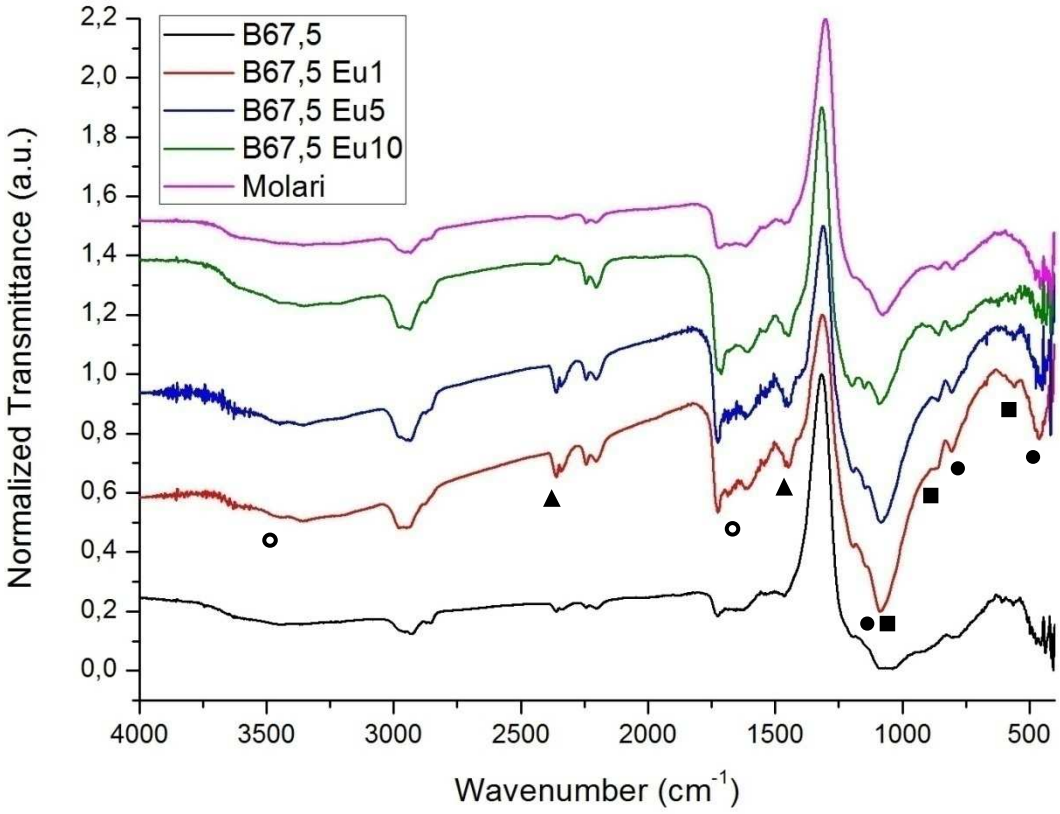

Fig. 4.29: Normalized FTIR spectra of some of our as-synthesized bioactive glasses

In literature we found a great number of articles dealing with FTIR characterizations of bioactive glasses (see ref. [1], [2], [9], [13], [22], [32], [37], [40], etc), and since in almost each of them a comparison between samples before and after bioactivity testing is shown, we have a lot of information on how to interpret our spectra (much more than with Raman, for instance). Our measurements were carried out from 4000 to 400 cm^{-1} (128 accumulations with 2cm^{-1} resolution), even if the majority of publications show only the portion of spectrum ranging from 1600 to 400 cm^{-1}; in fact, at higher wavenumbers there's little information on Si−O and P−O bonds, and the plots are dominated by water vibrations.

The most important spectral features are summarized in Tab. 4.9, and highlighted in Fig. 4.29 using the symbols of Tab. 4.8.

Type of bond	Symbol	Type of bond	Symbol
Si−O	●	C−O	▲
P−O	■	O−H	○

Tab. 4.8: Symbols used in Fig. 4.29 to highlight and identify peaks

Wavenumber (cm^{-1})	Vibrational mode	Description
3600	ν_{sym}(O−H)	Symmetric stretching of O−H bonds
3300	$\nu(H_2O)$	Vibration of adsorbed water molecules (humidity in the samples)
2360 and 2340	ν_{asym}(C=O)	Antisymmetric stretching of CO_2 atmospheric molecules (bad background subtraction)
1600 ÷ 1700	ν(O−H)	O−H deformation mode and H_2O bending
1450	ν(C−O)	C−O bonds asymmetric deformation
1000 ÷ 1200	ν_{asym} (P−O)	Asymmetric stretching of amorphous phosphate groups (mainly at 1035 cm^{-1})
	ν_{asym} (Si−O−Si)	Asymmetric stretching of Si−O−Si bonds (mainly at 1085 cm^{-1})
900	ν_{asym} (P−O) in Q^2	Asymmetric stretching of bridging oxygens in Q^2 phosphate tetrahedra (PO_4^{3-} groups with only two connection to the glass network)
800	ν_{sym} (Si−O)	Symmetric stretching of Si−O bonds
560 and 600	ν_{cryst} (P−O)	Stretching of P−O bonds in apatitic environment
450	δ_{bend} (Si−O−Si)	Symmetric bending of Si−O−Si bonds
	δ_{abend}(P−O)	Antisymmetric bending of P−O bonds in amorphous environment

Tab. 4.9: Summary of the most important vibrational modes detected in our samples

As easily noticeable from Fig. 4.29, the spectra of our samples look all very similar to each other: the same peaks are present, approximately in the same positions, and their intensities vary only slightly. Since in this work we are interested in identifying the modifications induced by the introduction of Eu ions in the composition of our glasses, our attention must focalize above all on the doublet of peaks at 560 and 600 cm^{-1}, connected with phosphate vibrations in an apatitic environment (see ref [70]): since it is not present in B67,5 Eu10 and Molari, this means that no crystallization takes place upon calcination at high Eu concentration. On the contrary, for low up to none Eu content those peaks can be detected (though their intensity is really faint), therefore, as already inferred from XRD and Raman data, we can further confirm that Eu has a hindering effect on the devitrification of HA.

4.3.7: Structural characterization by luminescence spectroscopy

In Chapter 5 we will describe in full detail the experimental path we followed to discover and explore the luminescence features of our doped bioactive glasses, while the theoretical

bases of the characterization technique and the experimental set-up we employed are described in Chapter 3; therefore, for a deeper understanding of what will be said in the following pages we invite the reader to refer to said parts of this work, as well as to consult more specialized, but yet didactic textbooks like: G. Blasse, B.C. Grabmaier, *Luminescent materials*, Springer-verlag, 1994. Here we will just show what kind of information site selective luminescence spectroscopy can provide when the analyzed samples are glasses before *in vitro* bioactivity testing.

As we will see in Chap. 5, by carrying out site selective luminescence spectroscopy measurements on post-interaction samples it is possible to identify the presence of two "families" of Eu^{3+} ions, occupying radically different sites:

- one selectively excitable in the $^5D_0$ emitting level by tuning the incident laser at **579 nm**, and corresponding to Eu cations inside the **amorphous** network (broad band emission);
- and one selectively excitable in its $^5D_0$ by tuning the laser at **574 nm**, and corresponding to Eu centers within a crystalline environment (narrow peaks), in particular occupying the Ca(II) sites of an **apatitic** lattice (see Par. 4.1.2).

Using the same two laser wavelengths to excite the as-synthesized glasses calcined at 700°C, we can obtain the emission spectra reported in Fig. 4.30 (beam at 579 nm - glass) and 4.31 (574 nm - apatitic crystal):

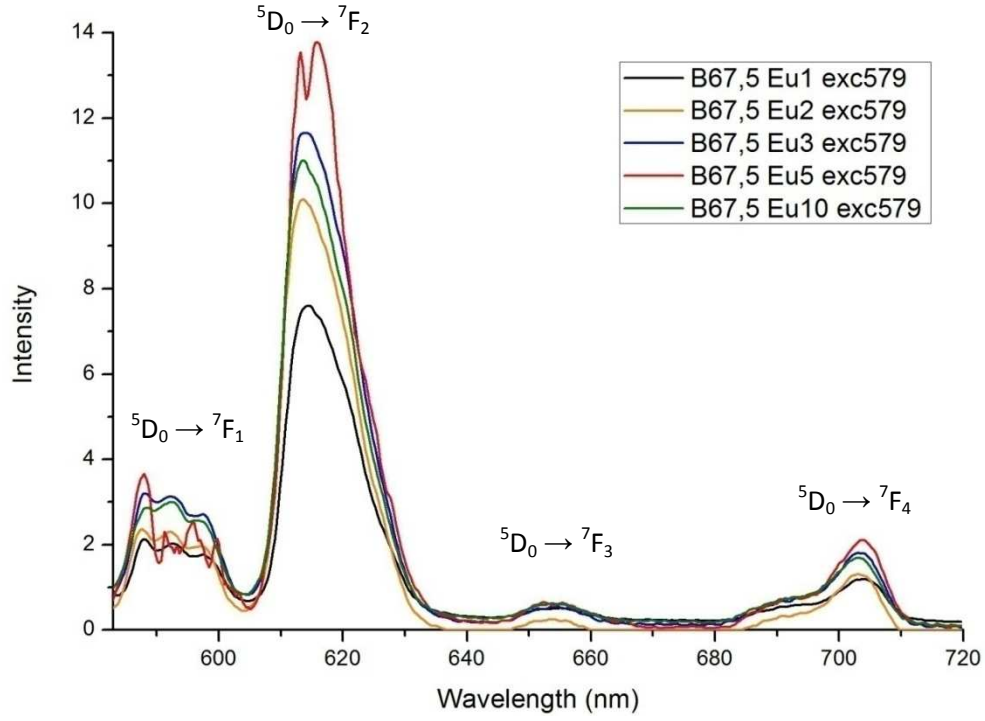

Fig. 4.30: Emission spectra of our glass powders when excited at 579 nm (no offset)

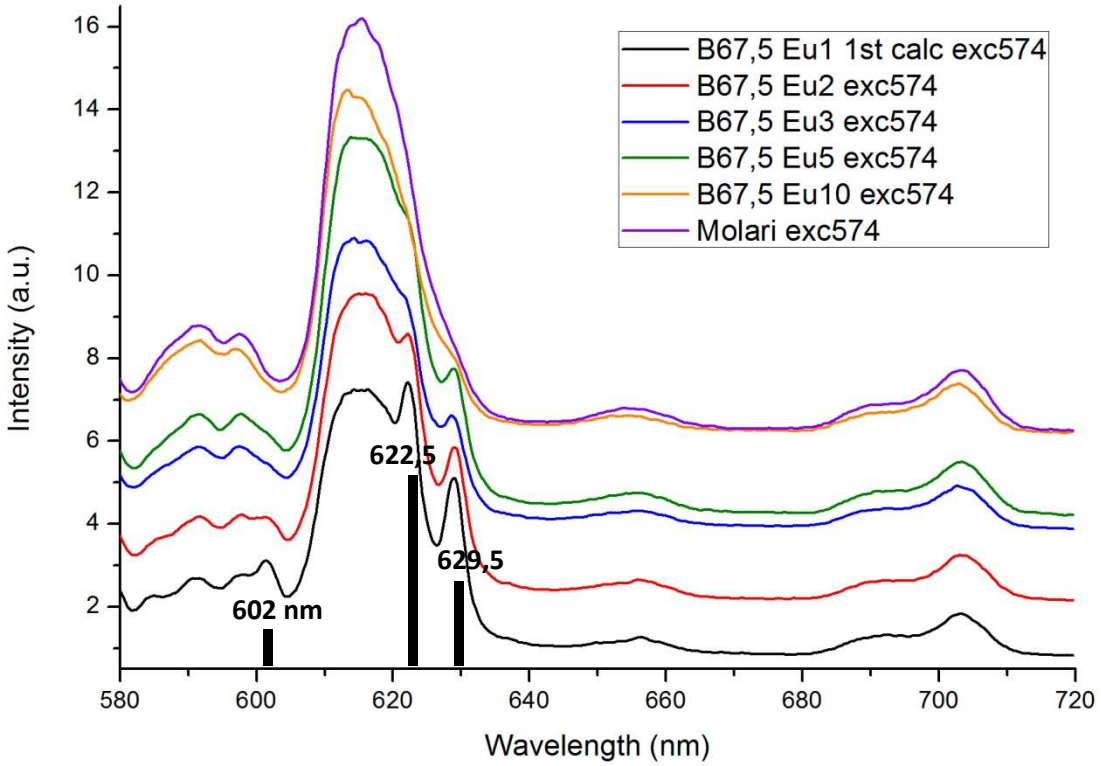

Fig. 4.31: Emission spectra of our 700°C glass samples when excited at 574 nm (with offset)

The spectra acquired with excitation at 579 nm (Fig. 4.30) look all very similar, with broad emission bands located within the most common wavelength ranges for Eu^{3+} ions; the only relevant difference is in their intensity, and in particular in the height of the $^5D_0 \rightarrow {}^7F_2$ transition, which increases with Eu content up to $5\%_{wt}$, but then decreases in the case of B67,5 Eu10. This effect might seem illogical at a first glance, but it is not: in fact, even if in the beginning increasing the amount of emitting centers causes reasonably an increase in peak intensity, when a certain concentration of ions is exceeded the equation "more excitable luminescent centers = more intense emission" becomes no more valid.

This is due to the fact that the higher the doping degree, the closer Eu ions will be inside the amorphous network (supposing an homogeneous distribution[28]), and thus, beyond a certain point, Energy Transfer (ET) between centers becomes possible. Therefore, in highly doped glasses (and this is true for any kind of emitting ion, not only for Eu) the luminescent ions can cross-desexcitate between each other, that is center A_1^*, in the excited state, can relax non

[28] Even worse is the case when emitting centers tend to segregate, phase separate or clusterize, because this way they get within the critical distance for energy transfer much earlier, and thus the emission intensity starts to drop at considerably lower concentrations. It's in this optics that the presence of P in our glasses' composition is highly beneficial, since it helps in preventing RE clusterization (see ref. [21]).

radiatively to its ground state A_1 by effectuating an ET towards another identical center A_2, present in its proximity, which consequently is promoted to an excited state A_2^*.

This effect alone, however, cannot explain the so called "*Concentration self-quenching (CSQ) of luminescence*", that is, in our case, B67,5 Eu10's low emission, but:

- since in our bioactive glasses there is a considerable amount of residual −OH groups, due to the sol-gel route we exploited for their synthesis (see also FTIR spectra of Par. 4.3.6);
- and since hydroxyl moieties are very powerful luminescence quenchers, because they provide a most favorable non-radiative desexcitation path, due to the high characteristic energy of their vibrational mode,

then the explanation becomes almost straightforward: beyond a certain concentration of dopant, the statistic probability of hydroxyl as well as of other types of luminescence quenching becomes higher, because now, thanks to the possibility of ET between centers, it is more probable for an excited center to be located in the vicinity of a quencher. And, obviously, more quenching equals less emission intensity.

Let's make an example to make things clearer: if ion A_2 is within the critical distance for non radiative coupling from an hydroxyl group, and is also next to an excited center A_1^*:

- if Eu's % is higher than the critical value for CSQ, then the ions are close enough for A_1^* to effectuate ET towards A_2, and thus A_2^*'s emission will be quenched by the −OH;
- if on the contrary we are below said critical concentration, then ET is impossible, and A_1^* is "forced" to desexcitate by emitting a luminescence photon, leaving A_2 undisturbed.

In other words, below the CSQ point the excitation can be regarded as "bound" to the actually excited centers, while beyond that dopant concentration it becomes "mobile", that is it can migrate from a center to another via ET, thus rendering more probable the encounter with a quenching trap.

All of this said, it seems highly probable that concentrational self quenching takes place in the case of B67,5 Eu10, but unfortunately we cannot state with precision which is the critical CSQ concentration for our bioactive materials; we can only estimate that it's located somewhere in between 5 and 10%$_{wt}$ of Eu_2O_3, since no intermediate doped glasses have been synthesized between the B67,5 Eu5 and B67,5 Eu10 compositions.

Switching now to Fig. 4.31, this time we can easily spot some considerable differences

between emission spectra: some thin peaks (characteristic of a crystalline phase), located at around 602, 622,5 and 629,5 nm, tend to disappear with increasing Eu content. As it will be clearly demonstrated in Chapter 5, those peaks can be attributed to Eu ions occupying Ca(II) sites of Hydroxylapatite crystals, and thus their decreasing intensity with doping degree[29] means that Eu has a hindering effect on the devitrification upon heating of apatitic phases, as confirmed by FTIR, Raman and XRD analyses on samples calcined at 700°C.

A further validation of the attribution of said emission peaks to Eu ions inside HA can be found in Fig. 4.32, where we report the emission spectra upon excitation at 574 nm of B67,5 Eu5 powders calcined at different temperatures (700, 800, 900 and 1100°C): it's straightforward to recognize the same three peaks of Fig. 4.31, increasing in height with calcination T. Now, since increasing T yields larger, better crystallized crystals, and since from XRD analyses (see Par. 4.3.4) we identified the devitrified phases as mainly HA, than a reasonable connection can be established between XRD and luminescence peaks.

In Chapter 5 the same correlation will also be found with Raman and FTIR measurements on post-interaction samples, and, moreover, again in Chap. 5 we will report a comparison between an experimental emission spectrum with HA-like peaks and the plot detected by Ternane (see ref. [11]) for his sol-gel derived Eu doped Hydroxylapatites; the perfect match we will find shall be the ultimate proof of the validity of our peak attribution.

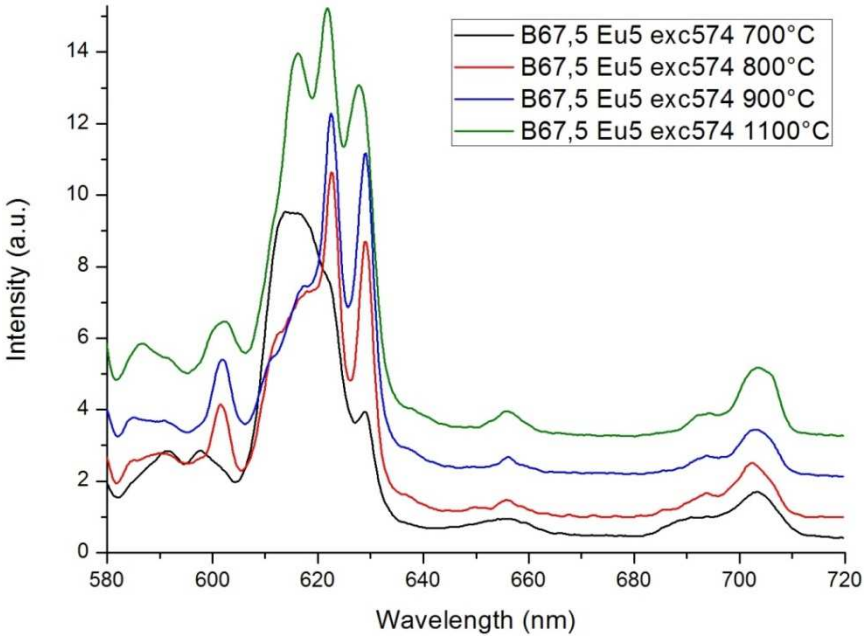

Fig. 4.32: Emission spectra (λ_{exc} = 574nm) of B67,5 Eu5 samples calcined at various T (offset)

[29] However, in the case of B67,5 Eu10 and Molari this effect might also partly be due to the concentrational self quenching of luminescence.

Last but not least, we want to report the emission spectrum upon excitation at 574 nm of one of the "anomalous" glasses we synthesized: B67,5 Eu1 2nd calc (see Par. 4.3.3), having the same composition of B67,5 Eu1, the same T_{calc} = 700°C, but fired only a few months after the drying step. In Fig. 4.33 we can see enormous HA peaks, even higher than those normally detected after 4 days of interaction with biological fluids (Chap. 5) or after stabilization at 900°C (Fig. 4.32).

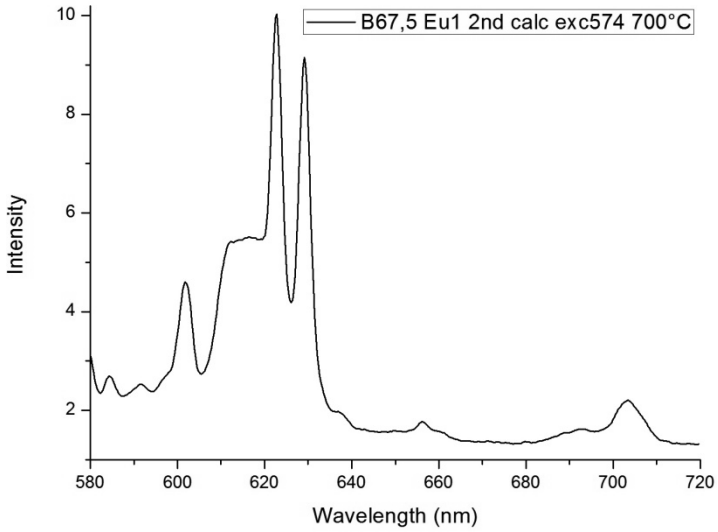

Fig. 4.33: Emission spectrum (λ_{exc} = 574nm) of the anomalous sample **B67,5 Eu1 2nd calc**

This is the reason why in Par. 4.3.3 we said that delayed calcination, besides yielding much more mesoporous samples, enhanced also devitrification upon heating at 700°C.

4.3.8: Conclusions

In this chapter we have presented the issue we faced during the research activity, i.e. the need of a new tool for characterizing biomineralization processes, and shown why, at least in theory, our idea, that is doping bioactive glasses with Eu^{3+} ions and carrying out site selective luminescence spectroscopy measurements on post-interaction samples, might be an effective solution. Then we have described first our experimental approach to this thesis, and second how we actually synthesized our materials, pointing out advantages and drawbacks of the sol-gel protocol we employed. Finally, we have reported the results of the various analyses we carried out on our pre-interaction doped samples, demonstrating how site selective luminescence spectroscopy can be a useful tool for detecting devitrification upon heat treatment in our glasses.

Finally, by cross referencing all the data we gathered, we reached the conclusion that Eu^{3+} ions at high concentrations hinder the devitrification of Hydroxylapatite upon calcination at 700°C.

Chapter Five: The bio-mineralized samples

In this chapter we will first describe the procedure we followed to carry out *in vitro* bioactivity tests on our doped and undoped sol-gel derived glass powders, pointing out its strengths and its weaknesses; then we will explain the experimental path that, through site selective luminescence analyses, led us to the identification of the characteristic spectral signature of doped Hydroxyl-carbonate-apatite crystals formed during interaction with biological simulated media; finally, we will present all the data we gathered through various characterization techniques in order to validate the results of our luminescent structural probe.

5.1: In vitro bioactivity testing

5.1.1: The simulated biological medium, DMEM

The synthesized bioactive powders have been tested following a well established protocol, already used by other researchers of the team (see ref. [23] and [49]), and very similar to many static procedures reported in bibliography (for example see ref. [31] or [40]), which in turn are all more or less derived from the milestone article by Kokubo et al, *Solutions able to reproduce in vivo surface-structure changes in bioactive glass ceramic A-W*, J. Biomed. Mater. Res., **26,** 1147–1161 (1992).

A major difference exists from this latter article: instead of SBF (Simulated Body Fluid) we employed Dulbecco's Modified Eagle Medium (DMEM), a cell culture medium. While the former is merely an ionic solution mimicking human plasma's composition, the latter, besides Na^+, Ca^{2+}, Cl^- and other ions, contains also vitamins, amino acids, glucids and other bio-organic molecules meant to sustain cell growth. The ionic compositions of human plasma, SBF and DMEM are reported in Tab. 5.1, while the organic components of DMEM are listed in Tab. 5.2:

	Na^+	K^+	Mg^{2+}	Ca^{2+}	Cl^-	HCO_3^-	HPO_4^{2-}	SO_4^{2-}
Human Plasma	142,0	5,0	1,5	2,5	103,0	27,0	1,0	0,5
Kokubo's SBF	142,0	5,0	1,5	2,5	148,0	4,2	1,0	0,0
DMEM	155,3	5,3	0,8	1,8	115,7	44,1	0,9	0,8

Tab. 5.1: Ionic concentrations (in mmol/L) of natural and simulated biological media

Amino Acids	Concentration	Vitamines	Concentration
Glycine	30	Choline chloride	4
L-Arginine hydrochloride	84	D-Calcium pantothenate	4
L-Cysteine 2HCl	63	Folic Acid	4
L-Glutamine	580	Niacinamide	4
L-Histidine hydrochloride	42	Pyridoxine hydrochloride	4
L-Isoleucine	105	Riboflavin	0,4
L-Leucine	105	Thiamine hydrochloride	4
L-Lysine hydrochloride	146	i-Inositol	7,2
L-Methionine	30		
L-Phenylalanine	66	**Other components**	**Concentration**
L-Serine	42	D-Glucose (Dextrose)	1000
L-Threonine	95	Phenol Red	15
L-Tryptophan	16	Sodium Pyruvate	110
L-Tyrosine	72		
L-Valine	94		

Tab. 5.2: Concentration of bio-organic species inside the DMEM (in mg/L)

This choice was made with three principal aims:

- to grant as much continuity as possible between the two most common stages of the *in vitro* bioactivity testing protocol, that is: first, interaction with simulated biological fluids (carried out in the present work); and second, cell adhesion or cell culture assays (maybe possible in the future developments of this thesis);
- to follow the path already laid by other researchers of the team (all of which used DMEM as biological medium), in order to be able to exploit also their published experimental data to better understand the biomineralization processes;
- to avoid the need of manually preparing SBF right before interactions: in fact, this latter is a home-made solution "brewed" by mixing appropriate amounts of salts in deionized water, so during its preparation operative errors as well as biologic contaminations of the liquid can take place; on the contrary, DMEM is a commercial product, sold in a sterilized state and with certified ionic and bio-organic compositions (in our case our supplier was Biochrom AG), whose sealed bottles can be stocked in a fridge for reasonably long periods of time and be opened when the need arises (however, they must then be consumed or disposed of within a few days).

Moreover, it has been demonstrated by J.E. Gough, L.L. Hench *et al*[1] that the differences in bioactive behavior brought about by the use of DMEM instead of SBF are extremely small, and consist of a slight decrease in HCA precipitation kinetics and of a reduced apatitic layer thickness. This is due to the fact that DMEM's organic molecules can adsorb onto the granules of bioactive glass, thus hindering a little the dissolution and precipitation processes that take place on their surfaces upon immersion in simulated biological fluids.

5.1.2: Our interaction protocol

The doped glasses' bioactive behavior has been tested by immersion of appropriate amounts of powders in appropriate volumes of DMEM for various interaction delays; in particular, the assays were performed inside closed disposable polyethylene 50mL bottles (obviously, one for each time interval of each different glass composition), kept in an oven at a constant temperature of 37°C (more or less the same as the human body) and manually shaken several times a day to avoid localized concentration effects.

Since the main interest of this work is to prove that site selective luminescence spectroscopy is capable of detecting HCA formation even after just a few hours of interaction, the delays we decided to study were: **1 hour, 6h, 12h, 1 day, 2d, 3d, 4d**; therefore, each type of glass required a series of 7 bottles to be tested. To obtain in practice such samples, one can exploit two principal approaches:

- Start all the biological interactions of a series at the same time: this way any possible degradation of the DMEM caused through time by biological contamination or oxidation of the solution is completely avoided;
- End all the biological interactions of a series at the same time: this way all the liquids deriving from bioactivity tests can be analyzed via ICP-AES in one shot.

Due to the fact that the employed ICP-AES instrument was not located in the same department of our laboratory, and to the fact that it was impossible to use it "at will", but we needed to reserve analysis time in advance, we were forced to follow the second method.

On the other hand, since we had to work with materials under the form of powders to be able to carry out a series of characterizations with the existing equipment, a serious problem arose regarding our luminescent probe's validity: biomineralization during interaction with

[1] D.C. Clupper; J.E. Gough; M.M. Hall; A.G. Clare; W.C. LaCourse; L.L. Hench; *Journal of Biomedical Materials Research Part A* **2003**, *67A*, 285-294.

biological media is fundamentally a surface driven process[2], and our samples do have different specific surface area values (see Par. 4.3.3), owing to their different compositions, so they naturally would react with DMEM at different rates and thus to different final extents.

Moreover, bioactivity tests, besides yielding biomineralized samples to be studied via site selective luminescence spectroscopy and other techniques, are also meant to identify the effects of the dopant alone on leaching, hydrolytic resistance and HCA formation for probe validation purposes, so, in order to make well grounded comparisons between results belonging to different glasses, we had to design some strategy that could allow us to isolate the contribution of the increasing Eu concentrations from that of the different surface areas.

To solve this issue at the best of our possibilities, we used the same solution exploited by other researchers of the team (see ref. [23] and [49]) as well as by some other famous academics (see for example ref. [31] by Rehman, Bonfield and Hench), that is we tailored the amount of glass powders and the volume of DMEM[3] in order to always achieve a fixed ratio between total surface area of the sample and volume of liquid. In particular, with the purpose of exploiting the data already gathered by the group on undoped bioactive glasses, we calculated the weight of powder to be put into each interaction bottle by using the following simple formula, extracted from J. Lao's PhD thesis (ref. [49]):

$$\mathbf{M_{glass} = 500 \cdot (V_{DMEM}\ [in\ mL] / Specific\ Surface\ Area\ [in\ m^2/g]) \cdot 10^{-4}}$$

We recognize that this approach might be considered questionable, so a critics on it will be developed in depth inside the next paragraph. In the following table we report the combinations weight of powder / volume of DMEM we actually used in bioactivity tests:

	B67,5 1st syn	B67,5 2nd syn	B67,5 Eu1 1st calc	B67,5 Eu1 2nd calc	B67,5 Eu5	B67,5 Eu10	Molari
Surf. Area	225 m^2/g	64 m^2/g	66 m^2/g	184 m^2/g	131 m^2/g	113 m^2/g	49 m^2/g
Combination	110.9 mg 500 mL	31.18 mg 40 mL	30.24 mg 40 mL	16.27 mg 60 mL	19.08 mg 50 mL	22.04 mg 50 mL	40.55 mg 40 mL

Tab. 5.3: Experimental parameters used for our bioactivity tests

[2] Because, as already said in Chap. 1, the actual amount of surface available for ionic exchange and nucleation & growth processes deeply influences the kinetics of apatite precipitation.

[3] This latter, however, was limited by the capacity of the container, and thus was almost always kept equal to 50mL, except for the cases when "extreme" specific surface area values would have yielded too little or too big values for the weight of the powders.

As it can be easily noticed, not all the synthesized glasses have undergone *in vitro* biomineralization assays: since these tests and the consequent characterizations are both expensive and time consuming, we chose to perform biological interactions only for the base bioactive glass and for three samples respectively at low ($1\%_{wt}$), medium (5%) and high (10%) doping degrees.

However, a few exceptions were made: since it was impossible to carry out ICP-AES characterizations on the B67,5 Eu1 1st calc series due to a malfunction of the instrument in the date scheduled for the analyses, and since the available amount of said powder was not enough to perform a second test, the interactions for the 1% dopant concentration were repeated also on a newly calcined material: B67,5 Eu1 2nd calc. Therefore, while all the FTIR, Raman, luminescence, etc characterizations have been carried out on post-interaction powders of the first test, ICP-AES data refer to post-interaction DMEMs of the second series.

Moreover, in order to have enough biomineralized material for XRD analyses, a considerable amount of B67,5 Eu5 (190.8 mg in 500 mL of DMEM) and of B67,5 powders (110.9 mg of 1st synthesis glass in 500 mL of fluid) has also been tested. In particular, for this latter composition we had the possibility of choosing between powders deriving from the first (SSA = 225 m^2/g) or from the second (SSA = 65 m^2/g) synthesis; since our aim was to compare their diffraction patterns to B67,5 Eu5's ones (SSA = 131 m^2/g), we decided to test the powders with higher specific surface area value.

The exploited interaction protocol described in full detail consists of the following points:

1. Each and every vessel used in the test is marked with the name of the sample it will contain (both type of glass and interaction delay); in particular, it is necessary to prepare and classify for each glass composition: 7 PE 50mL Nalgene® bottles, in which the assay itself is carried out; 7 Eppendorf caps, where powders are collected after interaction; 7 tiny 10mL glass bottles, where an aliquot of post-interaction DMEM is stocked, in order to be successively analyzed via ICP-AES;
2. An appropriate amount of powder, calculated using the above reported formula, is weighed and put inside each PE bottle;
3. Depending on the scheduled hour and date for the delivery of liquid samples to the ICP-AES analysis center (and keeping into account the time needed to practically recover each biomineralized glass from its solution), at the right time each interaction with biological medium is started by pouring into the bottle the required volume of DMEM

(usually 50mL); for this operation, carried out under aspiration hood, an Eppendorf pipette with carefully Ethanol-cleaned disposable tips is used.

4. The filled bottle is tightly closed, vigorously shaken and put inside an oven at 37°C, where it is left for the required amount of time, periodically agitated to prevent localized concentration effects.
5. When the interaction delay has expired, the bottle is withdrawn from the oven, and an aliquot of DMEM is collected with a pipette from the top of the solution (to avoid aspiration of powder grains, located mainly on the bottom part of it) and poured into the corresponding 10mL glass bottle.
6. The pH of the interaction medium is quickly measured using a pH-meter;
7. Using another pipette, the biomineralized powders are withdrawn from the solution and put inside the correct Eppendorf cap, where they are centrifuged at 3000 rpm for a few seconds; the residual DMEM is eliminated from the cap and the powders are then redispersed and rinsed in ethanol.
8. Finally, the powders are centrifuged again, the excess ethanol is eliminated and the Eppendorf cap is put inside an oven at 37°C for drying purposes.

At the end of this procedure, 7 liquid samples of post-interaction DMEM and 7 samples of post-interaction biomineralized powders are obtained for each tested glass composition.

5.1.3: Drawbacks of the employed method

The first critic one might express about our interaction protocol is that it is far from being adequate from the technical-biological point of view: even though the utmost attention and care were paid in cleaning bottles and pipette tips, though we always worked under aspiration hood, etc., nevertheless we operated in a chemistry lab, where obviously sterile equipment (gloves, vessels, spatulas, pipettes, etc) is not available; we employed a common oven, normally used for drying lab glassware, instead of a dedicated incubator; we shook manually the bottles instead of using a continuous mechanical device, etc. However, even if this critic is grounded, what we did was actually the best we could do with our available resources.

Another interesting criticism might be that we started the various interactions of each series at different times: it would have been far better to start them all together, and to stop each one after the right delay, because DMEM deteriorates slightly over time once its bottle is opened, even if it's stocked in the fridge. For example, the solution's pH passes from 7.44 (just after

the removal of the seal) to 7.78 after two days and 7.86 after three days, so this means that some alterations take place within the liquid, maybe due to oxidation processes, maybe due to bacterial contamination. However, since we couldn't perform ICP analyses at will[4], this method was out of discussion, and we were forced to make all the interactions end at the same time.

The most important drawback of our protocol, however, lies in its unavoidable sensitivity to the specific surface area (SSA) value of the samples: in fact, keeping a constant S_{tot} / V_{DMEM} ratio can only help compensating little differences, and works mainly for ICP analyses, but with very distant SSA values the alterations in biomineralization kinetics become too significant to be balanced. Let's explain this point in better detail.

From a theoretical but simplistic point of view, at least for what concerns the leaching behavior the "constant ratio trick" should work: in fact, even if wider surfaces release more ions because they are more easily attacked by the liquid phase, compensating this effect by increasing the volume of biological medium should yield comparable final ionic concentrations (i.e. amount of ions / volume).

This argument, however, neglects a series of issues that might happen:

- Specific surface area values are determined from nitrogen adsorption measurements, and from those values we calculate the total surface of the powders we put inside the interaction bottles; however, we don't know whether the biological medium can infiltrate the interconnected porosity to the same extent N_2 molecules can, or not, therefore we don't know either if the whole calculated surface actually interacts with DMEM or, more likely, only a part of it is interested in biomineralization processes. This way, the calculated S_{tot} / V ratio might be different from the actual one, since the "effective surface" might be smaller than the BET-derived S_{tot}.
- Our approach neglects the possible evolution of porosity with interaction time: some pores might become initially wider due to glass network dissolution, while, later, others might be blocked by the growing Ca-P amorphous layer and HCA crystals. Evidently, these effects cannot be easily quantified, so keeping them into account in a formula or in the protocol is practically impossible.

[4] Moreover, due to the high ionic concentrations of our samples, a costly and time consuming thorough cleaning process of the instrument was necessary after each batch of analyses.

- Samples with different total pore volumes, or pore sizes, or pore shapes, or pore tortuosities might experience different solution stagnation effects, which in turn influence in a non-negligible way the overall ionic releases.
- The leaching process in a sample with high SSA receives a considerable surface-induced kinetic boost if compared to what happens in a glass with low SSA, therefore their ionic releases will be different not only in their absolute values, but, above all, in their timing: i.e. a powder with high SSA reaches a certain degree of ionic release way before than a sample with low SSA, and this effect cannot be compensated by the "constant ratio trick".

Summarizing, it appears evident that keeping a constant ratio between total surface of the sample and volume of DMEM can help us in compensating the differences in SSA values existing between our powders, but cannot eliminate them; therefore, ICP-AES data on ionic release can be rigorously compared only between pairs of samples having close SSA values (for example B67,5 Eu5 with B67,5 Eu10; and B67,5 2nd syn with Molari).

As regards HCA biologically-induced precipitation, the effects brought about by diversities in SSA are completely unavoidable and unbalanceable: more surface yields more nucleation sites and more space for crystal growth, therefore the amount of HCA formed (and its rate) is highly dependent on the total surface of the sample[5]. Therefore utmost care must be paid in the interpretation of results provided by characterization techniques.

All of this said, even with all these issues, yet we believe that, by paying attention to the correct interpretation of data, our interaction protocol can provide us useful information on our samples. On the contrary, better comparable results would have surely been obtained if we had tailored each time the synthesis protocol in order to create powders with identical SSA values, that's true, but this way we would have completely lost reproducibility in the syntheses, and therefore those rigorous results would have yielded no information about the modifications intrinsically induced in our bioactive glasses by the dopant, because further extrinsic and unaccountable alterations would have been introduced.

[5] In our case, with our fixed S_{tot} / V ratio value, ions contained in DMEM were never a limiting condition for precipitation, that is they were never completely depleted.

5.2: Site selective luminescence spectroscopy analyses on post-interaction samples

Before starting to describe the path we followed in the exploration of our luminescent structural probe's potential, we have to warn the reader that in the following pages he won't find almost any complete (covering the "usual" range 200 ÷ 550 nm, as in most literature about Eu^{3+}) excitation spectrum of our samples. This is due to an exceptional dose of bad luck with the Xe lamp used as excitation source in the measurements, which actually worked only for one afternoon in six months, the rest of the time remaining out of order. We anticipate also that in the following paragraphs we won't present our data in a strictly organized way, but, on the contrary, we will really describe almost in a chronological way the little discoveries that, step by step, led us to the demonstration of the validity of our probe. For more information on the experimental set-up or on the characterization technique itself, please refer to Chapter 3.

5.2.1: Emission spectra with excitation in the $^5D_2$ level

Due to the above mentioned impossibility of performing excitation analyses on our biomineralized samples, we started out with emission luminescence measurements by trying to selectively excite Eu^{3+} ions located inside the amorphous glass network; to do so, we referred to an excitation spectrum (reported in Fig. 5.1) previously acquired by another member of the team on a B67,5 Eu5 composition by monitoring the emission of the $^5D_0 \rightarrow {}^7F_2$ transition (i.e. λ_{obs} = 614 nm).

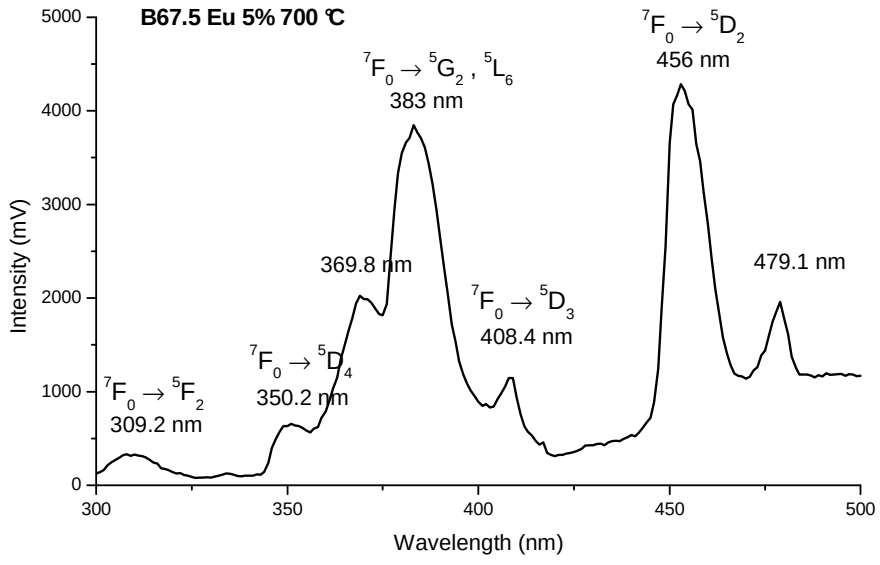

Fig. 5.1: Excitation spectrum of a B67,5 Eu5 glass calcined at 700°C (λ_{obs} = 614 nm)

Since the synthesis of this latter glass was carried out following our very same protocol, we hopefully made the hypothesis that the excitation wavelengths remained identical also in our case; in the following pages we will see that this is not completely true (see Par. 5.2.4), but the little mismatch between λ was highly providential, since it allowed us to detect also a faint emission from Eu^{3+} ions inside apatitic crystals.

In order to reach the maximum possible emission intensity, we decided to excite the samples in the $^5D_2$ level, at 456 nm (highest peak in Fig. 5.1); as already said in Chapter 3, however, the main emitting level of Eu is the $^5D_0$, and in fact what actually happens upon excitation in the $^5D_2$ is that the excited electrons non radiatively relax to the $^5D_0$, and thence they return to one of the levels of the ^7F_j (j = 0 .. 6) fundamental manifold by emission of a luminescence photon (and this latter emission is the one we detect; see red arrows in Fig. 5.2).

However, emission from the $^5D_2$ as well as non radiative relaxation to the $^5D_1$ and then radiative desexcitation to the ^7F_j manifold are also possible, even though much less probable, and therefore their detectable intensities are much much lower.

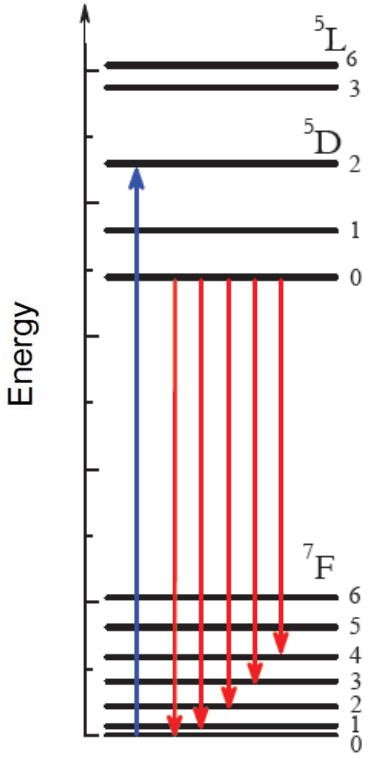

Fig. 5.2: Simplified energy level scheme of Eu^{3+} ions

To obtain a 456 nm beam with our dye **laser** we had to employ the Anti-Stokes 1 beam of its H_2 Raman cell attachment; in particular, the exploited settings were as follows:

- Pumping laser: pulsed frequency doubled Nd:YAG (532 nm).
- Dye solution: pure Rhodamine 590.
- Laser fundamental: **564.5 nm**; this is the wavelength of the beam at the exit of the dye laser, that is before it enters the Raman cell.
- H_2 Raman cell beam selection: **Anti-Stokes 1** (shift of +4155 cm^{-1}) → **456 nm**; this beam is separated from the four other components (i.e. fundamental, Stokes 1 and 2, Anti-Stokes 2) coming out of the Raman cell by means of multiple dispersion prisms (Pellin Broca prisms), and is focalized and directed onto the sample by means of focusing lenses.
- Degree of focalization: high, in order to compensate as much as possible for the low

intensity of the Anti-Stokes beam.

To **detect** the emission of our samples we used a Jobin-Yvon HR1000 monochromator coupled with a Hamamatsu R1104 photomultiplier and with a EG&G PAR 162/164 Boxcar Averager (to perform time-resolved spectroscopy analyses), exploiting the following settings:

- Analysis range: 550 → 712 nm.
- Lambda step: 0.325 nm.
- Photomultiplier voltage: 800 V.
- Variable resistance: 100 kΩ.
- Acquisition delay from front laser pulse: 60% of 2 ms.
- Integration gate interval: 5 ns.
- Temperature: room temperature.

Since the available excitation data were acquired from a B67,5 Eu5 pre-interaction glass, the described analytical setup was first employed to analyze our B67,5 Eu5 series of biomineralized samples; the resulting emission spectra are reported in Fig. 5.3. In particular, being interested in the evolution of the relative intensities of the various transitions, we have normalized the spectral data to the intensity of the $^5D_0 \rightarrow {}^7F_4$ peak, whose detected height is practically independent from the interaction delay.

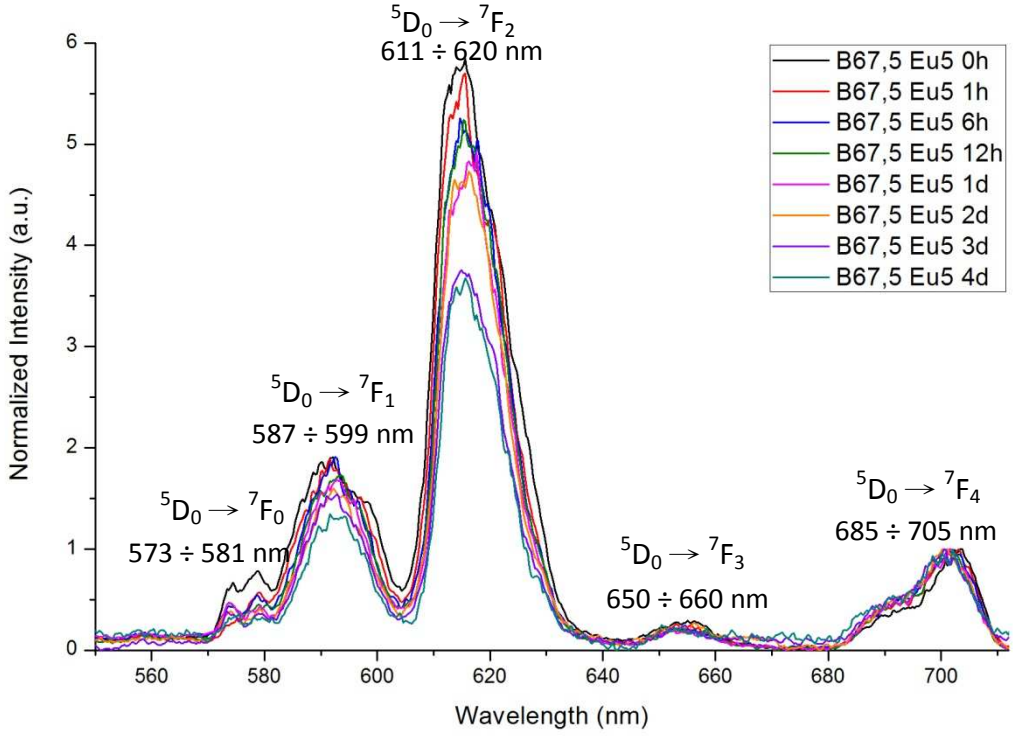

Fig. 5.3: Global emission spectra acquired for the B67,5 Eu5 biomineralized glasses series with excitation in the $^5D_2$ level, at 456 nm

First of all, the obtained spectra certainly bear the distinctive mark of Eu^{3+} ions located inside an amorphous matrix: in fact, we detected the typical wide emission bands caused by inhomogeneous broadening, and their positions and relative intensities are perfectly consistent with what is published in literature about Eu doped bioactive glasses (see ref. [4], [10], [20])

From the reported plots and, above all, from absolute curves (not shown), we can easily notice a global lowering in the emission intensity with interaction time, which is perfectly consistent with the fact that Eu ions are progressively leached from the bioactive glass network; from ICP-AES data we will also see that they do not remain in solution, but, on the contrary, they are quickly depleted, which means that during interaction with biological media Eu is increasingly incorporated inside the amorphous calcium phosphates layer and inside the HCA crystals (as we will demonstrate later) in development on the surface of the powders.

In fact, it is reasonable to state that in these two latter phases Eu ions occupy sites significantly different both in site symmetry and crystal field intensity from those present in the silicate amorphous network, and thus their $^7F_0 \rightarrow {}^5D_2$ transitions shift to different energies due to different Stark splittings of both the manifolds; therefore, Eu ions in HCA and Ca-P layer are no more effectively excitable at 456 nm, and thus the global intensity of the detectable emission becomes lower and lower with interaction delay.

A decrease in emission intensity is also consistent with the formation of a highly silanol-rich silica gel layer on the surface of the grains (just below the Ca-P and HCA layer) owing to ionic exchanges between glass and biological medium (see Chap. 1): the increasing amount of luminescence-quenching −OH groups renders non-radiative desexcitation routes more probable, and thus the REE emission intensity becomes increasingly lower.

Another interesting characteristic of the acquired spectra is that the relative intensity of the $^5D_0 \rightarrow {}^7F_2$ peak decreases with bioactivity testing time; in literature this transition is reported to be hyper-sensitive to the degree of symmetry of the CF (high asymmetry, like in crystals, yields high intensity; and *vice versa*), so this might mean that the progressive break-up of the glass network consequent to the interaction with H_2O and OH^- molecules of DMEM renders the amorphous lattice increasingly disordered, and thus, increasingly symmetric (i.e. we move towards compensation isotropy).

The most important spectral feature we can identify in the curves of Fig. 5.3, however, is the couple of peaks at around 574 and 579 nm, within the typical wavelength range of $^5D_0 \rightarrow {}^7F_0$

transitions: as previously said in Chapter 3, the 0 → 0 transition is non degenerated, thus it manifests itself with one single peak for each different emitting site present in the sample; the detection of two perfectly resolved peaks in that high energy region of the spectra clearly indicates the existence of Eu ions occupying two different sites, both somehow excited by the incident 456 nm laser, but emitting at slightly different wavelengths.

Intrigued by this double peak, we decided to repeat the emission measurements by focalizing our attention only on the $^5D_0 \rightarrow {}^7F_0$ and $^5D_0 \rightarrow {}^7F_1$ transitions; in particular, the new settings used for this batch of analyses were:

- Analysis range: 570 → 605 nm;
- Lambda step: 0.075 nm;
- Photomultiplier voltage: 950 V;

(all the parameters not cited above remained unchanged), and the obtained spectra are reported in Fig. 5.4; for clarity purposes, the curves have been normalized to their maximum intensity and presented adding a certain offset between them.

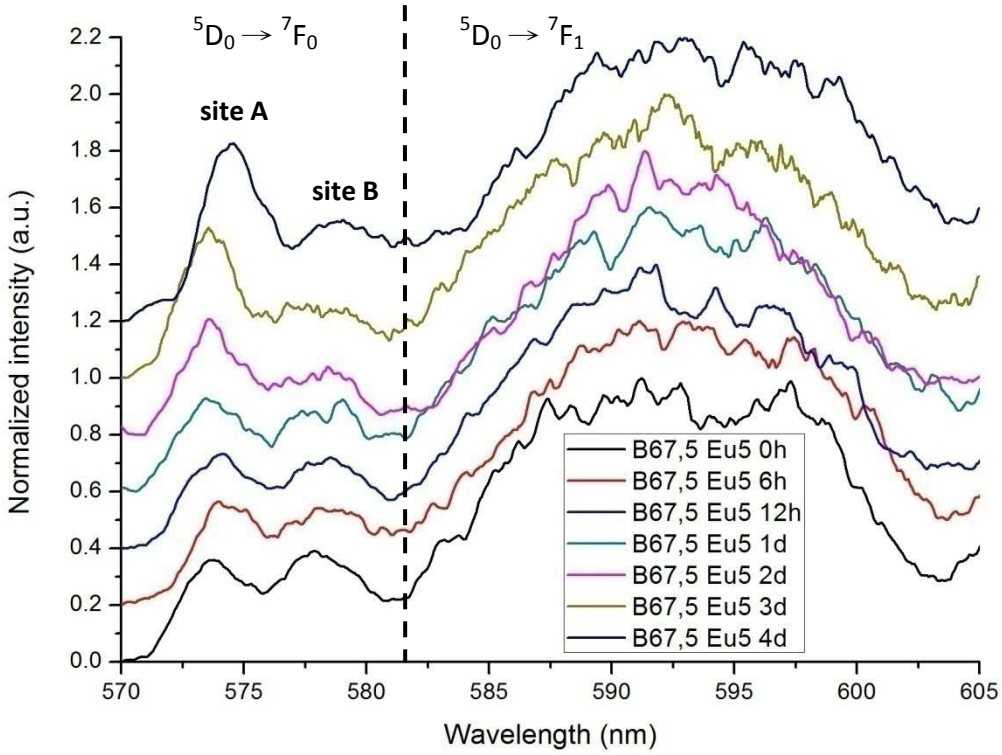

Fig. 5.4: Emission spectra acquired from post-interaction samples of the B67,5 Eu5 series (λ_{exc} = 456 nm); zoom on the $^5D_0 \rightarrow {}^7F_0$, $^7F_1$ transitions

This time the presence of two different peaks at around 573 ÷ 574 and 577 ÷ 579 nm is clearly evident, and it is also straightforward to notice a trend in their relative intensities: the

peak at 574 nm becomes progressively higher than the one at 579 nm with increasing interaction delay. This means that the phase where Eu occupies the site responsible for the 574 nm emission (site A) becomes more and more abundant with increasing bioactivity testing time. Moreover, a difference in emission wavelengths of as much as 4 ÷ 5 nm is very high, which means that the crystalline fields in which Eu ions are embedded inside the two sites are radically different.

Now, a feature like this was exactly what we hoped to detect in order to demonstrate the effectiveness of our structural luminescent probe, since a similar behavior is perfectly consistent with our hypothesis of Eu entering inside the precipitated HCA crystals (that indeed grow with interaction time): in fact, if the emission at 574 nm was actually connected with Eu in HCA (and in the following pages we will demonstrate so), then the increase in peak intensity would be the tangible sign of the biologically induced growth of an apatite incorporating Eu^{3+} ions, and therefore these latter could actually be considered a useful tool in detecting and quantifying biomineralization processes in bioactive glasses.

Before going on with the discussion, we need to point out a few things:

- A low 574 nm peak is present also in the spectrum acquired from the as-synthesized B67,5 Eu5 glass (i.e. before bioactivity testing; black curve in Fig. 5.4); this is consistent with the slight devitrification of Eu doped apatitic phases upon calcination at 700°C showed and discussed in Chapter 4.
- The only detected peak belonging to Eu:HA here is connected to the $^5D_0 \rightarrow {}^7F_0$ transition (574 nm); as we have already stated in Par. 4.1.2, and as we will experimentally see in Paragraph 5.2.3, this is due to the peculiar point group symmetry of the site occupied by Eu in the HCA lattice, which renders the $0 \rightarrow 0$ transition allowed and thus the most intense of the emission spectrum.
- The intensity of the site A $^5D_0 \rightarrow {}^7F_0$ peak is very low not only because the excitation was site selective towards site B (Eu^{3+} in glass), but also because our analytical settings enhanced the detection of luminescence signals arising from slow emitters, like Eu ions occupying type B sites. In fact, site A emission has, as we will see in the following pages, a much faster decay lifetime than site B's (approximately 0.45 ms VS 1.28 ms of site B) so the intensity detected after 1.2 ms (our acquisition delay from the laser pulse) is way lower than it was at the beginning.

Now, even though the faint peak at 574 nm exhibits a series of features that induce us to

believe it is connected with Eu doped HCA, it has also very low intensity upon excitation at 456 nm, so it results of very little use for a characterization, especially if our ultimate purpose is to derive quantitative information from the spectra; on the other hand, it is also true that in the preceding analyses we tuned our laser in order to selectively excite in their $^5D_2$ level the Eu ions located inside the amorphous glass (site B), and thus necessarily the emission from Eu ions occupying different sites could not be other than faint.

Therefore, in order to enhance the emission of the phase responsible for the 574 nm peak, and thus to be able to better identify its complete spectral signature (i.e. all of its peaks), we needed to find a way to selectively excite it, that is, in practice, we needed to find the correct value of lambda for our laser. From a theoretical point of view, achieving this result is very simple: it's just a matter of acquiring a complete excitation spectrum by monitoring the emission at 574 nm.

In practice, however, without the appropriate equipment (unfortunately the Xe lamp of the instrument was broken at that time), overcoming this issue became much more challenging, especially if we wanted to excite Eu ions in their most emissive level: our dye laser's wavelength was tunable over a small range of lambdas (around 30 nm), centered on the fundamental of the selected dye, therefore a complete excitation spectrum could have been obtained by merging a lot of localized 30-nanometers-wide excitation spectra, acquired using different dyes to cover all the spectrum. Nevertheless, a similar procedure would have been considerably time consuming, and moreover would have required compensation for the different intensity outputs obtained with different dyes.

Therefore, we decided to act in a different, more cost-effective way: instead of searching the most emissive one, we went for the level whose energetic whereabouts were approximately known, i.e. the $^5D_0$; in fact, since the transition from $^5D_0$ to $^7F_0$ takes place with emission of a quantum of radiative energy at around 574 nm, and since the Stokes effect[6] in REE luminescent centers is limited, then exciting our samples at around 574 nm should yield the exactly inverse transition, that is $^7F_0 \rightarrow {}^5D_0$; and once the luminescent centers occupying type A sites are selectively promoted into their fundamental excited state ($^5D_0$), selective site A emission by radiative desexcitation towards the ^7F_J manifold would be detectable.

[6] Eu's spectroscopic levels are all deriving from 7f orbitals, so the configurational coordinate change upon transition between them is practically negligible; therefore, when excitation brings an electron in the $^5D_0$ level, there is practically no need of non-radiative relaxation prior to fluorescence emission, and thus the λ of the emitted photon is almost coincident with the wavelength of the previously absorbed exciting quantum.

This approach surely allows to selectively excite Eu ions occupying either type A and/or type B sites (if we tune the laser at 579 instead of 574 nm), thus permitting to detect the specific spectral signature of the two different crystalline fields, but obviously has the big drawback of unavoidably losing any information about the $^5D_0 \rightarrow {}^7F_0$ transition, whose intensity is completely masked by the scattered component of the incident laser beam light.

5.2.2: Emission spectra with site selective excitation in the $^5D_0$ level; part 1

In order to maximize the emission intensities not only from a site selective, but also from a global point of view, for this new batch of analyses we changed many of the experimental settings; some modifications were also made with the purpose of obtaining spectra as much quantitatively comparable as possible. In particular, for the **laser**:

- Dye solution: mix Rhodamine 610 + Rhodamine 590 (respectively 30% and 70%$_{vol}$); with this combination we centered the maximum output intensity right at 579 nm.
- Laser fundamental: either **574** or **579 nm**.
- H_2 Raman cell beam selection: this time the Raman cell was useless, since we had no need of shifting our beam's wavelength, therefore it was excluded; this yielded a far more intense incident laser, thus allowing for less amplification of the signal.
- Degree of focalization: very low; we tried to obtain a laser "spot" more or less as broad as the target (a circle with 3 mm diameter), so that the unavoidable little displacements of the sample holder from measure to measure[7] would cause only negligible changes in the focalization of the beam, thus allowing us to achieve quantitatively comparable results.

As for what concerns the **detection**:

- Analysis range: 570 → 720 nm.
- Scansion step: 0.30 nm.
- Photomultiplier voltage: variable between different series of samples and different laser wavelengths:
  600 V for B67,5 Eu5's series with laser at 574 nm;
  500 V for B67,5 Eu5's series with laser at 579 nm;
  500 V for B67,5 Eu10's and Molari's series with laser at 574 nm;
  400 V for B67,5 Eu10 with laser at 579 nm;
  700 V for B67,5 Eu1's series with laser at 574 nm;
  600 V for B67,5 Eu1's series with laser at 579 nm;

[7] To place the sample inside the optical set-up exploited for the emission measurements it was necessary to physically remove from its support the sample holder; therefore, each time this latter was put again in its working place, a little mismatch with the previous position was possible.

- Variable resistance: 10 kΩ.
- Acquisition delay from front laser pulse: 27,25% of 1 ms; this way we can detect with high efficiency both slow (Eu in site B) and relatively fast (Eu in site A) emitters.

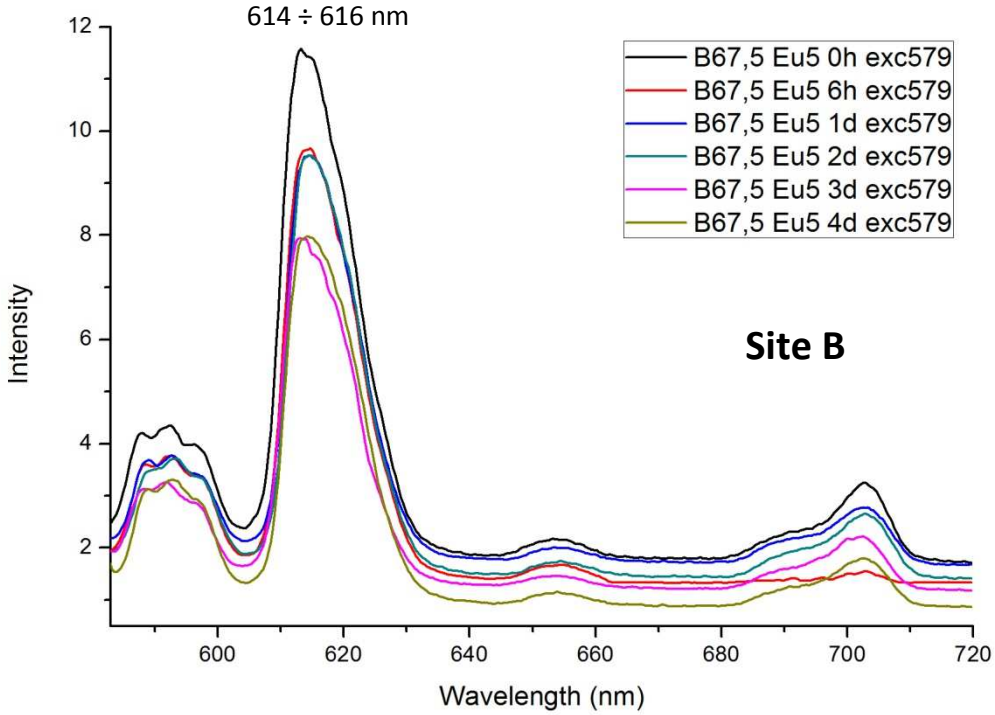

Fig. 5.5: Emission spectra acquired from post-interaction samples of the B67,5 Eu5 series upon excitation in the $^5D_0$ level of site B Eu ions (λ_{exc} = 579 nm; no offset)

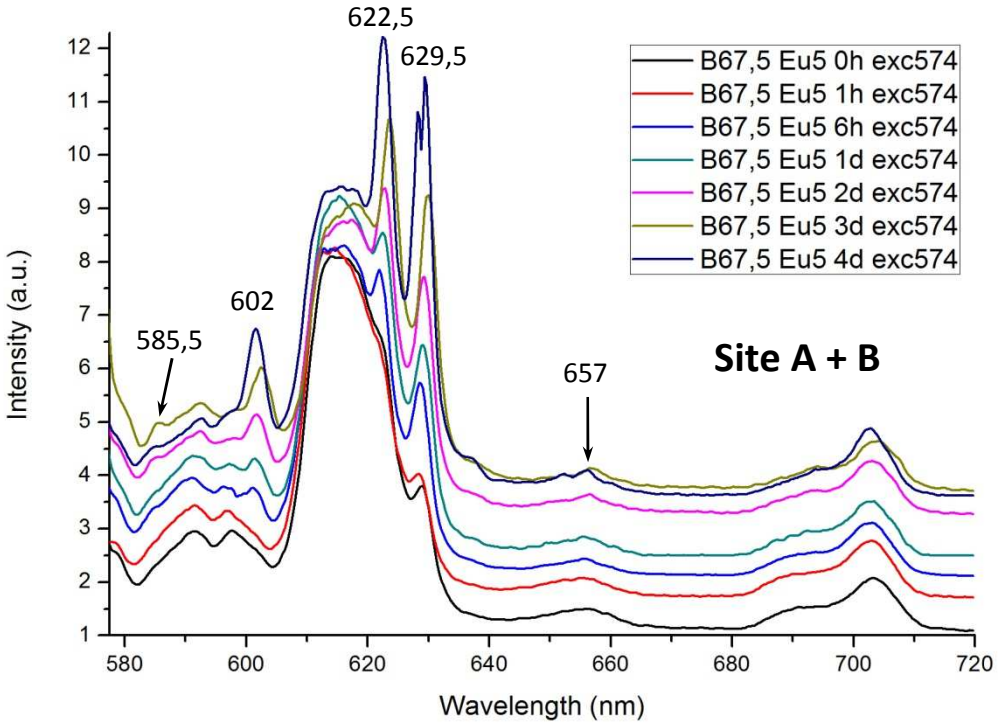

Fig. 5.6: Emission spectra acquired from post-interaction samples of the B67,5 Eu5 series upon excitation in the $^5D_0$ level of site A Eu ions (λ_{exc} = 574nm; with offset)

With such experimental parameters we analyzed first the B67,5 Eu5 biomineralized glasses series, for which we already knew the correct excitation wavelengths to be used; then we extended this approach to the B67,5 Eu1 series and eventually also to a small part of the B67,5 Eu10 and Molari series (but we will discuss these data in detail in Par. 5.2.5). The emission spectra acquired from post-interaction B67,5 Eu5 samples have been reported in Fig. 5.5 for selective excitation at 579 nm (site B), and in Fig. 5.6 for selective excitation at 574 nm (site A); no normalization of the data has been done.

As it is clearly evident, for what concerns the emission arising from Eu ions occupying type B sites, nothing different can be noticed from Fig. 5.5 with respects to what we already saw in Fig. 5.3 (always the same broad bands, in the same positions and with the same intensity ratios), whereas Fig. 5.6 is overflowing with new information on the phase containing type A sites. While in Fig. 5.3 the sole 574 nm peak appeared for the already mentioned reasons, thanks to site selective excitation and to the faster detection time interval it is now possible to appreciate the full spectral signature of site A Eu ions, though overlapped with site B's one.

In particular, the phase containing type A sites is manifestly crystalline, since the emission from Eu ions located inside it exhibits characteristic narrow, well resolved peaks at: **574** (not shown in Fig. 5.6 because masked by the laser; but it was evident in Fig. 5.3 and will appear also in Par. 5.2.3), **602**, **622.5** and **629.5 nm** (maybe it has also some minor peaks at 585.5 and 657 nm). Moreover, as already noticed in the previous paragraph, it clearly registers a gradual development with interaction time, since the above listed peaks become progressively more intense for longer delays; in particular, most probably said development involves both the growth of the crystals and an improvement in their crystallinity degree, as testified by the resolution of the two convoluted peaks at around 629.5 nm possible for the B67,5 Eu5 4days sample (dark blue in Fig. 5.6).

Once again, a behavior like the one we've just described would be perfectly consistent with the identification of the phase containing type A sites with HCA, since this latter crystal is known to actually grow on the surfaces of bioactive glasses during *in vitro* biological testing, and to attain increasing mean size and degree of crystallization with interaction time. In the next section (5.3) we will report a series of complementary evidences, gathered through various characterization techniques, that will support this attribution, showing that HCA crystals precipitating on our samples actually exhibit the same trend as the one detected via site selective luminescence spectroscopy.

Another important fact to be noticed is that in the case of Fig. 5.5, excitation was rigorously site B selective, and thus only the typical emission of Eu ions inside an amorphous environment was detected; this, by the way, was absolutely obvious, since the energy of a laser beam at 579 nm (λ_{exc} for site B measures) is clearly not enough to excite site A Eu ions, which require at least a λ_{exc} = 574 nm.

On the contrary, in the case of Fig. 5.6, together with site A Eu ions we excited also a part of type B luminescent centers, therefore the resulting emission spectra show the overlap between features characteristic of site B (broad bands) and site A (sharp peaks). This effect is due to two main reasons: first, a radiation at 574 nm has enough energy to excite also centers having λ_{exc} = 579 nm; and second, as we will see from excitation spectra, site B's $^7F_0 \rightarrow {}^5D_0$ excitation band is very wide, due to inhomogeneous broadening; therefore a laser at 574 nm is capable of exciting also site B centers, even though with less effectiveness than a beam at 579 nm, as testified by the need of a higher PM tension to obtain a good signal.

5.2.3: Localized excitation spectra in the $^7F_0 \rightarrow {}^5D_0$ transition range

Now, once identified the distinctive features of the emissions of Eu ions occupying type B and type A sites, we decided to perform some localized excitation measurements to verify that promotion of electrons from the $^7F_0$ to the $^5D_0$ level actually took place upon absorption of photons having the very same wavelengths (579 for site B and 574 nm for site A) as the ones we exploited for the acquisition of our emission spectra.

To practically achieve this without proper equipment, we employed the same optical set-up used for the collection of emission spectra (dye laser as excitation source + monochromator + boxcar + photomultiplier as detector), but this time we continuously changed the incident beam's wavelength by scanning the whole range allowed by the radiant dye (compatibly with maintaining the beam intensity within reasonable constancy limits; **570 → 595 nm**), while contemporaneously fixing the detection at:

- $\lambda_{observed}$ = **616 nm** for Eu ions occupying **type B** sites; this lambda was chosen because in its correspondence we register the highest type B emission band (see Fig. 5.5); in this case the photomultiplier's tension was set at **500 V**.
- $\lambda_{observed}$ = **629.5 nm** for Eu ions located in **type A** sites; this time the most intense emission would actually be at 622.5 nm, but this latter peak is too close to 616 nm, where a type B-characteristic band is located; on the contrary, the peak at 629.5 nm, besides

being quite intense too, is also less overlapped with site B's $^5D_0 \rightarrow {}^7F_2$ broad band[8], and thus yields more selective information; for these analyses the PM was set at **600 V**.

The acquired excitation spectra are reported in Fig. 5.7 for Site B and Fig. 5.8 for Site A.

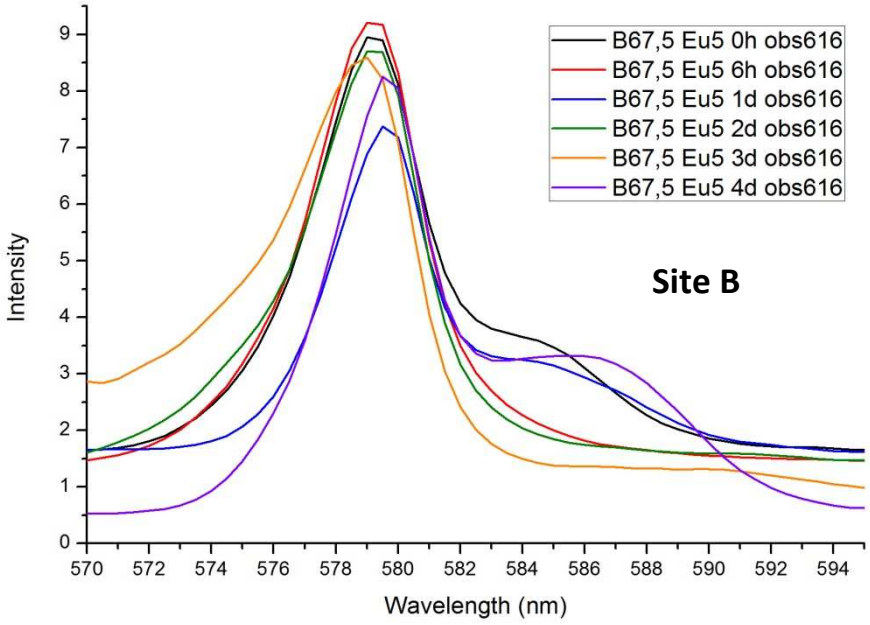

Fig. 5.7: Localized excitation spectra acquired from post-interaction samples of the B67,5 Eu5 series upon observation of site B's $^5D_0 \rightarrow {}^7F_2$ emission band (λ_{obs} = 616 nm)

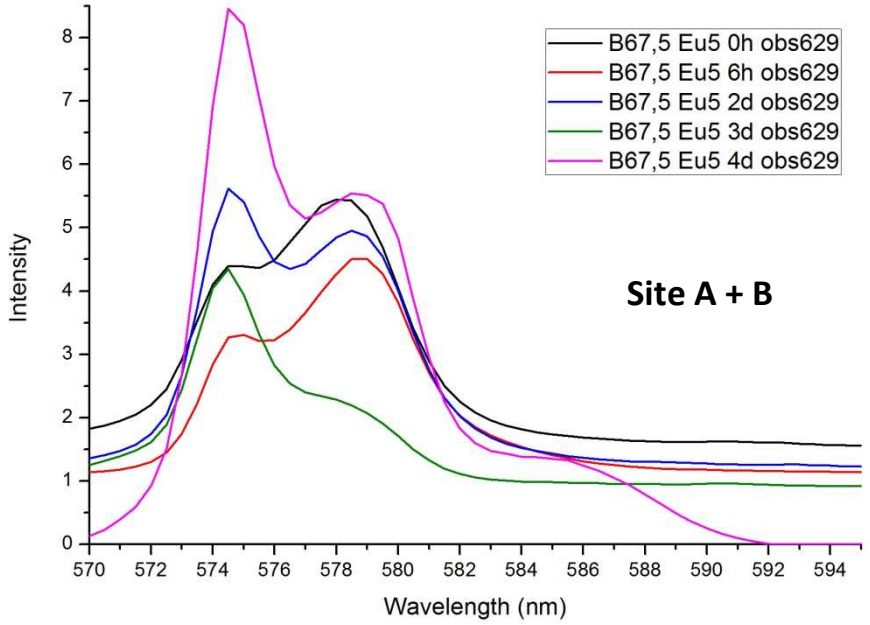

Fig. 5.8: Localized excitation spectra acquired from post-interaction samples of the B67,5 Eu5 series upon observation of site A's 629.5 nm emission peak

[8] We might say that type A 622.5 nm peak stands on the "right shoulder" of type B's $^5D_0 \rightarrow {}^7F_2$ band, while type A 629.5 peak stands at its "right foot"; therefore, this latter peaks gives us more specific information on site A.

Fig. 5.7 confirms that for Eu ions located inside the amorphous silicate network (site B) the transition from the ground $^7F_0$ state to the excited $^5D_0$ state takes place upon absorption of a quantum of radiative energy having a wavelength of 579 ÷ 579.5 nm.

In turn, from Fig. 5.8 we can notice a few interesting things:

1. Since in correspondence of the observation wavelength we have both the foot of site B's $^5D_0 \rightarrow {}^7F_2$ emission band and a site A's characteristic peak, the excitation spectra show both a site A $^7F_0 \rightarrow {}^5D_0$ absorption peak at 574 ÷ 574.5 nm and a site B broad band centered at around 579 nm;
2. In the beginning (0h, 1h, 6h), when site A's characteristic emission at 629.5nm is almost negligible (in Fig. 5.6 we can only see tiny peaks emerging from the amorphous bands), the excitation peak at 574 nm remains just a shoulder of the 579 nm band (red and black curves in Fig. 5.8);
3. For longer interaction delays the peak at 574 nm progressively increases in intensity over the band at 579 nm, which means that, as already inferred from emission spectra, the number of Eu ions occupying type A sites increases with bioactivity testing time, due to the biologically induced growth of the apatitic phase hosting said sites.

At this point of the research we have gathered a good number of evidences leading us to the conclusion that the emission and excitation behavior of type A Eu ions is consistent with what we would expect from luminescent centers inside a phase capable of growing on bioactive glasses' surfaces while they are immersed in biological simulated fluids; in the next section (5.3) we will demonstrate through FTIR, Raman and XRD analyses that a layer of HCA is actually developed on our samples upon interaction with DMEM, thus confirming the bioactivity of all of our synthesized glasses (though with some considerable differences in the degree of biomineralization between them); therefore, a reasonable connection can be established between biologically precipitated HCA and the phase containing the sites giving rise to Eu's type A emission, thus reasonably demonstrating that Eu doped bioactive glasses develop a layer of Eu doped HCA on their surfaces during *in vitro* bioactivity testing.

However, no strictly rigorous proof of this latter statement has so far been exposed, and, without any experimental evidence that type A emission arises really from Eu ions inside the HCA lattice, one could object that it is also possible that type A sites are located inside some other crystalline phase precipitating on our powders during immersion in DMEM: in fact,

even though in Par. 5.3.1 we will see that via XRD only HA can be found on the surface of our bioactive grains, nevertheless some other undetectable Eu doped nanocrystals could have been formed.

Fortunately, this is not the case, but before demonstrating so, we need to make a little digression and show the results we obtained analyzing the emission of our samples by exploiting a different excitation source: a nitrogen laser.

5.2.3: Emission spectra with non selective excitation in the UV range

Nitrogen lasers exhibit an emission peak at 337.1 nm (FWHM: 0.01 nm; duration 8 ns), in the UV domain, so, as we will see from the few complete excitation spectra we managed to acquire (see next paragraph), using such source on our samples results in non selective excitation.

Therefore, exploiting the N_2 laser to excite the emission of fluorescence photons from all the types of emitting centers present in our powders would have been the most clever thing to do since the beginning of our luminescence measurements, but a series of technical problems with the available old instrument induced us not to act in that way. In particular, the power output was never very stable; frequent security shutdowns took place right in the middle of our measures, due to problems with the faulty gas pressure management system; a lot of artifacts connected to the equipment appeared and almost dominated the spectra, etc.

However, in the impossibility of acquiring complete excitation spectra of site A Eu ions, and thus of knowing exactly where their $^5D_1$ or $^5D_2$ levels are located, if we wanted to have some detailed intensity information also on site A's $^5D_0 \rightarrow {}^7F_0$ peak (obviously masked by the laser when exciting in the $^5D_0$ level) we had to use this instrument.

The experimental **detection** parameters are reported below:

- Analysis range: 400 → 725 nm.
- Lambda step: 0.65 nm.
- Photomultiplier voltage: 1100 V.
- Variable resistance: 1000 Ω.
- Acquisition delay from laser pulse: 34.2% of 50 µs; with such a small delay it is possible to detect both slow and relatively fast (obviously not nanosecond) emitters.
- Integration gate interval: 5 ns.

The acquired emission spectra are shown in Fig. 5.9; no normalization or offsetting of the data has been done.

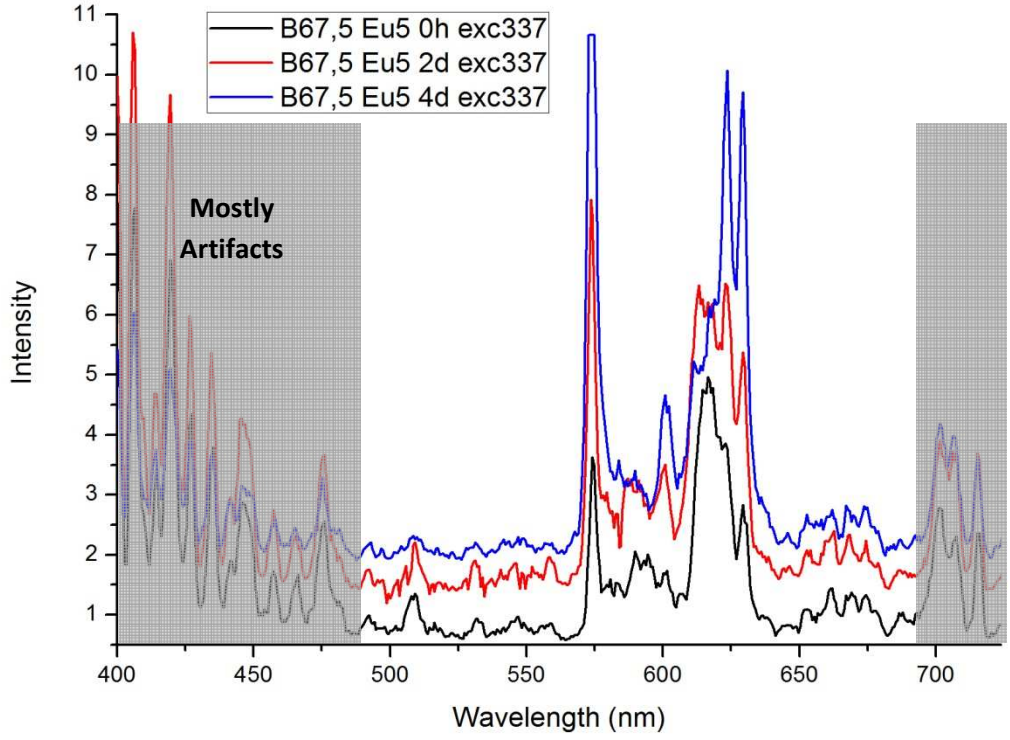

Fig. 5.9: Emission spectra acquired from samples of the B67,5 Eu5 series upon non selective excitation at 337.1 nm (N_2 laser)

The really interesting feature emerging from the reported plots, besides the usual increasing height of type A peaks with interaction time, is that the most intense site A emission arises from the $^5D_0 \rightarrow {}^7F_0$ transition. This is a highly uncommon characteristic, since the $0 \rightarrow 0$ dipolar electric transition is strongly parity forbidden by Laporte's rule (see Chapter 3), and normally gives rise to one of the faintest peaks of Eu's emission spectrum (if we exclude the $^5D_0 \rightarrow {}^7F_3$ transition, the most feeble of all due to its forced dipolar electric nature), as we can notice from our site B spectra or in ref. [5], [10], [21] etc.; here, on the contrary, it overwhelms also the usually dominating $^5D_0 \rightarrow {}^7F_2$ peak.

Nonetheless, if we look up in Eu luminescence literature, we can find that one of the few crystal families where this abnormal $^5D_0 \rightarrow {}^7F_0$ intensity is present is exactly that of the apatites (hydroxylapatite, chloroapatite, fluoroapatite, etc). Moreover, in an article by Ternane *et al.* (see ref. [11]) we found the emission spectrum upon non selective excitation at 254 nm of an Eu doped sol-gel derived HA; we report it below in Fig. 5.10, together with the spectrum of B67,5 Eu5 4d acquired upon excitation at 574 nm (we have more confidence in

those data than in the ones acquired with the nitrogen laser; our values have been converted to wavenumbers to yield a more straightforward comparison):

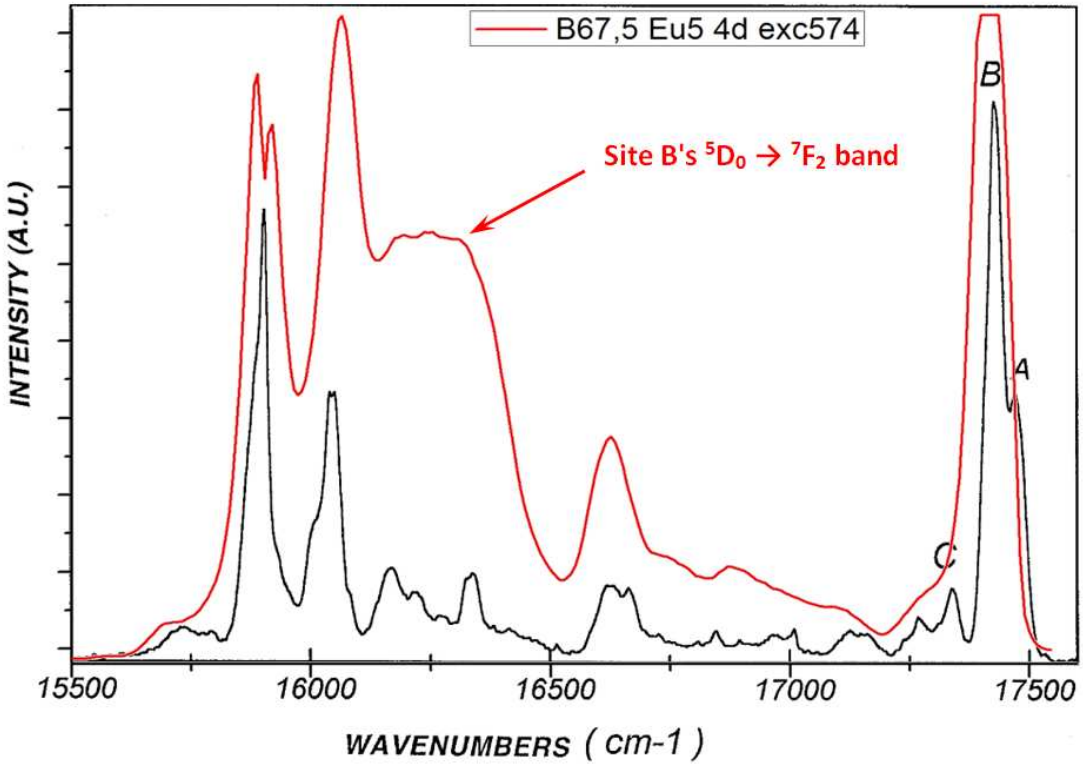

Fig. 5.10: Comparison between emission spectra of Ternane's Eu doped HA (in black, λ_{exc} = 254 nm) and of our B67,5 Eu5 4d sample, excited at 574 nm (in red)

If we exclude the $^5D_0 \rightarrow {}^7F_2$ broad band belonging to our site B Eu ions, the similarities between spectra are absolutely blatant: all our site A peaks[9] almost perfectly coincide with Teranane's ones. Moreover, the abnormally high intensity of our $0 \rightarrow 0$ transition finds an explanation in light of the peculiar charge compensation mechanism Eu must exploit to substitute for Ca in the HCA lattice; for more information on this point, we invite the reader to refer back to Par. 4.1.2. Here we shall just say that the sites we have called up to this moment "site A" coincide with HCA's Ca(II) sites (Ternane's type B sites in Fig. 5.10).

Since Eu ions have high sensitivity to their crystalline environment (both in site symmetry and intensity), and show abnormally intense $^5D_0 \rightarrow {}^7F_0$ transitions only in presence of peculiar distortions of site symmetry and high degrees of bond covalence, then a level of

[9] In Fig. 5.10 our 574 nm ≈ 17422 cm^{-1} peak is actually due to the dye laser, but from nitrogen laser measurements we've just seen that at that very same wavelength a really strong emission peak exists.

similarity such as the one we have encountered between our spectra and Ternane's can only be justified by the identity of the host crystals we studied.

Therefore, we have found the ultimate evidence that proves the identification of the phase containing type A Eu sites with Hydroxyl-carbonate-apatite, and thus we have proved that our initial hypothesis, "Eu doped bioactive glasses form Eu doped HCA layers on their surfaces during interaction with biological media", was correct.

As further and complementary evidence of said identification we can also report the results of some luminescence decay lifetime measurements: in particular, we selectively excited in their $^5D_0$ level in turn site B and site A Eu ions of a B67,5 Eu5 4d sample, and we registered the evolution of their specific emissions with time by coupling a Lecroy 9310A 400Mhz digital oscilloscope to the PM detector. What we found is reported in Fig. 5.11.1 for site B (excitation at 579 nm and detection at 613[10] nm; semilogarithmic in Fig. 5.11.2) and Fig. 5.11.3 for site A (λ_{exc} = 574 nm; λ_{obs} = 629.5 nm; semilogarithmic in Fig. 5.11.4):

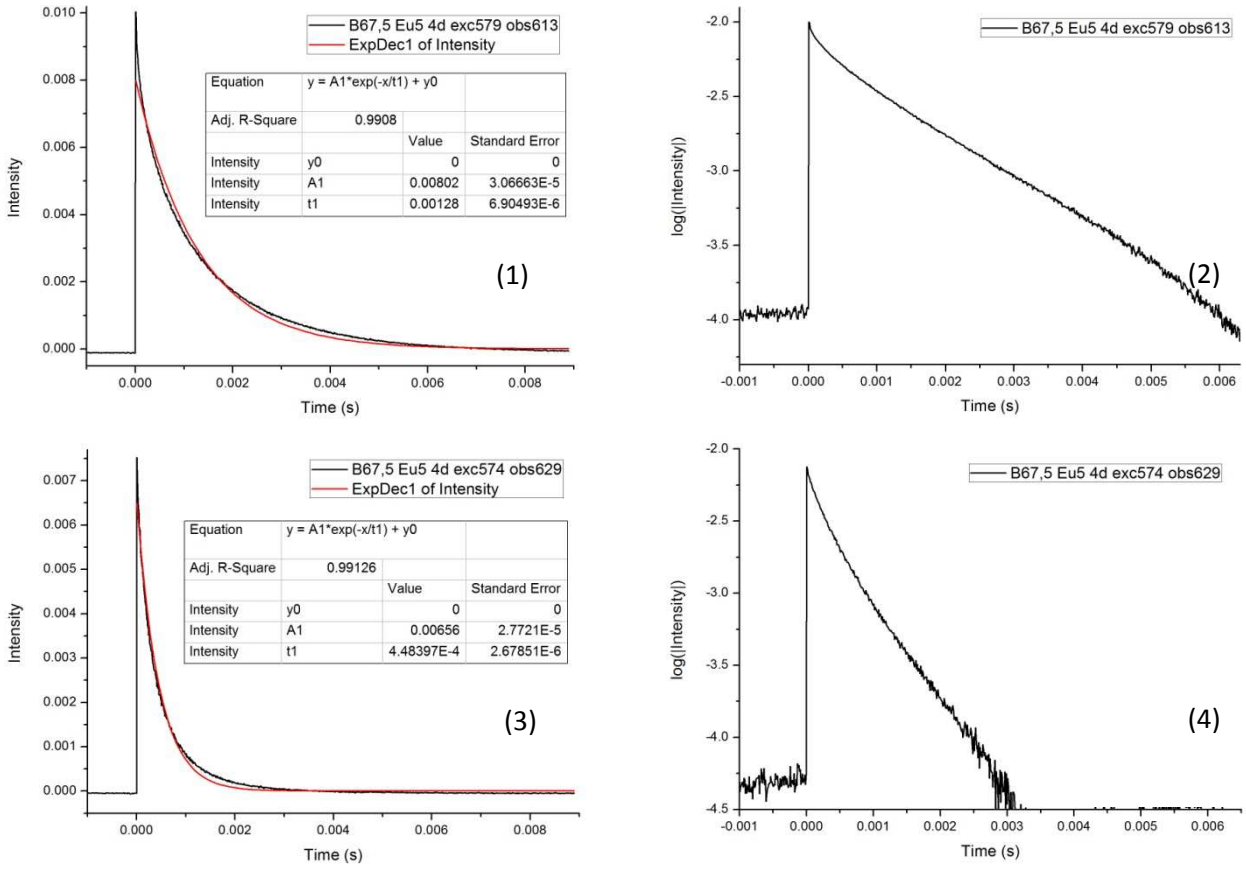

Fig. 5.11: Site selective luminescence decay measurements on a B67,5 Eu5 4d sample

[10] We chose to observe site B's emission at 613 nm and not at 616 nm (where its maximum is located) because at 613 nm we are still on top of the $^5D_0 \rightarrow {}^7F_2$ band, but we are more distant from the 622.5 Site A characteristic peak than at 616 nm, so this way we can acquire more site B selective information.

As it is clearly evident, the two characteristic values of luminescence decay lifetime of Eu ions occupying type A and type B sites are quite different: site A is a faster emitter than site B, as testified by the fact that in plots (3) and (4) the completely desexcited state is attained much earlier than for the curves number (1) and (2). In particular, by fitting the experimental data with exponential decay functions: $Intensity = A \cdot exp\left(-{time}/{\tau}\right)$ we calculated:

- Site B (Eu in glass): τ = 1280 ± 7 µs
- Site A (Eu in HCA): τ = 448 ± 3 µs

These values are very close to those published in literature: for Eu^{3+} ions occupying Ca(II) sites inside HA's lattice Ternane in ref. [11] reports τ values in the range 436 ÷ 486 µs; while for Eu^{3+} ions inside an as synthesized doped bioactive glass very similar to ours Krebs and Brownstein in ref. [4] report a τ value of 1.53 ms[11].

As a further confirmation of the fact that Eu ions inside HCA crystals desexcite faster than Eu ions inside the amorphous network, we report below in Fig. 5.12 an example of time resolved luminescence spectroscopy measurements on a B67,5 Eu5 3d sample with excitation at 574 nm (the plots have been normalized to the intensity of the $^5D_0 \rightarrow {}^7F_4$ transition).

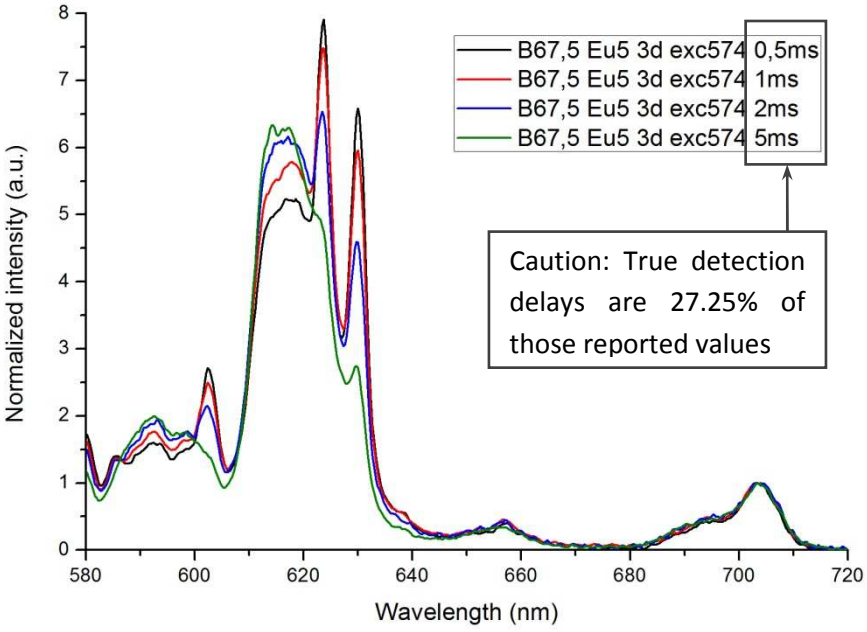

Fig. 5.12: Time resolved luminescence spectroscopy analyses on a B67,5 Eu5 3d sample (λ_{exc} = 574 nm)

[11] This slight difference might be ascribed partly to the compositional differences between Kreb's glass: 71%$_{mol}$ SiO_2 – 22.5% CaO – 6% P_2O_5 – 0.5% Eu_2O_3 and our B67,5 Eu5 glass: 72.6%$_{mol}$ SiO_2 – 23% CaO – 3.4% P_2O_5 – 0.9% Eu_2O_3; and partly to the fact that our sample has been in contact for 4 days with DMEM, so its amorphous network has been considerably altered (cation leaching, hydrolytic dissolution, formation of a silica gel layer, etc). In fact, for a B67,5 Eu5 pre-interaction glass (data not shown) we measured a τ value of 1.81 ms.

As usual, tuning the laser at 574 nm results in excitation of both site A and Site B luminescent centers, and it is straightforward to notice that site A characteristic peaks increase in intensity when the detection interval after laser pulse is shorter, while they almost disappear for the longest acquisition delays.

This is perfectly consistent with type A Eu ions being faster emitters than type B: in fact, while for example for these latter increasing the acquisition delay to approximately 1.35 ms (that is 27.25% of 5 ms) induces an intensity drop of only around 1/e ≈ 1/3 (because $\tau_{siteB} \approx$ 1.3 ms), for type A Eu ions, having $\tau_{siteA} \approx 450$ µs, after 1.35 ms 3τ have passed, so the emission intensity is reduced by a far larger factor $e^3 \approx 20$; therefore, site A peaks are more "time-sensitive" than site B ones, and decrease dramatically in intensity upon increasing acquisition delays.

5.2.4: Complete site B selective excitation spectra of the B67,5 Eu5 glass series

During the only one afternoon the Xe lamp excitation source worked, we were able to acquire the following series of spectra from B67,5 Eu5 post-interaction samples; since the observation wavelength was set at 614 nm, the information we acquired is Site B selective (spectra are normalized and offsetted for clarity purposes).

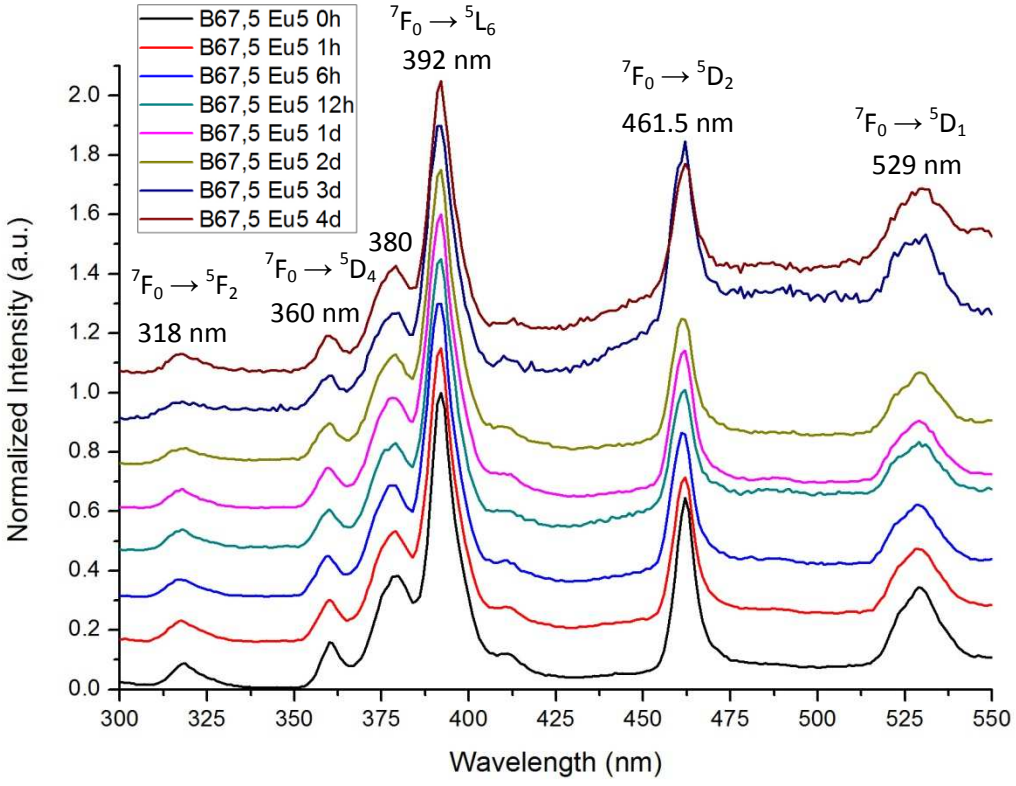

Fig. 5.13: Complete Site B selective excitation spectra acquired from the B67,5 Eu5 series (λ_{obs}=614)

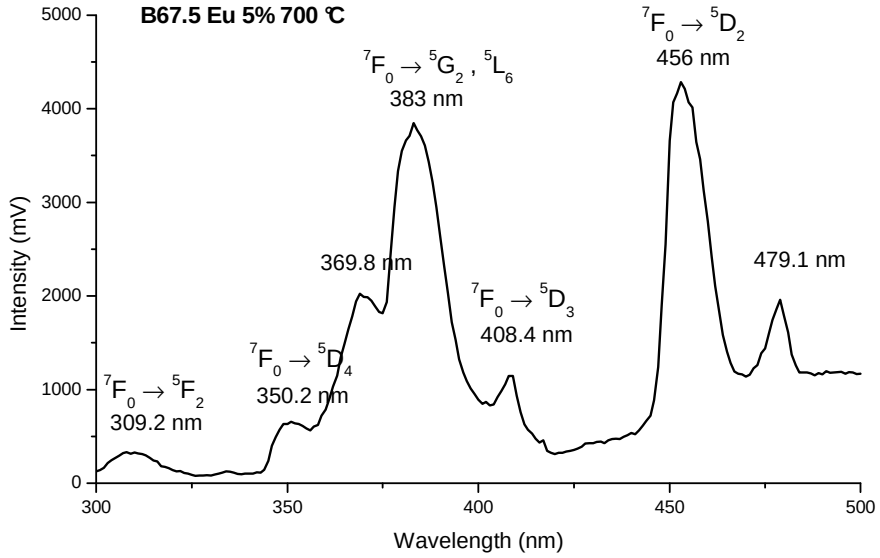

Fig. 5.1: Excitation spectrum of a B67,5 Eu5 glass calcined at 700°C (λ_{obs} = 614 nm)

A comparison between our spectra (Fig. 5.13) and Fig. 5.1 (reported again above) shows that the positions and relative intensities of our excitation peaks are quite different from those registered by the previous member of the research team. This, however, did not have a negative effect on our work, but, on the contrary, probably helped us in identifying the first "apatitic Eu" emission peak at 574 nm: in fact, if we had excited our samples exactly at 461.5 nm (site B's $^5D_2$ level), type B Eu emission would have been too overwhelming to allow the detection of site A's $^5D_0 \rightarrow {}^7F_0$ transition.

Unfortunately, at the time we carried out these measurements we did not have yet recognized the peak at 574 nm as arising from a different emitting site; when we understood that, it was too late, and the excitation source was again under maintenance, so we were not able to acquire complete excitation spectra also of Eu ions hosted inside the HCA lattice.

5.2.5: Emission spectra with site selective excitation in the $^5D_0$ level; part 2

In the preceding paragraphs we have described the experimental path that led us to the identification of two "families" of Eu ions inside our B67,5 Eu5 biomineralized samples:

- **type A Eu ions**, located inside the HCA layer formed on the surfaces of our bioactive glass powders during interaction with DMEM (or inside the HA crystals devitrified during calcination at 700°C) and occupying Ca(II) sites (position 6(h) inside the apatitic lattice), with C_s symmetry, but degenerating into pseudo $C_{\infty v}$ due to the high covalence of the Eu^{3+}–O^{2-} bonds that can be formed in those sites; these Eu ions can be excited in their

$^5D_0$ level by tuning the laser at 574 nm, and exhibit a characteristic spectral signature with narrow, well resolved emission peaks at 602, 622.5 and 629.5 nm; their desexcitation is relatively fast, and their luminescence decay lifetime is $\tau \approx 450$ µs.

- **type B Eu ions**, located inside the amorphous bioactive glass network and excitable in their $^5D_0$ level by tuning the laser at 579 nm; due to the high disorder of the glass structure, they occupy a great variety of sites, both in symmetry and crystal field intensity, so their characteristic spectral signature is made up of broad (inhomogeneous broadening) emission bands, connected with radiative transitions from the $^5D_0$ to the ^7F_j manifold (J = 0 .. 6, but only transitions up to J = 4 are observed); their luminescence decay lifetime in the millisecond order of magnitude ($\tau \approx 1.5$ ms average) is in line with the most common values encountered in literature for Eu ions inside amorphous hosts.

Once we gathered all these theoretical data, we decided to apply them to the characterization of the other series of post-interaction samples we obtained from *in vitro* bioactivity tests (see Par 5.1.2): B67,5 Eu1's, B67,5 Eu10's and Molari's ones; in doing so, we brought about the first embryonic application of site selective luminescence spectroscopy to the study of biomineralization processes in doped bioactive glasses.

In particular, since for the analysis of these latter series we exploited the same experimental settings and parameters used for measurements on B67,5 Eu5, we were able to establish some interesting comparisons between the bioactive efficiencies of our samples, at least from a qualitative point of view, therefore proving the usefulness of our luminescent structural probe in studying the bioactivity behavior of bioglasses.

In the following pages we will first show the data we acquired from the B67,5 Eu1 series: both emission spectra with selective excitation in the $^5D_0$ level at 574 (site A, Fig. 5.15) and 579 nm (site B, Fig. 5.14), and excitation spectra (always in the $^7F_0 \rightarrow {}^5D_0$ domain) with site selective detection at 629.5 (Fig. 5.16.2) and 616 nm (Fig. 5.16.1) will be reported. Then we will pass to the highly doped samples (B67,5 Eu10 and Molari in Fig. 5.17), which however will turn out to be a bit more "troublesome" than the others.

As already said above, for more information about analysis parameters and experimental set-ups refer to paragraphs 5.2.2 and 5.2.3, since the values we used here are the same as for B67,5 Eu5's series; the exploited photomultiplier tensions have already been reported in paragraph 5.2.2 for emission measurements, while for localized excitation spectra they are:

- 600 V for B67,5 Eu1 with detection at 616 nm (site B);
- 700 V for B67,5 Eu1 with detection at 629.5 nm (site A).

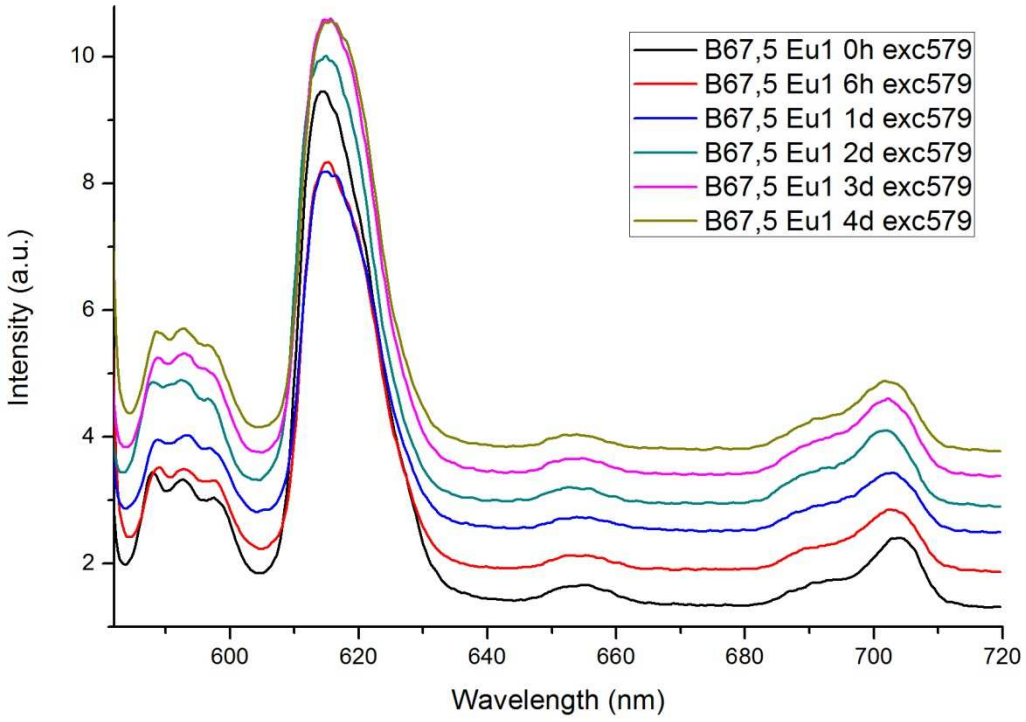

Fig. 5.14: Emission spectra acquired from post-interaction samples of the B67,5 Eu1 series upon excitation in the $^5D_0$ level of site B Eu ions (λ_{exc} = 579 nm; with offset)

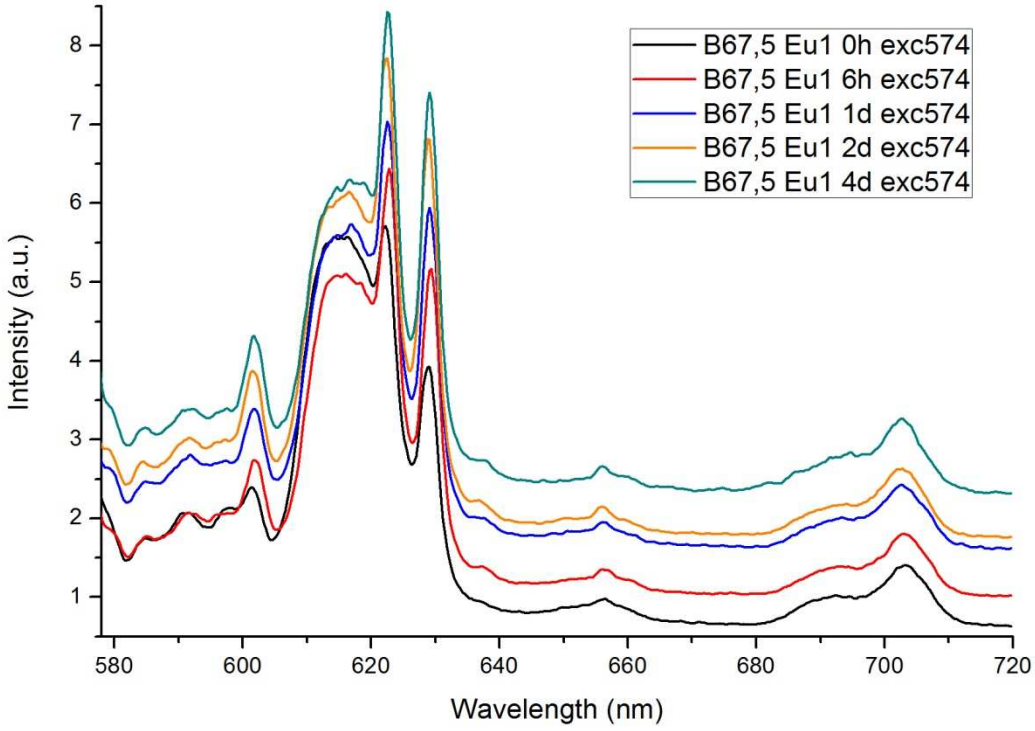

Fig. 5.15: Emission spectra acquired from post-interaction samples of the B67,5 Eu1 series upon excitation in the $^5D_0$ level of site A Eu ions (λ_{exc} = 574nm; with offset)

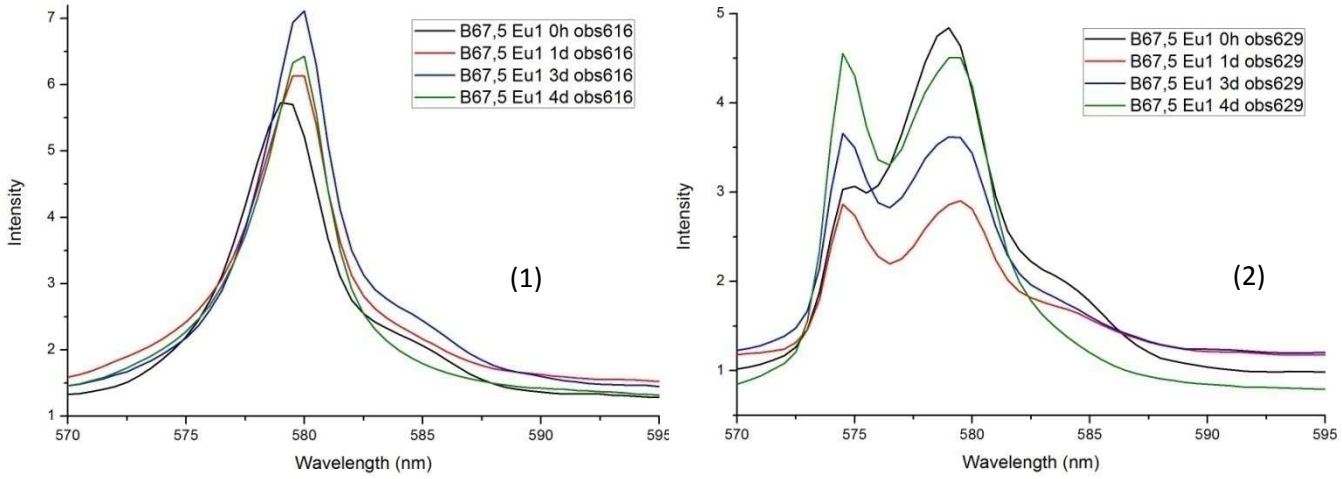

Fig. 5.16: Localized excitation spectra acquired from samples of the B67,5 Eu1 series upon observation of: (1) site B's $^5D_0 \rightarrow {}^7F_2$ emission band (λ_{obs} = 616 nm) and (2) site A's 629.5 nm characteristic peak

From the reported plots we can infer some useful information:

- Since in Fig. 5.15 we can recognize the typical Site A emission signature, and since we have already demonstrated that such peaks are connected with Eu ions located inside HCA crystals, then we can confidently state that also B67,5 Eu1 is a bioactive glass, capable of developing an apatitic layer on its surfaces during interaction with simulated biological media like DMEM;
- The energetic whereabouts of the $^5D_0$ levels of both type A and type B Eu ions do not change very much with doping degree, since the two $^7F_0 \rightarrow {}^5D_0$ transitions in B67,5 Eu1 samples remain excitable by tuning the laser respectively at around 574 ÷ 574.5 (site A) and 579 ÷ 579.5 nm (site B), as they were for the B67,5 Eu5 series;

If we now compare site A quasi selective emission spectra of B67,5 Eu5 and B67,5 Eu1 series:

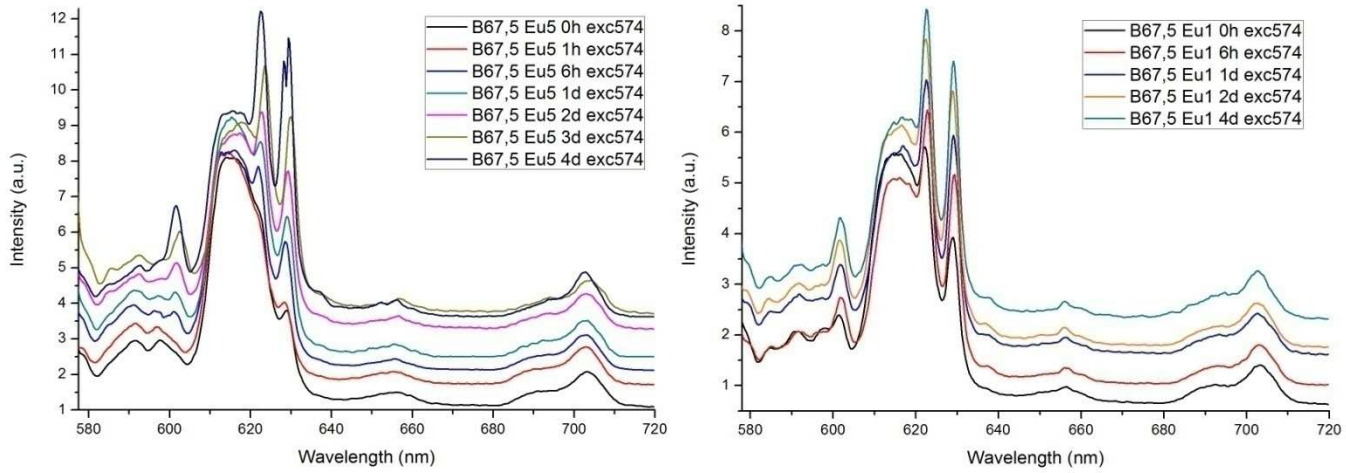

We can easily notice that:

- Coherently with what reported in section 4.3, B67,5 Eu1 at the beginning contains larger crystallites of HCA, as testified by the higher intensity of type A peaks in the low interaction time curves (black, red);
- The final degree of biomineralization should be practically the same, since in the 4 days plots the relative intensities of site A peaks with respect to site B bands are very similar; at such an embryonic stage of development of the method, however, this statement must indeed be interpreted in a qualitative way, but FTIR measurements seem to confirm this hypothesis.

  Now, since B67,5 Eu1 1st calc powder has a lower specific surface area value than B67,5 Eu5 (see Tab. 5.3), and since biomineralization processes are surface driven, this might mean that our B67,5 Eu1 glass is intrinsically more bioactive than B67,5 Eu5 (so that the intrinsic boost and the surface drawback compensate each other), and therefore we could think that Eu ions have a slight kinetic hindering effect not only on HA devitrification upon calcination, but also on HCA precipitation during immersion in biological fluids. This supposition will be confirmed by XRD, FTIR and Raman analyses.

If we now switch to the more heavily doped materials (containing $2\%_{mol}$ of Eu_2O_3), that is B67,5 Eu10 and Molari biomineralized glasses series, and we try to detect the characteristic site A emission by tuning the exciting laser at 574 nm, we get an unpleasant surprise:

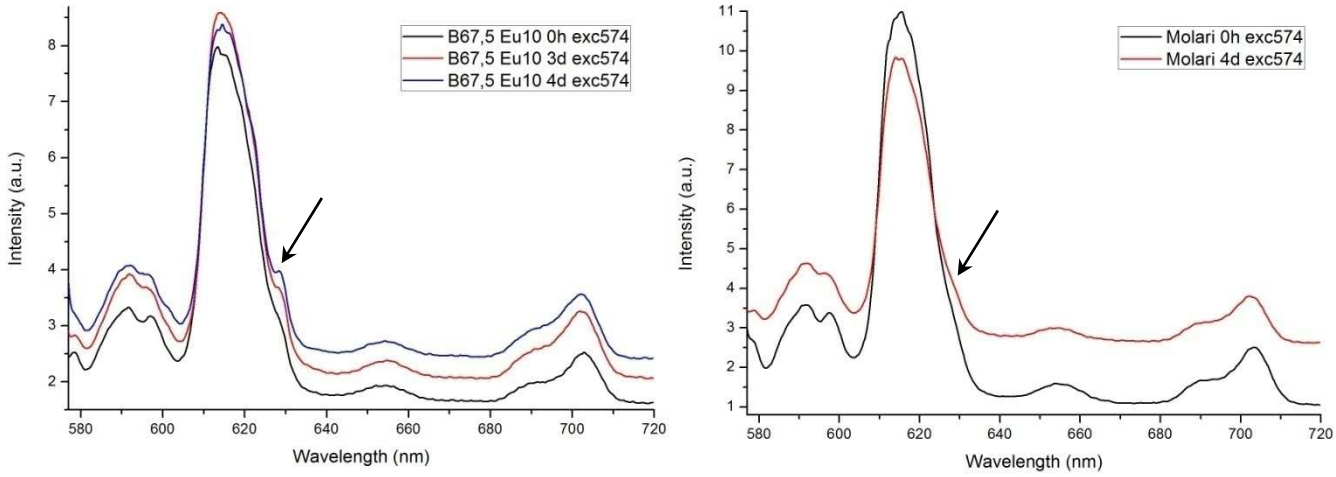

Fig. 5.17: Emission spectra acquired from post-interaction samples of the B67,5 Eu10 (left) and Molari (right) series upon excitation in the $^5D_0$ level of site A Eu ions (λ_{exc} = 574nm; with offset)

As we can see from Fig. 5.17, even for the longest interaction delays type A Eu peaks are extremely faint (highlighted by a black arrow), and in the case of Molari samples they are almost completely undetectable. This might potentially be due to various reasons:

- At such high concentrations, Eu's hindering effect on HCA crystallization might completely inhibit the formation of the apatitic layer on the surface of the glass grains, thus rendering them no more bioactive;
- For high concentrations Eu ions might clusterize or segregate (see ref. [21]), thus becoming less easily leachable from the glass network and therefore lowering their availability in solution for the precipitation of Eu doped HCA;
- At these high concentrations Eu might prefer entering inside phases different from HCA, therefore the precipitated apatitic crystals would not give rise to a luminescence signal because no emitting centers are integrated inside their lattice;
- At high Eu content concentrational self quenching (CSQ) of luminescence might take place: due to the great number of silanols existing in the silica gel layer present in the vicinity of the biologically precipitated apatitic crystals, massive energy transfer between type A emitting centers followed by hydroxyl-mediated non radiative relaxation might cause the almost complete quenching of site A fluorescence emission.

The data we gathered through complementary characterization techniques (see section 5.3) suggest that a combination of the preceding hypotheses might be the correct explanation: though the formation of HCA crystals is confirmed by both FTIR and Raman measurements, thus fortunately excluding the complete inhibition of biomineralization by high concentrations of Eu ions, the actual extent of the process seems quite lower than in less doped samples, even when specific surface area values are comparable (we refer to B67,5 Eu5 and B67,5 Eu10 series); therefore on our glass powders most probably we have fewer doped apatitic crystals, which moreover emit only feebly because of CSQ. Moreover, also the precipitation of phases containing Eu but different from HCA (thus not excitable at our wavelengths) is highly probable, as reported in ref. [21].

5.3: Validation of the luminescent structural probe

With all the data we have shown so far we have demonstrated that if we dope our bioactive glasses with appropriate amounts of Eu^{3+} ions and then we perform *in vitro* bioactivity tests on them, through site selective luminescence spectroscopy measurements on post interaction

samples we are capable of detecting the apatitic crystals formed during immersion in DMEM by identifying the characteristic spectral signature of Eu ions hosted inside the HCA lattice. Therefore we have demonstrated the actual detection effectiveness of our luminescent structural probe.

However, in order for a probe to be considered rigorously valid for analytical purposes, it's also absolutely essential that it does not introduce any alteration in the material it is meant to characterize; therefore it is necessary for us to demonstrate that Eu ions do not change too much our bioactive glasses, or at least that they do not alter those features intrinsically connected to the biomineralization processes we want to study.

To do so, we will report the results gathered on our post-interaction samples and fluids through some complementary characterization techniques such as ICP-AES, XRD, FTIR spectroscopy and micro Raman spectroscopy.

5.3.1: XRD measurements on biomineralized samples

In paragraph 5.2.3 we have shown a comparison between luminescence emission spectra of our type A Eu ions and of Eu ions inside a sol-gel derived HA, and we have recognized an almost perfect match between the curves, so we were able to state that on our post bioactivity testing samples there exists a layer of Eu doped HCA, whose precipitation is induced by the interaction of the doped glass with DMEM. Since HCA is a crystalline compound, it should be detectable via XRD analyses, provided it is sufficiently well crystallized and present in sufficient amount; therefore, with the aim of gathering further evidences of biomineralization, we decided to try and acquire a pair of diffraction patterns from 4 days old samples.

As already said in Par 5.1.2, in order to have enough material to get a detectable X ray diffraction signal from our post interaction glasses we carried out two "special" 4 days long bioactivity tests on relatively big amounts of B67,5 1st syn and B67,5 Eu5 powders.

In these two cases we directly put the correct amount of material (calculated with the formula of Par. 5.1.2) inside the original bottle (V_{tot} = 500 mL) of DMEM bought from Biocrom A.G., and then put the two containers inside our oven at 37°C with occasional shaking. After four days, due to the considerable quantity of material to be recovered, instead of using pipettes and centrifuge to stop the interactions, we exploited some vacuum filtration equipment (buchner funnel + buchner flask + paper filter + vacuum pump).

The two obtained samples were named **B67,5 1st syn 4d grosso** and **B67,5 Eu5 4d grosso**, and underwent XRD analyses with thin films geometry by using the same instrument, the same experimental parameters ($\theta_{glancing}$ = 3°, 30 kV, 40 mA, etc.) and approximately the same amount of powder (double sided tape completely covered by sample). The acquired diffraction patterns are reported in Fig. 5.18.

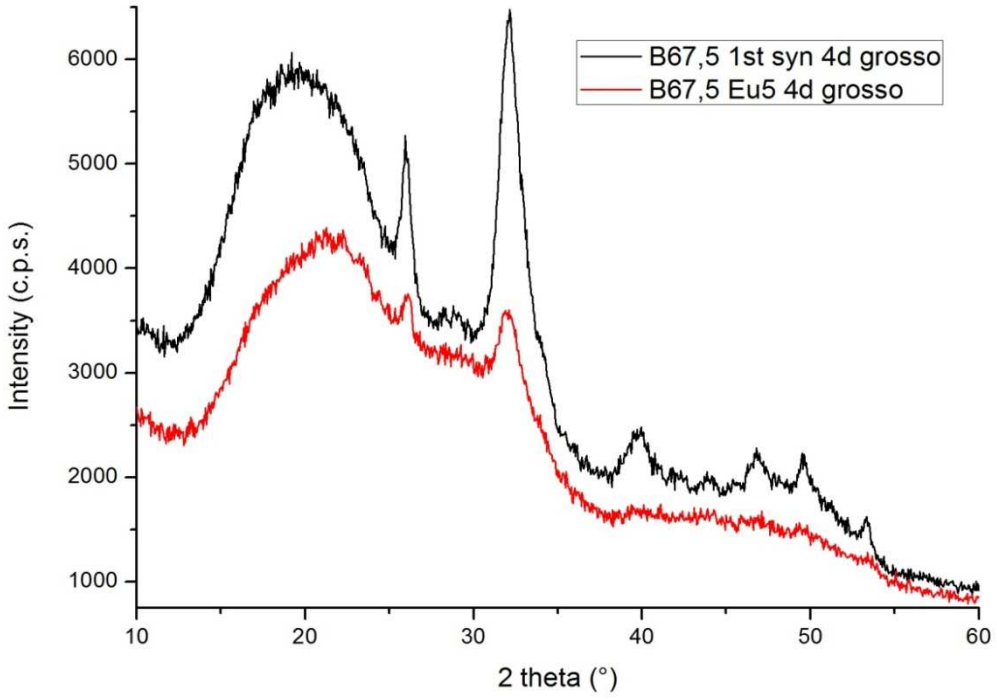

Fig. 5.18: Comparison between thin films XRD patterns of B67,5 1st syn 4d grosso and B67,5 Eu5 4d grosso biomineralized samples (no offset)

If we compare the above reported curves with what reported in Par. 4.1.1 (especially Fig. 4.3), we can easily recognize the typical biologically precipitated apatite's XRD signature: mainly a single peak at 26° and two convoluted peaks at 32°, plus minor peaks at 39.5°, 46.5°, 49°, etc. However, distinguishing an HA from an Eu doped HCA from those poor quality plots is practically impossible.

Moreover, since the black curve exhibits higher and better resolved diffraction peaks than the red one, it is straightforward to understand that the B67,5 undoped glass grains grow on their surfaces a more developed and better crystallized apatitic layer with respect to B67,5 Eu5. This effect is for sure partly due to the higher specific surface area of the former material, that unavoidably boosted its reactivity in DMEM, but, nevertheless, in our opinion also a kinetic hindering effect of Eu on HCA bio-precipitation is imaginable, and many other experimental evidences (FTIR, Raman, see further) support this hypothesis.

5.3.2: FTIR spectroscopy measurements on biomineralized samples

The various biomineralized glass powders we obtained from in vitro bioactivity tests have undergone a series of transmission FTIR spectroscopy measurements in order to demonstrate and possibly quantify the actual precipitation of HCA crystals during immersion in DMEM.

As already explained in Chapter 3, in order not to lose our powders as we would have done by using the KBr compress method, we exploited a home-made solution: we put our powders in between two KBr (transparent to IR light) windows normally used to carry out analyses on liquids; though being very simple and effective, this "trick" has the problematic drawback that it renders very difficult to obtain the same signal quality from all the measurements, since forcibly each time the amount and distribution of powder grains is slightly different from the others. Therefore, rigorous quantitative information cannot be inferred from the spectra we will report, but, nevertheless, by comparing the detected curves it is possible to gather many important and interesting data on biomineralization processes.

The analyses were carried out at the *Dipartimento di Ingegneria Meccanica - Settore Materiali* of the University of Padua on a Perkin-Elmer 2000 FTIR spectrophotometer, and covered the whole Mid-infrared range (400 → 4000 cm^{-1}), with a resolution of 2 cm^{-1}; in order to obtain good quality spectra, we averaged 128 acquisitions, and for "aesthetic" purposes we slightly smoothed the raw profiles. Each series of post interaction glasses has been characterized in a sequential way (i.e. first all the B67,5 Eu5 powders, then all the B67,5 Eu1 ones, etc), but we decided to skip the 1h, 6h and 12h samples, since they yielded almost equivalent spectra (at least for those features that interest us most).

Due to the aforementioned unavoidable differences in amount and dispersion of the powders placed in between the KBr windows, the absolute transmittance values provided by the instrument for different samples turned out to be quite distant; therefore, in order to establish at least a qualitative comparison between our curves, the acquired data have been normalized to their respective maxima and minima.

In Fig. 5.19 we show the spectra detected for the B67,5 Eu5 post-interaction series; for an identification of the most interesting peaks of our plots, we invite the reader to refer back to Tab. 4.9, where we've summarized the information we collected from various bibliographic references (see ref. [1], [2], [7], [9], [13], [22], etc).

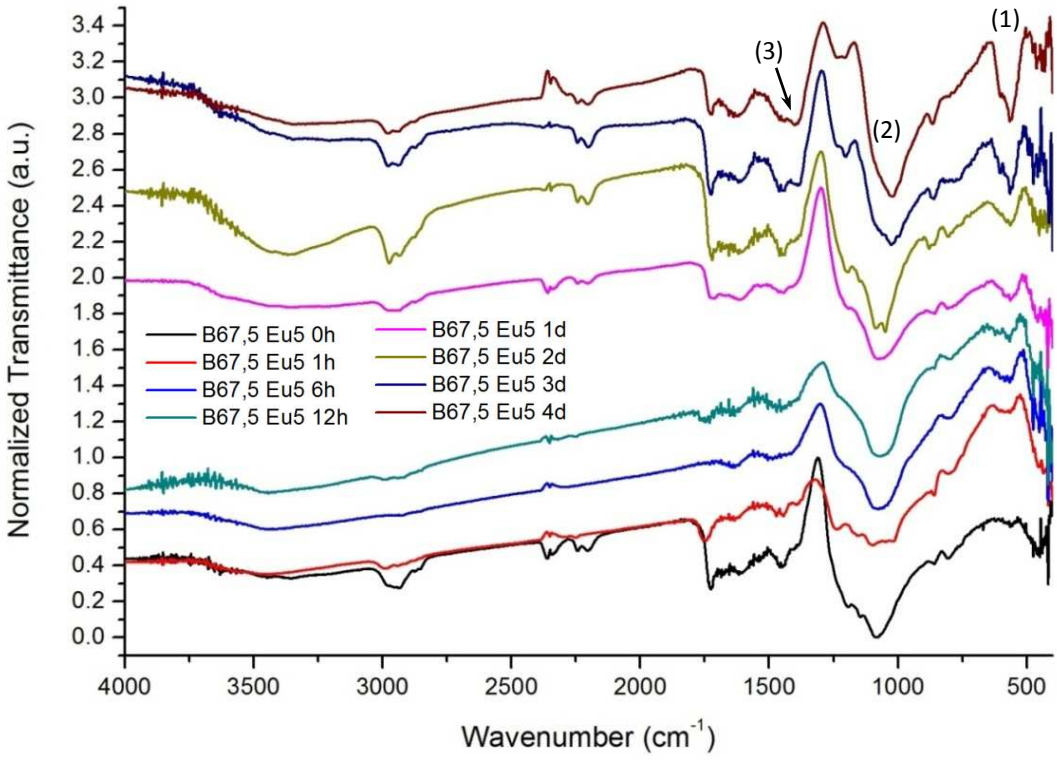

Fig. 5.19: FTIR transmission spectra of the biomineralized samples belonging to the B67,5 Eu5 series (normalized and offsetted for clarity purposes)

The evolution of our curves is perfectly consistent with what is commonly reported in literature for bioactive glasses:

(1) The most straightforward and important feature we can notice with increasing interaction delay is the appearance and progressive intensification of the doublet of peaks at around 560 and 600 cm^{-1}, connected, as previously said (see Par. 4.1.1 and 4.3.6), with the symmetric stretching vibration of P−O bonds of phosphate groups located inside a crystalline apatitic environment. Moreover, the longer the immersion time, the better resolved from each other are such peaks, so we can consider them as an effective evidence of HCA crystals precipitation and growth on the surfaces of our glasses during bioactivity testing (see above all the article in note 2 of Chap. 4 by Elliot).

(2) With increasing immersion time, the initial intense IR absorption peak at around 1085 cm^{-1}, attributed to the symmetric stretching of Si−O bonds, becomes progressively flanked by a peak at 1035 cm^{-1}, connected with the asymmetric stretching of P−O bonds, which then becomes dominant for longer delays.

(3) After long immersion periods, at around 1385 cm^{-1} we notice the appearance of a new peak, connected with the deformation of C−O bonds of carbonate groups of HCA;

Based on these results, we can state that B67,5 Eu5, even if containing the $5\%_{wt}$ of Eu_2O_3, remains still a bioactive glass (at least of class B, i.e. osteoconductive), since it maintains the capability of developing a layer of hydroxyl-carbonate-apatite on its surfaces when left in contact with natural or simulated body fluids; in particular, this IR finding confirms what already inferred from site selective luminescence analyses.

More or less the same kind of evolutions of transmittance peaks are also detectable for the other glass compositions that underwent *in vitro* bioactivity testing. The results are shown in Fig. 5.20 (B67,5), 5.21 (B67,5 Eu1), 5.22 (B67,5 Eu10) and 5.23 (Molari):

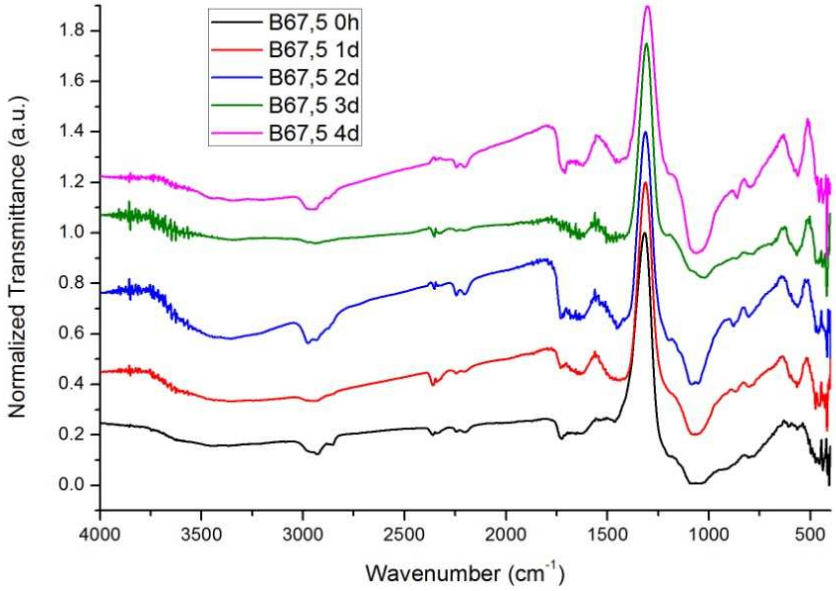

Fig. 5.20: FTIR transmission spectra of the B67,5 glass series (normalized and offsetted)

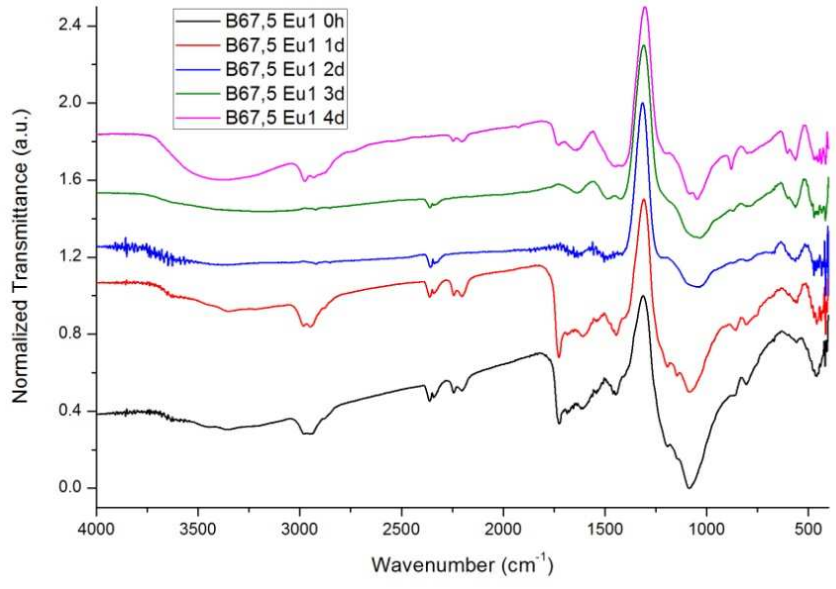

Fig. 5.21: FTIR transmission spectra of the B67,5 Eu1 glass series (normalized and offsetted)

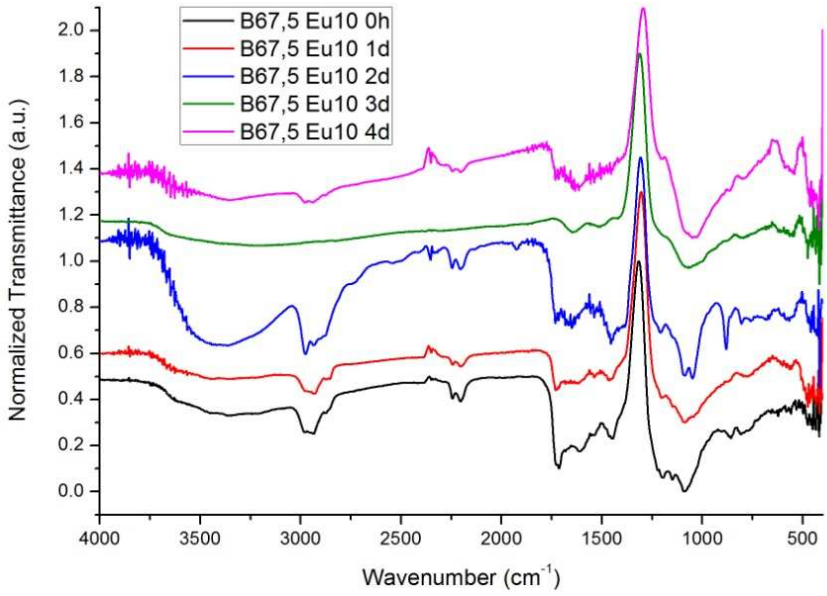

Fig. 5.22: FTIR transmission spectra of the B67,5 Eu10 glass series (normalized and offsetted)

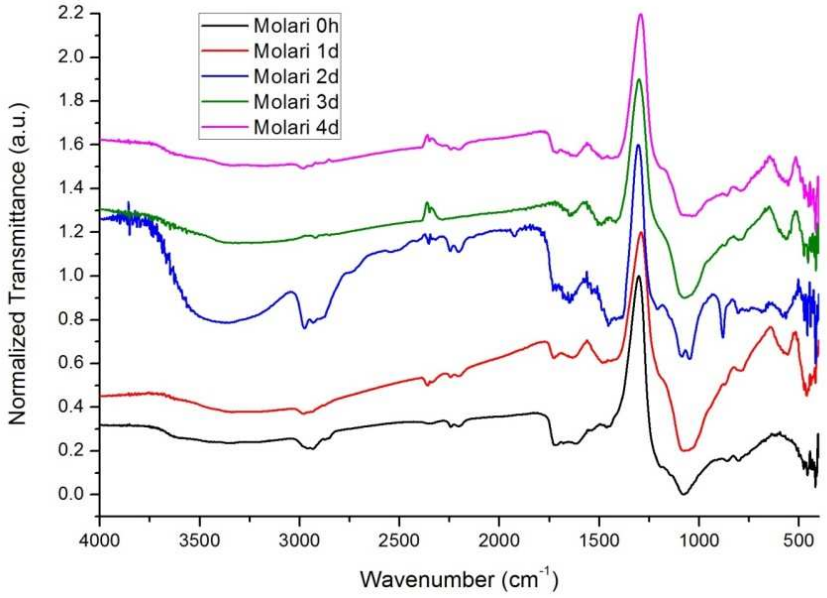

Fig. 5.23: FTIR transmission spectra of the Molari glass series (normalized and offsetted)

In all the reported plots we can recognize the three above mentioned characteristic features, so we can reasonably state that, during immersion in DMEM, HCA crystals precipitate on the surface of all our doped glasses, which therefore can all be considered actually bioactive.

In particular, the detection of the apatitic vibrational signature in the case of B67,5 Eu1 confirms what already deduced through luminescence analyses, and constitutes further proof of the identification of type A emission with Eu ions hosted inside HCA's lattice. On the other hand, detecting biomineralization through FTIR measurements on highly doped glasses such

as B67,5 Eu10 and Molari, whose fluorescence spectra did not exhibit typical site A peaks, fortunately excludes a total inhibiting effect of high concentrations of Eu ions on HCA biological precipitation, and thus makes us think that most probably the lack of site A's luminescent signature from site selective emission plots is connected to some concentration self quenching effect.

Nevertheless, if we analyze the five series of spectra we have reported by focusing our attention on the apatitic P−O stretch peaks at 560 and 600 cm^{-1}, we can easily notice that their height (or better, their depth) is not always the same; if we establish a reasonable connection between IR absorption intensity from said peaks and development of the HCA layer, then it is possible to infer that this latter does not reach the same final extent in all our samples, but a scale of bioactive effectiveness actually exists.

In order to be able to make a comparison as rigorous as possible between 4 days old samples deriving from different glass compositions, and thus to estimate the impact of the doping degree on bioactive behavior, we decided to repeat the analyses on our 4 days powders by trying to be extremely reproducible in sample preparation; the results are reported in Fig. 5.24.

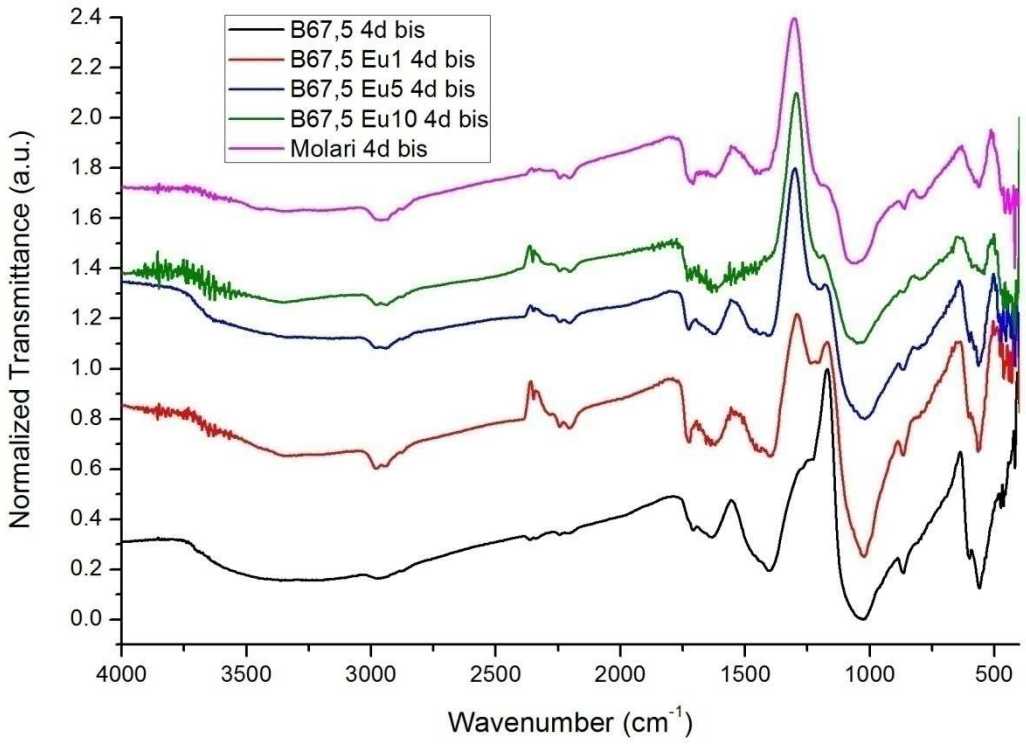

Fig. 5.24: Comparison between 4 days old samples belonging to different series of bioactivity tested glasses (spectra normalized and offsetted)

However, even if utmost care was paid in the measurements, the differences in specific surface area values of the original (pre-interaction) powders remain uneliminable, and thus the differential kinetic boosts to biomineralization processes must still be kept into account while interpreting the acquired spectra. As a reminder, we report again below a table summarizing the SSA values of our relevant samples.

	B67,5 2nd syn	B67,5 Eu1 1st calc	B67,5 Eu5	B67,5 Eu10	Molari
Surf. Area	64 m^2/g	66 m^2/g	131 m^2/g	114 m^2/g	49 m^2/g

Tab. 5.4: Specific surface area values of our bioactive glasses prior to bioactivity testing

From picture 5.24 we can extract a lot of useful and interesting information:

- From a comparison between B67,5 and B67,5 Eu1 curves we can notice that the doublet of apatitic peaks at 560 and 600 cm^{-1} has almost the same intensity, B67,5 Eu1's one being just slightly lower; by the way, the two starting powders had practically the same SSA values (64 VS 66 m^2/g), therefore, all of this seen, it is highly probable that these two bioactive glasses have developed on their surfaces HCA layers having similar thicknesses and degrees of crystallization. This experimental evidence is of fundamental importance, since it constitutes a step forward towards the demonstration that at low doping degree the alterations to bioactive behavior induced by the substitution of Ca^{2+} ions with Eu^{3+} ions are practically negligible.
- Let's now compare B67,5 Eu1 and B67,5 Eu5: it is evident that the apatitic doublet in this latter's spectrum is somewhat less intense than in the former's, even though the 5% doped glass has almost exactly a double SSA value (131 VS 66 m^2/g); if we make the reasonable assumption that the intensity of those peaks is directly proportional to the amount of HCA formed, then this means that some hindering effect of Eu^{3+} ions on biomineralization has compensated the surface kinetic boost (otherwise Eu5 should exhibit much higher peaks than Eu1).
- This statement seems to be confirmed by the comparison between B67,5 Eu5 and B67,5 Eu10: these two samples have very similar surface areas (131 VS 114 m^2/g), but their IR transmittance plots show quite different intensities (Eu10 < Eu5) at 560 and 600 cm^{-1}; this means that the most doped glass has developed an inferior amount of HCA, i.e. is less bioactive, and thus confirms that Eu has a hindering effect on the precipitation of

apatitic crystals during immersion in DMEM. However, in decreasing the bioactivity of the B67,5 Eu10 composition a considerable role might be played also by the different molar ratio modifier oxides / former oxides (see Par. 4.2.2).

- In fact, this latter effect becomes evident if we compare B67,5 Eu10 and Molari, glasses both containing the same molar amount of Eu_2O_3: even though Molari has a far lower SSA value (50 VS 114 m^2/g), and thus the biomineralization processes that take place on its surfaces should be less boosted, from IR spectra we notice similar intensities for the apatitic doublet (even higher for Molari), so we can deduce that similar amounts of HCA are formed in the two cases. Therefore, we are forced to conclude that for B67,5 Eu10 some other effect detrimental to bioactivity must exist, and we identify it exactly with the lower modifiers / formers molar ratio: being less modified makes B67,5 Eu10 more hydrolytic and leaching resistant, which renders it less reactive when immersed in solution, and therefore less prone to the biologically induced development of an HA layer.

Summarizing what we have learnt on our materials from FTIR measurements, we can say that: all the synthesized glasses are bioactive, because in all the long delay spectra it is possible to detect the typical apatitic vibrational signature; the substitution of considerable amounts of Ca ions with Eu ions for analytical purposes reduces the bioactive effectiveness of our glasses, therefore it is imperative to minimize the dopant concentration; a decrease in the value of the molar ratio network modifiers / network formers is harmful for the bioactive behavior of the glass, as seen for the B67,5 Eu10 series.

5.3.3: Micro-Raman spectroscopy measurements on biomineralized samples

The very same samples analyzed via FTIR spectroscopy have also undergone some micro-Raman characterizations, with the purpose of cross referencing all the obtained evidences, and thus to confirm or controvert our observations.

This technique has the great advantage of requiring absolutely no sample preparation, and it is completely non destructive too, therefore it proved to be optimal for our needs (very little amounts of powder available , no admissible sample loss, etc); moreover, the great capability of focalizing excitation and detection on micrometric spots of the sample granted by the coupling of a Raman spectrophotometer with a confocal microscope allowed us to analyze principally the interaction layer developed on our doped glasses, minimizing the contribution of the underneath amorphous network.

However, working with micro-Raman equipment turned out to involve also some problematic drawbacks:

- first of all, the acquired plots exhibit a low degree of quantitative reproducibility: in fact even if the relative intensities of the various peaks are more or less identical from spot to spot of a single sample, moving the analysis from a grain to another often results in a considerable change in absolute intensities; therefore, to make our spectra comparable between each other we were forced to normalize our data.
- secondly, the local nature of this technique is a double-edged sword, in the sense that to be sure that one detected spectrum is representative of the whole sample it is necessary to repeat the analysis on various spots and verify the concordance of the acquired data; moreover, if the sample itself is non homogeneous, the validity of each measurement remains of localized character[12].
- third, the amount of time needed to collect a micro Raman spectrum of decent quality is quite long: in our case, it was of 10 minutes, and since at least three measurements must be performed on each sample to understand if the acquired information can be considered of global validity, then at least a 30 ÷ 45 minute analysis time must be accounted for each sample.
- last but not least, for some Eu doped samples the Raman Stokes signal was almost completely masked by background fluorescence (see for example B67,5 Eu5 6h).

The experimental parameters (200 → 1560 cm^{-1} Raman Shift range, 0.6 cm^{-1} average spectral resolution; 41 mW laser intensity on sample, etc) employed for our measurements have already been reported in Chapter 3 and 4, and in Chapter 3 we have already described the theoretical bases of the technique; therefore hereby we will only show the curves we acquired with the help of Me.lle Elodie Petit by exploiting the micro-Raman instrument of the *Laboratoire des Materiaux Inorganiques* of Clermont-Ferrand.

In Fig. 5.25 we reported the curves obtained from biomineralized glasses belonging to the B67,5 series; in Fig. 5.26 we covered the B67,5 Eu1 samples; in Fig. 5.27 we showed the B67,5 Eu5 plots; in Fig. 5.28 we presented the B67,5 Eu10 data; and, eventually, in Fig. 5.29 we exhibited the information we gathered from Molari post interaction powders.

[12] Fortunately our materials turned out to be quite homogeneous, since only rarely we found relevant discordances between spectra acquired from different spots of the same sample.

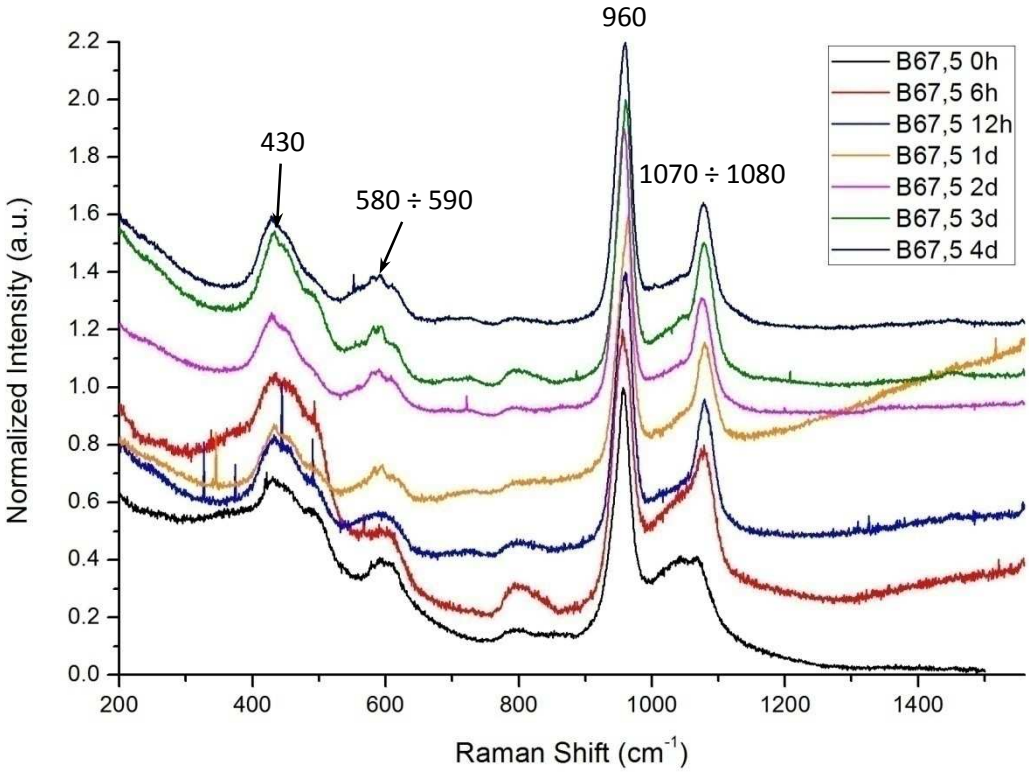

Fig. 5.25: Raman spectra of biomineralized samples of the B67,5 series (normalized to the maximum value and offsetted)

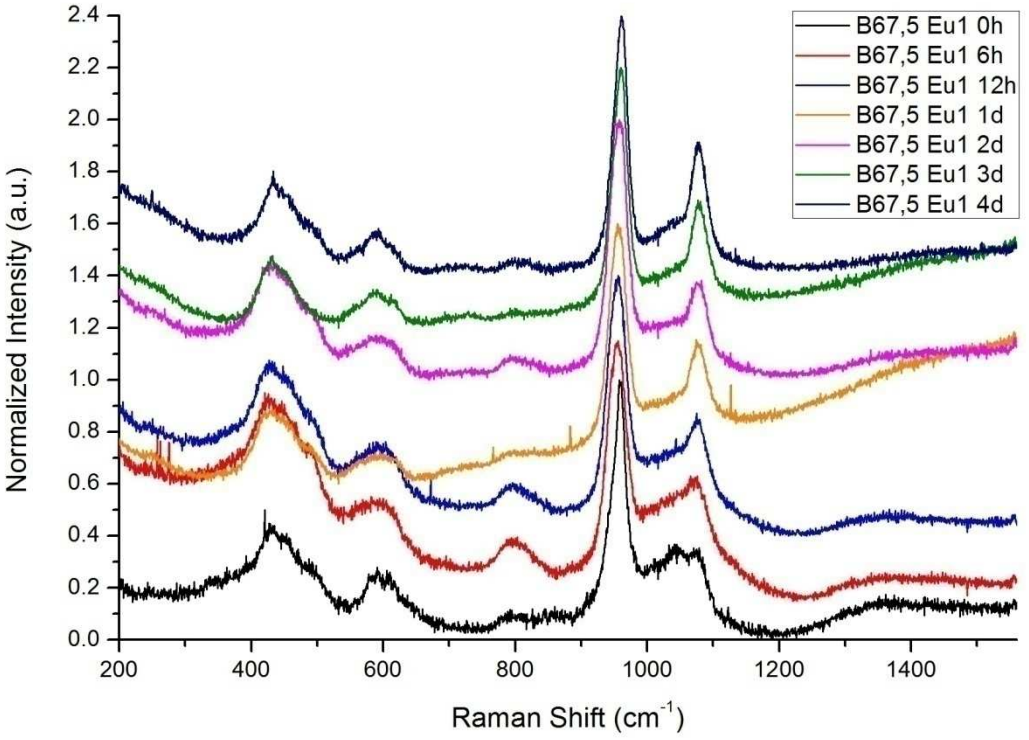

Fig. 5.26: Raman spectra of biomineralized samples of the B67,5 Eu1 series (normalized to the maximum value and offsetted)

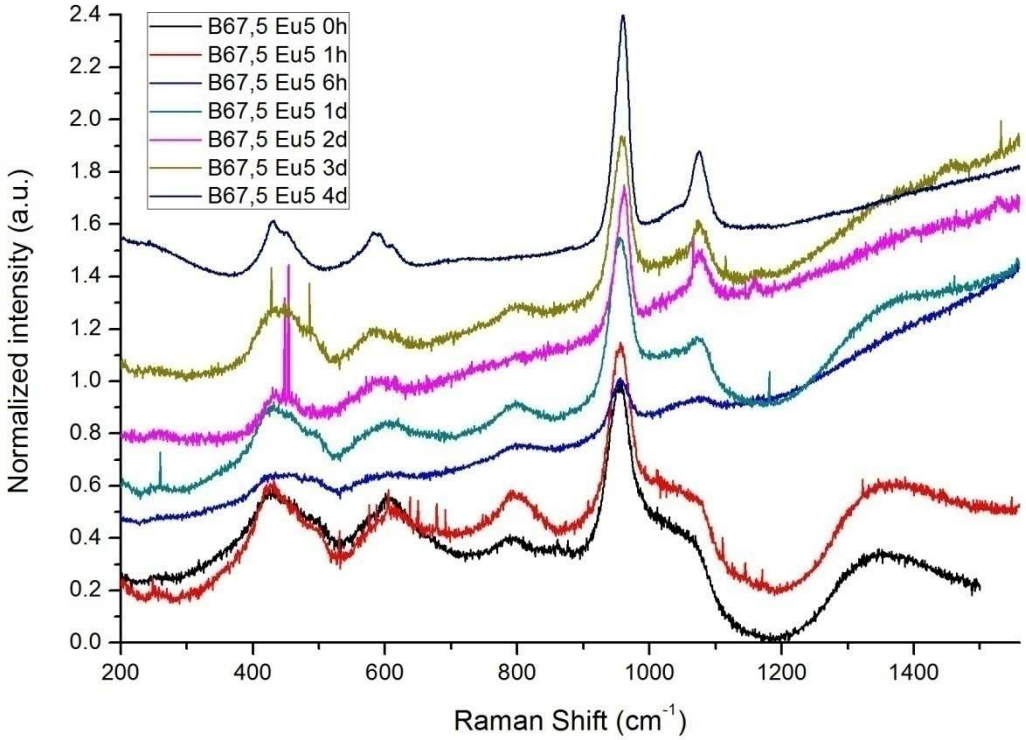

Fig. 5.27: Raman spectra of biomineralized samples of the B67,5 Eu5 series (normalized to the maximum value and offsetted)

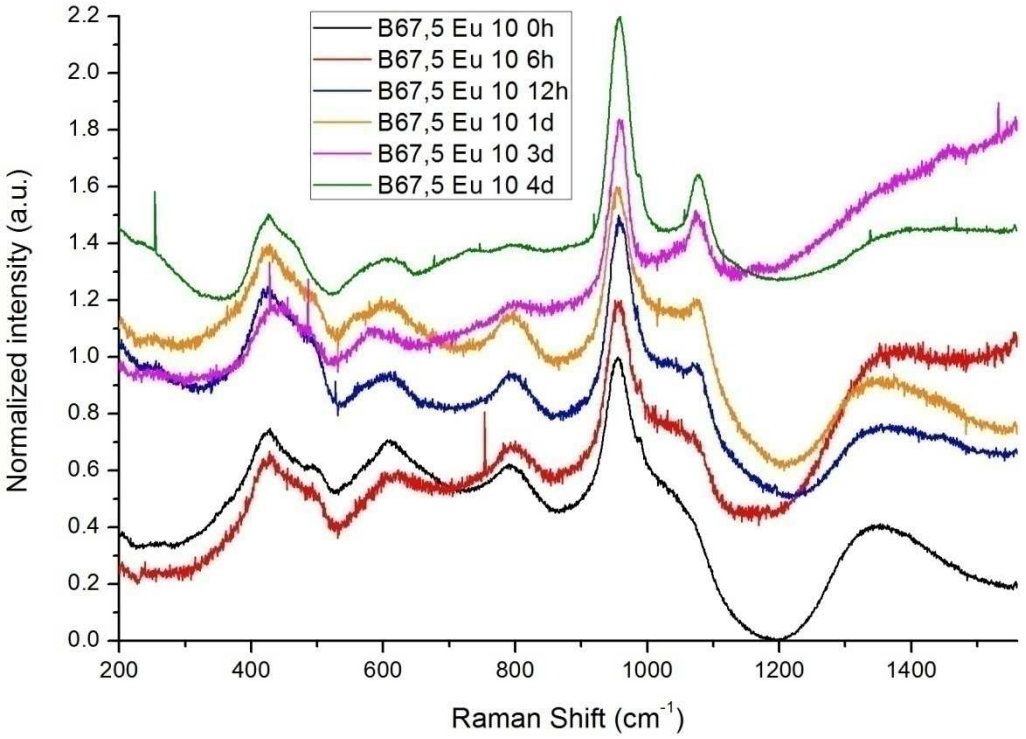

Fig. 5.28: Raman spectra of biomineralized samples of the B67,5 Eu10 series (normalized to the maximum value and offsetted)

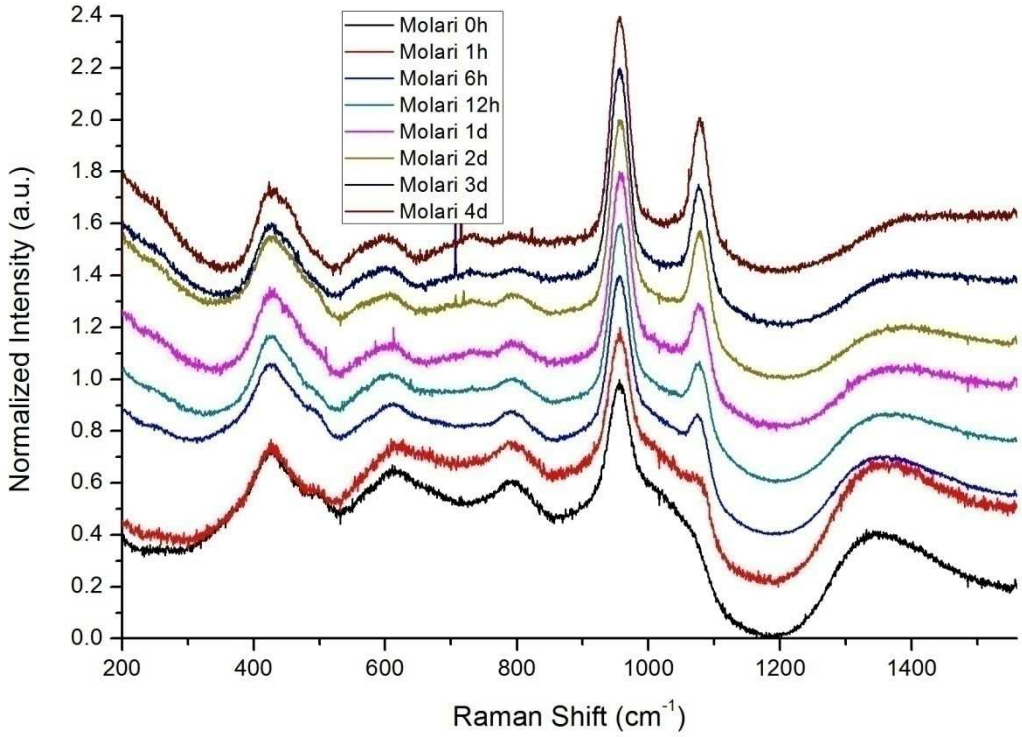

Fig. 5.29: Raman spectra of biomineralized samples of the Molari series (normalized to the maximum value and offsetted)

All the reported plots bear more or less the same spectral features, already summarized inside Tab. 4.7 of Par. 4.3.5; in particular, since we are interested in demonstrating the actual precipitation of HCA crystals on our samples, we will focus our attention basically on the ν_{sym}(P−O) peaks at 960 cm^{-1}, on the ν_{asym}(P−O) peaks at 1070 cm^{-1}, convoluted with the carbonate C−O vibrations at 1080 cm^{-1}, and on some other minor apatitic peaks like the tiny ones at around 430, 580 and 590 cm^{-1} (all the mentioned peaks are highlighted in Fig. 5.25 for the B67,5 series; literature reference on their attribution may be found in ref. [21], [33], [36] and [39]).

Since all of these peaks can be actually found in the longer interaction delay curves of the five reported graphs, we can confirm what deduced from FTIR measurements, i.e. that all of our doped glasses are capable of developing an apatitic layer on their surfaces during immersion in simulated biological media, and thus can all be considered bioactive. However, from Raman analyses we can notice again the existence of a scale of bioactive effectiveness: in fact, the final (4 days) heights of the two main phosphate peaks at 960 and 1070 cm^{-1} are not always the same, and the appearance of the minor apatitic peaks takes place at different times (and in some cases they are not even detectable).

In particular, if we establish a reasonable connection between amount of HCA formed and height of the mentioned peaks (as done for example in ref. [33]), we can make the following observations:

- The original B67,5 is the glass that forms on its surfaces the most developed apatitic layer, since its peaks at 960 and 1070 cm^{-1} are the highest detected; moreover, it exhibits the fastest biomineralization kinetics, with an intense 1070 cm^{-1} peak already after 6 hours, and minor apatitic peaks present already after 1 day.
- B67,5 Eu1 has almost the same specific surface area as B67,5, so their reactivity in solution should be identical from a textural point of view; however, the final intensity of the peak at 960 cm^{-1} is a bit lower, therefore the total amount of precipitated HCA is slightly inferior. Other important difference is that B67,5 Eu1 has a slower development with respect to B67,5, since the peak at 1070 cm^{-1} becomes strong only after 12 hours, and the minor peaks at 430, 580 and 590 cm^{-1} appear only after 2 or 3 days of immersion. Given that the difference between these two glasses lies only in the doping, we conclude that the small substitution of CaO with Eu_2O_3 ($1\%_{wt}$) alters a little the bioactive behavior of the doped glass; in particular, the effect seems to be of kinetic nature, since the evolution of the curves seems somewhat delayed in the case of B67,5 Eu1.
- If we switch to B67,5 Eu5, which has an almost double SSA value with respect to the two preceding samples, we notice a further decrease in bioactivity: the main peaks are slightly lower, the minor ones appear only after 4 days, and, above all, the development of the apatitic layer is considerably slower, since we need to wait 2 days to have a good 1070 cm^{-1} peak. This confirms the hindering effect of Eu_2O_3 on the biomineralization processes: from a textural point of view B67,5 Eu5 should be more reactive, so detecting less apatite formation means that the doping process has altered the bioactivity of the glass.
- Further evidence of this fact comes from the B67,5 Eu10 series, which exhibits even lower peaks and the slowest reactivity ever: here we don't even detect minor apatitic peaks, and to see a decent 1070 cm^{-1} peak we have to wait 3 or 4 days. However, as already pointed out in Par. 5.3.2, here the kinetic hindering effect of Eu_2O_3 is surely coupled to the relevant diminution of the molar ratio network modifier oxides / network former oxides, that renders the glass less reactive in solution (even if it has approximately the same SSA value of B67,5 Eu5).
- This latter statement is consistent with the trend of Molari's spectra, that testify a return to a level of bioactivity much higher than in B67,5 Eu10's case: even if Molari has half the

SSA of this latter glass (so its kinetics should be less surface boosted), its curves exhibit intense apatitic peaks (except for the minor ones, still undetectable), just a bit lower than B67,5 Eu1's ones, and a relatively fast development, with a good 1070 cm^{-1} peak after 12 hours. This means that the molar ratio modifiers / formers plays a fundamental role in the bioactivity behavior.

From what reported, it seems evident that most of the experimental evidences provided by FTIR and micro Raman measurements are in perfect agreement, and lead us to the same conclusions: B67,5 is the most bioactive glass, even though B67,5 Eu1 has a very similar biomineralization effectiveness; the specific surface area values of the powders are extremely important in driving the reactivity in DMEM; the substitution of increasing weight percentages of CaO with equal weight percentages of Eu_2O_3 progressively reduces the in vitro bioactivity of the samples, both because of the consequent increase in hydrolytic and leaching resistances (due to the decrease of the molar ratio modifiers / formers) and because of a kinetic hindering effect of Eu ions themselves on the precipitation of HCA, testified by the slight (but still detectable) differences in HCA development between B67,5 and Molari (having the same ratio modifiers / formers, but the latter containing $2\%_{mol}$ of Eu_2O_3).

The only relevant difference between FTIR and Raman data lies in the relative importance of the two aforementioned factors detrimental to bioactivity: if we look to Raman spectra, the molar ratio network modifiers / network formers seems much more important than the intrinsic Eu ions hindrance effect to HCA precipitation, since, as we've just said, Molari's, B67,5's and B67,5 Eu1's plots are quite close to each other (and all the three share practically the same ratio and SSA value); on the contrary, if we look to FTIR spectra, we notice a certain difference between Molari's and the other two's curves, which would lead us to think that it's the presence of Eu ions the factor that dominates the biomineralization kinetics slowdown.

However, Raman spectroscopy is said to be more sensitive to the vibrations of phosphate groups immersed in a crystalline environment than infra-red spectroscopy (see ref. [31], pag. 99), so it is plausible that the most correct interpretation is the one provided by Raman measurements, i.e. that the alteration of the molar ratio modifiers / formers connected to the peculiar (and maybe not so keen) way we operated the doping with Eu_2O_3 is more important than the intrinsic precipitation hindering effect of Eu ions themselves in spoiling the bioactivity behavior of our doped glasses.

5.3.4: ICP-AES measurements on post-interaction simulated biological media

The inductively coupled plasma atomic emission spectroscopy (ICP-AES) is a very powerful technique, capable of providing a very accurate compositional characterization of the analyzed samples, in some cases reaching the remarkable sensitivity of a few parts per billion (ppb); however, in order to be fed into the plasma torch that constitutes the heart and soul of the instrument, the samples must necessarily be in the liquid form, so only solutions and dissolved samples[13] are suitable to undergo ICP-AES measurements (for more detailed information, refer back to Chap. 3).

Being basically an ionic solution containing a few bio-organic species, DMEM is perfectly compatible with this characterization technique, and can be fed directly to the flame, without any need of prior processing; unfortunately, though, since it contains a lot of different ions and in considerable amounts, it can turn out to be a little instrument polluting, therefore after a batch of analyses it might be positive to thoroughly clean the whole equipment (especially the feeding circuit, the nebulizer and the plasma chamber) before passing to different samples.

In order to validate the results obtained exploiting our luminescent structural probe, we are highly interested in estimating the extent of the alterations to the hydrolytic and leaching behavior induced in our glasses by the increasing substitution of CaO with Eu_2O_3; to shed some light on this subject, and thus to discover whether our probe significantly alters its target or not, we decided to monitor via ICP-AES the evolutions with *in vitro* bioactivity testing time of Ca, P, Si and Eu ionic concentrations in the interaction media.

In fact, up to this point all of our efforts were concentrated on the biomineralized powders, but to reach a more complete understanding of the complex phenomena that take place upon immersion of our doped glasses in DMEM, we need also some information on the compositional evolution of this latter liquid with interaction time. Then cross referencing these data with what already deduced from other measurements, and always keeping into account the importance of the specific surface area and of the molar ratio modifiers / formers (whose values are reported as a reminder in Tab. 5.5) of the powders, we will be able to reach some preliminary conclusions, that might become a new starting point for further researches of the team on this topic.

[13] The dissolution must be carried out in an adequate solvent and by exploiting an appropriate method, such as the alkaline fusion (also referred as "alkaline pearl") method, direct acidic digestion, etc.

Glass series	Modifier/Former oxides molar ratio	Specific Surface Area (m^2/g)
B67,5	0,379	64
B67,5 Eu1	0,366	184
B67,5 Eu5	0,315	131
B67,5 Eu10	0,252	113
Molari	0,379	49

Tab. 5.5: SSA values and network modifier / network former oxides molar ratios for the five series of glass powders that underwent bioactivity tests

As already anticipated in Par. 5.1.2, from each interaction bottle, corresponding to a particular glass series and to a particular immersion delay, a sample of biological liquid has been collected and analyzed; Si and Ca concentrations were determined exploiting the built-in multi-element scanner of the instrument[14], while for P and Eu contents the use of reference solutions, containing known concentrations of said elements, was necessary, and the analysis was carried out using the single-element scanner. This time, differently from the alkaline fusion ICP-AES measurements of Par. 4.3.1, a certificated standard solution containing 10 ppm of metallic Eu was fortunately available, so it was possible for us to quantify also the Eu^{3+} ionic releases for each type of glass and for each interaction delay.

The results we gathered have been reported in four graphs, one for each dosed element: Eu in Fig. 5.30.1, P in Fig. 5.30.2, Si in Fig. 5.30.3 and Ca in Fig. 5.30.4; obviously, therein the 0 hours data correspond to analyses on pristine DMEM. To make the reading of the graphs as straightforward as possible, we connected with colored lines the various dots corresponding to detected values, but in none way we intend to mean that the real ionic concentration trends are those shown by said lines.

The interpretation of these plots is unfortunately a complicated matter, since the effect of the dopant itself on biomineralization processes is superimposed first to the different kinetic

[14] Since the instrument was property of the Volcanology Department, it was tailored on "geologist" needs, therefore it was specifically equipped to provide rapid, simultaneous and accurate data on Si and Ca concentrations (but also on Al, Fe, K, etc), because these elements are extremely abundant in rocks (families of the silicates and of the limes).

boosts induced by the different specific surface area values of our powders, and second to the different leaching and hydrolytic resistances of our glasses, connected with the peculiar way we operated the doping, i.e. via substitution of equivalent weight percentages of oxides (which progressively changed the molar ratio modifiers / formers).

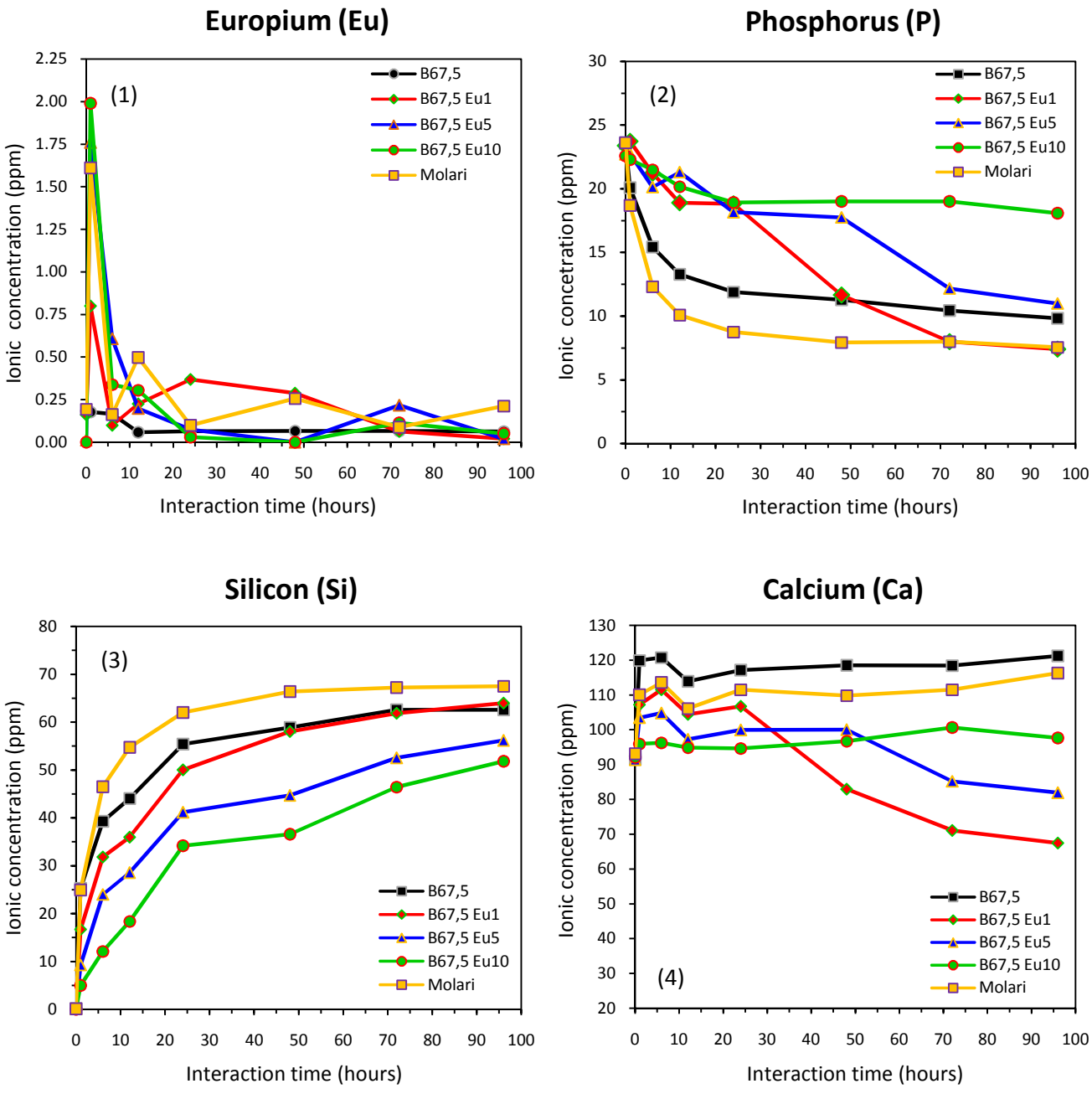

Fig. 5.30: Evolution of ionic concentrations in DMEM throughout *in vitro* bioactivity testing

Let's start commenting from Fig. 5.30.1, that is from the evolution of **Europium**'s release inside the biological medium: the first interesting thing to notice is that even in the case of the

undoped B67,5 glass, concentrations up to 0.2 ppm of ions are detected in solution; the material, however, was synthesized with utmost care to avoid REE contamination (for example using brand-new Teflon vessels and alumina crucibles for the gelation and calcination steps), so what we can first conclude is that the sensitivity of the instrument in dosing Eu content is not much better than 0.2 ÷ 0.3 ppm.

Excluding B67,5, the other four above reported plots exhibit a similar trend: after an initial release peak after 1 hour, Eu concentrations decrease considerably, attaining values of around 0.3 ppm, really close to the detection limit, as soon as after 12 hours of immersion time; this seems to confirm the hypothesis we made on the behavior of our probe during bioactivity tests: after an initial step during which Eu ions are leached from the glass network, and thus can be found in considerable amount inside the solution, they are then progressively incorporated inside the amorphous Ca-P layer (and eventually in HCA crystals) growing on the surfaces of powder grains, leading to their almost complete depletion from DMEM.

The maximum concentration attained after 1 hour is, as it was natural to suspect, in some way proportional to the Eu_2O_3 molar percentage, but deepening the observations on this effect is rendered really difficult by the different SSA values and modifiers / formers molar ratios of our samples: for example, passing from B67,5 Eu1 to B67,5 Eu5 we can easily detect an increase in Eu release, and the same we notice passing from B67,5 Eu5 to B67,5 Eu10, but understanding if a direct or a different type of proportionality exists is practically impossible, since we must also keep into account that the SSA value of Eu1 > Eu5 > Eu10, and that the hydrolytic and leaching resistance of Eu1 < Eu5 < Eu10 (due to the doping procedure we employed), etc.

Moreover, the values we can detect at 1 hour almost certainly are not the real maximum Eu concentration attained in the solution, since the leaching process is very fast and most probably reaches its climax in the very first few minutes of interaction; the maxima themselves are also sure enough reached at different times for different samples, since these latter have different leaching resistances and surfaces available for the attack[15].

[15] As already mentioned in Par. 5.1.3, even if we did keep for all the glass series a constant ratio between total surface of the immersed powders and total volume of DMEM put in each interaction bottle, it was impossible to completely compensate for the different kinetic surface boosts given to *in vitro* reactivity by the considerably different specific surface area values of our samples.

Therefore, in order to deduce more detailed and precise information, we should have performed briefer tests, in the scale of minutes, but from the research team's experience these kind of assays often turn out to be not much reliable (see ref. [23]): in fact, when the total immersion time is of 10, 20 or 30 minutes, even the smallest operational delays in the interaction protocol can yield unacceptable errors; moreover, 10 minutes assays cannot really be considered to take place at constant temperature, since the time needed to pass from the fridge's T (4°C) to the oven's T (37°C) is of around a couple of minutes. All of this seen, we decided not to carry out additional short term tests.

Let's now switch to commenting Fig. 5.30.3: since **Silicate** ions are not present inside DMEM's original composition and are released inside the medium due to the hydrolytic dissolution of the glass network operated by water molecules (and OH^- ions), their concentration increases with interaction time. Moreover, all the curves exhibit a behavior typical of a saturation phenomenon, that is after a steep rise in the first 20 hours, they then bend towards the horizontal: this means that at a certain point the dissolution processes slow down and eventually stop, and that Silicate ions are not integrated inside the Ca-P layer[16].

This effect is mainly due to two different reasons: first, once a certain concentration of Si ions is attained, the driving force for further dissolution of the amorphous network becomes inferior; second and most important, at a certain point the Ca-P layer formed on the surfaces renders the underneath silica gel layer (i.e. the outer part of the silicate network, depleted of modifier cations by the initial ionic exchange/leaching processes; see Chap. 1) no more easily reachable for water molecules, so the hydrolytic attack becomes less and less effective with immersion time.

Si ions release seems more influenced by the hydrolytic resistance of our glasses (tightly connected to their molar ratio network modifiers / network formers) than by their specific surface area values: the most straightforward evidence of this is the fact that B67,5 Eu1, having around three times the SSA of B67,5 but almost the same aforementioned ratio value, has practically the same behavior of this latter glass for what concerns the evolution of Si concentrations; and the tiny negative difference detectable is perfectly consistent with its slightly lower ratio, and thus with its slightly higher hydrolytic resistance.

[16] We could also make the hypothesis that a dynamic equilibrium state is reached, with Si depletion perfectly balanced by its hydrolytic release, but from literature evidences we can state that this is not the case.

Further proof of the statement underlined above can be found in the fact that B67,5 Eu10, having the lowest modifiers / formers ratio, and thus the strongest amorphous network, has also the lowest Si release of all our samples.

It is also very interesting to notice that B67,5 and Molari exhibit very similar shapes in their curves (and this is a feature that can be found also in P and Ca plots), even though a little difference in absolute values exists (Molari releasing somewhat more Si than B67,5): this means that the doping with Eu_2O_3, when operated via substitution of equivalent **molar** (and not weight) percentages of oxides, does not alter too much the hydrolytic and leaching behavior of our bioactive glasses. And since this is true for a huge $2\%_{mol}$ of Eu_2O_3, this shall be even more true when the doping degree is kept as low as possible, compatibly with the obtainment of a good quality luminescence signal.

Moreover, maintaining for our doped glasses a Si release kinetic tightly comparable to B67,5's is crucial to ensuring a satisfactory Type A bioactivity (demonstrated for B67,5 in ref. [49]): in fact, as already exposed in Chap. 1, silicate ions have a highly beneficial effect on osteo-integration, because they play an important role in a series of biological mechanisms leading to the activation and acceleration of bone regeneration (see ref. [42]). And even if Eu doped glasses are not meant to be used for *in vivo* tests, being sure that the doping process does not alter such a critical feature of our materials is a very positive aspect for the validation of our luminescent structural probe.

If we now switch to Phosphorus or Calcium graphs, we enter inside the domain of the ions more directly involved in biomineralization, that is first in the formation of the surface layer enriched in Ca and P, commonly referred to as the amorphous calcium phosphates layer, and, later on, in the precipitation of hydroxyl-carbonate-apatite crystals; since these processes take place on the surface of the glass grains, they turned out to be more deeply influenced by the specific surface area value of the powders than what we noticed for Si release.

Starting from **Phosphorus**, we notice that all the plots show a considerable decrease in its concentration with interaction time, which means that phosphate ions are progressively depleted from DMEM to build the Ca-P layer and HCA crystals; in fact, differently from Ca, P is not sufficiently abundant and easily available in the glass to cover the needs of the growing interfacial layer, so it must always be drawn from the biological medium.

The curves seem to reflect what emerged in Par. 5.3.3: from Raman measurements we noticed that B67,5 Eu10 formed the smallest amount of HCA, and here we find out that it also consumed the smallest amount of DMEM's phosphate ions; B67,5 Eu5 spectra exhibit more intense apatitic peaks, and from Fig. 5.30.2 we notice that in its case the decrease in P concentration is stronger. The case of B67,5 Eu1 is peculiar, since the sample that eventually underwent ICP-AES measurements had a different SSA value from the one that underwent Raman characterizations[17], so we cannot establish a direct connection between the two sets of data; however, the high SSA of B67,5 Eu1 2nd calc (bioactivity tested) makes us hypothesize that a strong biomineralization might have taken place, and this would be perfectly consistent with the considerable amount of P taken from the solution.

If in the end we compare B67,5's and Molari's plots, we discover that the curves have practically the same shape, but differ a bit in the final attained concentrations; this is highly encouraging, since it means that, as already pointed out for the silicate ions release, if we operate the doping of our bioactive glasses with Eu_2O_3 by substitution of equivalent molar percentages of CaO, it is actually possible not to alter significantly the leaching and dissolution behavior of our samples.

Moreover, we can find a very good agreement between phosphate ions' depletion kinetics and Raman spectra: B67,5 and Molari exhibit steep decreases in P content in the first few hours, and parallel fast evolutions of apatitic Raman peaks, with intense 1070 cm^{-1} asymmetric P−O vibrations as early as after 6 ÷ 12 hours; on the contrary, B67,5 Eu10 consumes phosphate ions very slowly, and a slow development of the apatitic peaks is shown in Fig. 5.28.

B67,5 Eu5's ICP-AES plots exhibit a considerable decrease in phosphate content starting from 2 days, and in Raman spectra we notice that HCA precipitation becomes really relevant only after 2 ÷ 3 days.; exactly the same trend can be noticed also from B67,5 Eu5's site A emission spectra of Fig. 5.6, where the typical peaks of Eu^{3+} ions hosted inside HCA's lattice exhibit a considerable intensity only after 2 days. This very good agreement between data provided by three different characterization techniques can be seen as a further proof of the identification we made earlier.

[17] As already stated in Par. 5.1.2, this was due to a technical malfunction of the instrument, that was not able to perform the required analyses on the **B67,5 Eu1 1st calc**'s series of post interaction fluids the day it was delivered to the Department of Volcanology.

Let's finally pass to Pic. 5.30.4, that is to commenting the evolution of **Calcium**'s ionic concentrations in DMEM throughout bioactivity testing; in the first few hours[18] all the reported plots exhibit a steep increase, which corresponds to the leaching of modifier cations (amongst which, in our case, Ca plays the most important role) from our glasses' networks as a consequence of fast ionic exchanges between said ions and H^+ (H_3O^+) ions present in the liquid phase (see Chap. 1).

In particular, it's easy to notice that the higher the network modifiers / network formers molar ratio, i.e. the lower the leaching resistance of the glass, the higher results also the maximum value reached by calcium's concentration. Therefore, since we operated the substitution of CaO with Eu_2O_3 in terms of weight percentages (see Par. 4.2.2), and since this *modus operandi* brought about a progressive diminution in said ratio, we can find out that higher doping degrees involve lower releases of Ca^{2+} ions inside the biological medium: in fact, B67,5 has the highest initial Ca concentration value, while B67,5 Eu10 has the lowest.

It is also extremely interesting to observe that Molari glass, which has exactly the same modifiers / formers ratio and almost the same specific surface area value as B67,5, and thus is quite well comparable to this latter, exhibits a Ca release just a bit lower than the original undoped glass; this means that, just as we thought, Eu^{3+} ions, though still behaving as network modifiers (as testified by the fact that they can be leached from the glass; see Fig. 5.30.1), are less effective then Ca^{2+} in breaking the continuity of the silicate amorphous lattice, and therefore slightly alter (slowing it down) the leaching behavior of the glass.

The difference in maximum detected values of Molari and B67,5 (112 VS 121 ppm), however, is less than the 7.5%, and in this case the molar percentage of Eu_2O_3 assumes the very high value of $2\%_{mol}$. On the other hand, as we have previously seen, at such high doping degrees a series of undesirable problems (alteration of devitrification behavior, kinetic hindering of HCA precipitation, concentrational self quenching of luminescence, possible precipitation of phases different from Eu doped HCA, clusterization of REE ions inside the amorphous network, etc) arises, so the optimal dopant concentrations are far lower, around $0.1 \div 0.3\%_{mol}$. Therefore it is reasonable to state that for a bioactive glass doped in the correct way (i.e. working in molar percentages) with the optimal amount of Eu the alterations to

[18] Up to 6 hours, according to the available data; however, without concentration measurements in between 1h and 6h, it is impossible for us to know if after 1h the concentration of Ca ions continues to grow slowly but steadily, or, on the contrary, if it reaches a spike maximum, and then it steeply decreases again.

biomineralization processes should be largely negligible, and thus that our luminescent structural probe should not change significantly the target it is meant to study.

When we consider longer interaction delays, the precipitation of amorphous and crystalline calcium phosphates on the surfaces of our glass grains becomes the dominant phenomenon, so that the Ca concentration curves start to behave in a way more deeply influenced by the SSA values of our samples: for example, B67,5 Eu1, having the widest surface area (184 m^2/g), undergoes a very intense biomineralization, leading to a strong and fast depletion of Ca^{2+} ions from DMEM to feed the development of the growing Ca-P and HCA layer.

In the case of B67,5 Eu5 (SSA = 131 m^2/g), whose Raman plots show a slower onset of apatite crystallization, the drop in Ca concentration (exactly as we have just noticed for phosphorus) is somewhat delayed: it starts after 2 days, and not after 1 day as in B67,5 Eu1; for B67,5 Eu10 (SSA = 113 m^2/g), suffering strong hindering effects to HCA precipitation due to its high hydrolytic resistance and high Eu content, the plots show an almost constant Ca concentration, clear sign of slow biomineralization processes: the slowly growing crystals have no need of drawing ions from the biological medium, since the leaching and dissolution phenomena ensure themselves a sufficient and timely supply.

Once again, as already seen for Si and P, even in the case of Ca concentrations Molari and B67,5 exhibit trends very close to each other; however, having SSA values (respectively 49 and 64 m^2/g) considerably lower than the previously mentioned three glasses, they seem not to deplete the biological medium of Ca ions to the same extent, probably because Ca is released in sufficient amount to constantly feed the growth of the apatitic layer.

Summarizing the most important information we have learnt from ICP-AES data, we can say that the ionic release of our doped glasses is deeply influenced by their hydrolytic resistance, in turn influenced by the peculiar way we operated the doping; however, if this latter is carried out in a proper way, a good agreement can be found between doped and undoped samples behaviors, thus demonstrating that if some conditions are respected, the data we obtain from our luminescent probe can be considered rigorously valid.

5.3.5: Conclusions

In this Chapter we have dealt with the core of our research activity, that is with the first steps in the development of an alternative method of characterization that allows to study with high

sensitivity the biomineralization processes that take place on the surfaces of bioactive glasses by exploiting a luminescent structural probe such as Eu^{3+} ions.

In particular, first we have designed and tailored to our needs an *in vitro* interaction protocol, in order to establish some reproducible way to estimate the bioactive efficiency of our synthesized materials; then we have discovered a way to actually detect the formation of Eu doped HCA crystals on our Eu doped glasses' surfaces through site selective luminescence measurements, and we've tried to translate it into some embryonic analytical method; finally, we tried to gather as many evidences as possible through various characterization techniques to demonstrate the validity of our probe: that is we tried first to find indisputable proof that the peculiar emission feature we exploited to detect biomineralization, i.e. the characteristic luminescent spectral signature detectable when exciting our samples with a laser beam having λ = 574 nm, is actually due to Eu^{3+} ions hosted inside HCA's lattice; and second we tried to prove that our probe does not alter too much the behavior of our glasses while immersed in biological fluids, both for what concerns the ionic release and the precipitation kinetics.

From all we have seen so far, we can confidently state that if the doping process is carried out in an opportune way (in molar percentages), and sufficiently low amounts of Eu_2O_3 are employed, the Eu doped glasses behave in the same way as the original, undoped ones, and thus the information we can acquire through site selective luminescence spectroscopy analyses is actually representative of these latter's bioactive behavior.

Conclusions and future perspectives

Facing the new challenges connected to the progressive ageing of the population in developed countries, especially the need of ensuring a satisfactory quality of life to the increasing number of elderly people, requires a great and united effort to many different and usually not communicating research fields, such as biology and biochemistry, medicine and surgery, materials science and engineering, etc.

In the last decades biomedical research has made giant steps forwards, and impressive achievements have been reached so far, like the creation of permanent implantable total artificial hearts (Abio Cor II, 2009), or of advanced bionic prosthetic hands responding to the myo-electric signals of the patient (i-LIMB hand, 2007). Even in the field of bone substitutes the progress has been really considerable, and nowadays there exist a lot of commercial products (NovaBone, PerioGlass, Novamin, Biogran, etc.) capable not only of filling bone defects, but also of actively stimulating the growth of osseous tissue, eventually leading to the complete resorption of the implant, i.e. to its substitution with newly formed natural bone.

To continue on this path and achieve new conquests in the biomedical field, one of the possible strategies is to improve the performances of the existing materials, as well as developing new, more effective ones; and to succeed in doing so, it is extremely important to further deepen our knowledge on the processes that take place at the interface between implants and host tissues.

In the case of bioactive materials, designed to interact with osseous tissue (e.g. bone substitutes or coatings for metallic prostheses), this means delving into the biomineralization processes, to better understand their dynamics and kinetics; in the past decades much has been written on this subject, but extensive quantitative information is somewhat lacking, mostly due to technical and technological difficulties in detecting and quantifying the formation of the hydroxyl-carbonate-apatite surface layer developed during interaction with biological fluids, distinctive feature of this class of biomaterials.

Striving to overcome this latter problem, we have laid the first steps in the development of a novel characterization technique, based on the use of Eu^{3+} doping ions as a luminescent

structural probe and on site selective luminescence spectroscopy measurements; in particular, we made the hypothesis that the Eu doped bioactive glasses to be studied were able to develop an Eu doped interfacial HCA layer upon interaction with biological environment, and that therefore the characteristic emission of Eu^{3+} ions hosted in the apatitic lattice could be detected and isolated by site selective excitation.

Following the path described in Chapter 5, we were able to demonstrate that this assumption was correct by reporting a series of evidences, gathered through various characterization techniques (XRD, FTIR, micro-Raman; see the whole section 5.3), that proved right the attribution of the detected typical Site A emissive spectral signature (see Par 5.2.2) to Eu^{3+} ions hosted in Ca(II) sites of the HCA lattice. This laid the foundations for the development of an embryonic characterization method, that proved to be capable of providing data perfectly consistent with what could be deduced by other characterization techniques (see Par. 5.2.5). Moreover, we demonstrated also that our novel technique was capable of detecting the formation of HCA even when the crystals were of nanometric size and represented only a tiny mass fraction of the whole sample, i.e. even for the shorter biological interaction delays.

The method then underwent validation trials, that is we tried to understand whether our luminescent probe had any influence on the very same biomineralization processes it was meant to study, or not; exploiting a series of characterization techniques (XRD, FTIR, micro-Raman, N_2 gas sorption, ICP-AES) we were able to demonstrate that, at least in the case of the base bioactive glass we studied, B67,5 (see Par. 4.2.2):

- High weight percentage substitutions of CaO with Eu_2O_3 yield samples with an increased degree of microporosity and with larger specific surface area values.
- High $\%_{wt}$ of Eu_2O_3 hinder the devitrification of apatitic phases upon calcination at 700°C;
- High $\%_{wt}$ of Eu_2O_3 slightly alter the leaching and hydrolytic dissolution behavior of the doped glasses, due to a strengthening effect on their networks that decreases the ionic release and its rate.
- High $\%_{wt}$ of Eu_2O_3 result in a decreased formation of HCA during immersion in DMEM.

Nevertheless, we also proved that when the doping is carried out by substitution of equivalent molar percentages of CaO with Eu_2O_3, the above mentioned alterations are considerably reduced (see all data regarding Molari glass), up to a point of being practically negligible if the dopant content is kept as low as $0.2 \div 0.5\ \%_{mol}$.

This demonstrates that if the concentration of Eu^{3+} ions is properly tailored, our luminescent structural probe does not alter the targets it is meant to study, and, therefore, that the acquired site selective luminescence spectroscopy data can be actually considered representative of the true biomineralization processes taking place on the bioactive glass surfaces.

Our novel characterization method, however, still has a very long way to go before it can be considered fully developed; in particular, future directions of study might be:

- Individuation of the $^5D_2$ level energetic position for Eu^{3+} ions hosted in HCA: this result could not be achieved during our research activity due to the protracted malfunction of the light source (Xe lamp) exploited for excitation measurements. Once the correct wavelength for the promotion of type A Eu ions into their $^5D_2$ level determined, it will be possible to acquire site selective emission spectra exhibiting the complete[1] spectral signature of Eu ions hosted in the apatite layer, $^5D_0 \rightarrow {}^7F_0$ peak included.

- Localized chemical composition measurements: following the evolution of the composition of our doped bioactive glass grains at a microscopic and sub-microscopic scale, both in the surface region and in the bulk, might provide further useful information on the influence of Eu_2O_3 on biomineralization processes; in particular, PIXE-RBS microprobe data for the base bioactive glass B67,5 are already available (see ref. [49]), so carrying out this type of analyses also on our samples would allow an interesting comparison between compositional evolutions during *in vitro* bioactivity tests to be made. Moreover, electron microprobe chemical analyses on HCA crystals developed in the case of B67,5 Eu10 and Molari glasses would let us know with certainty if the lack of Site A characteristic emission peaks from their luminescence spectra is actually due to some concentration self quenching effect, or if at high doping degree Eu ions are integrated with less efficiency into the HCA lattice[2].

- Individuation of the optimal doping degree: carrying out in vitro bioactivity tests on new B67,5 EuX samples with very low Eu content (< $1\%_{wt}$, i.e < $0.2\%_{mol}$) would permit to estimate which is the lowest $\%_{mol}$ of Eu_2O_3 capable of returning a Site A luminescence

[1] On the contrary, the spectra we reported in Par. 5.2.2 and 5.2.5 all lack the $^5D_0 \rightarrow {}^7F_0$ peak, since we excited our samples in the $^5D_0$ level, and therefore the above mentioned transition is masked by the laser scattering.

[2] This information, however, is of pure theoretical value, since such high Eu_2O_3 contents ($2\%_{mol}$) have proven to be not suitable for the application of our method, due to the not completely negligible alterations to biomineralization processes they induce.

emission signal of sufficient quality to be exploited in our method.

- Development of quantitative measurements: the technique we have elaborated so far does not provide any quantitative, "numeric" information on the analyzed samples, but relies on the comparison between acquired spectra. Since a precise quantification of HCA precipitation on bioactive glasses is the final aim of this research, the next fundamental step will be a quantitative calibration of the method, coupled with a greater exploitation of time resolved measurements (Eu ions in HCA have shorter luminescence decay lifetimes than Eu ions in glass) to better isolate the emission of type A Eu^{3+} ions.

- Application of the method to other bioglasses: our novel characterization technique has been developed in the case of a B67,5 composition, but aims to be applicable to all bioactive glasses; therefore, a series of tests and measurements very similar to those carried out in the present work should be performed on other sol-gel derived doped samples, to verify the actual reliability of the provided results also for compositions different from that of B67,5 (see Tab. 4.1).

- cell culture assays: last but not least, the applicability of our characterization method could also be investigated in the case of cellular *in vitro* tests; obviously, the potential cytotoxic effect of Eu^{3+} ions on osteoblasts and other cells might render our protocol not suitable for these applications, so performing some verification tests would be extremely interesting to assess its limits.

Summarizing and concluding, in this thesis we have developed up to an embryonic stage a novel method to study the biomineralization processes taking place at the interface bioactive glass / biological fluids; this method has proven to be effective in detecting the precipitation of hydroxyl-carbonate-apatite crystals on the surfaces of the samples, and, under opportune conditions, the acquired data have proven to be truly representative of the actual bioactive behavior of the analyzed material.

At the moment this technique cannot be considered cost-effective, that is the quality of the results it can provide does not yet justify the high costs connected to the use of an expensive dopant such as Europium. Nevertheless, we believe that, once fully developed even in its quantitative aspects, our novel characterization method might turn out to be a valuable asset in the biomedical research on bioactive glasses.

Bibliography

[1] A. Ramila, F. Balas, M. Vallet-Regi, *Synthesis Routes for Bioactive Sol-Gel Glasses: Alkoxides versus Nitrates*, Chem. Mater. 2002, *14*, 542-548.

[2] A. J. Salinas, M. Vallet-Regi I. Izquierdo-Barba, *Biomimetic Apatite Deposition on Calcium Silicate Gel Glasses*, J. Sol-Gel Sci. Tech. 21, 13–25, 2001.

[3] W. Cao, LL. Hench, *Bioactive Materials*, Ceramics International 22, 1996: 493-507.

[4] J.K. Krebs, J.M. Brownstein, J.T. Gibides, *Decay dynamics of europium excited states in bioactive glasses*, Journal of Luminescence 128 (2008) 780–782.

[5] A. Doat, M. Fanjul, E. Hollande, *Europium-doped bioapatite: a new photostable biological probe, internalizable by human cells*, Biomaterials 24 (2003) 3365–3371.

[6] A. Krajewski, A. Ravaglioli, *Bioceramica e corpo umano*, Faenza Ed., 1984.

[7] M. Vallet-Regi, A.J. Salinas, D. Arcos, *From the bioactive glasses to the star gels*, J. Mater Sci: Mater Med (2006) 17:1011–1017.

[8] J.D. Bronzino, *The biomedical engineering handbook, volume 1*, CLC Press LLC: Boca Raton (Florida), 2000.

[9] D. Arcos, D. C. Greenspan, M. Vallet-Regi, *Influence of the Stabilization Temperature on Textural and Structural Features and Ion Release in SiO_2-CaO-P_2O_5 Sol-Gel Glasses*, Chem. Mater. 2002, *14*, 1515-1522.

[10] Ting Cao, Guitang Chen et al, *Intense red and cyan luminescence in europium doped silicate glasses*, Journal of Non-Crystalline Solids 355 (2009) 2361–2364.

[11] J. Park, *Biomaterials: An Introduction.* New York: Plenum, 1979.

[12] P. Saravanapavan, L.L. Hench, *Mesoporous calcium silicate glasses. I. Synthesis*, Journal of Non-Crystalline Solids 318 (2003) 1–13.

[13] D. Hreniak, M. Jasiorski et al., *Nature and optical behavior of heavily europium-doped silica glasses obtained by the sol–gel method*, Journal of Non-Crystalline Solids 298 (2002) 146–152.

[14] L.R. Avila, P.F.S. Pereira, E.J. Nassar, *Preparation and properties of europium-doped phosphosilicate glasses obtained by the sol–gel method*, Journal of Non-Crystalline Solids 354 (2008) 4806–4810.

[15] N.L. de Macedo, *Bone defect regeneration with bioactive glass implantation in rats, J of Apll. Oral Sci.*, 12 (2) 2004, 137-143.

[16] D. W. Ball, *Theory of Raman Spectroscopy*, Spectroscopy 16(11), November 2001.

[17] Bing Hu, Jianlin Shi, *A novel MCM-41 template route to $Eu_8(SiO_4)_6$ crystalline nanorods in silica with enhanced luminescence*, J. Mater. Chem., 2003, 13, 1250–1252.

[18] M. Ferrari, A. Piazza, *Site Selection Spectroscopy of SiO2:Eu^{3+} Gels*, Journal of Sol-Gel Science and Technology, 2, 783-786 (1994).

[19] T. Kokubo, H. Kushitani, *Solutions able to reproduce in vivo surface-structure changes in bioactive glass-ceramic A-W*, J. Biomed. Mater. Res., 1990 (24): 721-734.

[20] J.K. Krebs, J.M. Brownstein, *Site-selective spectroscopy of Eu^{3+} in bioactive glass*, Journal of Luminescence 124 (2007) 257–259.

[21] K. Raulin-Woznica, *Étude du dopage par des ions actifs et des nanoparticules sémi-conductrices de materiaux sol-gel pour l'optique. Interaction dopant-matrice et croissance localisée de nanoparticules par irradiation laser*, PhD thesis, Université des Sciences et Technologies de Lille, 2008.

[22] S. Padilla, A. Carenas, M. Vallet-Regi, *The influence of the phosphorus content on the bioactivity of sol–gel glass ceramics*, Biomaterials 26 (2005) 475–483.

[23] J. Soulié, *Synthèse par voie sol-gel et réactivité in vitro de verres bioactifs dopés, mésostructurés et macrostructurés. Caractérisation par micro-faisceaux d'ions*, PhD thesis, Université Clermont II - Blaise Pascal, 2010.

[24] Piaoping Yang, Zewei Quan, *Bioactive, luminescent and mesoporous europium-doped hydroxyapatite as a drug carrier*, Biomaterials 29 (2008) 4341–4347.

[25] P.L. Roeder, D. Mac Arthur, G.R. Palmer, *Cathodoluminescence and microprobe study of rare-earth elements in apatite*, American Mineralogist, Volume 72, p. 801-811, 1987.

[26] A. Rodrigues, A. Lebugle, *Influence of ethanol in the precipitation medium on the composition, structure and reactivity of tricalcium phosphate*, Colloids and Surfaces A: Physicochemical and Engineering Aspects 145 (1998) 191–204.

[27] R. Ravikrishna, K. T. Valsaraj, *Low-temperature synthesis of porous hydroxyapatite scaffolds using polyaphron templates*, J Sol-Gel Sci Techn (2006) 38:203–210.

[28] C. Rey, C. Drouet, A. Al-Kattan, *Medical Potentialities of Biomimetic Apatites through Adsorption, Ionic Substitution, and Mineral/Organic Associations*, Advanced Engineering Materials 2010, 12, No. 7.

[29] T. Ohnuki, N. Kozai, *Study on uptake of europium by a thin film of apatite-smectite mixture using RBS and micro-PIXE*, Nuclear Instruments and Methods in Physics Research B 181 (2001), 644-648.

[30] Mei Long, Fashui Hong, Wei Li, *Size-dependent microstructure and europium site preference influence fluorescent properties of* Eu^{3+} *doped* $Ca_{10}(PO_4)_6(OH)_2$ *nanocrystal*, Journal of Luminescence 128 (2008) 428–436.

[31] I. Rehman, L. L. Hench, W. Bonfield, *Analysis of apatite layers on glass–ceramic particulate using FTIR and FT-Raman spectroscopy*, Wiley and sons, 2000.

[32] I. Rehman, J. C. Knowles, W. Bonfield, *Analysis of in vitro reaction layers formed on Bioglass using thin-film X-ray diffraction and ATR-FTIR microspectroscopy*, Wiley and sons, 1998.

[33] I. Notingher, A.R. Boccaccini, J. Jones, L.L. Hench, *Application of Raman microspectroscopy to the characterization of bioactive materials*, Materials Characterization 49 (2003) 255– 260.

[34] E. Kontonasaki, T. Zorba, L. Papadopoulou, *Hydroxy Carbonate Apatite Formation on Particulate Bioglass In Vitro as a Function of Time*, Cryst. Res. Technol. 37 2002 11 1165–1171.

[35] B. T. Stone, V.C. Costa, K.L. Bray, *In Situ Dehydroxylation in Eu3+-Doped Sol-Gel Silica*, Chem. Mater. 1997, *9*, 2592-2598.

[36] F. Bonino, A. Damin, V. Aina, *In situ Raman study to monitor bioactive glasses reactivity*, J. Raman Spectrosc. 2008; 39: 260–264.

[37] M. Vallet-Regí, I. Izquierdo-Barba, A. J. Salinas, *Influence of* P_2O_5 *on crystallinity of apatite formed in vitro on surface of bioactive glasses*, Wiley and sons, 1999.

[38] A. Dey, P.H. H. Bomans, *The role of prenucleation clusters in surface-induced calcium phosphate crystallization*, Nature Materials Vol 9, December 2010.

[39] P. Gonzalez, J. Serra, *Raman spectroscopic study of bioactive silica based glasses*, Journal of Non-Crystalline Solids 320 (2003) 92–99.

[40] P. Saravanapavan, J. R. Jones, R.S. Pryce, L.L. Hench, *Bioactivity of gel–glass powders in the CaO-SiO_2 system: A comparison with ternary (CaO-P_2O_5-SiO_2) and quaternary glasses (SiO_2-CaO-P_2O_5-Na_2O)*, Wiley periodicals, 2003.

[41] P. Saravanapavan, L.L. Hench, *Low-temperature synthesis, structure, and bioactivity of gel-derived glasses in the binary CaO-SiO_2 system*, Wiley and sons, 2000.

[42] S. Tiozzo, R. Gallo, *Vetri per applicazioni biomedicali: breve analisi dello stato dell'arte nella progettazione dei biovetri*, Università degli Studi di Padova, 2010.

[43] *Confocal Raman Microscopy General Overview*, Princeton Instruments.

[44] A. Lopez-Sastre, J.M. Gonzalo-Orden, *Coating titanium implants with bioglass and with hydroxyapatite; a comparative study in sheep*, International Orthopaedics (SICOT) (1998) 22:380–383.

[45] C.R. Mariappan, D.M. Yunos, A.R. Boccaccini, *Bioactivity of electro-thermally poled bioactive silicate glass*, Acta Biomater. (2008), doi:10.1016/j.actbio.2008.11.005.

[46] J.M. Nedelec, C. Mansuy, R. Mahiou, *Sol-gel derived YPO_4 and $LuPO_4$ phosphors, a spectroscopic study*, Journal of Molecular Structure 651-653 (2003), 165-170.

[47] C. Mansuy, F. Leroux, R. Mahiou, J.M. Nedelec, *Preferential site substitution in sol-gel derived Eu^{3+} doped Lu_2SiO_5: a combined study by X-ray absorption and luminescence spectroscopies*, J. Mater. Chem., 2005, 15, 4129-4135.

[48] A. Saboori, M. Rabiee, *Synthesis, characterization and in vitro bioactivity of sol-gel-derived SiO_2–CaO–P_2O_5–MgO bioglass*, Materials Science and Engineering C 29 (2009) 335–340.

[49] J. Lao, *Caractérisation par micro-faisceau d'ions des réactions physico-chimiques induites in vitro par des verres bioactifs nanostructurés élaborés par la methode sol-gel*, PhD thesis, Université Clermont II - Blaise Pascal, 2007.

[50] S. Lin, C. Ionescu, J.R. Jones, *Nanostructure evolution and calcium distribution in sol–gel derived bioactive glass*, J Mater Chem (2009) 19:1276–1282.

[51] Commission on colloid and surface chemistry, *Reporting physisorption data for gas/solid systems* (recommendations 1984).

[52] F. Rouquerol, P. Llewellyn, L. Luciani, *Texture des matériaux pulvérulents ou poreux,* Techniques de l'Ingénieur, traité Analyse et Caractérisation, 2004

[53] S. Lowell et al, *Characterization of porous solids and powders: surface area, pore size and density,* Kluwer Academic Publishers, 2004

[54] G. Blasse, B.C. Grabmaier, *Luminescent materials*, Springer-verlag, 1994

[55] R. D. Shannon, Acta Cryst 1976, A32, p.751

[56] J.C. Bunzli, *Mineral Chemistry notes*, Chap 4, 2001

[57] L.L. Hench, J.M. Polak, I.D. Xynos, L.D.K. Buttery, *Bioactive materials to control cell cycle,* Mat Res Innovat (2000) 3:313–323.

[58] E. Jallot, P. Bonhomme, *Dissolution Kinetics, Selective Leaching, and Interfacial Reactions of a Bioglass Coating Enriched in Alumina*, Journal of Colloid and Interface Science 233, 83–90 (2001).

[59] L.L Hench, *Bioceramics: From Concept to Clinic,* J. Am. Ceram. Soc., 74 [7] (1991).

[60] LL. Hench, J.W. Hench, D.C. Greenspan, *Bioglass®: a Short History and Bibliography*, J. Aust. Ceram. Soc. 40 [1] (2004), 1-42.

[61] L.L. Hench, D.E. Day, *Glass and Medicine,* International Journal of Applied Glass Science 1 [1] 104–117 (2010).

[62] I. D. Xynos, M.V.J. Hukkanen, L. D. Buttery, L. L. Hench, J. M. Polak, *Bioglass® 45S5 Stimulates Osteoblast Turnover and Enhances Bone Formation In Vitro: Implications and Applications for Bone Tissue Engineering*, Calcif Tissue Int (2000) 67:321–329.

[63] L.L. Hench, J.M. Polak, I.D. Xynos, L.D.K. Buttery, *Bioactive materials to control cell cycle,* Mat Res Innovat (2000) 3:313–323.

[64] L.L. Hench, *Sol-gel Materials for Bioceramic Applications*, Current Opinion in Solid State & Materials Science 1997.

[65] I.D. Xynos, A.J. Edgar, L.D.K. Buttery, *Ionic Products of Bioactive Glass Dissolution Increase Proliferation of Human Osteoblasts and Induce Insulin-like Growth Factor II mRNA Expression and Protein Synthesis*, Biochemical and Biophysical Research Communications 276, 461–465 (2000).

[66] In-Seon Byun, Swapan Kumar Sarkar et al, *Initial biocompatibility and enhanced osteoblast response of Si doping in a porous BCP bone graft substitute*, J Mater Sci: Mater Med (2010) 21:1937–1947.

[67] B.D. Ratner, *Biomaterials science: an introduction to materials in medicine*, Academic press, 2004.

[68] L.L. Hench, J. Wilson, *An introduction to bioceramics*, World Scientific, 1993.

[69] J. Park, *Biomaterials An Introduction*, New York Plenum, 1979.

[70] Elliot J.C., *Structure and chemistry of the apatites and other calcium orthophosphates*, Vol. 18, Studies in inorganic chemistry, Amsterdam Elsevier 1994, p. 59.

[71] R. Lin, A.E. Clark, L.L. Hench, *An investigation of bioactive glass powders by sol-gel processing*, J. Appl. Biomater., 2: 231-239, 1991.

[72] D.C. Clupper, J.E. Gough, M.M. Hall, L.L. Hench, *Journal of Biomedical Materials Research Part A* (2003), *67A*, 285-294.

[73] C. Di Bello, *Biomateriali, introduzione allo studio dei materiali per uso biomedico*, Pàtron Editore, 2004, Bologna.

Acknowledgments

First of all, I would like to sincerely thank the three professors that helped and guided me both in the research activity and in the editing of this thesis:

The first one is prof. Alessandro Martucci, whose kindness and helpfulness were enormous; he helped me in understanding how to steer the things right when all seemed to go wrong; he gave me a lot of good scientific as well as personal advices; he gave me access to the Materials Engineering labs of the University of Padua, even if my research activity was meant to be completely carried out in France; and he corrected the drafts of this work. He did much much more than he was supposed to do for me, and for this I am deeply and sincerely grateful.

The second is prof. Jean-Marie Nedelec, who welcomed me in his labs and allowed me to carry out this research activity; I would like to thank him for the quick and efficient work of revision of the drafts I sent him, as well as for the useful advices he gave me; and I want to especially thank him for having let me participate in the ISGS Summer School 2010: that was truly a great scientific as well as life experience.

The third is prof. Rachid Mahiou, who taught me from scratch what Rare-Earth element luminescence is, and guided me in carrying out site selective luminescence spectroscopy measurements; his help has been really precious and crucial for my research.

Then I would like to thank the two PhD candidates that most helped me and guided me in the research activity:

Dr Jérémy Soulié (now he has graduated), who taught me all I know about practically carrying out sol-gel syntheses and *in vitro* bioactivity tests; who gave me more good advices than everyone else; and, besides and above all this, has been a very good and sincere friend. He has been my mentor, and my gratefulness towards him will never be enough.

And Olivier Raissle, who helped me so much in nitrogen adsorption measurements, and was a constant, reliable presence in Chimie 7; but the thing I want to thank him most for, is his great heart: he was the first to welcome me in the department, he promptly integrated me in between his friends, and opened the doors of his house and family to me. Without him, the life in Chimie 7 would have been really boring, and flat.

Then I would like to thank also Adeline Hardy-Dessources, PhD candidate as well, and lab neighbor; with her gentle and sensitive character, she has always been very kind to me and has been a really good friend; meeting her in the labs even on Saturdays, and Sundays, and at night, when I had to work with biological interactions, was always a pleasure: a trouble shared is a trouble halved, they say.

A special thank goes also to Mirek (Miroslaw Chorazewski), who was the most constant presence in Chimie 7, literally, even on week-ends, and was always so friendly and helpful, and always had a good thought (and excellent sweets too!) for me.

And I would like to thank also the other researchers working in Chimie 7 and Chimie 5: Alexis, Elodie, Medhou, Azzam and all the others with whom I spent many nice launch breaks in the campus.

Then a really huge thanks goes to Riccardo Gallo, fellow student at the University of Padua, with whom I embarked on the Erasmus adventure; during the six months we spent together in Clermont-Ferrand he has been a true and sincere friend, he has always been there when I needed, and has engaged with me countless discussions on the mutual experimental results. Without him life in Clermont-Ferrand would have been extremely difficult, both from a material and, especially, psychological point of view. You have been a great roommate, man!

Infine, due ringraziamenti in italiano alle tre persone che, seppur a centinaia di chilometri di distanza, più mi sono state vicino durante i sei lunghi mesi passati lontano da casa:

Il primo va a mamma Donatella e papà Gildo, che mi hanno permesso di intraprendere questa esperienza estremamente formativa, sia dal punto di vista umano che accademico; a causa della sfortuna, hanno dovuto affrontare delle grosse difficoltà mentre ero via, senza poter contare su di me, e ciononostante ogni sera erano lì per me su Skype, per informarsi su come stava andando, e soprattutto per farmi sentire l'atmosfera di casa. Grazie infinite!!!

Ma il più importante, profondo e sentito ringraziamento va a Medea, la donna che amo, che per nove lunghi e difficili mesi, sei di Erasmus, e tre di stesura di questa tesi, ha avuto una fiducia e una pazienza infinite nei miei confronti, rimanendo sempre salda al mio fianco nonostante la mia distanza, il mio nervosismo, la mia assenza, sostenendomi nei momenti difficili e perdonando le mie mancanze al di là di quanto chiunque altro avrebbe mai fatto, dandomi una volta di più dimostrazione di cosa significhi davvero amare. Grazie di esistere!!!